DOCTOR OF PHILOSOPHY

Coverage and performance prediction of DGPS systems employing radiobeacon transmissions

Poppe, Dorothy Carol.

Award date:
1995

Awarding institution:
Bangor University

Coverage and Performance Prediction of DGPS Systems Employing Radiobeacon Transmissions

Thesis Submitted in Candidature for the Degree of

Doctor of Philosophy

Dorothy Carol Poppe

School of Electronic Engineering and Computer Systems

University College of North Wales

Bangor

United Kingdom

Acknowledgements

First and foremost, I wish to thank Professor David Last for the care he has taken in guiding me through this research.

A special thanks goes to Mark Searle, Phil Lane and Tom Crummey for the many lively discussions and also for their outstanding assistance over the past three years.

I wish to thank my father, Marty, who has given so much, not only as Cambridge Engineering, but as Dear Old Dad too!

This research has been funded by the General Lighthouse Authorities of the British Isles, Scorpio Marine Electronics, Ltd. and the Overseas Research Students Awards Scheme.

Thanks to 'the gang', especially Trinka, the Matthews family, John, Charles, Emma and Teresa, who have supported me, encouraged me and kept me sane!

Summary

The NAVSTAR-Global Positioning System (GPS) is a state-of-the-art, satellite-based, world-wide, navigation system which was declared operational this year. With GPS, the position of a user can be determined to within 100 m; by employing differential techniques this uncertainty can be reduced to 10 m or less. In real time, this requires a Differential GPS (DGPS) system to measure and communicate correction information to the user.

This research considers DGPS systems employing modified marine radiobeacons and receivers, examining the factors affecting their coverage and performance. Existing techniques of coverage prediction have been examined and found to be inadequate. Improved methods of coverage and performance prediction are developed which take into account several new factors. The groundwave and skywave field strengths of a beacon are calculated, taking into account detailed information about the ground conductivity. A new method of determining own-skywave fading has been derived and the effect at night determined to be significant. Levels of interference from other beacons on the co- and adjacent channels, via groundwave and skywave, are shown to be dominant coverage limiting factors in the European environment. Atmospheric noise and its effect on receiver performance is evaluated and forms the basis of performance predictions.

These new techniques have been built into a computer model which automatically evaluates coverage and performance contours for DGPS radiobeacons and which is being used world-wide in the planning and evaluation of these systems.

Contents

Abbreviations

BER	Bit Error Rate
C/A	Coarse/Acquisition
CCG	Canadian Coast Guard
CCIR	International Radio Consultative Committee
CP-FSK	Continuous Phase-Frequency Shift Keying
DGNSS	Differential GNSS
DGPS	Differential GPS
DOD	United States Department of Defence
DOP	Dilution of Precision
DOT	United States Department of Transportation
EMA	European Maritime Area
HDOP	Horizontal Dilution of Precision
IALA	International Association of Lighthouse Authorities
IDB	Industrial Development, Bangor
IMO	International Maritime Organisation
ION	US Institute of Navigation
ITS	Institute for Telecommunication Sciences
ITU	International Telecommunication Union
ITU-R	International Telecommunication Union-Radio
GDOP	Geometrical Dilution of Precision
GLAs	The General Lighthouse Authorities of the British Isles
GNSS	Global Navigation Satellite System

GPS	Global Positioning System
JPO	Joint Project Office
LF	Low Frequency
Mbps	Megabits per second
MF	Medium Frequency
MSK	Minimum Shift Keying
NAVSTAR	NAVigation Satellite Timing And Range
P-code	Precise code
PDOP	Position Dilution of Precision
PPS	Precise Positioning Service
PRC	Pseudorange Correction
PRN	Pseudorandom-Noise
RRC	Range Rate Correction
RTCM SC-104	Radio Technical Commission for Maritime Services, Special Committee No. 104
SA	Selective Availability
SIR	Signal-to-Interference Ratio
SNR	Signal-to-Noise Ratio
SPS	Standard Positioning Service
TDOP	Time Dilution of Precision
TEC	Total Electron Content
UNH	University of New Hampshire, Durham
USCG	United States Coast Guard
VDOP	Vertical Dilution of Precision
WER	Word Error Rate
WPI	Worcester Polytechnic Institute
WGS 84	World Geodetic System 1984

List of Symbols

a	the 1-σ SA acceleration, 0.0037 m/s
A	skywave factor, $106.6 - 2\sin\Phi$
α	geographic latitude, degrees
β	geographic longitude, degrees
b_{Hz}	noise bandwidth, Hz
B_i	the clock bias of the i-th satellite
B_{user}	the GPS receiver's clock bias
c	the speed of light, $3 \cdot 10^{-8}$m/s
c_i	polynomial coefficient i
d	Great Circle path distance, km
dBμ	dB relative to 1μV/m
Δ_{path}	path difference $p - d$, km
Δ_{time}	skywave delay, s
$E(t)$	the GPS positioning error, m 2drms
$e(t)$	the 1-σ pseudorange error
E_n	the rms noise field strength, dBμ
F_{am}	the median noise level from a CCIR world noise map
f_{Hz}	frequency in Hz
f_{kHz}	frequency in kHz
f_{MHz}	frequency in MHz
F	fade vector
$\|F\|_{dB}$	the logarithmic magnitude of F
Gnd	groundwave field strength, μV/m

Gnd_{dB}	groundwave field strength, dBμ
G_S	sea gain factor, dB
G_V	antenna gain factor, dB
h	ionospheric height, km
h_0	the height to which groundwave depends on conductivity, m
H_{1MHz}	upper noise limit, at 1 MHz, from frequency conversion curve
H_{300kHz}	upper noise limit, at 300 kHz, from frequency conversion curve
$I_0(x)$	modified Bessel function of zero order
k	skywave basic loss factor
k_1	the 1-σ fixed station positioning error, m
ld	the logarythm of d
L_1	the GPS C/A code frequency, 1575.42 MHz
L_2	the GPS P-code frequency, 1227.6 MHz
L_{1MHz}	lower noise limit, at 1 MHz, from frequency conversion curve
L_{300kHz}	lower noise limit, at 300 kHz, from frequency conversion curve
M	RTCM message length in bits
N	the number of attempts needed to receive an RTCM message up-date
p	skywave slant-propagation distance in km
P_m	probability of RTCM message success
P_w	probability of RTCM word error
Δ_P	beacon power factor, dB
Φ	geomagnetic latitude, degrees
$PRC(t_o)$	pseudorange correction generated at time t_o
ρ_i	the pseudorange to the i-th satellite
$\Delta\rho$	the change in pseudorange due to timing errors
R_d	the radiobeacon MSK data rate in bps
R_i	the range to i-th satellite
$RRC(t_o)$	range-rate correction generated at time t_o
S	the scaling factor between 1 MHz and 300 kHz noise levels
sgr	skywave-to-groundwave ratio
$\overline{SGR}$	median skywave-to-groundwave ratio, dB

Sky	skywave field strength, μV/m
Sky_{dB}	skywave field strength, dBμ
T_{a_i}	the arrival time of the signal from the i-th satellite
T_{t_i}	the transmission time of the signal from the i-th satellite
θ	the phase of skywave relative to groundwave
$Total$	the combined groundwave and skywve field strength, μV/m
$Total_{dB}$	the combined groundwave and skywve field strength, dBμ
v	received signal envelope voltage/$\sqrt{2}$
v_l	the rms voltage of the groundwave component, Gnd
v_n	the rms value of the median skywave component, Sky.
W	the number of RTCM words in a message

Chapter 1

Introduction

The NAVSTAR-Global Positioning System (GPS) is a state-of-the-art, satellite-based, world-wide, navigation system which was declared operational this year. With GPS, the position of a user can be determined to within 100 m. This uncertainty can be reduced to 10 m or less by employing differential techniques. In real time, this requires a Differential GPS (DGPS) system to measure and communicate correction information to the user. With GPS now universally available, DGPS systems employing modified marine radiobeacons and receivers as the communication medium are being installed around the world. Unfortunately, these systems are being designed using an imperfect understanding of the factors that will determine their coverage and performance.

DGPS radiobeacons are medium frequency (MF) transmitters typically located along the coast and inland waterways which send differential navigation information to users within reception distance. These beacons can transmit well beyond line-of-sight using relatively low-powered transmitters. However, the coverage area of a beacon is only poorly described by the simple circle so often seen. The signal propagates along the surface of the earth, where it is attenuated more rapidly over land than over sea-water, and also by ionospheric reflection. Atmospheric noise and interference from other transmitters may cause the signal to become corrupted and the data to be lost. Such factors need to be considered when planning a system of DGPS radiobeacons and even more so when communicating the coverage of the system to potential users.

Considerations which affect all DGPS systems, radiobeacon and other, such as the accuracy limitations due to data loss and systematic errors, have been widely studied. But many factors specific to radiobeacon DGPS systems, excepting atmospheric noise and transmission delay, have been left out of system planning.

The goal of this research is to determine the major coverage factors affecting a radiobeacon-based DGPS system and to construct a computer model of the system's coverage and performance. Existing bodies of knowledge will be sought out and applicable methods incorporated. Where these prove to be insufficient, new work will be done and novel techniques verified and implemented. The resulting model should include the capability to produce maps displaying coverage boundaries and performance contours. Such a model will assist in the design of cost-effective and reliable radiobeacon DGPS systems.

1.1 Overview of the thesis

Chapter 2 gives an introduction to GPS and how it works, followed by a discussion of the causes of positioning error. An overview of civilian positioning and navigational requirements is followed by an introduction to DGPS, discussing especially radiobeacon system specifications and error sources.

An analysis of relevant existing coverage prediction techniques is given in Chapter 3. The inadequacies of these techniques are described and a number of major factors affecting coverage are identified which have previously been ignored. The framework of an improved coverage prediction model is proposed.

Chapters 4 to 9 discuss in detail the major factors affecting the coverage of radiobeacon DGPS systems. Chapter 4 discusses groundwave field strength attenuation. It explains the importance of ground conductivity and describes the implementation, for DGPS radiobeacon use, of an internationally-recommended calculation method.

Chapter 5 discusses the method adopted for calculating skywave field strength attenuation. It includes details of the many parameters which must be taken into account

in this calculation and the need for statistical modelling of the attenuation.

Chapter 6 begins with an analysis of existing methods of calculating the multipath fading due to the combination of the groundwave- and skywave-propagated components of the signal. Reasons are given as to why these methods are inadequate for use in DGPS coverage prediction and a novel fade-calculation method for use in the model is developed.

The calculation of an atmospheric noise database is described in Chapter 7. Averaging techniques are developed to determine the noise levels corresponding to different characteristic periods. Examples of noise-limited coverage contours are given.

Due to the large number of radiobeacon allocations in a limited frequency band in the European area, interference from unwanted signals is a major coverage limiting factor. Chapter 8 develops a method for identifying potential interference sources and calculating their effective interference levels. Examples demonstrate the resulting limitations to coverage when this factor is included in the model.

Chapter 9 links the above factors to the achievable radiobeacon DGPS positioning accuracy. Discussions of both the spatial and temporal decorrelation of DGPS data are included. An analysis of the relationship between accuracy and word error is presented. Experimental measurements relating word error to signal-to-noise ratio are described. Examples are given of beacon performance contours generated by the model when these factors are introduced.

Chapter 10 summarises the major conclusions from this research and proposes directions of future work needed in this area.

1.2 Contributions

The major contributions of this research to the coverage prediction of DGPS radiobeacons are as follows:

- The identification of deficiencies in the existing coverage prediction techniques
- The identification of the major factors affecting the coverage and performance of radiobeacon DGPS
- The organisation and computer implementation of existing information concerning radiobeacon DGPS and, more generally, MF broadcasting
- The construction of an improved coverage prediction model, building upon an existing software framework, with new code for the factors specific to radiobeacon coverage prediction
- The calculation of groundwave attenuation parameters relevant to DGPS radiobeacon signals
- The implementation of techniques for skywave attenuation calculation as it pertains to DGPS radiobeacon signals, including the effect of antenna type and ground characteristics
- The identification of deficiencies in existing fade-calculation techniques when applied to radiobeacon signals
- The derivation of a novel technique for predicting the statistical multipath-fading of DGPS radiobeacon signals
- The assembling of noise databases for several regions of Europe
- The automating of SNR-contouring, using interpolation for a continuous noise distribution
- The derivation of novel noise-averaging techniques to allow for different temporal and seasonal classifications
- The development and implementation of a novel technique for identification of potential interferers
- The automation of interference-limited contouring

- First-time field measurements of channel and receiver performance at two of the standard data rates used in DGPS radiobeacon systems
- The implementation of accuracy-contouring
- First-time predictions for both existing beacon systems in various areas and also for the planning of new systems

Chapter 2

Radiobeacon Differential GPS

2.1 Introduction to GPS

GPS is a state-of-the-art satellite navigation system, owned by the United States Department of Defence (DOD) and jointly managed by the DOD and the United States Department of Transportation (DOT) [1]. It is designed to provide 24-hour, all-weather, high-accuracy navigation for military and civilian users on a world-wide basis. The system is currently used for air, sea, land and space navigation and positioning.

GPS makes use of a constellation of 24 satellites in approximately 20,200 km circular orbits with 11 hr 58 min periods, as shown in Fig. 2.1 [2]. Four satellites orbit in each of six orbital planes, at an inclination of 55° to the equator. GPS provides two different levels of service, the Standard Positioning Service (SPS) and the Precise Positioning Service (PPS). Non-military users have access only to the SPS which is intentionally degraded to position the user within 100 m of the true two-dimensional position 95% of the time (written as *100 m, 2drms*) [3, 4]. This degradation, known as Selective Availability (SA), is imposed for political and military reasons, because the civilian system provides *too good* a position, an order of magnitude better than the original specification of 500 m! The US military did not wish to allow this level of accuracy for unauthorised users who include potential adversaries. SA causes the user's GPS position to wander in a random fashion about the true position, changing

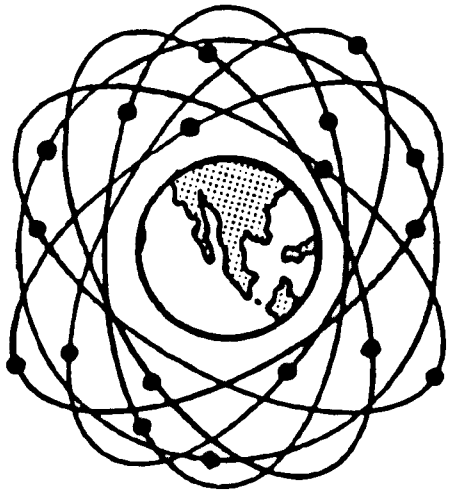

Figure 2.1: The GPS constellation, consisting of 4 satellites in each of 6 orbital planes at an altitude of 20,200 km, from [2].

at approximately 1 m/s. The radius of the circle containing 95% of the measured positions of a stationary receiver describes the 100 m, 2drms accuracy. Without SA, the SPS user would realise an accuracy of 30 to 40 m, 2drms [5, 6, 7]. The 'authorised' PPS user has a positioning accuracy of at least 22 m, 2drms [1, 8]. Despite this dilution of accuracy, SPS GPS is becoming widely used by the civilian community. Some of the variety of applications are listed in Table 2.1

The GPS satellites broadcast navigational information on two frequencies: the L_1 frequency of 1575.42 MHz and the L_2 frequency of 1227.6 MHz [9, 10]. GPS is a *code-division, multiple access system*, meaning that all satellites transmit their messages on the same carrier frequencies, but each modulates its carrier with a pseudorandom-noise (PRN) code, unique to that satellite, to produce a spread-spectrum signal. The PRN code used for the SPS is known as the Coarse/Acquisition (C/A) code; it is composed of a sequence of 1023 bits modulating the L_1 carrier at 1.023 Mbps (Megabits per second). The sequence repeats precisely every millisecond. The PPS service uses the longer-PRN *Precise code (P-code)*, which modulates both the L_1 and L_2 frequencies at a rate of 10.23 Mbps. The P-code may also be encrypted, being then known as the *Y-code*, to provide additional protection from jamming or *spoofing*. In addition to

Application Area	Application
Air Navigation	Nonprecision Approach and Landing
	Domestic En Route
	Oceanic En Route
	Terminal
	Remote Access
	Helicopter Operations
	Agricultural Spraying
	Aircraft Attitude
	Collision Avoidance
	Air Traffic Control
Land Navigation	Vehicle Monitoring
	Schedule Improvement
	Minimal Routing
	Law Enforcement
	Agricultural
Marine Navigation	Oceanic
	Coastal
	Harbor/Approach
	Inland Waterways
Static Positioning and Timing	Offshore Research Exploration
	Hydrographic Surveying
	Aids to Navigation
	Time Transfer
	Land Surveying
	Geographical Information Systems
Space	Launch
	In-Flight/Orbit
	Re-entry/Landing
	Attitude Measurement
Search and Rescue	Position Reporting and Monitoring
	Rendezvous
	Coordinated Search
	Collision Avoidance

Table 2.1: Some civilian applications of GPS.

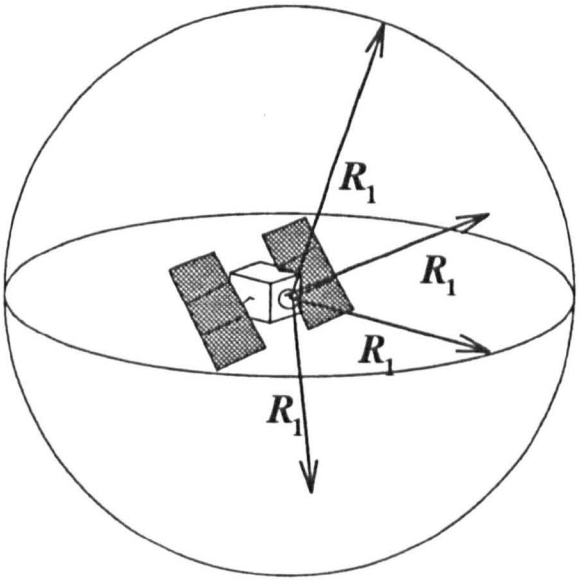

Figure 2.2: The range R_1 between the transmitter and the receiver defines the radius of a hypothetical sphere centred on the satellite, with the receiver located somewhere on its surface.

the PRN codes, both carriers are also modulated at 50 bps by a navigational message, containing satellite clock and ephemeris data, which repeats every 30 s. A full message, with almanac data, takes 12.5 min.

There is a similar system, owned and operated by Russia, called GLONASS [9]. It works like GPS in most important aspects, except that it is a frequency-division, multiple access system. Thus all the satellites use the same PRN code, but each has a unique carrier frequency. It has the equivalent of SPS and PPS, but no intentional degradation is applied to the civilian service. In Europe, the term Global Navigation Satellite System (GNSS) has been used to refer to either or both systems or to their successors [11]; it is a term now being adopted world-wide.

2.1.1 Range and pseudorange

The basis of most precision radio-navigation systems, including GPS and GLONASS, is the use of a radio signal to measure the range between a transmitter and receiver. As shown in Fig. 2.2, this range R_1 defines the radius of a hypothetical sphere centred on the satellite, with the receiver located somewhere on its surface. Fig. 2.3 illustrates the

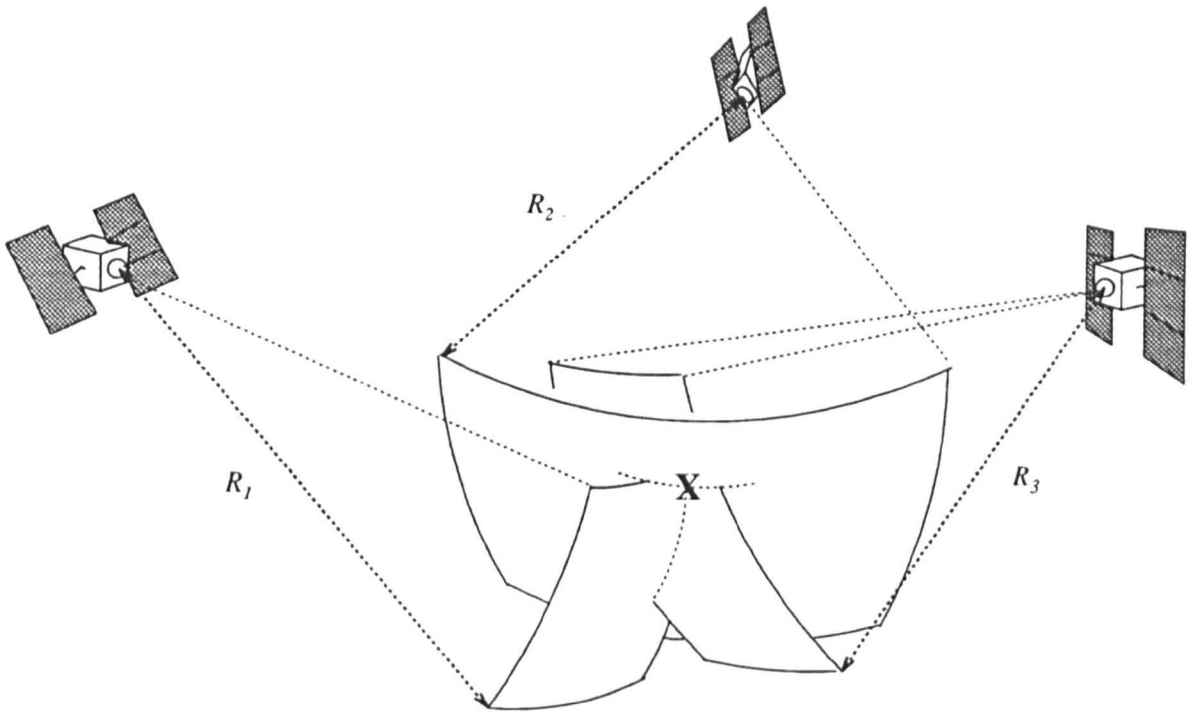

Figure 2.3: The three spheres, with radii determined by the ranges R_1, R_2 and R_3 from the three satellites, intersect at the point X which gives the location of the receiver.

addition of the ranges R_2 and R_3 from a second and third satellite, respectively. The receiver's position is X, the unique intersecting point of the three spherical sections.

Determining range requires the precise measurement of propagation time, that is, the time it takes the signal to propagate from the satellite to the receiver. This time is determined by subtracting the time-of-transmission (the time at which the signal is sent by the satellite) from the time-of-arrival (the time when the signal arrives at the receiver).

The receiver measures the time-of-arrival of a signal by correlating the received signal with a receiver-generated copy of the C/A code [12, 13, 14, 15]. An example of this correlation process is shown in Fig. 2.4. The receiver-generated copy is time-shifted until the correlation peak is found, at which point the received signal and the receiver-generated code are aligned in time. The time-shift necessary to find the correlation peak gives the time-of-arrival of the signal with reference to the receiver's clock. The receiver then retrieves the time-of-transmission of the signal relative to the satellite's atomic clock from the received navigational message. The signal travels at a velocity

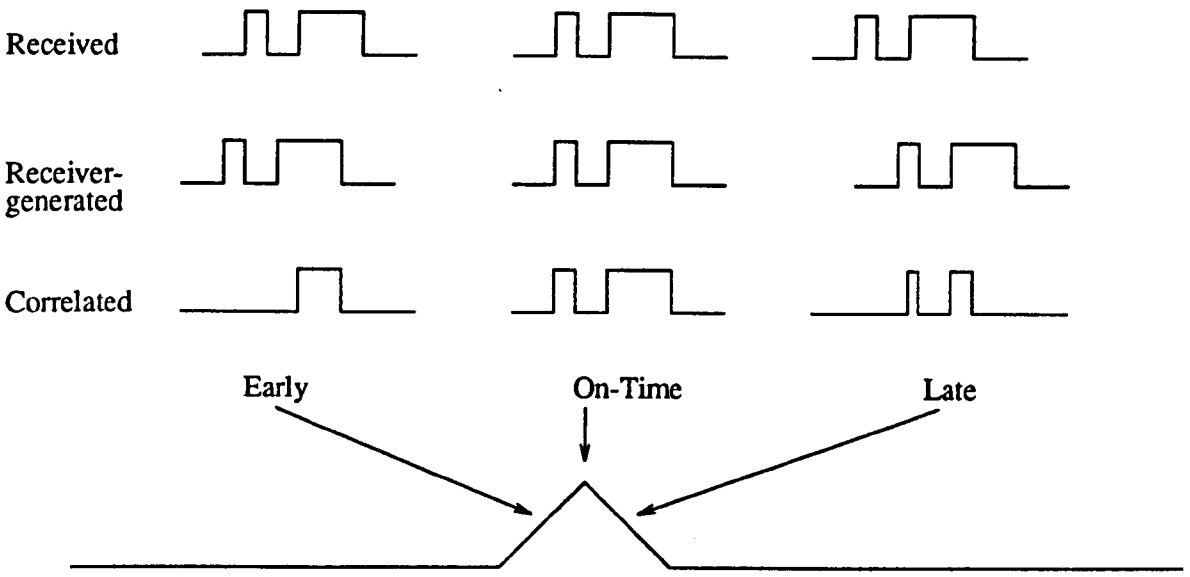

Figure 2.4: Response of the correlator, indicating the relative alignment of the received and receiver-generated C/A codes.

close to the speed of light, and thus the range R_i to the i-th satellite is given by

$$R_i = c(T_{a_i} - T_{t_i}), \tag{2.1}$$

where T_{a_i} and T_{t_i} represent the arrival and transmission times of the signal from the i-th satellite and c is the speed of light.

A precise measurement of propagation time could be achieved by the use in the receiver of a very accurate, very expensive, atomic clock, synchronised to the satellite's own atomic clock. In practice, a GPS receiver contains instead a less-accurate, less-expensive yet stable clock, with an unknown clock error or *bias*, B_{user}. When this clock is used, the measurement yields not the true range but rather a *pseudorange* to the satellite, based on a pseudo-propagation time composed of the real propagation-time plus the receiver's clock bias. The pseudorange ρ_i to the i-th satellite may be written as

$$\rho_i = c(T_{a_i} - T_{t_i} + B_{user}). \tag{2.2}$$

The pseudoranges and navigational messages for different satellites are recovered by correlating the received spread-spectrum signal, consisting of the transmissions from all the satellites, with their individual PRN codes.

2.1.2 Locating the satellites

Unlike terrestrial radio-navigation transmitters, the GPS transmitters are not located at fixed sites. The receiver needs to know the location of each satellite at the moment of transmission of the signal. For this information, the user relies on the satellite to broadcast its location. The satellite does this by sending, as part of its navigational message, a set of parameters defining its orbit [6, 10, 16]. This *ephemeris data* allows the receiver to calculate the position of the satellite at the moment of transmission. Satellite positions, and hence the positions computed by the receivers, are in the earth-centred, earth-fixed, reference frame known as the World Geodetic System 1984 (WGS 84).

The simultaneous measurement of four pseudoranges allows the solution of four unknowns: latitude, longitude, altitude and time. The four simultaneous equations are:

$$e_1 \cdot R_{user} - B_{user} = e_1 \cdot R_1 - \rho_1 - B_1, \quad (2.3)$$

$$e_2 \cdot R_{user} - B_{user} = e_2 \cdot R_2 - \rho_2 - B_2, \quad (2.4)$$

$$e_3 \cdot R_{user} - B_{user} = e_3 \cdot R_3 - \rho_3 - B_3, \quad (2.5)$$

$$e_4 \cdot R_{user} - B_{user} = e_4 \cdot R_4 - \rho_4 - B_4, \quad (2.6)$$

where the receiver measures the pseudoranges ρ_i, e_i and R_i are known from the position of the i-th satellite, B_i is the clock bias of the i-th satellite. The four unknowns are: position R_{user} $[x\ y\ z]$ and receiver clock bias B_{user}. If only two-dimensional positioning and time need be determined, (that is, altitude is known), only three simultaneous pseudoranges from three satellites are required in order to obtain the three unknowns: latitude, longitude and time.

2.2 Sources of error in GPS positioning

The accuracy of a user's measured GPS position is dependent on the precision of the determination of both the location of the satellites and its ranges to them. Both natural and man-made factors affect the receiver's ability to calculate its position precisely. The magnitudes of the sources of error are indicated in Table 2.2. The major source of

Error source	Expected range measurement error (m rms)		
	PPS	SPS	DGPS
Selective Availability	0	≤66	0
Ephemeris errors	2.5-7	2.5-7	0-0.1
Satellite clock errors	1-3	1-3	0
Ionospheric delay (after correction/modelling)	0.4-2	2-15	0.1-1
Tropospheric delay (after correction/modelling)	0.4-2	0.4-2	0.1-1
Multipath propagation	1-2	2-4	2-5
Resulting range error in receiver	3-8	≤66	2-6
Resulting 95% position error			
horizontally	4.5-12	100	3-9
vertically	7.5-20	150	5-15

Table 2.2: The error budget of a stationary receiver using the PPS, SPS, and DGPS services. The DGPS budget assumes a 90 km separation between the beacon and the user (after [16, 18]).

error for the SPS user is Selective Availability, designed to degrade the absolute and repeatable accuracy of the system to 100 m, 2drms.

2.2.1 Selective Availability

Selective Availability reduces the accuracy of the pseudorange measurements through two mechanisms: ephemeris manipulation and clock dither. Ephemeris manipulation is the intentional introduction of small errors into the broadcast orbital parameters. Clock dither is the time-varying de-synchronisation of the satellite's clock with respect to GPS time. The SA error is independent for each of the 24 satellites, with both its magnitude and its rate of change being set by the DOD. The expected levels of positioning error due to SA are based on both statistical data provided by the GPS Joint Project Office (JPO) [17] and off-air measurements [8, 18, 19].

2.2.2 Ephemeris error

In addition to (and much less than) the SA ephemeris error, there is a real uncertainty in the orbital location of a satellite [16, 18, 20]. This uncertainty normally results in

positioning errors of a few metres, but may exceptionally be as large as 20–30 m. The ephemeris data transmitted by the satellite is that of a predicted orbit based on past measurements made by GPS ground monitoring stations. Errors in this information arise due to irregularities in the orbit of the satellite which cause the ephemeris data to age. Post-processed information on the precise orbits is available *ex post facto*, but this is of no assistance in real-time navigation.

2.2.3 Satellite clock bias

As discussed in section 2.1.1, the receiver need not carry a very accurate clock, since the receiver clock bias is treated as an unknown and separated from the positioning coordinates in the navigation solution. This process assumes, however, that all the satellites' clocks are perfectly synchronised. Despite each satellite's carrying several atomic clocks, this is not the case and so there is also a satellite clock bias factor which can be of the order of tens of nanoseconds. The satellites broadcast clock corrections giving estimates of their current bias values which allow the broadcast time to be aligned to within 5 to 10 ns of GPS time by the receiver. This clock correction is supplied periodically to the satellite by a ground control station and is based on ground monitoring station observations. For each nanosecond of timing error introduced, the pseudorange error will increase by $\Delta\rho$, where

$$\Delta\rho = c \cdot 10^{-9} = 0.3 \ m. \tag{2.7}$$

Thus, typical residual satellite clock biases of 5–10 ns contribute 1.5–3 m of pseudorange error [18].

2.2.4 Additional signal delay

The range to the satellite may also be over-estimated due to uncompensated signal delays. During its propagation from the satellite to the receiver, the GPS signal passes through the earth's atmosphere where both the ionosphere and the troposphere reduce its propagation speed [21, 22, 23].

The signal delay due to the ionosphere depends on the Total Electron Content (TEC) of that region of the ionosphere through which the propagation path passes and on the angle of this path through the ionised layer. TEC is a measure of the ionisation in a vertical column with a 1 m^2 cross-sectional area. Signal delays at the L_1 frequency may be greater than 200 ns, but are more typically tens of nanoseconds. The ionospheric delay has a frequency-squared dependency; thus the dual frequencies available to the PPS user, L_1 and L_2, allow this delay to be measured by comparing the propagation times of the signals at the two frequencies, which would otherwise be the same. The single-frequency SPS user does not have this luxury; instead ionospheric modelling is employed which reduces the ionospheric error by some 50% [24, 25, 26]. Pseudorange errors due to ionospheric delay typically are greatest during the daytime, measuring 20–30 m before the ionospheric model is applied, but they fall to only 3–6 m at night.

GPS signals also suffer delays due to propagation through the troposphere [27]. These tropospheric delays are largely frequency-independent, producing errors for both PPS and SPS users. They are minor delays which can be partially modelled, one model being based on satellite elevation seen from the receiver. The tropospheric delay is typically of the order of nanoseconds, and so contributes position errors of only a few metres for satellites more than about 5° above the horizon. If satellites below this elevation are used, the delays can cause tens of metres of positioning error.

The range to the satellite may be miscalculated due to signal multipath propagation. This occurs when the signal reaches the receiver by reflection off a surface, not via the direct path from the satellite. This phenomenon affects both PPS and SPS users and can give errors of the order of tens of nanoseconds. It can be reduced through careful siting of the GPS receiver antenna, the use of a ground plane, or by signal processing techniques in the correlator of the receiver.

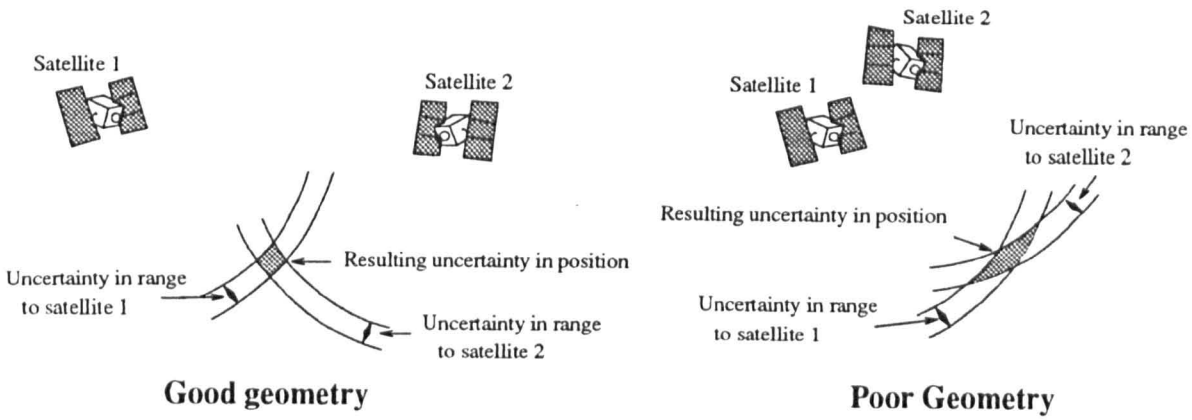

Figure 2.5: Illustration of GDOP. For the same uncertainty in range measurements, the uncertainty in position is greatly increased when the satellites are located close together. Good GPS geometry would be three satellites well spaced around the horizon and a fourth directly overhead.

2.2.5 Satellite geometry

As with other navigation systems, the accuracy of the system depends on the geometrical distribution of the transmitters. The effects on the position of small uncertainties in the measurements of pseudorange are magnified by poor satellite geometry, resulting in a Geometrical Dilution of Precision (GDOP). Fig. 2.5 illustrates this for a simple two-dimensional case. The uncertainty in the measurement of the range to the satellites is of the same magnitude in both the *good geometry* and the *poor geometry* scenarios. The resulting uncertainty in position is the shaded intersection of the two spherical sections. It is seen to be a much larger area in the case of the poor geometry, where the satellites are located close together. Good GPS geometry would be obtained from, say, three satellites well spaced around the horizon and a fourth directly overhead. GDOP can be broken down into two components, the Position Dilution of Precision (PDOP) and the Time Dilution of Precision (TDOP). Numerically, the larger the DOP, the more uncertain the position. PDOPs of not greater than 6 should normally be achievable by users with a clear view of the sky in all directions [1, 4, 10, 28]. PDOP can be further divided into the Horizontal Dilution of Precision (HDOP) and the Vertical Dilution of Precision (VDOP). HDOPs of less than 2 are normally achievable.

2.3 The need for DGPS

The SPS user has available a world-wide, nominally-100 m, navigation and positioning system. Table 2.3 lists the accuracy required for a variety of real-time navigation and positioning tasks, as determined by a recent Institute for Telecommunication Sciences' (ITS) survey of some 67 US Federal agencies and organisations [29]. Accuracy requirements vary widely, with many not being satisfied by SPS GPS [30, 31, 32, 33, 34]. What is needed is a way to enhance GPS, to improve the real-time accuracy so that it is within a few metres. This enhancement can be achieved by differential techniques.

Another very important requirement fulfilled by DGPS is that of providing GPS system *integrity*, the need to know that the GPS system is working as it should [35, 36, 37, 38]. The user assumes that the satellites signals are providing *healthy* broadcasts containing correct ephemeris and clock information, within the limits of SA. If the GPS accuracy falls below specification, most navigational tasks require notification of the user within seconds [29]. The GPS ground-based control group constantly monitor the GPS broadcasts, but inherent system delays can result in several hours delay between a satellite becoming *unhealthy* and the control group passing this crucial information the user [39, 40]. Positioning solutions calculated with the message or timing information from an unhealthy satellite can result in hundreds of metres of navigational error, yet cause no alarm in the user's GPS receiver.

The DGPS reference station works as a local ground-monitor station, constantly measuring the pseudoranges to all satellites in view. If a satellite's pseudorange should become too large or unstable, the reference station can alert the local user *immediately.* This notification is not dependent on news from the GPS control group; it is under the complete and independent control of the DGPS system operator.

Application	Accuracy (2drms)	Achieved with SPS ?
– – – Intelligent Vehicle Highway Systems – – –		
Navigation and Route Guidance	5 – 20 m	no
Mayday/Incident Alert	5 – 30 m	no
Fleet Management	25 – 1500 m	some
Automated Bus/Rail Stop Announcement	5–30 m	no
Vehicle Command and Control	30 – 50 m	no
Collision Avoidance	1 m	no
Accident Data Collection	30 m	no
Infrastructure Management	10 m	no
– – – Railroad Traffic Management – – –		
Train Position Tracking	10-30 m	no
Train Control	1 m	no
Automated Road Vehicle Warning at Crossing	1 m	no
– – – Marine Transportation – – –		
Harbor/Harbor Approach	8 – 20 m	no
Harbor Research Exploration	1 – 3 m	no
Coastal	460 m	yes
Ocean	3700 – 7400 m	yes
– – – Air Transportation – – –		
En Route Oceanic	23 km	yes
En Route Domestic	1000 m	yes
Terminal	500 m	yes
Approach/Landing: Non-Precision	100 m	yes
Approach/Landing: Precision Category I–III	horiz: 17.1– 4.1 m vert: 4.1– 0.6 m	no
Non-Transportation		
Search and Rescue	10 m	no
Aerial Crop Dusting	10 m	no
Aerial Surveillance	1 – 5 m	no
Emergency Management	8 – 10 m	no

Table 2.3: Navigation and positioning requirements for transportation and non-transportation tasks, many of which are not achievable with SPS, from [29].

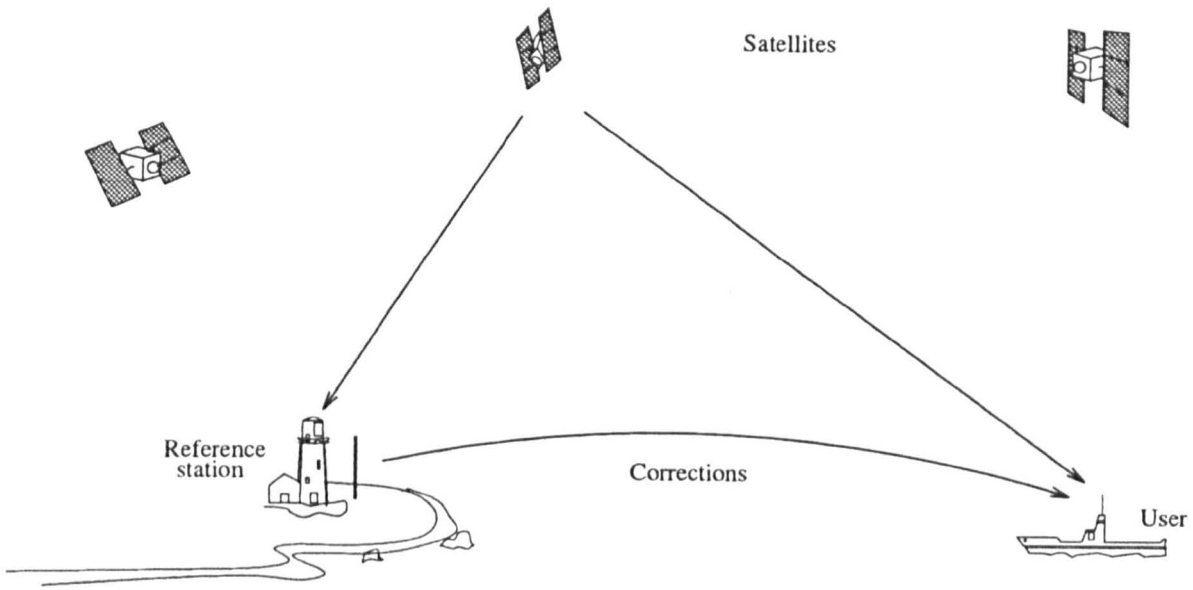

Figure 2.6: DGPS system which employs a local reference station with a high-quality GPS receiver and an antenna at a known, surveyed, location. Corrections generated at the reference station are broadcast to users within communication range and used to correct their measured positions.

2.4 Overview of DGPS

The most effective method of removing, or reducing, the effects of many of the GPS errors given above, most importantly SA, is to use GPS in a differential mode, that is differential GPS. DGPS works on the principle that at a given time, the errors affecting two receivers located in the same area are substantially correlated. Thus, the relative positions of the two receivers can be determined to within a few metres, even in the presence of SA. If the location of one of the receivers is accurately known, then the position of the second receiver can be determined to within those few metres.

Fig. 2.6 shows a typical DGPS system [5, 20, 41]. A local reference station and a user both receive the signals from the same, or *common-view*, satellites. The reference station compares each measured pseudorange with the pseudorange which it calculates using the satellite's ephemeris data and the reference station's known, surveyed, location. The difference between these two pseudoranges gives the *Pseudorange Correction (PRC)* of that satellite. The reference station tracks all satellites in view, up to 11 at a time, and calculates their PRCs. A data link passes the PRCs to the user, where

they are applied to correct the user's measured pseudoranges. By having the reference station deliver PRCs for all satellites in view, the user may select those providing the best geometry from the set of common-view satellites.

Assuming timely delivery of corrections to avoid temporal decorrelation, the use of PRCs allows the GPS positioning errors caused by SA ephemeris manipulation, SA clock dither, satellite ephemeris error and satellite clock bias to be largely cancelled. Partial correction of the errors due to ionospheric delay and tropospheric delay is also possible, the level of improvement depending on the spatial decorrelation of these errors due to the separation between the reference station and the user. No reduction in the errors due to multipath or other receiver-dependent error sources is possible; indeed, multipath errors at the reference station will be added to those of the user. Differential GLONASS operation is very similar, in practice, to DGPS.

2.5 DGPS data message and format

A recommended data message and format for broadcasting GPS and GLONASS PRCs has been devised by the Radio Technical Commission for Maritime Services, Special Committee No. 104 (RTCM SC-104) at the request of the US Institute of Navigation (ION) [18, 42]. This standard is still being developed. It establishes 64 possible different *Types* of RTCM messages, 26 of which have been defined tentatively or in final form, or retired, or reserved in the current version of RTCM SC-104, version 2.1. The eight that have been defined in a final fixed form, the most important ones, are listed in Table 2.4.

2.5.1 The DGPS data link

Using the RTCM data format, the data link can be any RF or other communications medium that allows the message to be communicated reliably at a data rate of at least 50 bps [18, 43]. This minimum data rate is driven by the expected rate of PRC varia-

Message Type No.		Description
GPS	GLONASS	
1	31	Differential GPS/GNSS corrections, full set of satellites
2		Delta differential GPS corrections
3	33	Reference station parameters
5		Constellation health
6	36	Null frame
7	37	Radiobeacon almanacs
9	39	Sub-set differential GPS/GNSS corrections
16	46	Special message

Table 2.4: GPS and GLONASS message type numbers and descriptions for the eight messages defined in final fixed form by RTCM SC-104 version 2.1.

tion, which is in turn dominated by the expected rate of SA clock dither [17]. A data rate of 50 bps, broadcast continuously, is required to provide a 5 m accuracy. One attractive technique for broadcasting corrections to mariners involves modulating selected MF marine radiobeacon signals with the RTCM message. The modulation scheme employed, Minimum Shift Keying (MSK), satisfies the requirement that the DGPS data should not interfere with the long-established marine direction-finding function of the beacon. Also the use of a very narrow-band signal increases the effective signal-to-noise ratio (SNR) of the data link. This type of differential system has been, or is being, adopted by many international and national bodies, including the International Association of Lighthouse Authorities (IALA), the International Maritime Organisation (IMO), The General Lighthouse Authorities of the British Isles (GLAs), the United States Coast Guard (USCG) and the Canadian Coast Guard (CCG) [11, 44, 45].

The use of marine radiobeacons for DGPS data links is attractive for several reasons. Foremost is that existing radio regulations allow for the transmission of supplementary navigational information in the radiobeacon frequency band. Additionally, MF radiobeacons, broadcasting on frequencies around 300 kHz, have good propagation characteristics and use equipment that is relatively inexpensive, reliable, and readily available commercially [46, 47]. Also, the propagation ranges are commensurate with the range over which reference station corrections are applicable. Many countries have existing systems of coastal marine radiobeacons; thus no new frequency allocations are

required to establish an international network, infrastructure costs for implementing the system are relatively low and the system can be implemented much more rapidly than could other potential systems [29, 48, 49]. DGPS broadcasts on marine radiobeacons have either been implemented, or are being planned, in Australia, Belgium, Canada, China, Denmark, Finland, Germany, Norway, Poland, Sweden, the United Kingdom, the United States and countries bordering the Arabian Gulf [18, 50]. The authorities in all these countries have taken advantage of the RTCM standard by prescribing it as the format for these broadcasts.

IALA has been active in setting standards in Europe. IALA works in collaboration with the United Nations organisation, formerly known as the CCIR (International Radio Consultative Committee) and now as ITU-R (International Telecommunication Union-Radio). As part of Differential GNSS (DGNSS), IALA specifies the correction standards for both GPS and GLONASS. The minimum message Types defined by IALA are RTCM SC-104 GPS message Types 1, 3, 6, 7, 9 and 16 and GLONASS Types 31, 33, 36, 37, 39 and 46 (Table 2.4). Recommended message formats for GLONASS PRCs are also included in the latest version of the RTCM document [18].

2.5.2 MSK modulation

The channel spacing of marine radiobeacons is 1000 Hz in the US and only 500 Hz in Europe. Thus a highly bandwidth-efficient modulation scheme is required. Standard data transmission rates of 50, 100 and 200 bps are specified by RTCM and IALA. The Minimum Shift Keying which has been adopted as standard by both the USCG and IALA may be thought of as a form of continuous-phase frequency shift keying (CP-FSK), with the frequencies separated by 0.5 times the bit rate [51, 52]. Thus, in a 100 bps transmission, MSK looks like CP-FSK with frequencies of 25 Hz above and below the carrier. MSK was originally developed to increase effective SNR by using a signal with a narrow bandwidth, resulting in a compact spectrum with good error rate performance and simple demodulation and synchronisation circuits [53, 54]. The power spectrum, shown in Fig. 2.7, confines 99% of the power to within a bandwidth

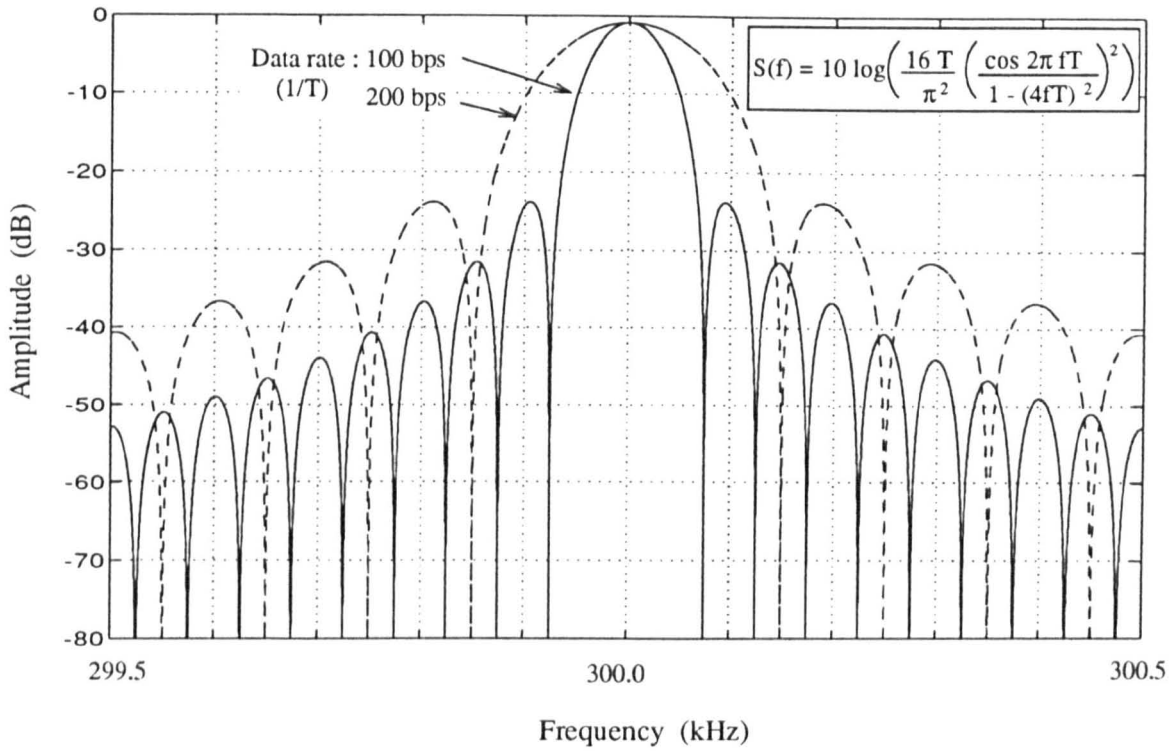

Figure 2.7: The spectrum of a 300 kHz DGPS radiobeacon MSK signal, after [55].

of 1.17 times the bit rate and 50% of the power within 0.59 times the bit rate [55].

2.5.3 Message format

Full details of all RTCM message types and parameters are given in [18]. This section introduces the primary RTCM message of a DGPS system, the Type 1 message, which contains the pseudorange corrections. Like all RTCM messages, it has a header containing a synchronisation preamble and the time at which the PRCs were calculated. It also contains a *Range Rate Correction (RRC)* which gives the rate of change of each PRC. The RRC allows the user to extend the period over which the PRC is valid by computing a *current pseudorange*, $PRC(t)$, as:

$$PRC\,(t) = PRC\,(t_o) + RRC\,(t - t_o)\,, \tag{2.8}$$

where t is the current time, $PRC\,(t_o)$ and $RRC\,(t_o)$ are the PRC and RRC values broadcast in the message and t_o is the time at which they were calculated by the reference station. The Type 1 message carries a PRC and an RRC for each satellite in

view, thus it is a variable length message. With a maximum of 11 satellites in view, it can be quite a lengthy message of 630 bits.

Instead of Type 1, a reference station can broadcast Type 9 messages. These consist of the same data format, but they are fixed length messages, containing PRCs for only 3 satellites at a time. Three or four such messages are required to encompass all the PRCs. It will be seen (Chapter 9) that the shorter length of the Type 9 message improves the DGPS accuracy in high-noise environments [56, 57].

The bias of the reference station clock contributes a factor to all the PRCs in a Type 1 message which may change from one message to the next. The receiver employs PRCs from a single message in each navigational solution. The reference station clock bias is thus effectively added to that of the receiver and isolated in the solution.

At 100 bps, Type 1 messages are updated typically every 10–12 s [18]. However, it takes only a single bit error to cause the whole message to be corrupted and all the 'new' PRCs to be lost. If this occurs, the user must wait for a preamble signalling the start of the next message, and try again.

The use of Type 9 messages requires an atomic clock at the reference station. This ensures that the reference station clock bias remains stable from one measurement epoch to the next. With this stability, PRCs from different messages can be combined to correct a single position solution. The shorter Type 9 message, containing corrections for just 3 satellites, is more immune to corruption by atmospheric noise. In addition, the PRCs are not as 'old' when received, that is, $t - t_o$ (in Equation 2.8) is smaller. At 100 bps, Type 9 messages are typically updated every 8–9 s [18].

The choice of Type 1 or Type 9 messaging has a significant and complex impact on the accuracy achievable by the user, as will be discussed in Chapter 9.

2.6 Sources of error in DGPS systems

The RTCM SC-104 standard is designed to provide 5 m positioning accuracy with a degree of redundancy [18, 58]. The accuracy of the DGPS system may be degraded by spatial or temporal decorrelation of the PRCs between the reference station and the user. Spatial decorrelation describes the variation with location of the GPS pseudorange errors due to ionospheric delay, tropospheric delay, and SA ephemeris error [20, 59]. PRCs are valid several hundreds of kilometres away from the reference station. This is a range greater than the ranges of radiobeacon DGPS signals, unless an exceptionally high-powered transmitter is used, thus spatial decorrelation is not usually a significant factor in radiobeacon DGPS systems.

Temporal decorrelation causes a reduction of DGPS accuracy because of the time varying nature of SA clock dither, SA ephemeris manipulation, ionospheric delay, tropospheric delay, satellite clock bias and satellite ephemeris errors. The SA clock dither has the fastest variation with respect to time, causing the PRCs to become 'old' within 10–30 s, the time depending on the rate of SA being applied to each specific satellite [17]. 'Old' PRCs will degrade the DGPS accuracy; beyond a certain point it will be worse than with non-differential measurements. Under ideal, error-free, MF broadcast conditions, a 'new' PRC will be received before this aging is significant, but as signal-to-noise ratio falls, more messages are lost, PRCs become older and accuracy falls. The minimum data rate of 50 bps was designed to allow as many as three consecutive PRCs to be lost while still meeting the 5 m accuracy specification. Correction data may be corrupted and PRCs lost due to inadequate SNR or high levels of interference from other radiobeacons.

These factors and their effects on the performance of the system are the topics studied in this research and will be the subjects of Chapters 4 to 9.

2.7 Conclusions

GPS can provide the civilian user with 100 m positioning accuracy on a world-wide, 24-hour a day, basis. This accuracy is insufficient for many phases of navigation and some positioning tasks. The use of differential techniques allows the errors common to all GPS receivers in a local area to be cancelled through the application of pseudorange corrections. The DGPS accuracy can be made as good as 1 to 3 m, but it depends upon the ability of the user to receive PRCs in a timely manner. This research focusses on modelling the factors that affect the ability of the user to receive these PRCs when broadcast from MF DGPS radiobeacons.

Chapter 3

Coverage Prediction

3.1 Introduction

Coverage prediction is the process of determining the area within which a radio system provides some minimum standard of service. For radio-navigation systems, the minimum standard is usually an accuracy or availability requirement. Determining coverage areas for DGPS radiobeacons is a complex procedure, with many factors affecting both the accuracy and availability. Radio signals attenuate more rapidly when travelling over land than over sea-water, limiting the range at which signals can be received. The radiobeacon band is prone to high levels of non-Gaussian atmospheric noise, due primarily to lightning-storms around the world. Fading and interference can cause degradation in the quality of service at certain times of the day and seasons of the year. Many system providers are unaware of these complex factors and simply represent the coverage as a circle centred on the beacon.

Automated techniques for predicting the coverage of radio-navigation systems are still relatively new. One of the first comprehensive models was developed for the Loran-C radio-navigation system, at the University of Wales, Bangor, in the early 1990s [60, 61, 62, 63]. At about the same time, a prototype DGPS radiobeacon coverage model was being developed at Worcester Polytechnic Institute (WPI), USA [64]. More recently, the U.S. Coast Guard has commissioned a model for use in North America [65]. These

DGPS coverage prediction models, however, are inadequate in many respects, especially when applied in Europe. This chapter will describe these early models, identifying the factors they incorporate and proposing reasons why they may prove inaccurate.

A number of additional factors which may affect the coverage area of a DGPS radiobeacon system are identified. It is the comprehensive analysis of how these factors affect DGPS radiobeacon systems which forms the backbone of this research. Additionally, a software framework for an improved model is described, a model into which all the additional factors will be incorporated.

3.2 Bangor Loran-C coverage prediction model

The Bangor Loran-C coverage prediction model was developed as an expert system to compute accurate coverage predictions of the low frequency (LF), 100 kHz, Loran-C pulsed-radio-navigation system, considering specifically the European radio spectrum [63, 66]. Fig. 3.1 shows the predicted coverage for a transmitter 'Shetland' located in Northern Scotland. This figure illustrates how the software framework makes use of calculation points defined to be at grid points spaced every 0.5° of latitude by 1° of longitude. The spacing of the points reflects the large areas covered by the high-powered Loran-C transmitters, this one being a relatively small Loran transmitter of only 2.5 kW. The points inside the *coverage area* of the Shetland transmitter are not shown. How has this coverage area been determined?

At each calculation point the model considers several *coverage-limiting* factors. The *groundwave attenuation* and the resulting strength of the signal propagating along the earth from the transmitter are calculated [66]. This groundwave attenuation in turn depends on the electrical characteristics, or *ground conductivity*, of the propagation path, with more attenuation being experienced over land than over sea [67]. When it reached the calculation point, is the signal strong enough? Propagation over ground also distorts the shape of the pulse, due to its frequency-dependent effect on signal velocity, the degree of distortion also depending on the conductivity of the path [62].

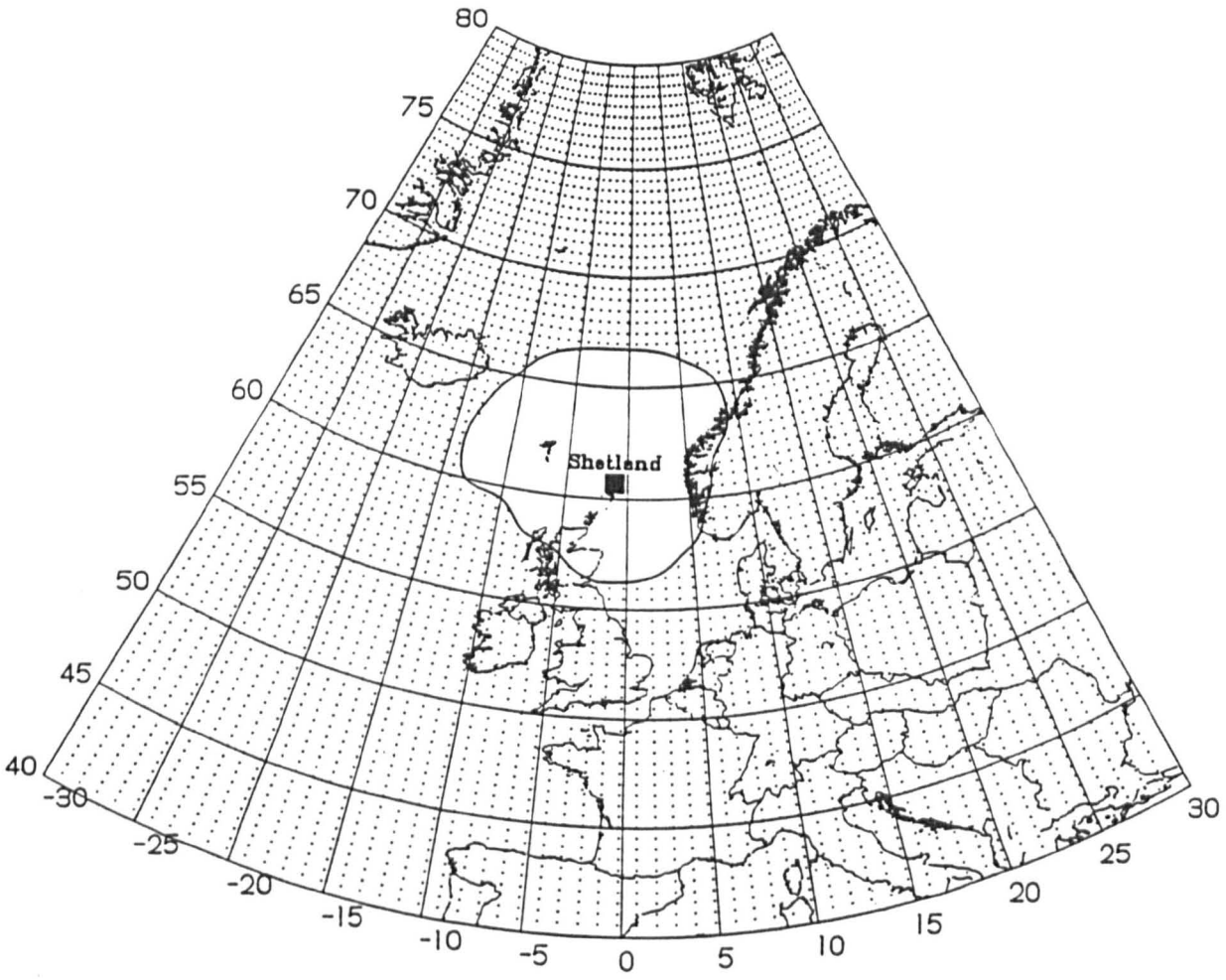

Figure 3.1: An example of the Bangor Loran-C model output for a single transmitter, 'Shetland', located in Scotland. The grid array of calculation points is shown here, except inside the coverage area.

Has the pulse been distorted beyond use?

The *skywave attenuation* and the resulting field strength of the signal propagating via ionospheric reflection are determined at the calculation point [68]. The Loran-C model applies curves of skywave attenuation based on empirical data [66]. These curves show the attenuation to be relatively high during the day, but at night the skywave signals may propagate over long ranges. Then the groundwave and skywave signals from the Shetland transmitter interact in a complex way - is the resulting signal still usable for navigation? Do the signals received via two propagation modes interfere with each other? Such questions are taken into consideration by the model, with the user controlling the minimum requirements.

The model considers not only the wanted signal, it also looks at the atmospheric noise level, checking whether or not the signal-to-noise ratio meets its minimum requirement. To do this, the model draws on a database of noise values derived from the CCIR Atmospheric Noise Report which presents a world-wide map of equal noise contours, at 1 MHz, for each of 24 different time periods throughout the year [69]. This Report includes a complex procedure which allows the 1 MHz noise values to be converted to those at other frequencies. The signal strength of the Shetland transmission is also compared to the strengths of the some *one thousand* potentially-interfering signals at frequencies close to that of Loran-C, to see whether the signal-to-interference ratio exceeds its minimum requirement [70].

Having completed all the calculations and compared them with the coverage-limiting criteria for one calculation point, the model then proceeds to the next point and repeats the process. It quickly becomes apparent how complex coverage prediction can be, and why it has to be automated. And this is for only a single transmitter. To navigate using Loran-C the receiver needs the signals from at least three Loran transmitters at each point. Even if these signals are available, the accuracy obtainable will depend on the geographical distribution of the transmitters with respect to the point.

The Loran-C model enhances the speed of its performance by pre-calculating as many

of the factors as possible, and saving the results to file. These files are then called upon when determining a coverage contour. For the Shetland transmitter shown, pre-calculated files of groundwave attenuation, skywave attenuation, atmospheric noise and interference have been employed. Each of the points is determined to be inside or outside the coverage area depending on the user-adjustable parameters. The model runs on a 80286 (or better) PC and has been extensively verified as to the correctness of its various algorithms.

Unfortunately, this Loran-C model does not operate at radiobeacon frequencies. Although several of the coverage-limiting factors do also apply to radiobeacons, others are unique to the Loran-C system. Groundwave attenuation is a factor that is similar at the Loran and radiobeacon frequencies. The methods employed by the Loran-C in calculating this factor will now be examined in greater detail.

3.2.1 Groundwave attenuation

Groundwave attenuation is calculated in the Loran-C model using the CCIR curves of attenuation at 100 kHz as a function of range and ground conductivity (Fig. 3.2). To determine the ground conductivity of the propagation path, the Loran-C model makes use of the *Bangor Ground Conductivity Database.* This database is unique to the Bangor Loran-C model, for which it was developed. It comprises a map of ground conductivity for all of Europe and portions of North America, Northern Africa and the Middle East with a resolution of 0.1°of latitude by 0.1°of longitude. It was assembled using the published CCIR ground conductivity information [67], more detailed information being added from other sources where it had been made available by the authorities of the various countries included. Where no information was in the public domain, geological maps were used to determine conductivity by identifying the ground type. The result is one of the most comprehensive, digitised, conductivity databases available, containing information essential for the precise calculation of groundwave field strength attenuation. Algorithms in the model draw on this database to determine the conductivity profile along the Great Circle path between the transmitter and

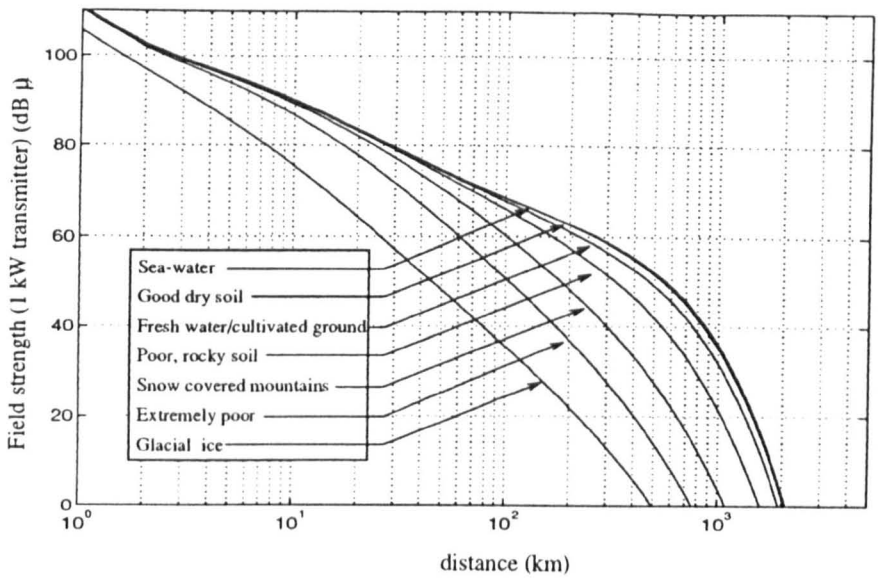

Figure 3.2: The CCIR curves of 100 kHz groundwave attenuation as a function of ground type. These curves have been plotted using the fifth-order polynomial coefficients drawn from the Bangor Loran-C coverage prediction model.

each calculation point.

The curves of groundwave attenuation and the detailed information on the conductivity of the propagation path is fed into an algorithm which employs *Millington's method* [71] - the semi-empirical technique recommended by the ITU for estimating attenuation over paths of mixed conductivity [67]. The result of the calculation is the value of the groundwave attenuation at the calculation point, which is stored to file. The algorithms for such tasks as calculating the Great Circle propagation paths, determining the path conductivity, applying Millington's method and storing the calculated attenuation values have been extensively verified. In fact, the model has been used to design the North West European Loran-C system currently being constructed. By changing the resolution of the calculation points (see 3.4.8 below) and employing CCIR 300 kHz attenuation curves in place of the 100 kHz ones, this model can be adapted to calculate the groundwave attenuation of radiobeacon signals.

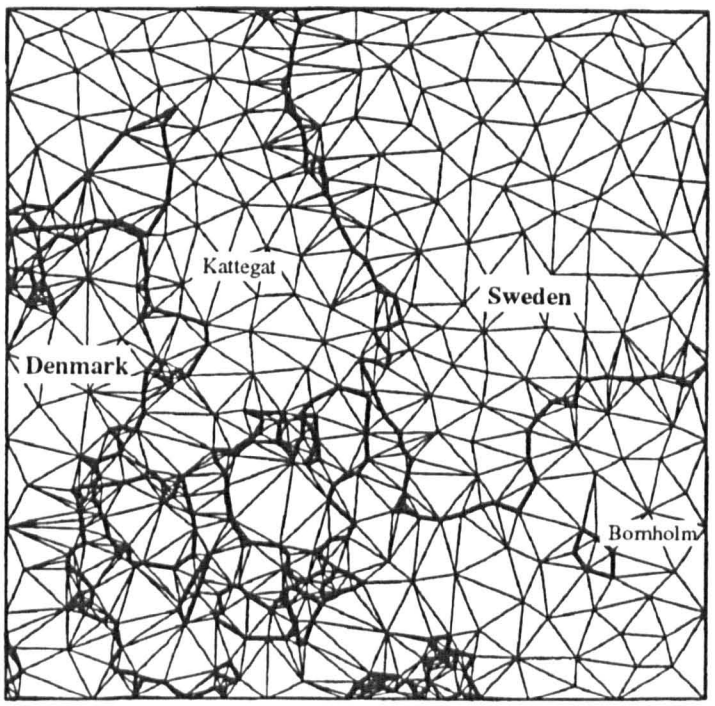

Figure 3.3: An example of the WPI model's Delauney mesh, taken from [64]. The heavy lines indicate the coastlines of a portion of Denmark and Sweden.

3.3 The WPI model

At about the same time as the Bangor Loran-C model was being implemented, a prototype DGPS radiobeacon coverage model was being developed at WPI, in Worcester, Mass [64]. Very different from the Loran-C model, the WPI model is structured around an algorithm called a *Delauney mesh generator* [72]. Instead of a regular array of geographical points, calculation are done at *Delauney mesh nodes.* A *Delauney mesh* is an intricate set of triangles, the edges of which approximate a given boundary. Delauney mesh nodes are the corner points of these triangles. Fig. 3.3 shows the Delauney mesh for those portions of the Danish and Swedish coastlines which are indicated by the heavy lines. The points defining the coastlines and islands have been drawn from a coastline database.

The WPI model examines three factors in determining the coverage area of a DGPS radiobeacon: groundwave attenuation, atmospheric noise and the required SNR.

As in the Loran-C model, standard CCIR curves of attenuation (for 300 kHz now) and Millington's method are employed by the WPI model. A major difference between the two models is that the WPI model does not employ a ground conductivity database. Instead, the user types in, at run-time, the conductivity of the regions outlined by the boundaries. In the prototype model this means one of two conductivities, 'land' or 'sea-water'. In the coverage example published, the 'land' conductivity value is based on limited measurements of over-land attenuation made in the area. Using the resulting field strength values at each node, contours of equal strength are determined.

The WPI model assumes range to be limited solely by atmospheric noise. However, it generates contours of equal signal strength, not of equal signal-to-noise ratio. Unlike the Loran-C model, it does not automatically calculate the SNR at each point. To determine the effect of atmospheric noise, the user must specify the expected noise level in the area and the SNR required, and thus which signal strength contour defines the limit of coverage.

To assist the user, a separate program calculates the noise level at user-specified co-ordinates. This noise calculation program makes use of the information contained in the CCIR "Atmospheric Noise" Report, [69]. No details are given as to how the user goes about determining the minimum acceptable level of SNR, but an SNR of 10 dB is used in the published example.

3.4 Proposed coverage limiting factors

The two early coverage prediction models were found to differ considerably. The Loran-C model includes a variety of coverage-limiting factors and makes use of a highly detailed conductivity map. The WPI model calculates only groundwave attenuation, applying either 'sea' or 'land' as the conductivity. As important as they may be, surely there must be coverage limiting criteria besides groundwave attenuation and atmospheric noise. With only a 3:1 ratio between the Loran-C and radiobeacon frequencies, the propagation modes would not be expected to differ considerably. This fact sug-

gested that certainly skywave attenuation needs to be considered. In addition, the radiobeacon spectrum in Europe is very crowded, so it is likely that interference from other beacons will prove a coverage-limiting factor.

Having examined the factors included in the existing models, the next stage of this project was an extensive study of DGPS and radio communication literature to determine what were likely to be the major coverage factors affecting DGPS radiobeacons. Discussion were also conducted with personnel at the GLAs and Scorpio Marine Electronics, who together were planning to establish a DGPS radiobeacon system covering the United Kingdom and Ireland. The result of this research and these discussions was the identification of eight factors which should be considered when modelling the coverage and performance of DGPS radiobeacons:

- attenuation of the groundwave-propagated component of the wanted beacon's signal,
- strength of the skywave-propagated component of the wanted beacon's signal,
- *own-skywave* fading resulting from the combination of the wanted signal's groundwave- and skywave-propagated components,
- atmospheric noise,
- groundwave-propagated interference from other beacons,
- skywave-propagated interference from other beacons,
- spatial decorrelation of the PRCs,
- temporal decorrelation of the PRCs.

Let us now examine each of these factors to identify the state of knowledge and the work required to create an appropriate component to be incorporated into a DGPS coverage-prediction model.

3.4.1 Groundwave attenuation

The rate of attenuation of a groundwave signal with distance depends on the conductivity of the surface over which the wave travels.

Databases of ground conductivity values, applicable at 300 kHz, are available for many geographical areas [66, 67, 73]. They vary in respect of their data resolution and the credibility of their contents. The Bangor Ground Conductivity Database offers good spatial resolution and has been assembled in a scientific manner. The digitisation block size, approximately 11×7 km, allows for reasonably detailed representation of coastline when compared to typical beacon ranges of several hundred kilometres and is adequate to preserve the resolution of the most detailed CCIR ground conductivity maps. The database contains the most complete and up-to-date records of ground conductivity available. Some information is available separately concerning the small seasonal changes which affect ground conductivity values [74].

The signal attenuation at 300 kHz as a function of distance at a single ground conductivity is known from the standard CCIR curves [67]. Millington's method provides a way of combining these curves and the ground conductivity information to deal with paths of inhomogeneous conductivity. The Bangor Loran-C model contains a software implementation of Millington's method which has been extensively tested and verified.

Work required

Since the Bangor Ground Conductivity Database supplies only a single conductivity value, the effect of seasonal freezing and thawing in the upper latitudes will need to be considered.

The information in the CCIR 300 kHz groundwave attenuation curves needs to be implemented in a computer-accessible form, most likely requiring some form of curve-fitting. The Loran-C implementation of Millington's method works at much too coarse a spatial resolution for use in a model for radiobeacons. Loran-C transmitters employ

power levels of hundreds of kilowatts and their signals propagate for thousands of kilometres. It will be necessary to reduce the resolution to reflect the much lower DGPS radiobeacon output powers, typically of the order of 1 W, which have typical ranges of only a hundred kilometres.

3.4.2 Skywave attenuation

The 300 kHz signal reaching the receiver has, in addition to the normal groundwave component, a skywave component due to reflection by the ionosphere. The level of skywave signal depends on both the time of day and the season in the year, with night-time levels expected to be significant compared to groundwave signals well within the ranges of the beacons. At night, skywave signals can propagate to ranges beyond those of the groundwave signal. The presence of skywave signals may allow radiobeacons to be used at greater ranges at night, so called *skywave recovery*, or may limit their ranges due to fading.

Empirical data on levels of skywave attenuation has been implemented in the Loran-C model [68, 75]. This data comes from USCG and Decca Navigator measurements at 100 kHz. Methods of calculating skywave attenuation at 300 kHz, suitable for use with radiobeacons, are recommended by the CCIR [76, 77, 78]. Information on the diurnal and seasonal variations of skywave intensity are available from both Decca Navigator System sources [79] and CCIR [77]. At least statistically, the groundwave-to-skywave ratio of the 300 kHz signal should be capable of being estimated with reasonable confidence.

Work required

The skywave data for 100 kHz may or may not be applicable to DGPS radiobeacon signals. A method for validating the data at 300 kHz, or possibly converting it to 300 kHz, needs to be devised. The CCIR information needs to be applied at 300 kHz as well. After a method has been selected for estimating the skywave attenuation at

300 kHz, it will need to be implemented in the model.

3.4.3 Own-skywave fading

Once the strength of the wanted skywave signal has been incorporated into the model, the interference between the groundwave and skywave components must be considered. Close to the beacon the groundwave signal will dominate. Moving further from the beacon the groundwave will be attenuated, the skywave will increase and the received signal will consist of a mixture of the two components. Still further away the groundwave may fall below a usable level and the only signal will be that due to skywave propagation. Where groundwave and skywave are of comparable strength, own-skywave fading is to be expected and this may cause the levels of the combined signal to fall below the specified limit for significant periods of time, and DGPS data to be lost.

The CCIR report detailing skywave attenuation also includes information on the statistical variation of this attenuation. CCIR recommend a method of calculating the severity of fading in Radio-Communication Systems Design Report 266 [80]. A different calculation method has been published by one of the co-authors of the WPI model [81].

Work required

The effect of own-skywave fading on DGPS radiobeacon signals needs to be determined. This can be broken down into three specific studies: the effect of different skywave-to-groundwave ratios, the effect of various skywave delays on the alignment of bit-transitions in the MSK signal and the effect of the random phase of the arriving skywave relative to the groundwave which causes the signals to either add or cancel. The statistics of the vector sum of the two signal components need to be determined as a function of their relative phases and amplitudes. The CCIR fade calculation method will be applied to the radiobeacon situation and compared to other calculation methods.

The implementation of this factor will depend on which method proves most suitable for use in the model.

3.4.4 Atmospheric noise

Atmospheric noise in the 300 kHz band is dominated by *spherics*, that is, non-Gaussian noise impulses. Of primary interest is the range at which a 300 kHz DGPS broadcast can be received and decoded properly. This range depends on the intensity of the received signal strength with respect to the spherics and on the behaviour of the receiver in the presence of these spherics. The greater the range of the receiver from the beacon, the weaker the received signal and the more likely it is that a message will be corrupted by noise.

The CCIR Atmospheric noise report plots world-wide noise contours at 1 MHz for 24 different time and season periods [69]. It also gives information on the probability distribution function of 300 kHz atmospheric noise [82]. Information on how this noise may affect the performance of a radiobeacon receiver is included in [83, 84]. Both USCG and ITU include minimum signal-to-noise requirements in their specifications for DGPS radiobeacon receivers [11, 44].

Work required

The CCIR noise data for the area of interest must be converted to 300 kHz. A decision will need to be made as to how this data is to be passed to the model and whether to apply averaged noise or the noise specific to some time period. The minimum SNR requirements must also be included.

3.4.5 Interference

Groundwave and skywave signals propagate not only from the wanted beacon, but also from every other beacon which is broadcasting. The levels of these unwanted

signals and their effect on the wanted signal depend on the powers, locations and frequencies of the unwanted beacons. As the intensity of the interference increases, the radiobeacon receiver may fail to demodulate the wanted signal correctly and the data will be corrupted or lost.

IALA allocates the frequencies and powers of all radiobeacon broadcasts in the European Maritime Area (EMA) and a list can be obtained from the ITU for the relevant frequency band [85, 86]. The strengths of the groundwave and skywave components of these unwanted signals may be determined in the same way as those of the wanted signal. The effect of interference on an MSK signal has also been investigated [53, 54, 87]. Both the ITU and the USCG specifications for radiobeacon broadcasts include maximum signal-to-interference ratios allowable inside coverage areas [11, 44].

Work required

A database of potential interferers to the wanted beacons needs to be created and a method devised for determining the interference level at any calculation point. This method then needs to be implemented in the model, together with the minimum signal-to-interference ratio.

3.4.6 Spatial decorrelation

Spatial decorrelation due to the geographical separation between the reference station and the user will affect the DGPS accuracy. Chapter 2 showed it to be due mainly to the difference in the ionospheric delay affecting the satellite signal received at the reference site and that received at the user's location.

Detailed information on the expected variation in ionospheric delay is not available. Preliminary estimates of the expected worst case variations have been made by the USCG and others [21, 24, 44].

Work required

The available information on worst-case ionospheric variation needs to be converted into a relationship between reference station–user separation and position error. The implementation in the model will need to embody this relationship.

3.4.7 Temporal decorrelation

Temporal decorrelation refers to the variation with time in the measured position of a static receiver. This variation will affect the DGPS accuracy as it causes the DGPS corrections to become less relevant with age. Chapter 2 showed it to be due primarily to SA clock dithering, with high DGPS accuracy requiring the continuous, error-free reception of data from the reference station.

The effect of temporal decorrelation on the achievable accuracy has been well studied by RTCM, USCG and others [18, 29, 44, 65, 81]. The published information relates the DGPS positioning accuracy to the performance of the data channel. The result depends primarily on the characteristics of Selective Availability [17, 88]. There is very little quantitative data on the DGPS channel performance.

Work required

A method of relating the predicted signal, noise and interference to DGPS channel performance needs to be devised. Due to the nature of the data and the noise corrupting it, this may best be done means of experimental measurements. A measurement procedure needs to be defined, a test bed established and channel performance measured. These measurements then need to be combined with the existing methods relating channel performance and DGPS accuracy and the results implemented in the model. Doing this will allow the accuracy at each calculation point to be estimated from the previously-calculated values of signal, noise and interference levels.

3.4.8 Proposed framework for a new model

In addition to determining the major coverage-limiting factors, a framework for the software model needed to be established at this point. The requirements for this framework are: that it provide sufficient resolution to show the details of individual radiobeacon coverage contours, yet still allow the coverage of an extensive system of many beacons to be viewed; that it allow coverage calculation to be run in a reasonable time; and that the final package be able to run on a PC.

It was decided to make use of the Bangor Loran-C model's framework. Although designed for high-powered transmitters, the source code was available and its resolution could thus be modified. It would be necessary to reduce the spacing of the grid points by about an order of magnitude, reflecting the relative output powers of beacons and Loran-C transmitters. The modified framework would use an array of grid points spaced every 0.1° of latitude by 0.1° of longitude (11×7 km at UK latitudes). These regularly-spaced points will be referred to as *calculation points* throughout this thesis. Groups of calculation points will form rectangular *beacon arrays* centred on each beacon; the outer limits of this rectangle define the *beacon window.*

For simplification, the field strength in dB relative to 1 μV/m will be written as 'dBμ' throughout the thesis.

A major advantage of using a modification of the existing model, rather than starting from scratch, is that it will be possible to re-use the algorithms for such fundamental processes as progressing through the calculation points, calculating Great Circle paths, accessing databases, applying Millington's method and, once the points in coverage have been determined, outputting coverage contours. These procedures have been tested and verified for several years now in the existing Bangor Loran-C model.

3.5 Conclusions

The primary objective of this research is to develop more precise and comprehensive techniques for predicting the coverage and performance of DGPS radiobeacon systems. Coverage prediction of DGPS radiobeacon systems, indeed navigation systems in general, is a complex process and one that is well suited to computer modelling.

Two existing coverage prediction models have been examined and found to be inadequate for predicting the coverage areas of DGPS radiobeacon systems. The first is inadequate primarily because it is intended for modelling a different radio-navigation system. The second, while designed specifically for radiobeacon DGPS, is overly simplified: in calculating groundwave attenuation it makes poor use of the available ground conductivity information. The skywave mode of propagation and the fading of the beacon signal are neglected. The dominant noise source is assumed to be atmospheric, ignoring the fact that, especially in Europe, range is potentially limited by interference from other beacons as well.

Following an extensive literature search and discussions with DGPS system planners, a list was compiled of the major factors determining coverage and existing bodies of work identified. During the period of this research, the data from a wide range of sources was brought together and the constant flow of new publications incorporated. A rich source of information on the propagation of MF signals is available in CCIR/ITU Reports and Recommendations, which compile the results of many years of experimental and theoretical research by various countries. These documents form the basis on which broadcasting systems are designed world-wide.

The following chapters discuss one-by-one the application of the coverage-limiting factors to DGPS radiobeacon systems. The implementation of these factors into an improved model is described and their effects will be illustrated using a group of Scandinavian DGPS radiobeacon stations.

Chapter 4

Groundwave Propagation

Groundwave field strength is one of the principal factors which must be calculated when predicting the coverages of DGPS radiobeacons. The attenuation of the signal as it travels away from the beacon depends on the quantity, quality and distribution of the land. This chapter identifies the methods and databases employed in calculating a beacon's groundwave field strength and includes a discussion of the constancy of groundwave with variations in temperature and altitude. The application of the existing information to DGPS radiobeacons and the implementation of this factor into the model are discussed. The methods which have been adopted to reduce the run-time and the storage requirements of the software are presented. Plots of field strength contours, produced using the model, are used to illustrate various aspects of groundwave attenuation.

4.1 Groundwave field strength

The groundwave field strengths at calculation points around a beacon depend on the power of the transmitter and the attenuation, due to ground losses, over the Great Circle path from the beacon to the receiver. The attenuation at each point is determined using the curves of groundwave attenuation versus distance in CCIR Report 717-2 [67]. CCIR has combined vast quantities of measured data to produce standard curves of groundwave field strength attenuation with distance for a range of ground types and

over a wide range of frequencies. The dominant parameter which controls the rate of attenuation of groundwave signals at a given frequency is the ground conductivity. Fig. 4.1 shows these standard curves of field strength of signals at 300 kHz as a function of distance from the beacon for the eight values of ground conductivity employed by CCIR and in the coverage prediction model. Signals are seen to be attenuated more rapidly over land paths (0.01–30 mS/m) than over sea-water paths (5000 mS/m).

In order to automate the calculation of groundwave field strength attenuation, it is necessary for the computer to have access to the CCIR field strength attenuation curves. A simple way to do this is to fit polynomial equations to the curves, so that for a given ground conductivity and distance the computer can calculate the corresponding attenuation. Given that the specification requires the radiobeacon radiated power level to be maintained within 3 dB of its advertised power [11], and that the CCIR graphs are of limited resolution, it was decided that a polynomial curve fit within ±1 dB would be sufficient. Additionally, the polynomial should be of as low an order as possible in order to reduce the calculation time. One way of meeting these two criteria, established by trial and error, is to use the logarithm of the distance instead of the distance itself in the curve-fitting process. This has a smoothing effect, spreading out the points around the knee of the curve. The curves shown in Fig. 4.1 are fifth-order polynomial fits to the CCIR data points shown. The curve fitting is generally much closer than ±1 dB. The polynomial coefficients are listed in Table 4.1. The polynomial expansion adopted to avoid the time-consuming C functions of squaring, cubing, etc. normally required in solving a polynomial, is of the form

$$Gnd_{dB} = c_0 + ld(c_1 + ld(c_2 + ld(c_3 + ld(c_4 + ld\, c_5)))). \qquad (4.1)$$

The CCIR standard curves extend over a wide frequency band, with one located at 300 kHz. One must consider whether more than one set of coefficients is required to accommodate the 283.5 kHz to 325 kHz frequency range of the world-wide marine radiobeacon band at ranges up to 550 km. Using linear interpolation between the adjacent CCIR curves, at their frequencies of 270 kHz and 400 kHz, the attenuations for beacons at the edges of the band are found to be in error by at most ±1 dB

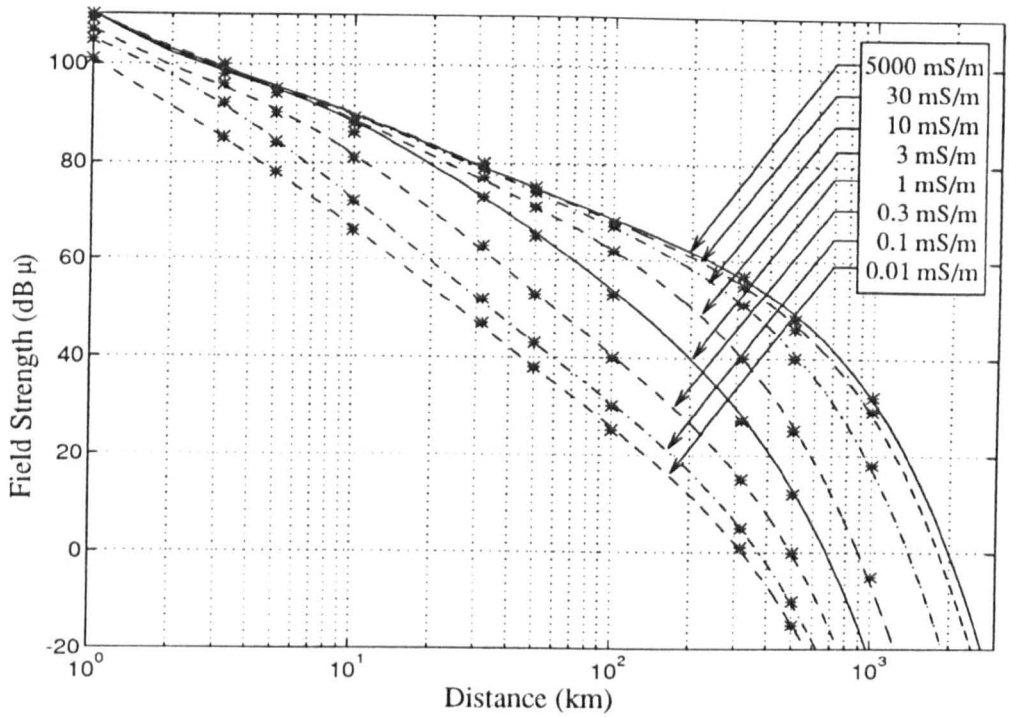

Figure 4.1: Attenuation of groundwave field strength with range and ground conductivity at 300 kHz for a 1 kW beacon; '$*$'s mark the CCIR data points.

Conductivity (mS/m)	$Gnd_{dB} = c_0 + c_1 ld + c_2 ld^2 + c_3 ld^3 + c_4 ld^4 + c_5 ld^5$					
	c_0	c_1	c_2	c_3	c_4	c_5
5000	110.1146	-29.6602	26.3555	-26.7689	11.4738	-1.7841
30	110.1486	-32.0708	32.5899	-31.9379	13.2058	-2.0021
10	110.1066	-28.4962	23.4802	-24.7357	10.9790	-1.8120
3	110.0843	-24.5033	12.7588	-16.2357	8.0360	-1.5237
1	109.0808	-35.9430	45.1628	-47.4954	19.2751	-2.9201
0.3	107.0787	-33.6107	41.7486	-54.3445	24.4572	-3.8412
0.1	105.0632	-22.2583	-5.8686	-12.2449	9.7756	-2.0293
0.01	101.0332	-35.3790	15.8569	-26.1701	13.6865	-2.4260

Table 4.1: The coefficients for fifth-order polynomial fits to the CCIR 300 kHz groundwave attenuation curves. Gnd_{dB} is the field strength in dBμ. Parameter ld is the logarithm of the range in km.

compared to using the 300 kHz curve, at the maximum range of 550 km. This worst-case error occurs with the lowest conductivity path. The error falls to only 0.25 dB for a sea-water path. These discrepancies fall within the curve-fitting criterion above and so the 300 kHz attenuation data alone is used in the model. Using this single data set simplifies and speeds up the field strength calculations. If the frequency band were much broader, it would be necessary to include a number of frequency curve sets and implement an interpolation algorithm, as was done in a related project in which the DGPS model was modified for use with aeronautical radiobeacons, ranging in frequency from 190 to 850 kHz [89].

4.1.1 The use of nominal range values

Radiobeacon antenna systems are invariably small compared with the wavelengths (c 1 km) of their signals. Consequently, they have low efficiencies, radiating only between 1 and 20% of the transmitter power. The efficiency depends on the site, the earthing arrangements and the antenna of the individual station. Thus transmitter power is not a good measure of the radiated power, as it is with many other kinds of radio transmitting installation. Instead, the transmitter power is actually adjusted to give a specific level of field strength at a calibration point established at a known range over a sea-water path. It is conventional in radiobeacon practice to quote the *nominal range* of a beacon, rather than its power in Watts. In the EMA [90], the nominal range is that range at which a beacon's field strength falls to 50 μV/m (34 dBμ) over a sea-water path. This minimum field strength is increased to 75 μV/m (37.5 dBμ) for beacons located below 45° latitude. Specifications for other parts of the world are broadly similar.

The standard CCIR field strength curves are plotted assuming a station which radiates 1 kW. The corresponding higher latitude nominal range, at which the field strength has fallen to 34 dBμ over a sea-water path, is 950 km. In Europe, most DGPS radiobeacons are relatively low-powered and have much shorter ranges, normally between 70 and 180 km. Changing the power does not, of course, affect the shapes of the curves, but only results in a vertical shift. Thus, in employing the standard curve set to predict

the field strengths of beacons, the number of dBs required to achieve a field strength of 34 dBμ, or 37.5 dBμ as appropriate, over a sea-water path at the nominal range of the beacon is first determined, Δ_P. That number, which represents the effective radiated power of the beacon relative to 1 kW, is then subtracted from the attenuation values determined for the specific range and ground conductivity type for which the attenuation is being computed. The method employed in this modelling work is always to calculate and store field strength values. Subsequent adjustment of the beacon's nominal range can then be easily accommodated at any later time by relating the modified nominal range to the original nominal range.

4.2 Millington's method

Many real-world propagation paths are inhomogeneous; that is, they have sections of different ground conductivities. The model estimates attenuation over such paths by using Millington's method [71], a semi-empirical technique, the use of which is recommended by the ITU. This method is represented pictorially in Fig. 4.2. Here the path is composed of three homogeneous sections: sea-water for the first $d1$ km from the beacon, then a land section of length $d2$ km and then $d3$ km of sea-water out to the receiver. The attenuation over each homogeneous section is determined from the CCIR curves. This gives attenuations of $A1$ dB over $d1$ km of sea-water, $A2$ dB over the $d2$ km of land and $A3$ dB over $d3$ km of sea-water. Notice that the attenuation due to the land section depends not only on its length, $d2$, but also on the distance $d1$ between the beacon and the start of the land section. The three attenuations are added together to give a *forward path* attenuation. The process is then repeated assuming the location of the beacon and the transmitter are swapped, giving a *reverse path* attenuation. The average of the forward and reverse path attenuations is then taken as the calculated value of groundwave attenuation at the user's location. This 'swapping and averaging' is the characteristic feature of Millington's method. It is based on the principle that the true attenuation is the same both ways and thus the average represents the best guess, given discrepancies between the *forward* and *reverse* estimates.

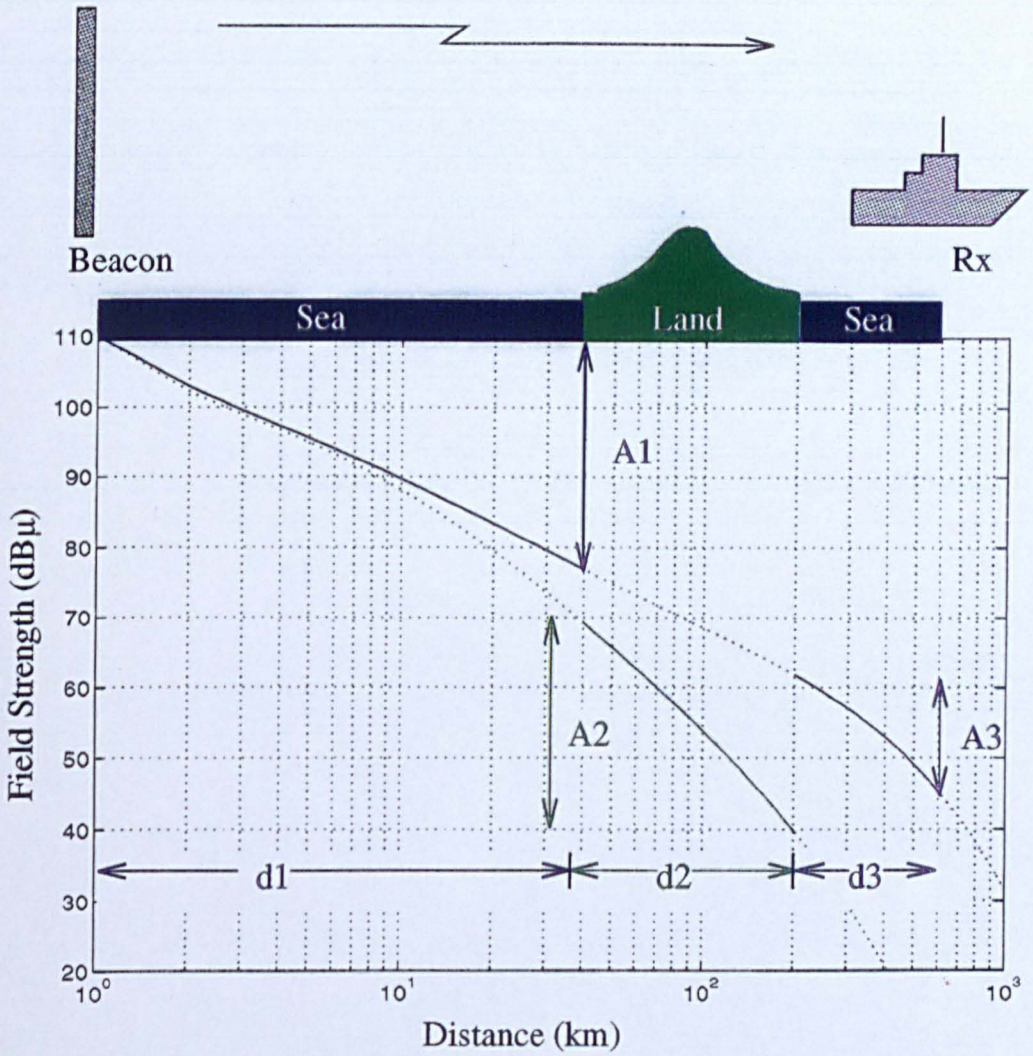

Forward Path Attenuation = (A1 + A2 + A3)

Figure 4.2: Illustration of Millington's method. The attenuations, $A1$,$A2$ and $A3$, due to the three homogeneous sections are summed up to give the *forward* attenuation over the inhomogeneous path.

Following the flow of the software implementation of Millington's method:

Compute the Great Circle path between the beacon and the calculation point,

Using the conductivity data base, determine the points along the path at which transitions in conductivity occur,

Starting at the beacon, calculate the attenuation over each homogeneous path section,

Sum the attenuations, to give the *forward path* attenuation,

Starting at the receiver, calculate the attenuation over each homogeneous path section,

Sum the attenuations, to give the *reverse path* attenuation,

Average the forward and reverse path attenuations, to estimate the total path attenuation.

4.2.1 Ground conductivity

It has been seen that the most important electrical characteristic of the earth, as far as the attenuation of low- frequency groundwave radio signals are concerned, is its electrical conductivity. This coverage model incorporates the *Bangor Ground Conductivity Database*, a digitised conductivity map which covers all of Europe with a resolution of 0.1° latitude by 0.1°longitude (see Chapter 3). This corresponds to a digitisation block size of approximately 11 × 7 km in the latitudes of the United Kingdom and Baltic Sea, the regions which have been studied most closely in this work. Local databases with the same resolution have been created for other areas of the world, the data having been extracted wherever possible from the CCIR "World Atlas of Ground Conductivities" [67]. The database quantises ground conductivity values into the eight standard levels adopted by the CCIR which are listed, along with the types of land of which they are characteristic, in Table 4.2. The model extracts from this database the ground conductivity value of each section of the propagation path from the station to each calculation point in the array.

Fig. 4.3 shows, by way of example, that part of the ground conductivity database which

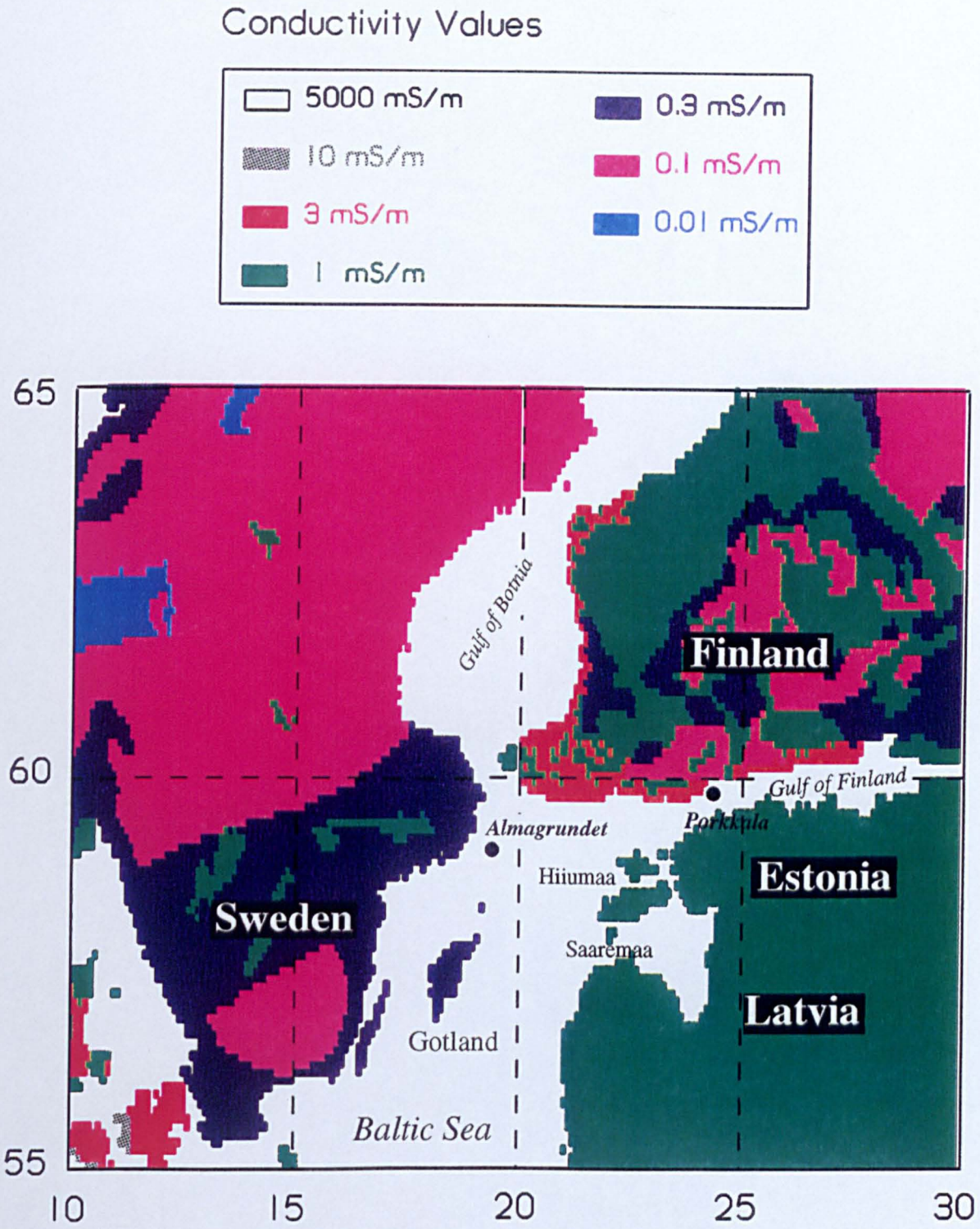

Figure 4.3: Ground conductivity in the Baltic region. This data is drawn from the Bangor Ground Conductivity Database. The low conductivities of southern Finland and most of Sweden provide a sharp contrast to the high sea-water values.

Conductivity (mS/m)	Ground Type	Penetration Depth (m)
5000	Sea water	0.45
30	Very good ground	$\approx$5
10	Wet ground, good dry soil	9.5
3	Fresh water, cultivated ground	20
1	Medium dry, average ground mountainous areas	30
0.3	Dry ground, permafrost, snow covered mountains	$\approx$75
0.1	Extremely poor, very dry ground	100
0.01	Glacial ice	$\gg$100

Table 4.2: Electrical characteristics of various types of ground. The ground conductivities are the standard values, in milliSiemens per metre, recommended by the CCIR [67] and which are used in the Bangor Ground Conductivity Database.

covers the Baltic Sea region. Areas of low ground conductivity are seen along the coast of Southern Finland and throughout most of Sweden. The southern coast of Finland, along the Gulf of Finland, provides an area with rapid variation between high and low conductivity. The contours of the field strengths of the signals from the radiobeacons at Porkkala and Almagrundet will be used to illustrate the effects of ground conductivity on groundwave field strength. Looking south-south-west from Almagrundet, the Baltic Sea and Gotland presents a 'sea-land-sea' pattern, as used in Fig. 4.2 to demonstrate Millington's method.

Fig. 4.4 shows a 3-d contour plot of the groundwave field strength distribution for Almagrundet computed using the model; the x and y axes are longitude and latitude, respectively. The height is the calculated field strength, with the beacon located at the peak. The field strength is seen to fall off less rapidly to the north and east, over the sea-water of the Gulf of Bothnia and the Gulf of Finland, than over the land in the other directions. The attenuating effect of Gotland is evidenced by the more rapid fall-off in strength to the south, with a definite 'valley' formed by the island's shadow. Similar attenuation patterns are seen over Sweden and Finland, with a less pronounced rate of attenuation over the higher conductivity region of Estonia.

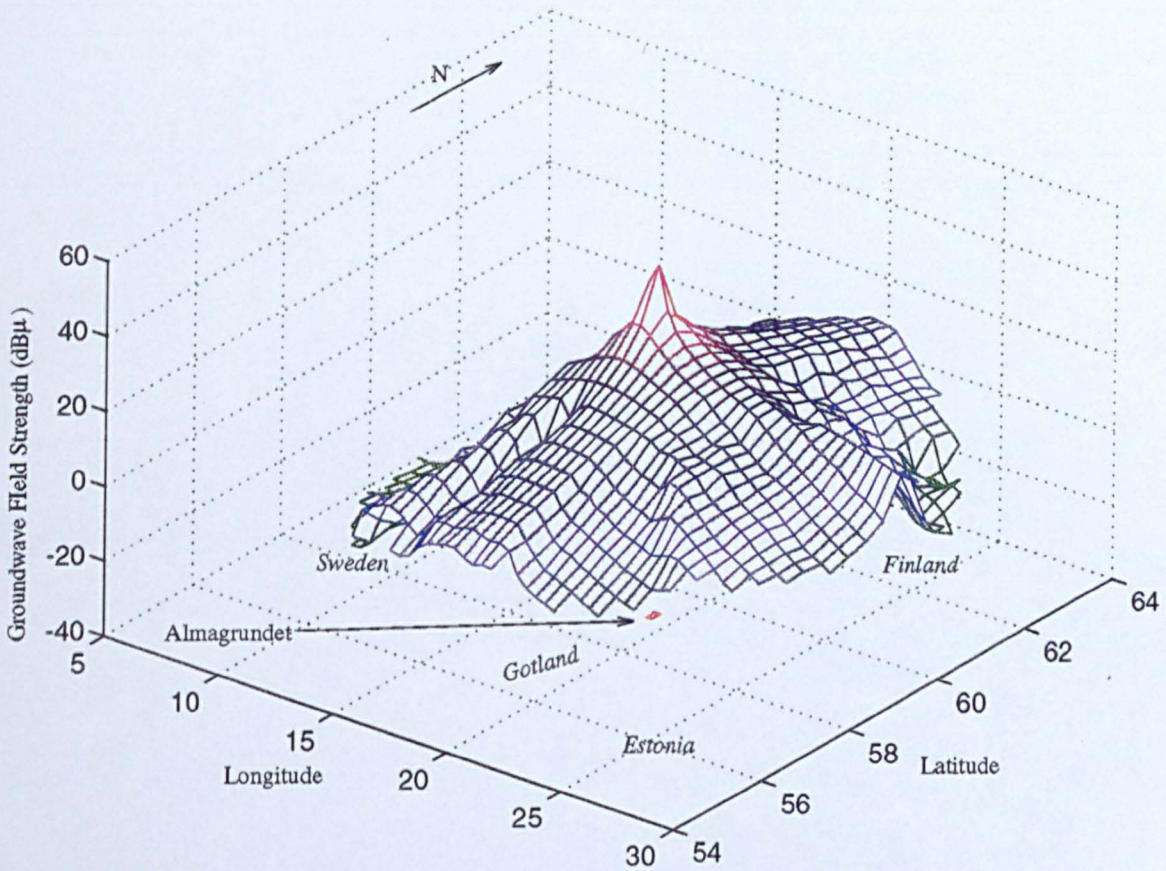

Figure 4.4: The attenuation of field strength around the beacon at Almagrundet in Sweden. Height is proportional to field strength, with the beacon located at the peak. The rapid attenuation to the west, north-west and north-east are evident, as well as the more gradual attenuation over the sea-water paths to the north and east.

4.3 Constancy of the groundwave attenuation

Applying Millington's method is one of the most time-consuming aspects of computing groundwave-propagated field strengths. Thus it would be desirable to pre-calculate an array of groundwave attenuation values for each beacon and store it for use each time a coverage prediction is carried out. This can only be done, however, if the attenuation is constant over time or, at worst, varies in a known way.

In general, groundwave attenuation is extremely constant over the year. There are, however, variations in the mid- and upper-latitudes due to seasonal freezing and thawing which alter the ground conductivity and the losses of the ground [74]. The effect of such temperature variations is significant only when the ground freezes down to depths which are commensurate with the depths to which the groundwave signal energy penetrates. The penetration depth defines the depth into the earth at which the signal has lost 63% of its energy [91]. Penetration depths of 300 kHz waves into earth of different conductivities are listed in Table 4.2. The lower the conductivity, the deeper the groundwave energy penetrates. Seasonal freezing and thawing, however, affect only the first couple metres of ground at most. Thus it is deduced that they cause negligible variation of groundwave field strength.

It should be noted that ground conductivity also determines the velocity of propagation of groundwave signals. The small variations of velocity which result from freezing and thawing are, in contrast to the attenuation effects, significant for low-frequency radionavigation systems such as Loran-C and Decca Navigator [66, 91].

Sea water can also freeze and, since the conductivity of ice is much less than that of sea-water, its effect on field strengths needs to be considered. According to reference [74], when a layer of low conductivity material (such as ice), thinner than its penetration depth, covers a layer of higher conductivity material (such as sea-water), the conductivity of this sub-stratum must be considered. This information needs to be applied to the radiobeacon situation. Consider the case of sea-water with a surface layer of, say, 1 m of ice. The conductivity of the ice is on the order of 0.01 mS/m, and

the penetration depth therein is in excess of 100 m - much greater than the thickness of the surface layer. Thus, the energy lost in the 1 m-thick surface ice is negligible. The conductivity of sea-water is 5000 mS/m and the penetration depth only 0.45 m. So the signals easily penetrate the ice and then penetrate only a further 0.45 m into the sea-water below. The conductivity of the sea-water sub-stratum is the dominant factor, and the standard curve for attenuation over sea-water may be applied. Thus it is concluded that the effect of the freezing and thawing of sea-water paths is also insignificant when predicting groundwave field strengths. Again it is noted that the effect on velocity is significant.

A related question, which also affects the use of stored field strength values, is the variation of groundwave field strength with height. Differential GPS broadcasts are used not only by surface vehicles but also by aircraft, notably helicopters and crop-dusters [92, 93, 94]. From [71], the height h_0 (in metres) up to which field strength is still predominantly dependent on groundwave, rather than space-wave, propagation and so on the ground-type is related to the frequency f_{Hz} by

$$h_0 = 50 * (c/f_{Hz})^{2/3}, \tag{4.2}$$

where c is the speed of light (m/s). Hence the groundwave field strengths of 300 kHz signals are applicable up to an altitude of 5 km (approximately 16000 feet). This is sufficient to ensure that the groundwave field strength values may be used for most aeronautical applications of DGPS. Above h_0 , field strength increases with height until it reaches the line-of-sight (free-space) value.

We conclude that groundwave attenuation is sufficiently constant to allow their values to be computed once only at each geographical grid point and the set of such values for each station stored in an array for subsequent use by the model.

4.4 Implementation considerations

If the model is to be a valuable tool for coverage prediction and planning, its running-time should be kept as short as possible. One way this can be achieved is by limiting

the region within which point-by-point field-strength calculations are carried out. Let us consider the maximum range from a beacon at which such computations are likely to be required.

The most powerful DGPS radiobeacon allocation in the EMA is the Finnish station 'Mantyluoto', which has a nominal range of 180 km. The minimum signal strength with which a DGPS radiobeacon receiver is required to work is 20 dBμ [11, 44]. The groundwave signal from this 180 km beacon reaches this 20 dBμ threshold at a range of 550 km over the path with minimum attenuation, an all sea-water path. So the maximum possible range of this strongest DGPS signal is 550 km and there is thus no call to compute conditions further from any wanted beacon than this.

The software employs rectangular arrays of calculation points with the wanted beacons at their centres, rather than circular arrays (see Chapter 3). Thus we would wish to set the geographical limits of our array automatically to correspond to a circle of 550 km radius. Although this radius means an array will always extend approximately 5° north and south of the beacon (since 1° latitude is always 111 km), the east-west spread in degrees will depend on the latitude of the beacon. This is because 1° longitude is equivalent to a distance of $111 \cdot cos(latitude)$ km. Thus the sizes of the arrays required (rounded to the nearest integer degree values) will range from 10°×14°to 10°×20°in the mid-latitudes. The larger longitudinal spread corresponds to more northerly beacons. The resulting range of arrays contain 14,000–20,000 points at their spacing of 0.1°×0.1°.

Applying the radius limit of 550 km means that calculations need only be done at points within a circle of this radius, not at all points within the array. This circle will contain about 70% of the array points, the corner points which lie more than 550 km from the beacon being excluded with a corresponding reduction in calculation time. In fact, the reduction is even greater than would be expected: the use of Millington's method means that the attenuation of a long path takes more time to compute than that of a short path, and the longest paths of all - those from the beacon to the corners of the window - are removed. A groundwave field strength file for an individual beacon now takes approximately 7.5 minutes to compute on a 486, 20 MHz, PC. Its size is

normally 32 to 40 Kbytes.

4.5 Groundwave field strength contours

The Finnish beacon of Porkkala and the Swedish beacon of Almagrundet are used as examples throughout this work. These beacons form part of the earliest European DGPS radiobeacon system, established for test and evaluation to cover the route of the Stockholm-Helsinki ferry. They have been the subject of a number different studies [64, 95, 96]. Their situations are unique: on the coasts of the Baltic Sea and the Gulf of Finland, with paths from the two beacons to the ferry route being principally over sea-water. The conductivity of the land along the coasts is low, however, and the groundwave attenuation over land paths is high. Unlike many Atlantic coast beacons, the Baltic Sea beacons need only cover a relatively small body of water.

Groundwave field strength contours around Porkkala, nominal range of 160 km, are shown in Fig. 4.5. To explain the figure, a field strength contour of 20 dBμ, for example, encloses all points in the array at which the predicted field strength exceeds that value. The contours in Fig. 4.5 range from 20dBμ, the limiting value employed by DGPS system planning, to 35dBμ, a value close to the field strength of the beacon at its nominal range over a sea-water path.

The effect of the low-conductivity ground north of Porkkala is clearly indicated by the closeness of the contours to the beacon, and their close packing to one another. This is an area where the groundwave field strength is severely attenuated over a relatively short distance. In fact, the signal has been reduced to 35 dBμ at a range of only 40 km and to 20 dBμ at a distance of about 100 km. In contrast, the contours over the sea-water paths to the east and south-west lie much further from the station and are more widely spaced. Here the 35 dBμ contour extends out to 140 km from the beacon and the 20 dBμ contour to some 377 km. West of the beacon, the signal is again quickly attenuated by the low ground conductivity of Sweden and the 20dBμ contour lies close to the coastline. Note also the shadowing caused by Gotland, forming a

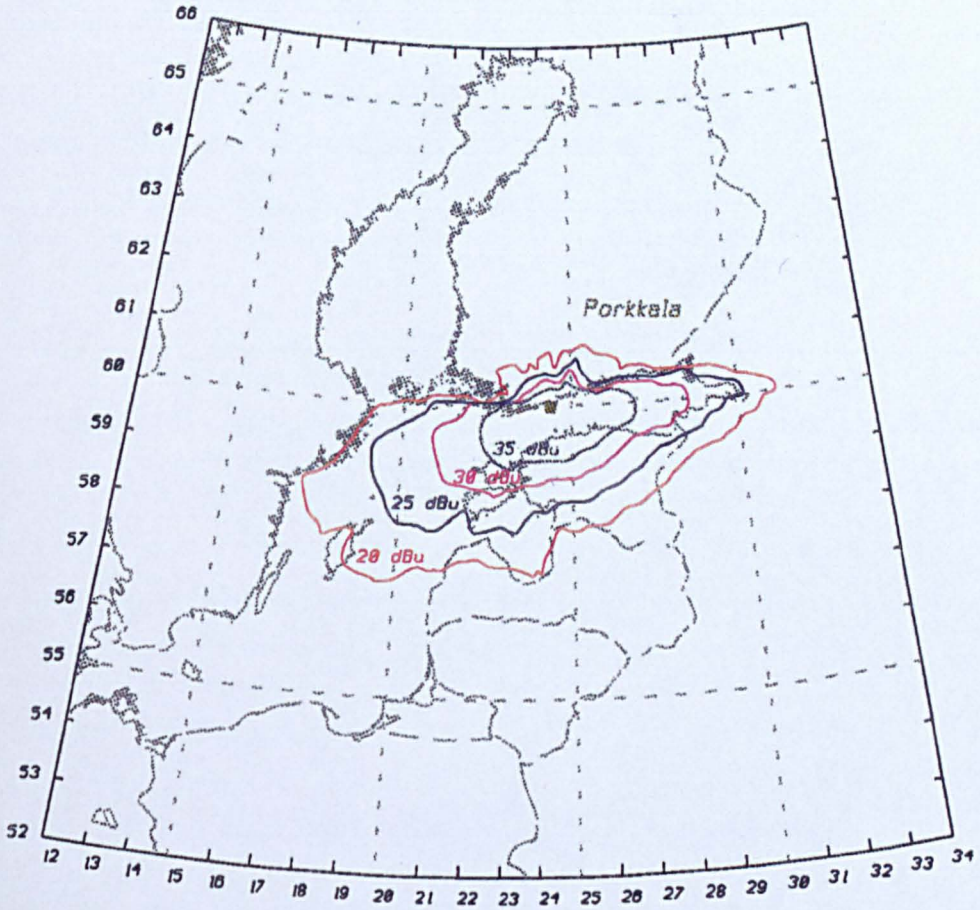

Figure 4.5: Contours of groundwave field strength around the Finnish beacon 'Porkkala' which has a nominal range of 160 km. The low conductivity land north of the beacon causes the contours to lie close to the station and be closely packed. The ranges are much greater over the sea-water paths to the east and west. The attenuation of the groundwave signal by the island of Gotland, south-west of the beacon, is also quite distinct.

distinct indentation in the 20 dBμ contour.

Not all land in the area is of low conductivity: the contours over the high-conductivity land of Estonia are closer together than those over the sea, but much more widely spread than those north of Porkkala. The 34 and 20 dBμ ranges in this area are about 90 km and 220 km, respectively.

Fig. 4.6 shows the equivalent field strength contours around Almagrundet, a beacon with a smaller nominal range of 88 km. Again, the effect of the different conductivities of land and sea may be seen and Gotland causes pronounced 'dips' in both the 20 and 25 dBμ contours. These two figures demonstrate dramatically the importance of the use of groundwave modelling and the inadequacy of simply citing the nominal range of the beacon and relating the DGPS coverage to it.

An additional feature of the model is that contours may also be drawn for systems of beacons, such as the combination of Porkkala and Almagrundet (Fig. 4.7). In this case, a calculation point is included inside the contour if the field strength of one or both of the beacons meets the limiting criterion.

Another way to present the data, which is valuable to the planners of DGPS systems, is shown in Fig. 4.8. Including the contours of the individual beacons allows the areas where redundant coverage is available to be identified. Here, for example, it can be seen that, at the 20 dBμ level, the area of the Baltic covered by Almagrundet is largely duplicated by its more powerful neighbour, Porkkala. Current guidelines for DGPS users recommend using the geographically-closest beacon for corrections, switching to an alternate beacon if this beacon should become unusable [44]. This type of plot both demonstrates the inappropriateness of using the closest beacon and allows the availability of alternatives to be examined.

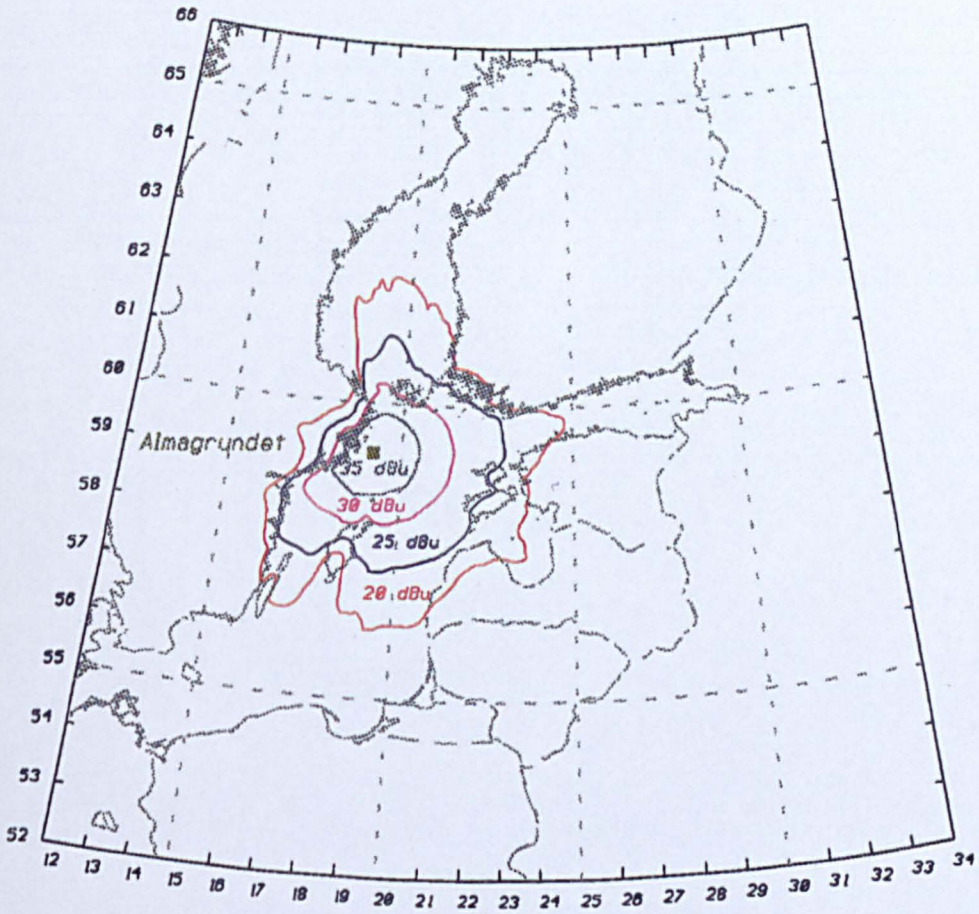

Figure 4.6: Contours of groundwave field strength around the Swedish beacon 'Almagrundet', nominal range 88 km. Note how the contours lie close to the Swedish and Finnish coastlines, and the attenuation caused by Gotland. This figure and the previous one demonstrate the importance of groundwave modelling and the inadequacy of assuming that the coverage may be represented by a simple *nominal range*.

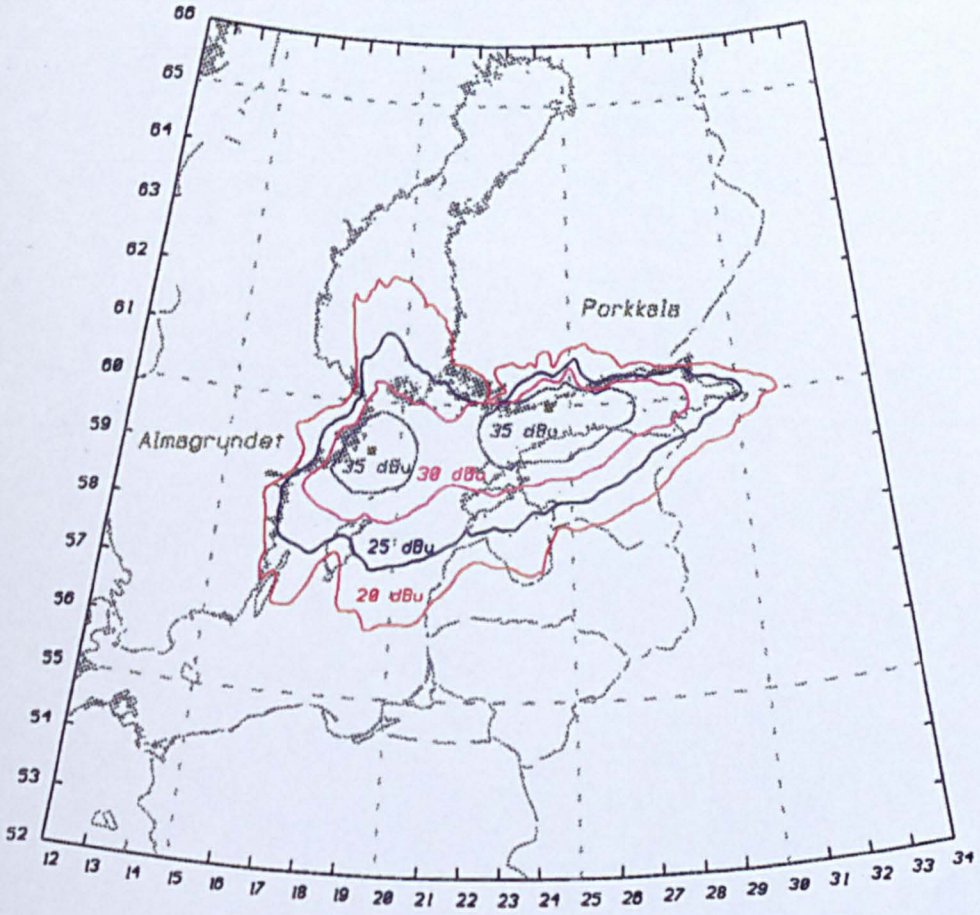

Figure 4.7: Groundwave field strength contours for a system of two beacons. A point is included in a contour if the signal from one or both beacons exceeds the quoted level.

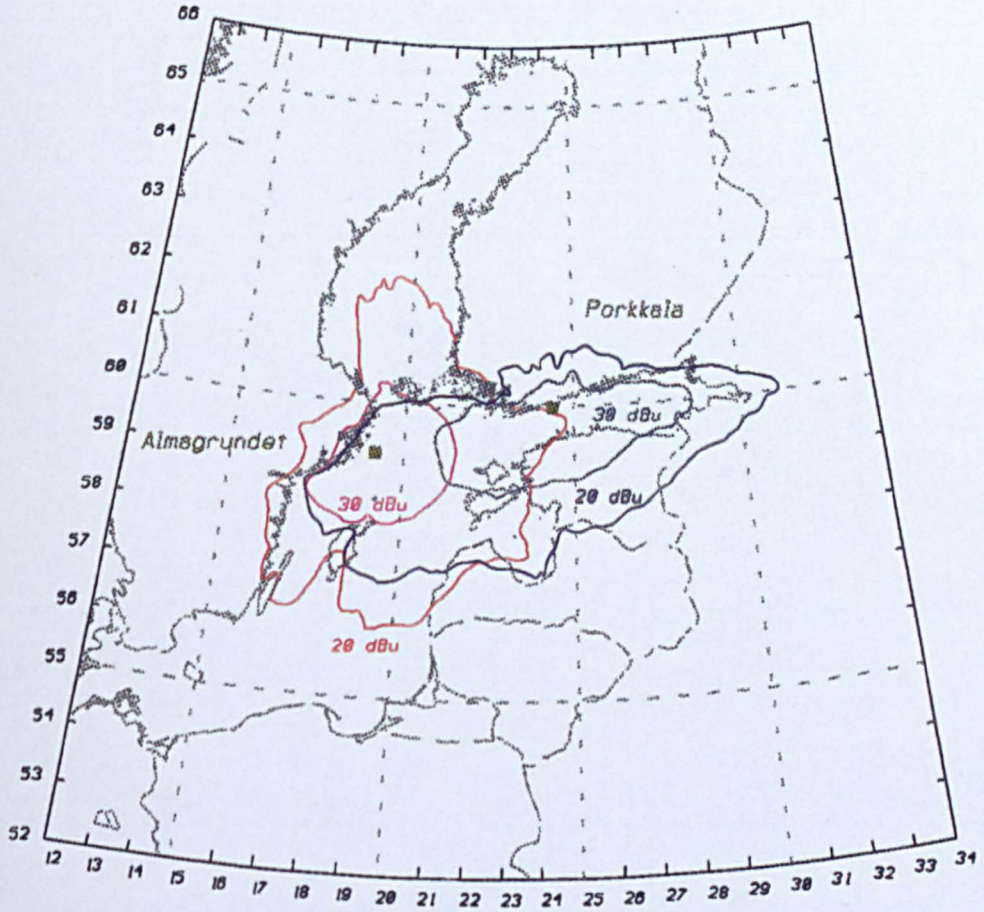

Figure 4.8: Overlapping contours of groundwave field strength around two beacons. The overlapping areas, within which the signal strengths from both beacons exceed the contour levels, show where alternate DGPS correction sources are available to the user. In the Baltic Sea, the 20 dBμ coverage of Almagrundet is largely duplicated by Porkkala.

4.6 Verification of predictions

The data and methods employed in calculating the groundwave attenuation are those recommended by the CCIR and are based on a large volume of measured data gathered in many countries over many years [66]. Verification of values predicted by the DGPS model does not (and cannot) seek to repeat the CCIR work, but to establish that the data and methods have been correctly implemented. Verification of the model is of great importance, building confidence in the 'truth' of the predicted coverage.

Independent measurements from the commissioning of DGPS radiobeacons around the British Isles were made available by the GLAs [97]. There are now 11 DGPS beacons in operation along the coasts of the United Kingdom and Ireland. During the commissioning of these beacons, a calibration site was established a few kilometres from each beacon over a sea-water signal path. Knowing the range, the field strength is calculated, assuming that the beacon has the correct nominal range. The power of the beacon is then adjusted so the measured level at this point agrees with this value. From knowledge of the power output of the transmitter, the antenna efficiency may also be calculated.

In validating the groundwave field strength function of the coverage prediction model, the levels of groundwave field strength, predicted (and measured) by the GLAs were compared with those computed from the model. Table 4.3 shows the data from the calibration sites of the 11 beacons. Fig. 4.9 plots the field strength measured, and those computed by the model, against range; the ranges of the calibration sites from their beacons varied between 20 and 130 km. There is excellent agreement between the measured field strengths and those predicted by the model over the full range of distances; the greatest discrepancy is only 1.4 dB. In addition to validating the model, the results also illustrate the characteristically low efficiencies of radiobeacon antenna systems.

Since the early stages of this research, requests have come from DGPS radiobeacon system planners (and users) for coverage predictions of their systems. These requests

Beacon	Range	Field Strength (dBμ)		Antenna
		Measured	Predicted	Efficiency
Tory Island	39.2	44.6	44.4	2.8%
Mizen Head	60.5	40.0	39.9	4.3%
Butt if Lewis	59.2	41.0	40.9	1.5%
Rinns of Islay	124.7	35.0	34.2	3.6%
Girdle Ness	41.0	44.0	43.2	1.0%
Sumburgh Head	31.1	46.5	46.5	4.5%
Flamborough Head	54.4	41.3	41.6	3.7%
Lizard	81.5	39.0	38.1	1.5%
North Foreland	25.6	47.5	48.4	1.8%
Point Lynas	18.6	52.0	50.6	1.1%
St Catherines	47.0	44.0	43.1	2.0%

Table 4.3: Measured field strength values at the calibration sites of 11 GLAs radiobeacons compared with values predicted using the coverage model. The agreement (within 1.4 dB) over a wide range of path lengths verifies the correct operation of the model.

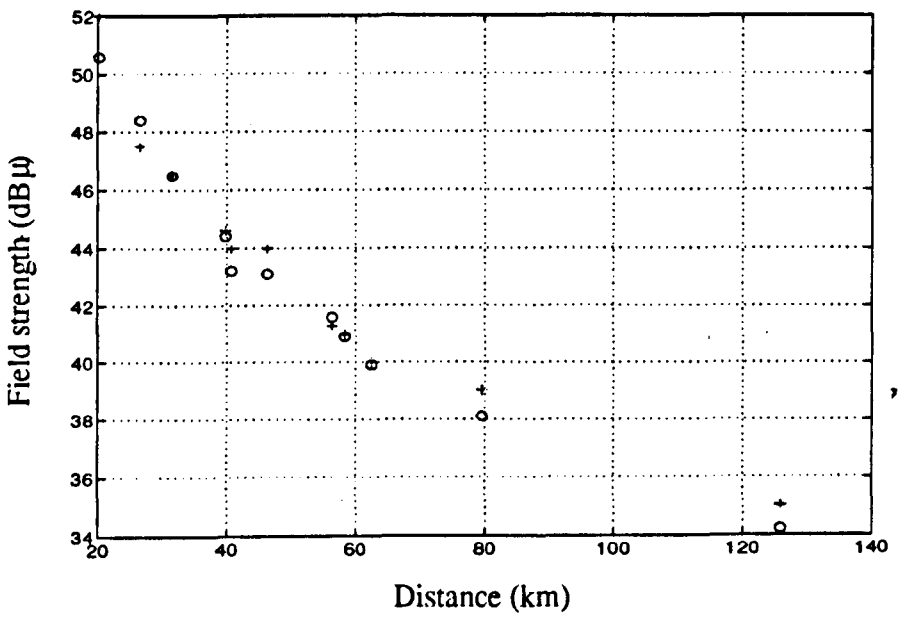

Figure 4.9: Comparison between measured (+) and predicted (o) field strengths at the calibration sites of 11 radiobeacons. The agreement (within 1.4 dB) over a wide range of path lengths demonstrates the correct operation of the model.

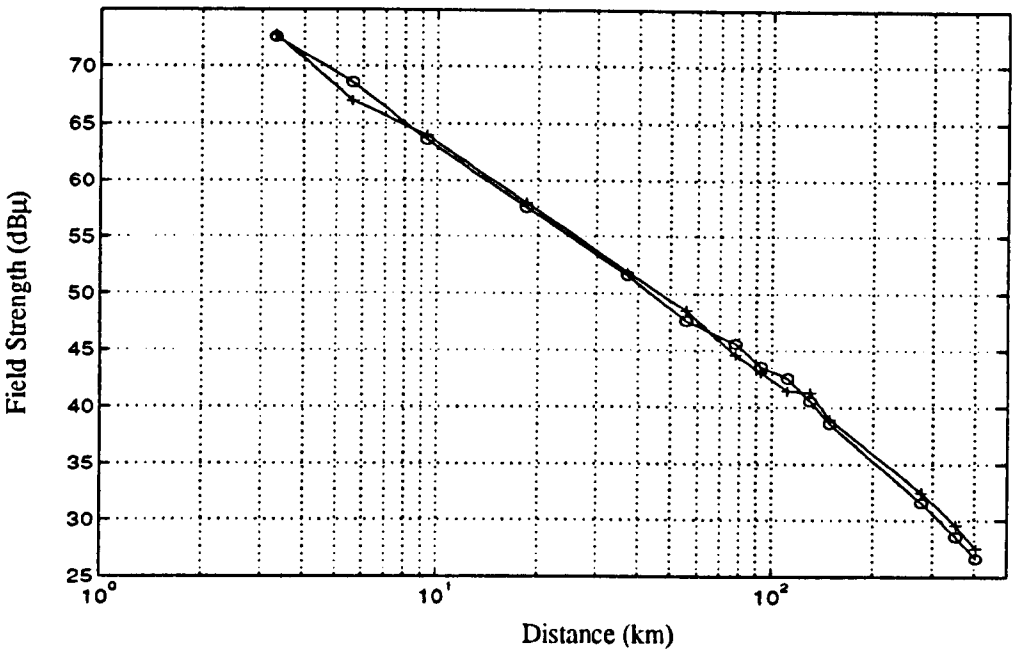

Figure 4.10: Comparison between predicted (o) and measured (+) field strengths over a sea-water from an experimental beacon in the Arabian Gulf, from [98].

have been fulfilled both by the candidate and by a company owned by the University called Industrial Development, Bangor (IDB). Appropriately modified versions of the model were supplied to IDB by the candidate, along with information on the databases required and recommendations on how to generate these databases when information is specific to a local area. The results of these predictions have been closely studied by IDB and the recipients, this scrutiny providing valuable, independent, verification of the model's implementation. An example of the coverage in each of the areas is included in Appendix C. Where not available in the public domain, permission has been obtained to reproduce these examples from confidential reports.

As a complement to the coverage predictions, high quality field measurements have also been made in locations around the world, contributing to the process of verifying the model. Fig. 4.10 shows a comparison made over a particularly wide spread of ranges in the Arabian Gulf, over sea-water paths. The plot compares the measured results with the model's predictions. The two sets of points show excellent agreement, regardless of the range from the beacon [98].

This close examination of the model's predictions by experts and comparison to in-

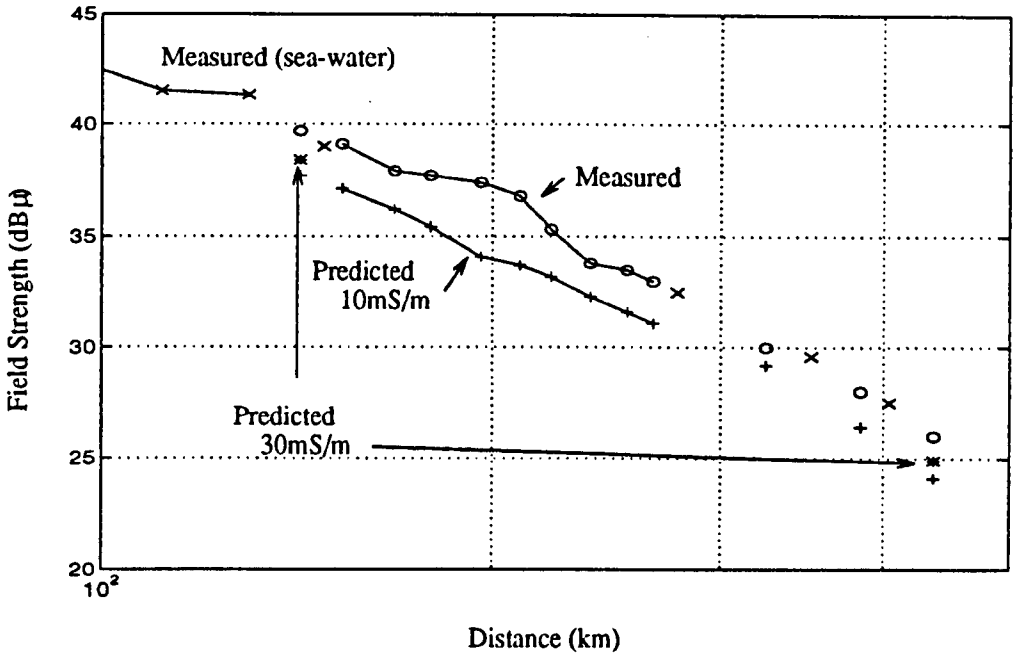

Figure 4.11: Comparison between predicted and measured field strengths from an experimental beacon in the Arabian Gulf. The predictions of the model were used to determine the conductivity of a peninsula over which the signal propagated, from [99].

dependent field strength measurements has built confidence in the validity of the model's results. In fact, Fig. 4.11 shows a measurement scenario that reflects this confidence [99]. In this case, the conductivity of a peninsula in the Arabian Gulf is not accurately known and the model has been used to determine the closest conductivity value. To do this, measurements were made of the beacon's field strength in the waters on the far side of the peninsula, recording the loss due to the land section. These measurements were then compared to the model's predictions, assuming in one case a ground conductivity of 10 mS/m for the peninsula and in the other 30 mS/m. From this comparison, it has been concluded that the ground conductivity of the peninsula is best represented by the 30 mS/m value.

4.7 Conclusions

The groundwave attenuation around a beacon is strongly dependent on the ground conductivity. A simple nominal range represents a beacon's coverage area poorly, neglecting the attenuating effects of islands and the variation in conductivity of different

types of land. To represent groundwave attenuation accurately, a coverage model needs access to a detailed conductivity database and to an algorithm that can work with propagation paths of mixed conductivity.

The data and methods recommended by the CCIR have been employed in the software implementation of a radiobeacon groundwave field strength prediction process. The Bangor Ground Conductivity Database supplies highly-detailed conductivity information, the importance of which has been highlighted in the examples. Novel methods of reducing the run-time, including the use of a maximum range, have been employed. Comparisons between predicted and measured data have been used to verify that the CCIR methods have been correctly implemented. These comparisons have shown very good agreement between measured and predicted groundwave field strengths over a range of distances, giving confidence in the foundation of the coverage prediction model.

Chapter 5

Skywave Propagation

The signal broadcast by a wanted DGPS radiobeacon can reach the user by groundwave or by skywave, that is, by ionospheric 'reflection' (actually, refraction). The navigational information transmitted is correction information, not timing or ranging signals, so that (unlike the signals of low-frequency navigation systems such as Loran-C or Decca Navigator) it is as valid when received via skywave as when received via groundwave. The pattern of attenuation of skywave signals around a beacon has very different characteristics from that of groundwave signals, being virtually independent of ground conductivity and varying with both the time of day and the season of the year. In practice, *skywave* is primarily experienced at night, when it can be of great significance for DGPS radiobeacon coverage. It is after dusk when, depending on the relative strengths of the groundwave and skywave, fading becomes possible.

This chapter identifies various methods of calculating the skywave field strength and selects one that is appropriate for radiobeacon systems. The different parameters determining the rate of attenuation of these signals will be detailed, including the effect of ground conductivity and the temporal variation. The implementation of the selected method in the model will be described. Field strength contour plots will be used to identify and emphasize the various parameters which control the attenuation of the skywave-propagated component of radiobeacon signals.

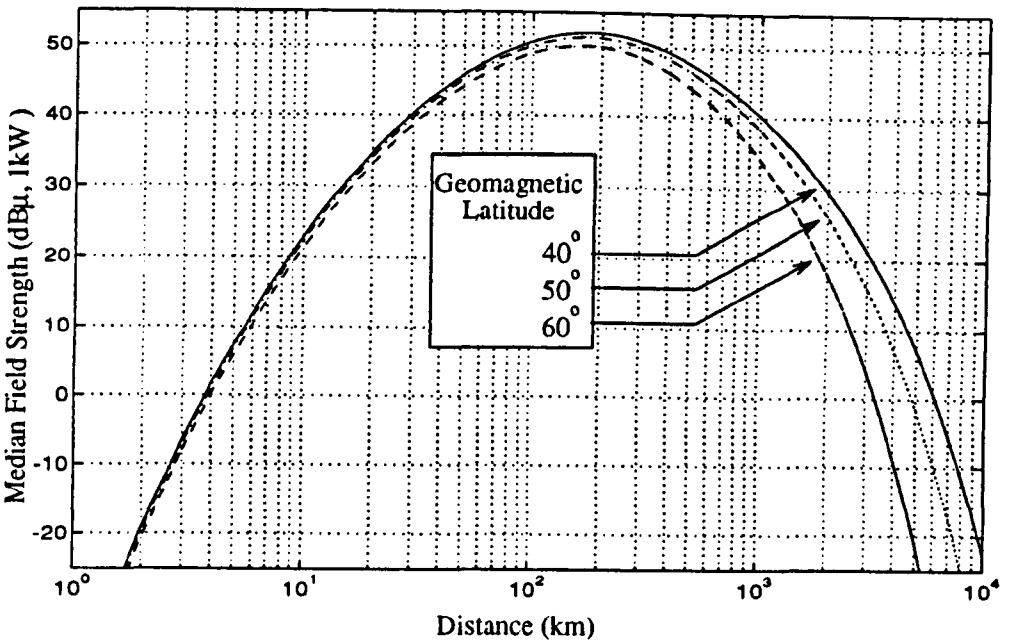

Figure 5.1: Median skywave field strength as function of distance for three different Geomagnetic Latitudes: 40°, 50°and 60°. The field strength close to the beacon is attenuated by the Antenna Gain factor.

5.1 Introduction

The skywave field strength of a 300 kHz signal at any point may be viewed as the combination of the signals arriving via multiple paths, but primarily reflected by the E-layer of the ionosphere. The effective height of this ionised layer depends on the level of solar activity and hence varies with time of day and season of the year. The lower effective height experienced during the day, together with the presence of the attenuating D-layer below the E-layer, greatly reduces the daytime skywave field strength compared to night-time values. Night-time skywave field strength in the 300 kHz band is strongest in the spring and autumn, with a pronounced minimum during the summer [77]. The DGPS model includes skywave as a night-time factor only. A typical 300 kHz beacon has the skywave field strength characteristics shown in Fig. 5.1. The strength is low near the beacon, increasing to a peak at a range of about 200 km, then falling off again relatively slowly with distance.

5.1.1 Candidate methods of calculation

CCIR Report 575-4 [78] discusses several different methods for calculating skywave levels in the LF and MF bands. These methods have been applied to the radiobeacon band, compared, and found to give quite similar results. This similarity can be seen in Fig. 5.2, where skywave field strength is plotted against distance. Note that the *Cairo* and the *USSR* curves are valid only for distances greater than 250 km.

The *Cairo* curve is the result of measurements made in the late 1930's on north-south paths on the American continent. Similar measurements in the former USSR form the basis of the *USSR* curve. This curve, dating from 1970, is calculated from an empirical formula derived from the statistical analysis of these measurements. The *Report 435-6* curve plots the results of a method of which details are presented in that CCIR document [77]. It is the result of further study and modifications to the *USSR* method. The *Region 2* curve is the result of a simplification to the *Report 435-6* method which takes into account a difference in the traditional reference hour, resulting in the $\approx$2.5 dB shift shown.

Of these methods, the *Report 435-6* method was selected for integration into the DGPS model, as it is applicable over the widest range of distances and in all regions of the world. Additionally, this calculation method includes several parameters which can be fine-tuned specifically for a DGPS radiobeacon scenario.

Another potential source of skywave field strength information is the Loran-C model discussed in Chapter 3, which includes curves based on measurements of the 100 kHz Loran-C and Decca Navigator systems. Fig. 5.3 compares these empirical curves with the 100 kHz curve given by the Report 435-6 method. While somewhat similar, the two curves differ enough that it would be better to replace this curve in the DGPS model with one for 300 kHz use based on Report 435-6.

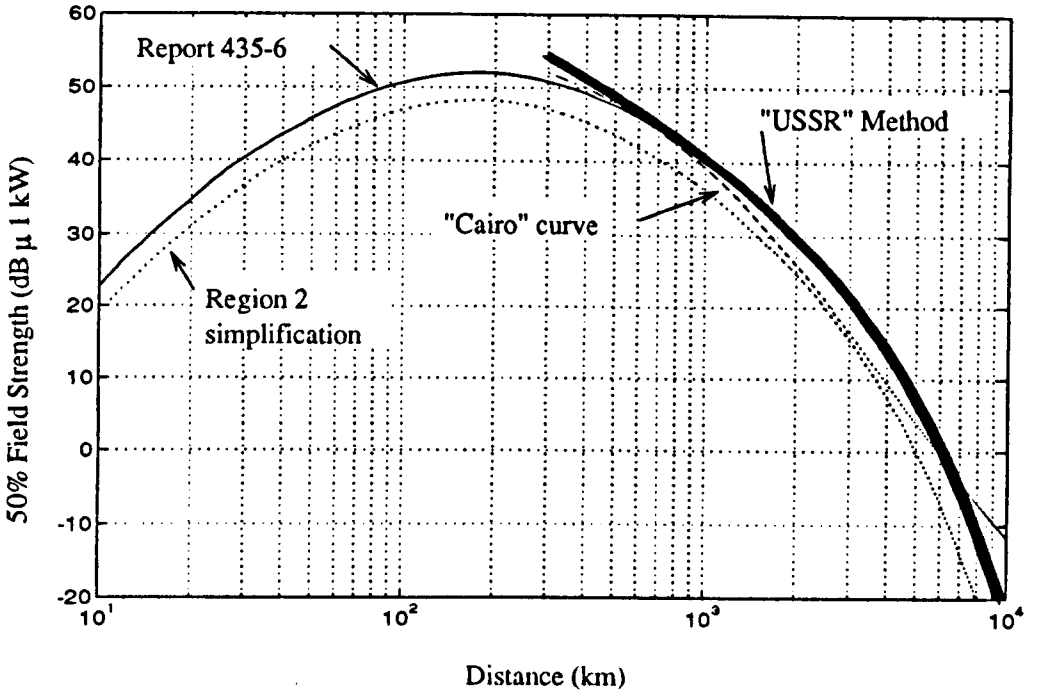

Figure 5.2: Comparison of four different skywave field strength calculation methods suggested by CCIR. The results given by the methods are plotted only over their regions of validity. It can be seen that all give similar results. *Report 435-6* is the method adopted for the DGPS model.

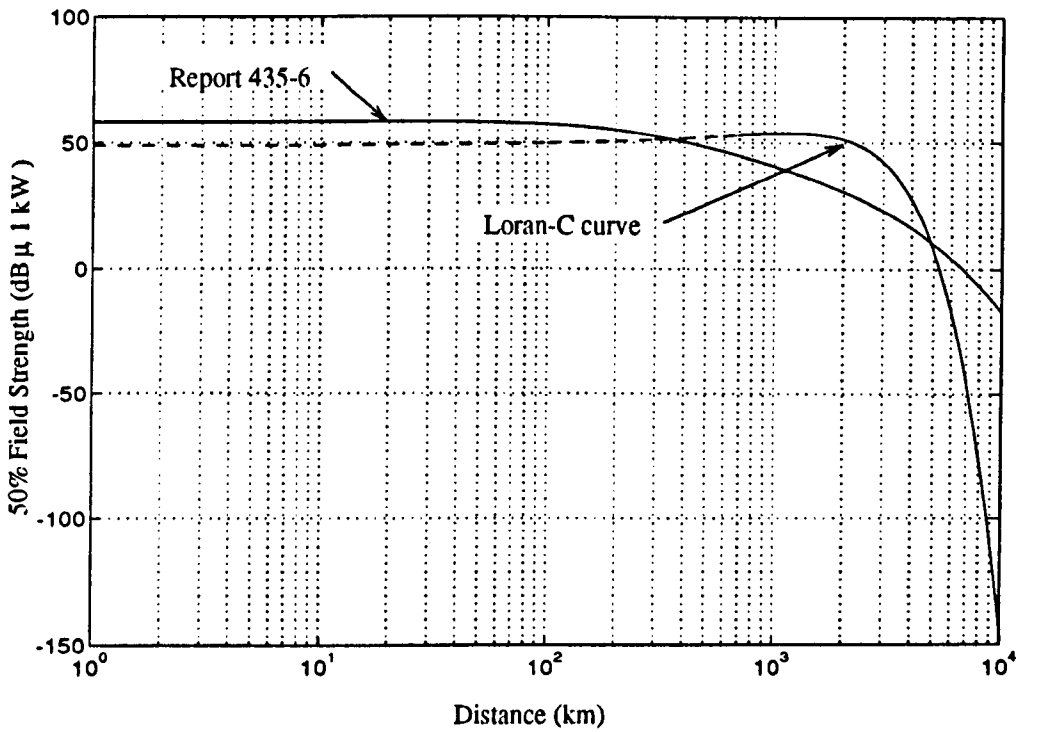

Figure 5.3: Comparison of the empirical skywave field strength curve employed in the Loran-C model and the method of CCIR Report 435-6. Both these curves apply to 100 kHz, Loran-C transmissions.

5.2 Skywave field strength

This section describes the application to DGPS radiobeacons of the information and techniques for calculating median values of annual average night skywave published in CCIR Report 435-6 [77]. This report is based on the extensive measurements of skywave-propagated signal levels described in [78].

In [77], the median field strength Sky_{dB} (dBμ) at any range d (km) is given by

$$Sky_{dB} = A - 20log\,p - 10^{-3}k\,p + G_S + G_V + \Delta_P \tag{5.1}$$

where:

Δ_P: a beacon power factor.
p: the slant-propagation distance in km,
k: the basic loss factor,
G_V: the antenna gain factor described in 5.2.1,
A: $106.6 - 2\sin\Phi$,
Φ: the geomagnetic latitude term described in 5.2.2,
G_S: the sea gain factor described in 5.2.3,

Equation 5.1 gives the skywave field strength for a beacon of 1 kW radiated power, or 950 km nominal range in radiobeacon convention. The range may be adjusted for beacons of different power (or nominal range) values by applying an appropriate beacon power factor, Δ_P dB. The magnitude of Δ_P for any given nominal range is determined using the groundwave propagation curve for sea-water paths, as described in 4.1.1.

The total path length, or *slant-propagation distance*, from the beacon to the receiver via the ionosphere depends on both the ionospheric height and the ground distance d. The calculation of slant-propagation distance is shown geometrically in Fig. 5.4. Using a typical E-Layer ionospheric height of 100 km, the slant-propagation distance is given by:

$$p = \sqrt{d^2 + 200^2}. \tag{5.2}$$

The *basic loss factor, k*, due to ionospheric absorption, is given by:

$$k = 3.2 + 0.19 f_{kHz}^{0.4} \tan^2[\Phi + 3] \tag{5.3}$$

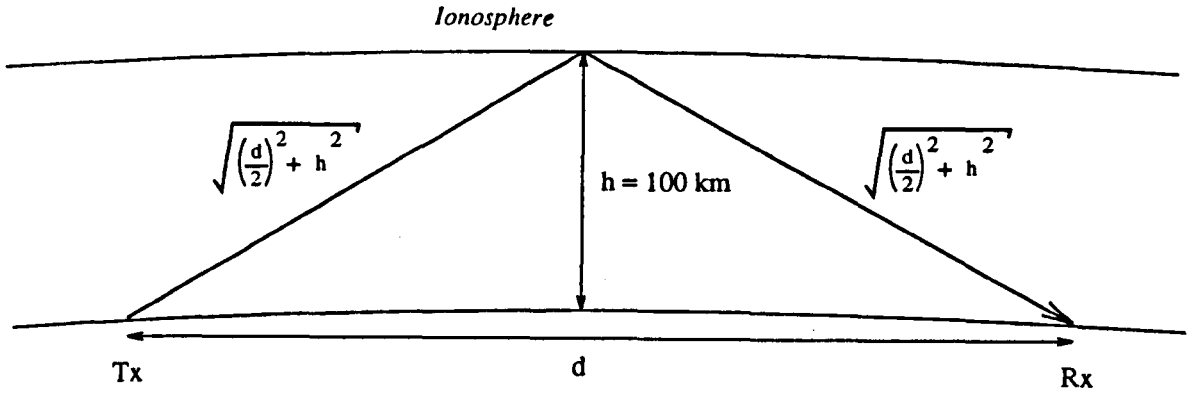

Figure 5.4: Calculation of the *slant-propagation distance,* given ionospheric height h and Great Circle path length d.

where f_{kHz} is the frequency in kHz.

5.2.1 Antenna Gain

The attenuation of skywave field strength at points close to the antenna due to the radiation pattern of the antenna is referred to conventionally (and misleadingly) as *antenna gain.* Radiobeacon antennas are omni-directional in the horizontal plane and this level of attenuation is dependent on the vertical polar diagram of the antenna. Both the beacon and the receiver antennas are assumed to be single monopoles, much shorter than a quarter wavelength (250 m). This is a reasonable assumption, as even the transmitting antennas are typically only 10 to 30 m in height. Receiver whip aerials vary in length from tens of centimetres to 2 m.

If a 300 kHz signal were to be transmitted vertically, it would be reflected back down toward the transmitter, with only the attenuation due to 200 km of free-space attenuation. The radiation pattern of a single monopole antenna imparts great attenuation to signals departing or arriving at vertical, or nearly-vertical, angles compared with low-angle signals. At distances of 2000 km or so, where the skywave is expected to be by single-hop reflection, departure angle is near-zero and the antenna gain near unity (0 dB) [78]. CCIR gives curves of antenna gain, *i.e.* signal attenuation, as a function of distance and antenna height (as a fraction of wavelength). For use by the DGPS model, the curve for antennas much shorter than a quarter wavelength was se-

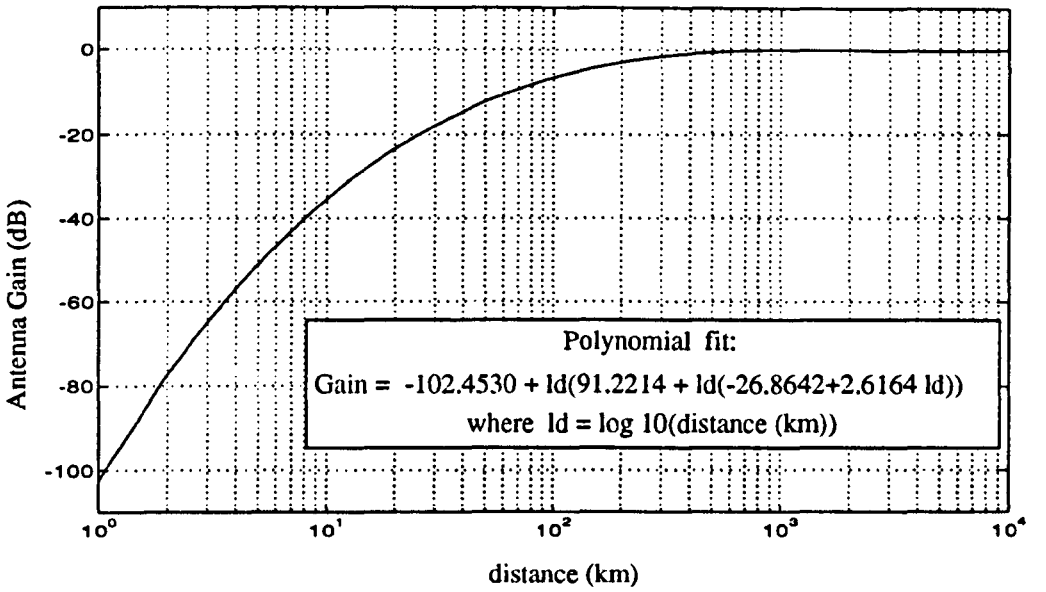

Figure 5.5: The effect of antenna gain on skywave-propagated signals as a function of the distance between the beacon and the receiver. The high level of attenuation close to the beacon is due to the vertical polar diagram of the antenna.

lected and a polynomial curve fitted to it. The result is shown in Fig. 5.5, this being a 3rd-order polynomial fit with the coefficients given. Attenuation due to antenna gain is seen to dominate the skywave field strength at points close to the beacon, but to have negligible effect beyond about 300 km.

5.2.2 Geomagnetic Latitude

Attenuation of the skywave field strength also depends on the geomagnetic latitude of the mid-point of the propagation path between the beacon and the receiver. Geomagnetic latitude is the latitude with respect to the geomagnetic poles, assuming an earth-centred dipole field model. The geomagnetic north pole is currently located at the geographic coordinates [78.5°N, 69°W] [91]. From [77], geomagnetic latitude may be related to geographical latitude by

$$\Phi = \arcsin(\sin\alpha \sin 78.5^\circ + \cos\alpha \cos 78.5^\circ \cos(-69^\circ + \beta)) \qquad (5.4)$$

where:

Φ: geomagnetic latitude,
α: geographic latitude,
β: geographic longitude.

This equation can be implemented directly in the model, such that it can itself compute the geomagnetic latitude of the mid-point of any propagation path. If Φ is greater than 60°or less than -60°, the limiting values 60°or -60°, respectively, should be employed and Equation 5.1 used with caution [77].

In the region of south Finland used in the examples which follow, centred on about [58° N, 25° E], the geomagnetic latitude is 65° N; that is, it is 7°greater than the geographic latitude.

5.2.3 Sea Gain

The original measurement campaign which formed the basis for equation 5.1 was carried out with the transmitting and the receiving aerials located on ground of average conductivity, 3-10 mS/m. Further measurements showed the skywave field strengths to be stronger when one or both of the aerials was located near the sea. To compensate for this, a *sea gain* correction term was incorporated into the method by CCIR [78].

Marine radiobeacons are normally located on coasts, or islands, and most of the points for which field strengths are to be computed are out to sea. Thus it is appropriate to include sea gain in the DGPS radiobeacon skywave field strength calculations. In doing so, the model employs the Bangor Ground Conductivity Database (see 4.2.1) to check for the presence of sea-water within 5 km (see below) of either the beacon or the calculation point, along the propagation path. Sea gain is calculated separately for each end of the path.

Basic sea gain, if there is no land between a point and the sea, is given by a curve against distance in [77]. To incorporate this information into the model, a polynomial curve was fitted: a 5th-order fit was required because of the complexity of the curve. The first 2500 km of this polynomial curve is plotted in Fig. 5.6. Although never a dominant factor, at a range of 1000 km and with both antennas on the sea, there is a correction of 1.5 dB at each end, or 3 dB total. Neglecting sea gain would introduce an avoidable error into the prediction process.

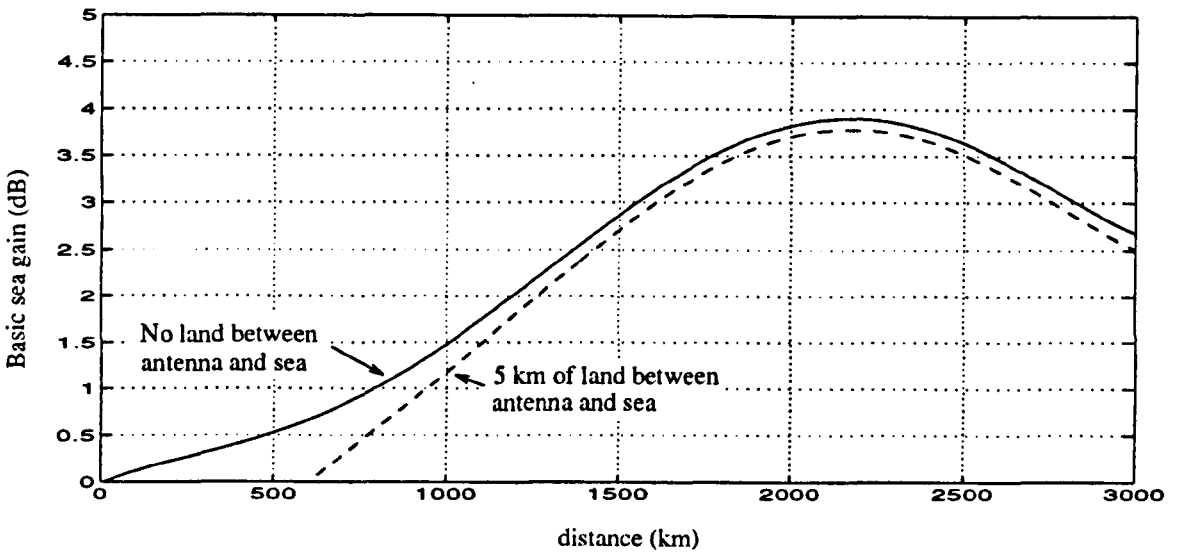

Figure 5.6: Basic sea gain as a function of Great Circle path distance between beacon and receiver. This gives the extra skywave strength if there is no land between either antenna and the sea. The curve of sea gain when there is 5 km of land between the antenna and the sea is also included, as indicated. Sea gain is computed separately for the beacon and receiver antennas.

The basic sea gain must be reduced where there is any land between the antenna and the sea. Also sea channels or islands close to either end of the path must be identified [77]. The 'close range' around the antenna within which the ground conductivity affects the skywave strength depends on the separation between beacon and receiver. Curves showing this relationship are also included in [77]; the 'close range' never exceeds the 200 km it reaches with 2000 km of path length. Fig. 5.6 also includes a curve showing the sea gain when the antenna is located 5 km from the sea. This is the limiting case for DGPS radiobeacons since 5 km is the 'close range' corresponding to the maximum radiobeacon range of 550 km over which field strengths are computed.

5.3 Temporal variation of skywave field strength

Unlike groundwave, the received skywave field strength at a point is not always the same. It is best described by a statistical distribution [76, 77, 81, 100]. Within any given time period, the upper decile, or 90th percentile, has been found experimentally to be 6.5 dB above median [77]; that is, 90% of the time the skywave field strength

will be below the median-plus-6.5 dB level.

In order to predict the statistics of fading and thus the percentages of time that signals can be received, it is necessary for the model to be able to predict the skywave field strength for different percentiles. To do this, it is necessary to fit some form of statistical distribution to the only two points, the 50th and 90th percentiles, at which CCIR have computed skywave levels from their measured data. Given this limited information, and the fact that skywave strength is a combination of many signals with similar distributions, it would appear appropriate to apply the Central Limit Theorem [101, 102]. This important theorem in probability theory states that when an infinite number of independent random variables (read 'skywaves' here) with the same probability distribution are combined, the result looks Gaussian. When combining a finite number of skywaves, the accuracy of this approximation will depend on the nature of the individual skywave probability distributions, but given the limited data published by CCIR, a Gaussian distribution appears to be the most appropriate. The 'Gaussian' column of Table 5.1 lists the resulting adjustments for different percentiles based on a Gaussian distribution fitted to the 50% and 90% points.

In calculations of the temporal variation of skywave by some authors, a Rayleigh curve is used to describe the probability distribution [66, 78]. A Rayleigh distribution results from the addition of a constant signal to one with a Gaussian distribution. It is completely described by just a single parameter. Thus, once the median skywave has been calculated, all other percentiles are known: the 90% is always 1.8 times the median (+5.1 dB) [91]. This 90th%-ile value is different from the +6.5 dB measured by CCIR and so it was concluded that a Rayleigh distribution did not give the best fit to the CCIR data. The 'Rayleigh' column of Table 5.1 shows the change in field strength (in dB) between the median (50%) and other percentiles given a Rayleigh distribution. The difference between the Gaussian and Rayleigh distributions at the 90% point is only 1.3 dB. It becomes more pronounced, however, as the percentile increases, reaching 7.7 dB at the 99.99% point. At the lower percentiles there is more discrepancy, 6.6 dB at the 1% point.

Percentile	dB above median		Gaussian-Rayleigh difference (dB)
	Gaussian	Rayleigh	
1%	-11.9	-18.5	6.6
5%	-8.5	-11.6	3.2
10%	-6.5	-8.18	1.7
50%	0	0	0
90%	6.5	5.2	1.3
95%	8.5	6.4	2.1
99%	11.9	8.2	3.7
99.99%	18.9	11.3	7.7

Table 5.1: Comparison between the Gaussian and Rayleigh dB shifts between median and other percentiles. The Gaussian 90% and 10% values are set to median±6.5 dB, respectively. As can be seen, the difference between the two distributions increases as the percentile moves away from median, with the greatest differences for values below the median.

Throughout this thesis, the term *wanted signals* refers to the groundwave or skywave signal propagating from the DGPS radiobeacon. *Unwanted signals* refers to both the groundwave and skywave signals coming from any other beacon. A clear distinction needs to be made as to what the percentile means when considering a wanted signal level as opposed to an unwanted signal level. A *percentile* gives the percentage of the time a signal will be *below* a certain level. In using the model, we are interested in knowing the percentage of time the wanted skywave signal will *exceed* a certain limit. The 90th-percentile gives the level of wanted skywave available only 10% of the time. Hence, the level of wanted skywave signal encountered at least 90% of the time is median-minus-6.5 dB.

Conversely, when considering unwanted signals from other beacons which are potential interferers, we are interested in the percentage of time the unwanted signal is guaranteed *not to exceed* a certain limit: the level of unwanted signal not exceeded 90% of the time is median-plus-6.5 dB.

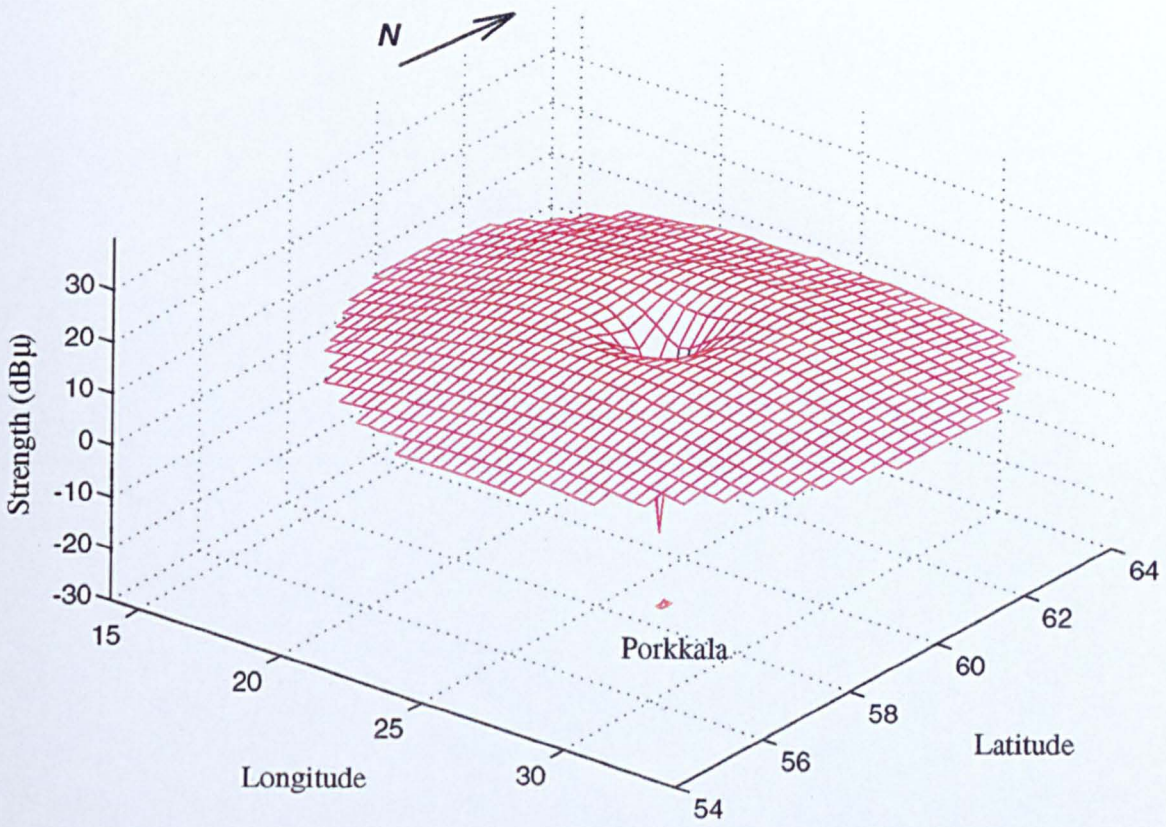

Figure 5.7: A 3-d contour plot of skywave field strength around the Porkkala beacon. The attenuation due to the antenna gain factor can be seen as a hole over the beacon. Sea gain causes the signal to be slightly stronger over the Baltic Sea to the east than over Finland to the north. The location of Porkkala is marked.

5.4 Skywave contouring

The curve-fitted polynomials corresponding to Figs. 5.5 and 5.6 and Equations 5.1, 5.2, 5.3 and 5.4 have been incorporated into the DGPS model, allowing skywave field strength values to be calculated at points throughout the array centred on each beacon (see Chapter 4). Fig. 5.7 shows a 3-d contour of the median skywave field strength around Porkkala. The x and y axes are longitude and latitude, respectively, and height is field strength. The plot is, of course, dramatically different from that of groundwave, with a nearly-uniform strength over most of the torus-shaped distribution. The steep drop in the centre, above the beacon, is due to the antenna gain factor. Much less obvious is the sea gain effect, which results in slightly higher signal levels over the Baltic Sea to the east compared to those over Finland to the north.

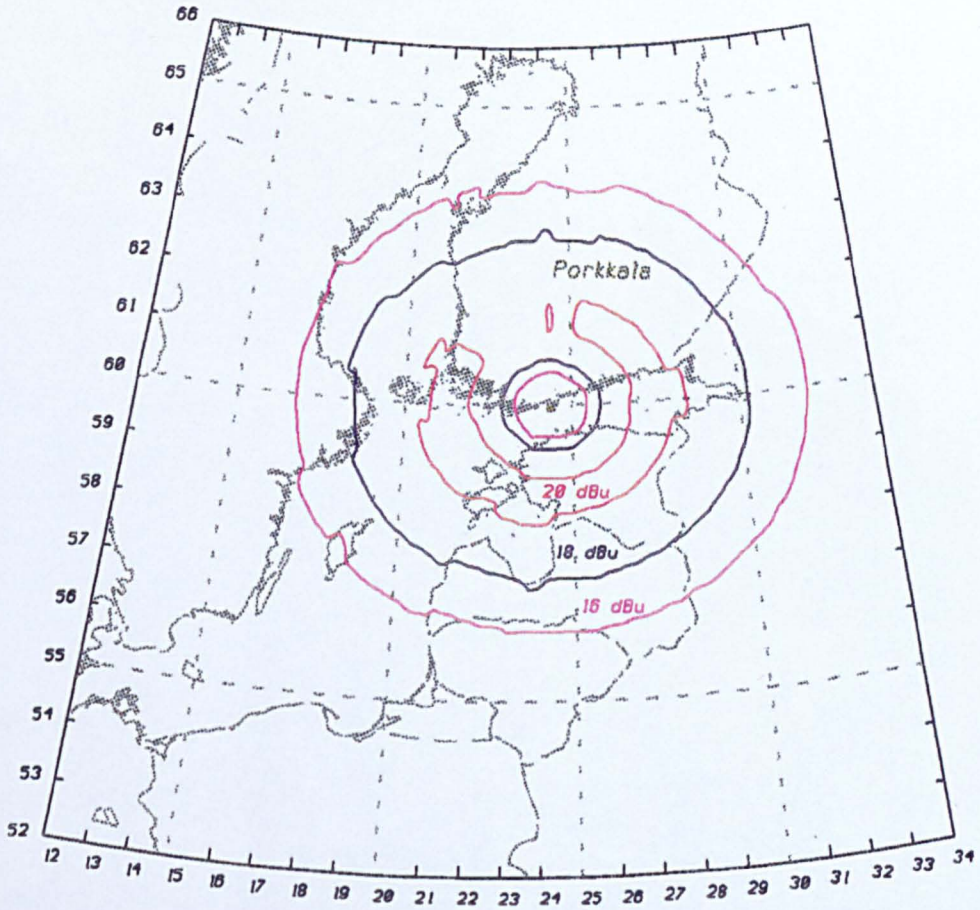

Figure 5.8: Contours of median skywave signal strength around the Porkkala DGPS beacon, nominal range 160 km. Field strength is virtually independent of ground conductivity: it is almost as strong over low conductivity ground as over the sea-water to the east. Points immediately around the beacon experience very low skywave signals because of the antenna's vertical radiation pattern.

Fig. 5.8 shows the median skywave field strength around the Porkkala beacon in the form of contours generated by the model. These, again, are greatly different from the contours of the groundwave signals shown in the previous chapter. The skywave contour has a torus shape; field strengths immediately around the beacon are too low to appear on the minimum, 16 dBμ, contour. The outer limit is principally dependent on distance and, of course, independent of ground conductivity, except that sea gain increases the range slightly on the over-water paths.

5.5 Verification

As with the calculation of groundwave attenuation, the CCIR methods employed are based on large volumes of measured data collected in various regions over several years. Verification of values predicted by the model cannot seek to repeat the CCIR work, but must be concentrated on establishing that the data and methods have been correctly implemented.

As part of this work a discussion was held with Dr. N. Ward of the GLAs as to how this verification might be carried out. As a result, an 'auditing' approach was adopted; the curves of skywave field strength which included the antenna gain factor and various values of geomagnetic latitude, were submitted to the GLAs without their source or the method used to evaluate them being discussed. These curves were cross-checked against values the GLAs derived working quite independently. Subsequent comparison of results and discussion showed that the curves were correct, although they initially disclosed that the $\pm 60°$limits to geomagnetic latitude had inadvertently been omitted from the model. This bound was then added into the model.

Measurement of skywave field strength is complicated by the statistical nature of the skywave signal and the continual presence of the groundwave signal. It is, of course, the combination of the two which the DGPS receiver experiences and the separate components are difficult to isolate. The nature of this combined signal forms the basis of the next chapter.

5.6 Conclusions

The attenuation of the skywave signal around a beacon is very different from that of the groundwave signal. There is less dependence on ground conductivity, only the land or sea within a few kilometres around the transmitting and receiving antenna having any significant effect. Skywaves are primarily a factor at night, during which time the signals propagate over long ranges with relatively uniform strengths. At points close

to the beacon the skywave is strongly attenuated due to the beacon's antenna gain in the vertical plane.

Several different methods of calculating skywave attenuation have been studied and considered for application to DGPS radiobeacon coverage prediction. The parameters of the method adopted and their implementation in the DGPS model have been discussed in depth. The resulting contour plots show skywave contours to have a characteristic torus-shape. The temporal variations of the skywave signal have been modelled as a Gaussian distribution rather than the more conventional Rayleigh; the model allows different signal availabilities to be calculated.

Over ground of low conductivity, skywave field strength falls off significantly more slowly than groundwave as the separation from the beacon increases. The levels of night-time skywave field strength in some locations around a beacon are comparable to the groundwave field strengths. This fact will be of great importance in the next chapter, which deals with the combination of groundwave and skywave signals, since it shows that deep fading of the combined signal is possible.

Chapter 6

Own-Skywave Interference: Fading

A DGPS radiobeacon operates as an aid to navigation by broadcasting correction data, not by providing timing information as do conventional navigation systems, including Loran-C and GPS. So DGPS radiobeacon coverage prediction is concerned with the receiver's ability to acquire the data, regardless of the propagation mode by which it arrives: correction data is just as valid whether it reaches the receiver via skywave paths as via groundwave - or both.

Previous coverage prediction analyses have invariably assumed that the radiobeacon signal reached the receiver by groundwave propagation alone. The foregoing chapter, however, has shown skywave from wanted beacons, *own-skywave,* to be present with significant levels at night. The question this raises is whether this skywave will cause fading of the received signal due to cancellation of the groundwave signal by skywave-propagated components.

This chapter will review existing methods of determining the effect of own-skywave interference on total field strength. The limitations of these methods, which make them unsuitable for application to DGPS coverage prediction, will be explained. A new method for calculating the effect of own-skywave interference will be presented. The implementation of this new method into the DGPS model will be described and coverage examples used to demonstrate the very significant effect of own-skywave interference on DGPS radiobeacon coverage.

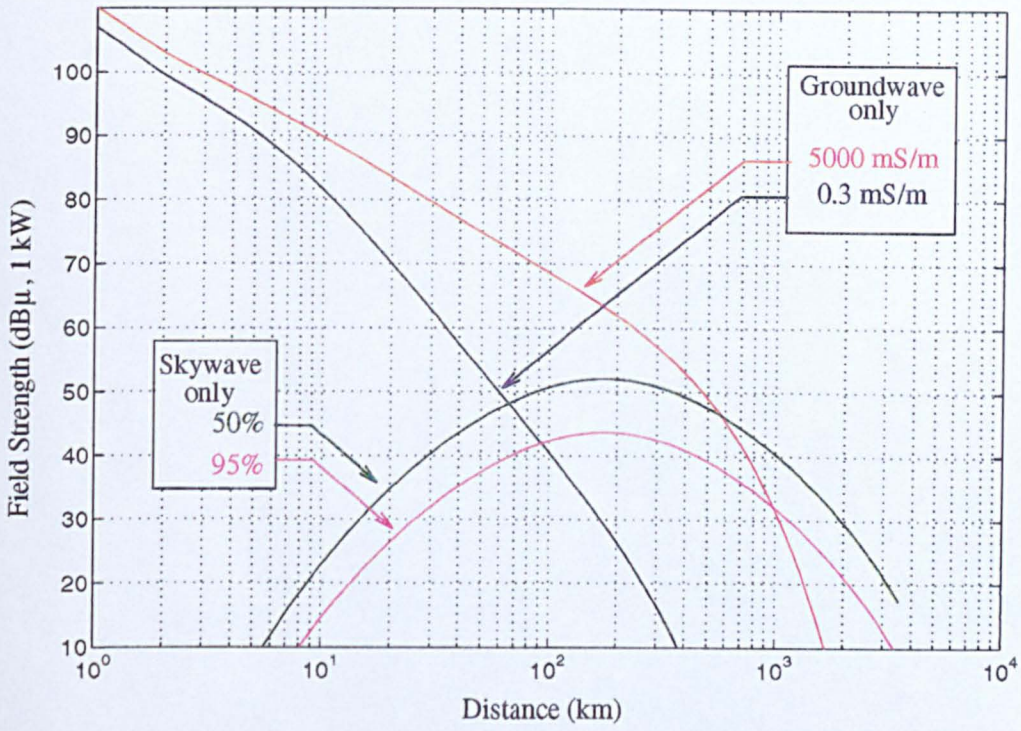

Figure 6.1: Curves of groundwave and 50% skywave field strength against distance. The distance at which the two become commensurate depends on the ground conductivity of the propagation path, but ranges here from 45 km to 550 km

6.1 Combining groundwave and skywave

From the discussions in Chapters 4 and 5 it can be argued that, close to the radiobeacon, the groundwave signal dominates the skywave signal. As the distance from the beacon increases, the groundwave signal falls, the skywave signal increases and there is a zone (the *fading zone*) where the two become comparable in amplitude. At still greater ranges, the groundwave will disappear below the noise and any coverage will depend solely on whether there is a usable skywave component. The area of greatest complexity is the fading zone, where signals of similar strength reach the receiver via the two modes of propagation. Fig. 6.1 shows that the groundwave and skywave strengths are comparable at distances from about 45 km to about 550 km, the extent of this zone depending on the ground type.

6.1.1 The effect of skywave delay

Because the sky path is longer than the ground path, the DGPS correction information arrives slightly later via skywave. *Skywave delay* relative to the groundwave is dependent on the range from the beacon, but is of the order of tens or hundreds of microseconds, an order of delay which results in serious coverage limitations for LF systems such as Loran-C and Decca [76, 75]. For DGPS beacons, the delay may be calculated using the Great Circle path distance (d) and the CCIR equation for slant-propagation distance (p), Equation 5.2, yielding:

$$\Delta_{path} = p - d, \tag{6.1}$$

$$\Delta_{path} = \sqrt{d^2 + 2 * h^2} - d, \tag{6.2}$$

$$\Delta_{time} = \Delta_{path}/c, \tag{6.3}$$

where Δ_{path} and Δ_{time} are the differences in path length and propagation time via the two modes and c is the speed of light. The result of Equation 6.3 is plotted against distance in Fig. 6.2, with the approximate boundaries of the groundwave-dominant, skywave-dominant and fade zones marked out. In the fade zone the skywave delay is calculated to be 0.03 to 0.24 ms. Standard DGPS radiobeacon broadcasts employ bit rates of 100 or 200 bps, with bit times of 10 or 5 ms. Hence, skywave delay is only a fraction of the duration of a bit and we conclude that the received signal is a mix of skywave and groundwave data streams in which bit transitions are approximately aligned. For an MSK broadcast, this means combining two sine wave signals of the same frequency, with transitions between frequencies occurring at the same time. Thus it is concluded that skywave delay should cause no significant inter-symbol interference to the data. However, the difference in path lengths and the reflection at the ionosphere result in significant phase differences at the carrier frequency (one cycle is approximately 0.003 ms) and the possibility of fading.

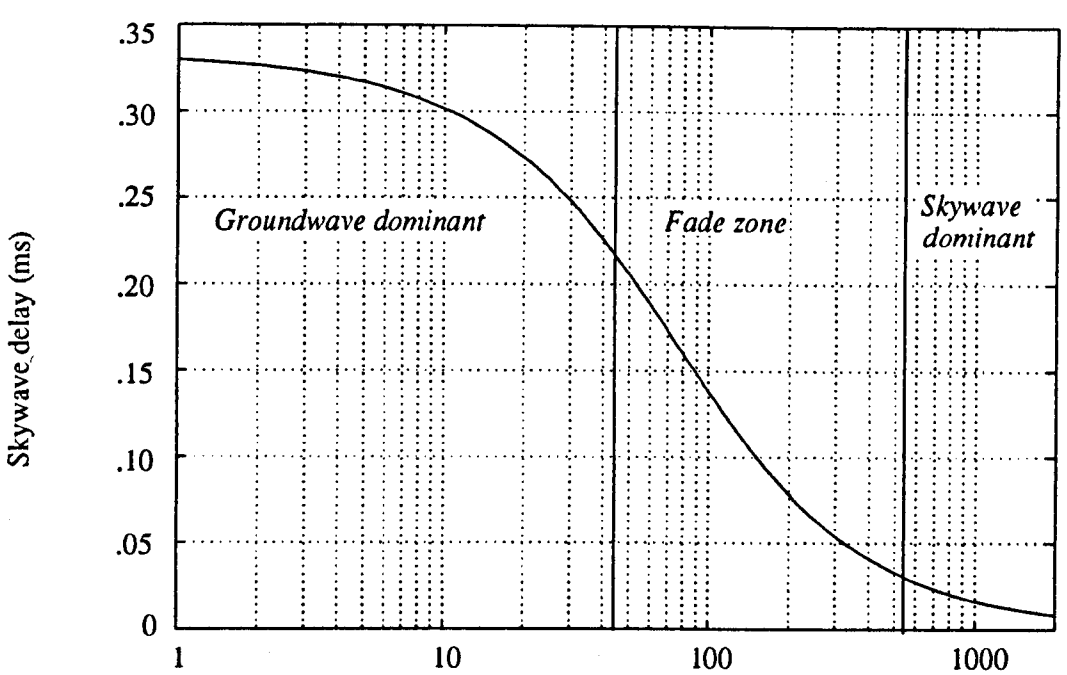

Figure 6.2: Skywave delay, relative to groundwave, as a function of distance from the beacon. Inside the *fade zone*, skywave delay is 0.03–0.22 ms which is only a fraction of a bit time at 100 or 200 bps.

6.2 Calculating fading

The model has access to separate arrays of groundwave and skywave field strengths. A method that could combine the information from these two arrays and come up with a total field strength would be one way of including an own-skywave factor into the DGPS model. Fig. 6.3(a) illustrates the problem of estimating the strength of the beacon's signal in the fade zone. *Total* is the vector sum of the groundwave *Gnd* and skywave *Sky* components, which can be written as

$$Total = Gnd + Sky\, e^{j\theta}. \tag{6.4}$$

The groundwave field strength at any point is constant and can be estimated by the method of Chapter 4. The median field strength of the skywave component may be calculated as in Chapter 5, with its short-term statistical distribution in time taken

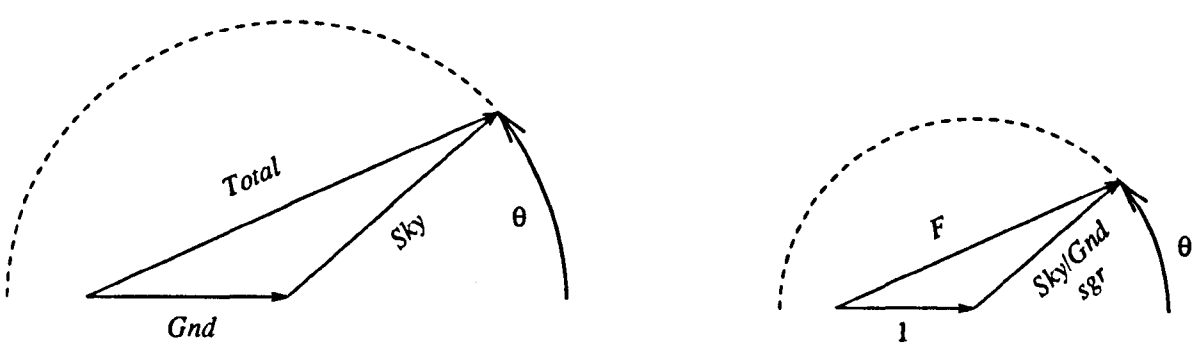

Figure 6.3: Vector representation of the calculation of the *Total* field strength, a combination of the groundwave and skywave components. This calculation needs to be applied when the two are of comparable strength.

to be Gaussian. The phase, θ, of the skywave relative to that of the groundwave is uniformly random within the range $0 \leq \theta \leq \pi$ and independent of field strength [80, 77].

The analysis may be simplified by dividing through by *Gnd,* resulting in a constant unit (groundwave) vector, a log-normally distributed *Sky/Gnd* or *sgr* vector and a fade vector F, where

$$F = 1 + sgr\ e^{j\theta}. \tag{6.5}$$

This normalisation is illustrated in Fig. 6.3(b).

The result of the analysis should be the statistical variation of $|F|_{dB}$, the logarithmic magnitude of F, as a function of $\overline{SGR}$, the median *Sky*-to-*Gnd* Ratio in dB. The distribution function $P_F(f)$ may also be derived for a given *sgr,* where

$$P_F(f) = Pr(|F| < f). \tag{6.6}$$

Note that f is fading depth, not frequency.

6.2.1 Nakagami-Rice Distribution

One existing method of analysing fading of this type is given in CCIR Report 266-5, 'Ionospheric Propagation Characteristics Pertinent to Terrestrial Radio-Communication Systems Design (Fading)' [80]. This method assumes that before they are combined,

the signal is composed of a constant groundwave component and a random Rayleigh-distributed skywave amplitude component, with uniform phase distribution. These assumptions result in the fading described by a *Nakagami-Rice* distribution. To determine whether this method correctly predicts the own-skywave effect, it first had to be adapted to the DGPS radiobeacon situation.

Following [80], the signal amplitude distribution $P(v_0)$ gives the probability of finding signal amplitude v, greater than v_0:

$$P(v_0) = \int_{v_0}^{\infty} p(v)dv, \tag{6.7}$$

with $p(v)$ given by:

$$p(v) = (2v/v_n^2)\exp(-(v_l^2 + v^2)/v^2)/v_n^2)I_0(2v_l v/v_n^2) \tag{6.8}$$

where:

$I_0(x)$: a modified Bessel function of zero order,
v: the received signal envelope voltage/$\sqrt{2}$,
v_l: the rms voltage of the groundwave component, *Gnd*
v_n: the rms value of the median skywave component, *Sky*.

For a given *Gnd* strength and median *Sky* strength, Equations 6.7 and 6.8 yield the probabilities of receiving various *Total* strengths. Fig. 6.4 plots 'Percentage of Time' against $|F|_{dB}$, the total signal level normalised with respect to the groundwave strength, for an $\overline{SGR}$ of 0 dB, that is $Gnd = Sky$. Four percentiles are marked with '*'s; the 50%, 90%, 95% and 99%. 50% corresponds to an $|F|_{dB}$ of 3 dB, meaning 50% of the time the level of signal can be guaranteed to be 3 dB stronger than *Gnd* alone. Similarly, 90% corresponds to an $|F|_{dB}$ of -5.3 dB, meaning that the signal strength that can be guaranteed 90% of the time is 5.3 dB weaker than *Gnd* alone. Percentiles of 95% and 99% correspond to $|F|_{dB}$s of -8.4 dB and -15.4 dB, respectively, the level of signal that can be guaranteed becoming weaker as the percentage of time increases.

Fig. 6.5 plots $|F|_{dB}$ against $\overline{SGR}$ for the 50%, 90% and 99%-iles. This figure has been constructed by generating a $P(v_0)$ for each $\overline{SGR}$, to find the values of $|F|_{dB}$ corresponding to the different percentiles graphed. A large negative $\overline{SGR}$ corresponds to the groundwave being much greater than the skywave, close to the station. The

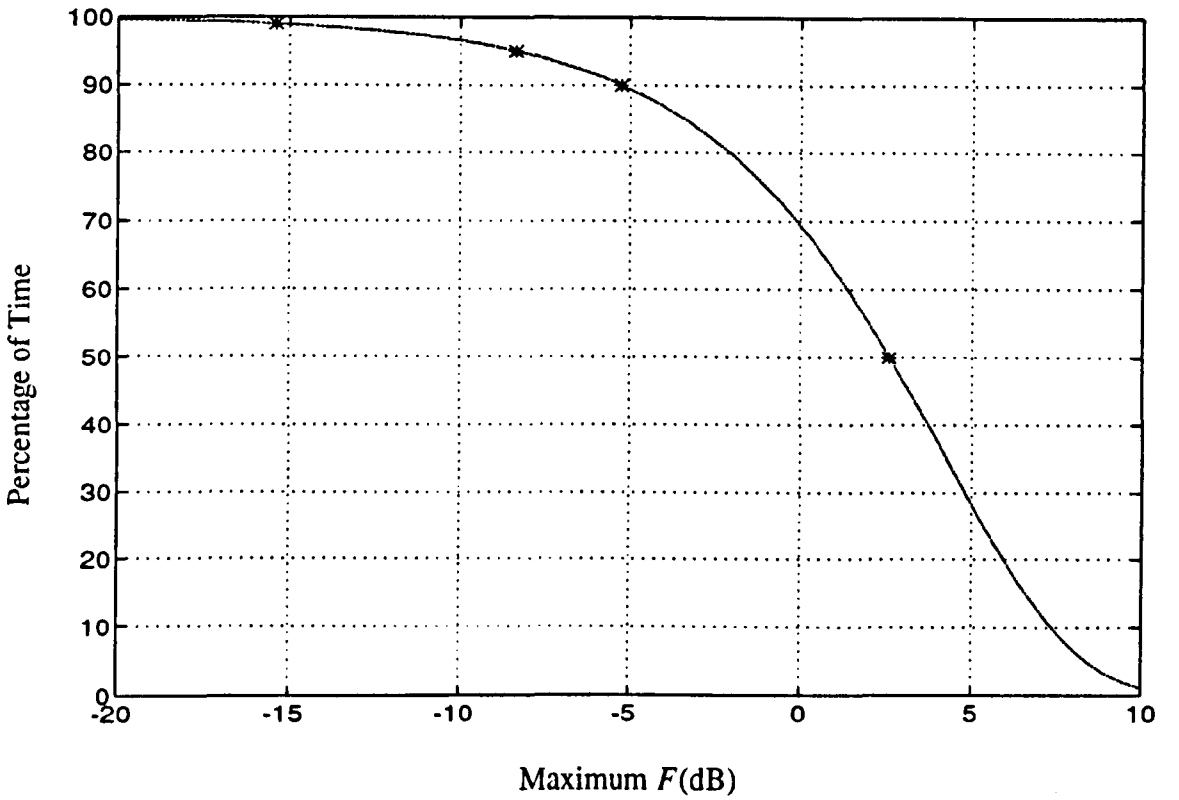

Figure 6.4: $|F|_{dB}$ against percentiles for an $\overline{SGR}$ of 0 dB, from the Nakagami-Rice distribution; '*'s mark the 50th, 90th, 95th and 99th percentiles. The higher the percentile, the more negative $|F|_{dB}$ and the deeper the fade. The 0 dB point represents no fading, negative values are fading, positive values *skywave recovery*

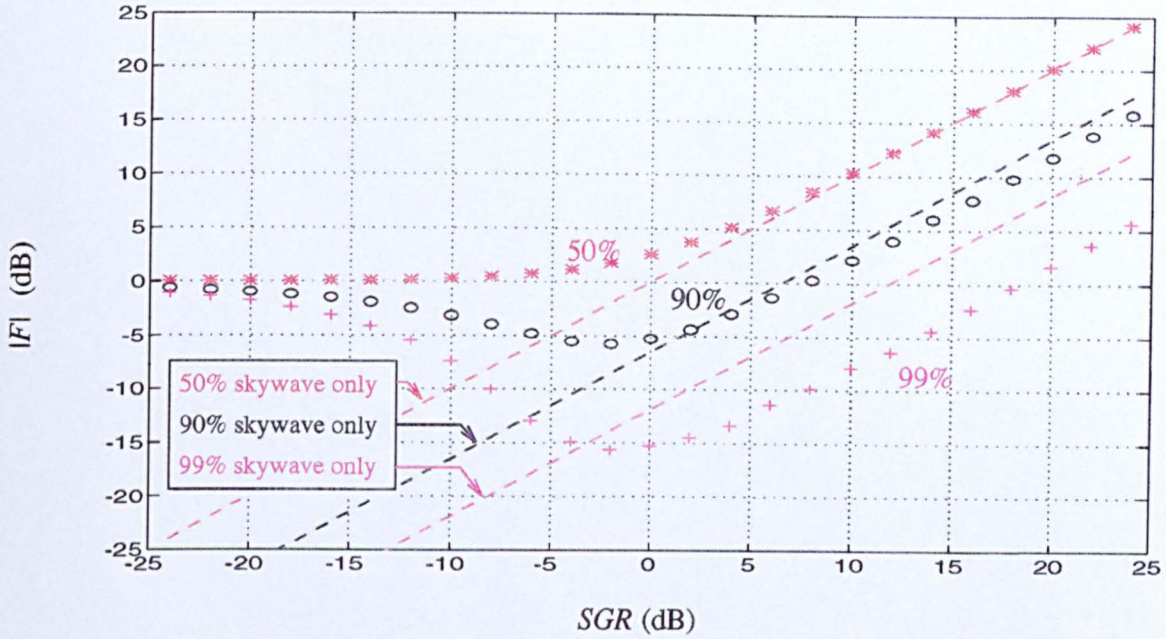

Figure 6.5: The total field strength with respect to the groundwave signal, $|F|_{dB}$, as a function of the skywave-to-groundwave ratio, $\overline{SGR}$, from the Nakagami-Rice distribution for the 50%, 90% and 99%-iles. There is a discrepancy between the 90% and 99% curves and their skywave-only asymptotes, due to the assumption of a Rayleigh distribution in the Nakagami-Rice analysis.

resulting values of $|F|_{dB}$ are close to zero, indicating little or no fading. The fade zone occurs in the region around zero $\overline{SGR}$ where the skywave and groundwave are of equal magnitude and the deepest fading occurs. Fig. 6.5 shows fading of less than 15 dB 99% of the time, for example.

A large positive $\overline{SGR}$ represents a skywave much greater than the groundwave. It would be expected here that all three curves would asymptote to their respective skywave-only availability levels, as determined from CCIR Report 435-6 [77]. This is true for the 50% median value since the Rayleigh distribution has been based on this median value. The 90% and 99% curves, in contrast, do not asymptote to their skywave-only levels. This is due to the Nakagami-Rice assumption that the skywave is Rayleigh distributed. As was noted in Chapter 5, the Rayleigh distribution does not provide as good a fit to the upper decile value given in [77] as a Gaussian distribution. In fact, while the Gaussian 90% availability can be set to median-minus-6.5 dB, the Rayleigh is fixed at median-minus-8.2 dB; this 1.7 dB difference is seen in the 90% asymptote. As the percentile increases, so does the discrepancy between the Gaussian skywave-only

and Nakagami-Rice asymptotes.

In conclusion, the Nakagami-Rice distribution provides reasonable fade values, that is little or no fading, for groundwave-dominant regions. Its assumption of a Rayleigh-distributed skywave component introduces a fixed error in the skywave-dominant regions, when compared to the skywave-only values from CCIR Report 435-6. The magnitude of this fixed error depends on the percentile. It is expected, therefore, that the predicted field strengths in the fading zone are accurate for percentiles around median, but become less so as the percentile is increased. Coverage prediction work and system planning employ specifications of signal availability at such percentiles, so getting the result right for these percentiles is important.

6.2.2 Enge-Olsen Method

Enge and Olsen [81] have published an analysis of this problem assuming a double-sided Gaussian distribution of skywave amplitude. Their method has been studied to see if it provides better results than the Nakagami-Rice in the skywave-dominant region. The equations in this section come from [81], but let us unravel these to look at their physical significance and the assumptions being made by Enge and Olsen.

Following [81], the analysis begins, not with Equation 6.4, but with

$$Total = Gnd + Sky\ cos\theta \tag{6.9}$$

where an important (and very restrictive) implicit assumption has been made that the groundwave is the dominant component. That is, by using $cos\theta$, Equation 6.9 deals only the component of the skywave which is in-phase with the groundwave. As was done in Equation 6.5, the next step in [81] is the normalisation of this equation with respect to *Gnd*, which yields the total field strength relative to the groundwave field strength:

$$F = 1 + sgr\ cos\theta \tag{6.10}$$

The Enge-Olsen distribution function of $|F|$ is given as

$$P_F(f) = \int_D \int p_{sgr,\theta}(sgr, \theta)\, dsgr\, d\theta \tag{6.11}$$

where D is the region where $|1 + sgr\, cos\theta| \leq f$. This region includes all possible results from combining *Gnd* and *Sky* (normalised), and comes from Equation 6.10. Applying the assumption that the skywave amplitude and the phase of the skywave relative to the groundwave are independent allows simplification of Equation 6.11. If $f < 1$, we get the probability of the total being less than the groundwave (*i.e.* fading) for a given skywave-to-groundwave ratio:

$$P_{|F|_{dB}}(f) = \frac{1}{\pi} \int_{\pi/2}^{\pi} P_{SGR}\left(20log_10\left(\frac{1+f}{-cos\theta}\right)\right) - P_{SGR}\left(20log_10\left(\frac{1-f}{-cos\theta}\right)\right) d\theta. \tag{6.12}$$

If $f > 1$, then we get the probability that the total is greater than the groundwave (*i.e.* skywave-recovery) again for a given SGR:

$$P_{|F|_{dB}}(f) = \frac{1}{\pi} + \int_0^{\pi/2} P_{SGR}\left(20log_10\left(\frac{f-1}{cos\theta}\right)\right) d\theta - \frac{1}{\pi} \int_{\pi/2}^{\pi} P_{SGR}\left(20log_10\left(\frac{f+1}{-cos\theta}\right)\right) d\theta. \tag{6.13}$$

Enge and Olsen assume a Gaussian distribution of skywave amplitude and so show that the distribution of the SGR is also Gaussian:

$$P_{SGR}(x) = 1 - Q\left(\frac{x - \overline{SGR}}{\sigma}\right) \tag{6.14}$$

where the value of σ can take one of two values; σ_l for $x \leq \overline{SGR}$, otherwise σ_u. $Q(x)$ is unity minus the Gaussian distribution function, that is, along the tails of the Gaussian distribution:

$$Q(x) = \frac{1}{\sqrt{2\pi}} \int_x^{\infty} exp(-y^2/2)\, dy. \tag{6.15}$$

If we now implement Equations 6.12, 6.13 and 6.14 numerically, Fig. 6.6 shows the resulting $|F|_{dB}$ as a function of $\overline{SGR}$ for the 50% and 90%. As would be expected, for $\overline{SGR}$s of -20 to -10 dB very little fading is predicted. For $\overline{SGR}$s around zero this method predicts severe fading, of the order of 13 dB for the 90%-ile. That the

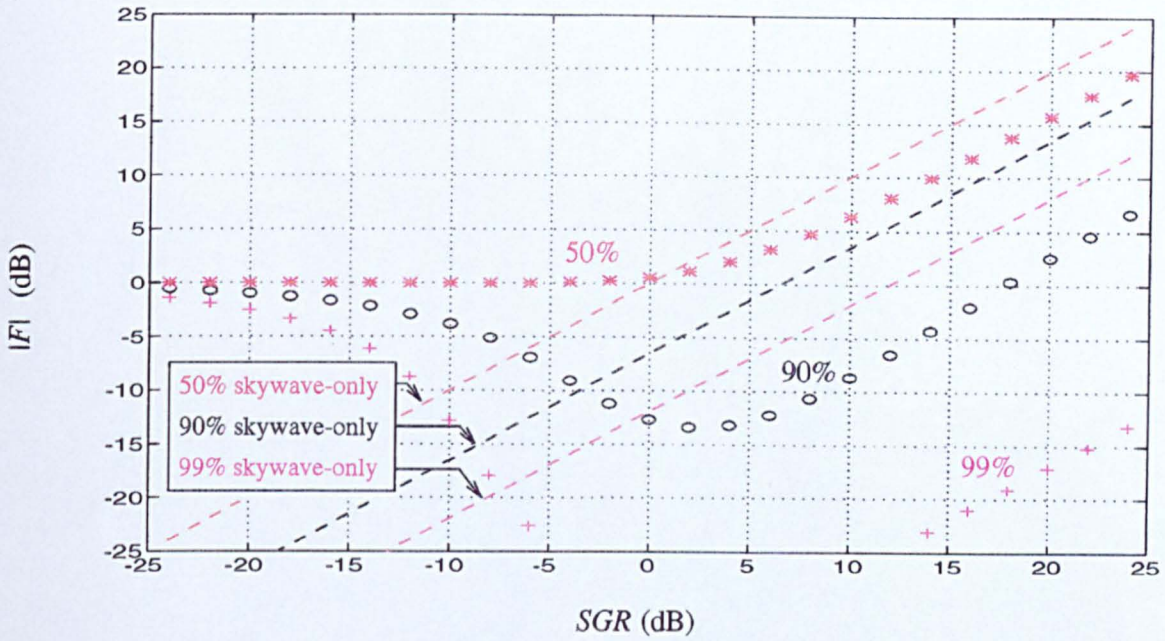

Figure 6.6: $|F|_{dB}$ as a function of $\overline{SGR}$ from the Enge-Olsen $P_{F_{dB}}$ for the 50%, 90% and 99%. This method predicts deep fades for the 90% and 99%. There are large discrepancies between all three curves and their skywave-only asymptotes, due to the assumption that only the portion of skywave in-phase with the groundwave need be considered.

point of deepest fade occurs above an $\overline{SGR}$ of zero suggests that the fading zone lies beyond the range at which the skywave and groundwave are of comparable strengths, which is unreasonable. When skywave dominates, *i.e.* $\overline{SGR}$ is much greater than zero, recovery to skywave signal levels would be expected. But because it includes only the portion of the skywave which is in-phase with the groundwave, this method never shows the signal recovering to the skywave-only levels. This is despite Enge and Olsen's use of Gaussian-distributed, rather than Rayleigh-distributed, values of *Sky*. Clearly the method is inadequate: it is obvious that far from the beacon where the groundwave signal has 'disappeared', only the skywave is present and its distribution must be dominant and correspond to skywave statistics.

It is concluded that the assumption of a dominant groundwave component, and the use of the in-phase term alone, limits the region over which the Enge-Olsen Method may correctly be applied to ranges less than those needed to reach the fading zone. More importantly, these ranges are less than those needed to reach the planned edge of coverage for most DGPS radiobeacons!

6.2.3 New Method

To predict the effect of own-skywave interference, a new method needs to be developed that combines a constant groundwave component more accurately with a skywave component of Gaussian amplitude and uniform phase distribution. In contrast with the Enge-Olsen method, it is important to place no restriction on the relative amplitudes of the two components.

The derivation begins with the vector summation from Fig. 6.3.

$$Total = Gnd + Sky\, e^{j\theta}. \tag{6.16}$$

From [101], the fade is described by

$$P_F(f) = \int_{D_F} \int p_{sgr,\theta}(sgr, \theta)\, dsgr\, d\theta \tag{6.17}$$

where D_F is the full region $|F| \leq f$, that is, all possible values of the total signal. No limitation is placed on the magnitude of *sgr*. The distribution of the skywave-to-groundwave ratio (*sgr*) is taken to be independent of the relative phase between the two signals (θ). Thus Equation 6.17 simplifies to:

$$P_F(f) = \frac{1}{\pi} \int_{D_\theta} P_{sgr}(\theta)\, d\theta \tag{6.18}$$

This equation calculates the probability of measuring a total signal level $|F| \leq f$ (relative to the groundwave strength) if we allow the *sgr* vector (whose magnitude is described statistically) to move uniformly over the range of θ values, as defined by the region D_θ. As we let f increase, there will be a higher probability of measuring a total signal less than f.

We want to find the region of integration D_θ. We know D_F is the region:

$$|F| \leq f, \tag{6.19}$$

and $|F|$ is defined in terms of *sgr* and θ in Equation 6.5. Let us determine the bounds on θ mathematically. Substituting Equation 6.5 into 6.19 will give f in terms if *sgr*

and θ:

$$|1 + sgr \exp j\theta| \leq f, \tag{6.20}$$

$$\sqrt{(1 + sgr\, cos\theta)^2 + (1 + sgr\, sin\theta)^2} \leq f, \tag{6.21}$$

$$sgr^2 + 2\, sgr\, cos\theta + 1 \leq f, \tag{6.22}$$

Solving the quadratic in Equation 6.22 will bound sgr as a function of θ and f:

$$-cos\theta - \sqrt{cos^2\theta - 1 + f^2} \leq sgr \leq -cos\theta + \sqrt{cos^2\theta - 1 + f^2}. \tag{6.23}$$

The phase of the skywave component is uniformly distributed between 0–π and sgr is an amplitude, thus a real number. For f greater than 1, sgr in Equation 6.23 stays a real number over the whole range of θ. Thus for $f > 1$, D_θ ranges from $0 \rightarrow \pi$.

For $f < 1$, sgr in Equation 6.23 is real only for the values of θ at which:

$$cos^2\theta - 1 + f^2 \geq 0, \tag{6.24}$$

$$f^2 \geq -cos^2\theta + 1, \tag{6.25}$$

$$f^2 \geq sin^2\theta, \tag{6.26}$$

$$sin^{-1}(f) \geq \theta. \tag{6.27}$$

We now know the integration regions D_θ:

$$\pi - sin^{-1}(f) \leq \theta \leq \pi, \quad \forall f \leq 1 \tag{6.28}$$

$$0 \leq \theta \leq \pi, \quad \forall f > 1. \tag{6.29}$$

The limits on θ in Equations 6.28 and 6.29 can be visualised by plotting the region of validity in the sgr-θ plane. Fig. 6.7 illustrates Equation 6.28, that is, $f < 1$. For $f \ll 1$ (deep fading), the groundwave and skywave components will have to be cancelling each other to a great extent. This implies that the two components are of similar magnitude, $sgr \approx 1$, and that they are out-of-phase, $\theta \approx \pi$. The region of D_F for $f = 0.1$ is shaded to indicate the area of validity from Equations 6.23 and 6.28 and indeed, it only includes values of sgr around 1 and values of θ up to near π. In general, for $f < 1$, $\theta = \pi - \arcsin(f) \rightarrow \pi$. To calculate the area of this region, the integration

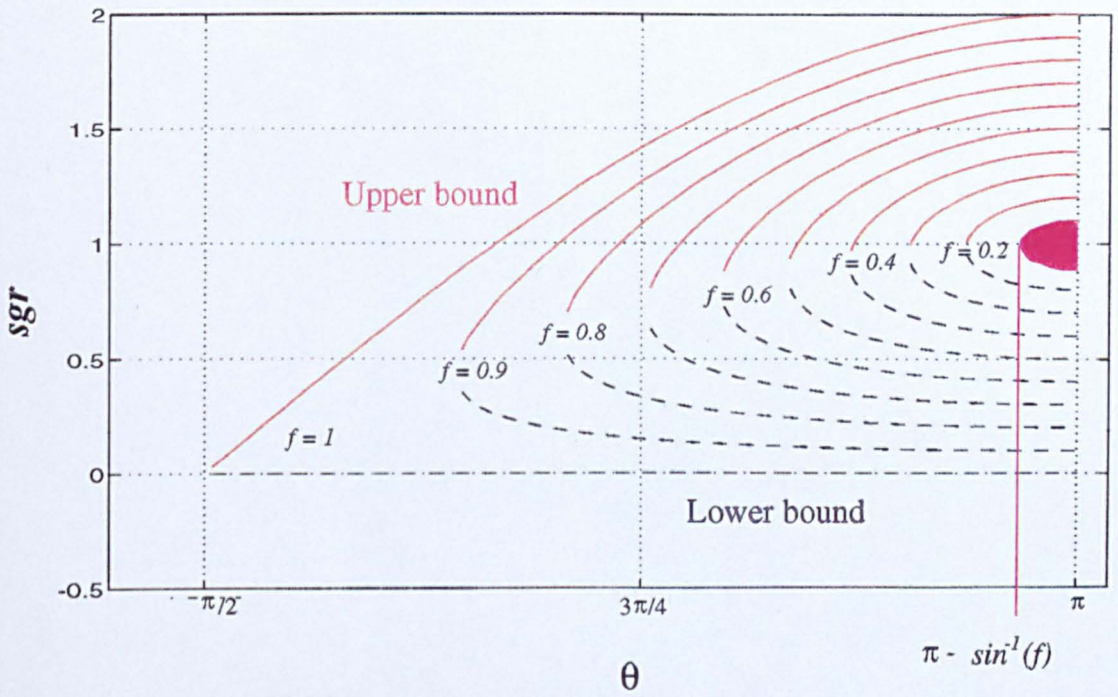

Figure 6.7: Visualisation of the integration regions in the *sgr*-θ plane, for f=0.1, 0.2,...1. The roots of the quadratic are plotted as functions of f and θ. The desired area is shaded for $f = 0.1$ and is seen to go from $\theta = \pi - \arcsin(0.1) \rightarrow \pi$. In general, for $f < 1$, $\theta = \pi - \arcsin(f) \rightarrow \pi$.

of the lower bound is subtracted from the integration of the upper bound, thus for $f < 1$,

$$P_{|F|_{dB}}(f) = \frac{1}{\pi}\int_{\pi-sin^{-1}(f)}^{\pi} P_{SGR}\left(20log_{10}\left(-cos\theta + \sqrt{cos^2\theta - 1 + f^2}\right)\right) - P_{SGR}\left(20log_{10}\left(-cos\theta - \sqrt{cos^2\theta - 1 + f^2}\right)\right) d\theta. \quad (6.30)$$

Fig. 6.8 shows D_F in the *sgr*-θ plane for values of $f > 1$. The region of D_F corresponding to an arbitrary f is now calculated by integrating the upper bound, over the full range of θ. There is no subtraction of the area under the lower bound, as this area is zero. Thus, for $f > 1$,

$$P_{|F|_{dB}}(f) = \frac{1}{\pi}\int_{0}^{\pi} P_{SGR}\left(20log_{10}\left(-cos\theta + \sqrt{cos^2\theta - 1 + f^2}\right)\right) d\theta. \quad (6.31)$$

Assuming a Gaussian-distributed skywave amplitude, P_{SGR} is given by:

$$P_{SGR}(x) = 1 - Q\left(\frac{x - \overline{SGR}}{\sigma}\right) \quad (6.32)$$

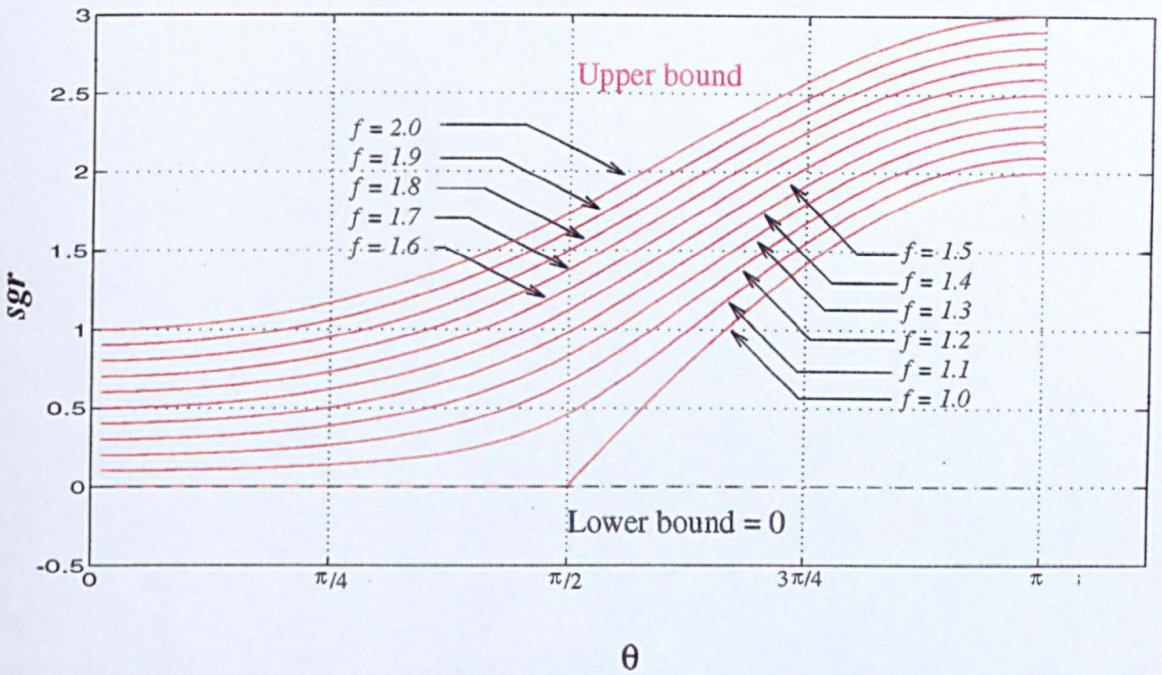

Figure 6.8: Visualisation of the integration regions in the *sgr*-θ plane, for f=1, 1.1, 1.2,...2. The quadratic roots form the upper and lower bounds, with the lower always zero here. Thus the desired area for a given $f > 1$ is below the upper bound with $\theta = 0 \rightarrow \pi$.

where σ is the standard deviation of the Gaussian distribution and may be written as 90th%-ile divided by 1.29, allowing us to apply the upper decile value from [77]. Q is given by Equation 6.15.

Equations 6.23– 6.32 have been implemented numerically. The resulting plots of $|F|_{dB}$ against $\overline{SGR}$ are given in Fig. 6.9 for the 50th, 90th and 99th percentiles. For the groundwave-dominant $\overline{SGR} \ll 0$, $|F|_{dB}$ is approximately zero, indicating little or no fading. All three curves now asymptote correctly to their respective skywave-only availability levels for skywave-dominant $\overline{SGR} \gg 0$.

In the fade zone, there is a 50% probability that the sum of the groundwave and skywave will be up to 3 dB greater than either of them alone which is physically reasonable. The signal level guaranteed to be exceeded 90% of the time is 5.3 dB below the groundwave, still stronger than the skywave-only -6.5 dB level. At 99% availability, the fade is down to 15 dB below the groundwave, well below the skywave-only -11.9 dB. A major merit of this New Method is that the predicted results accurately model the skywave-dominant

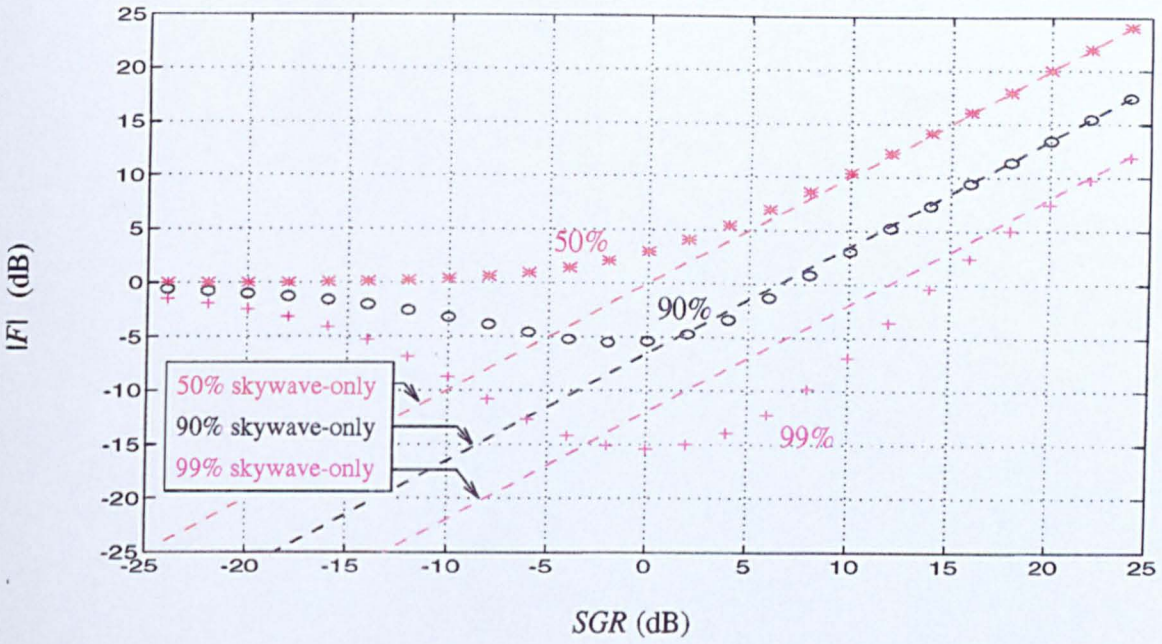

Figure 6.9: $|F|_{dB}$ as a function of $\overline{SGR}$ from the New Method, for the 50%, 90% and 99%-ile. This method predicts fading similar to the Nakagami-Rice around an SGR of 0. Note that all three curves now also asymptote correctly to their skywave-only levels.

zone, as the curves asymptote to their skywave-only levels.

Fig. 6.10 combines these newly-computed own-skywave values with the previously-available curves of the groundwave and skywave field strengths to give the two *Total* curves. Two different groundwave paths are considered, one over sea-water and the other over the sort of low-conductivity ground found north of Porkkala. Night skywave conditions are assumed to apply and both 50% and 95% availability skywave curves are shown. The total field strengths shown are the 95% availability values.

Over the sea-water path, the effect of fading is seen to begin at around 100 km. The resulting total signal is less than that of either the groundwave or the 95%-availability skywave component alone from there out to more than 1000 km. Over the lower-conductivity ground, fading begins at only 40 km, but, the signal level then recovers as the skywave signal takes over. A fascinating result is that, at ranges from about 600–1300 km, the 95%-availability signal received over this path actually exceeds that received over the sea-water path! That happens because, at those ranges, the sea-water path is still experiencing skywave-groundwave fading whereas over the poor land

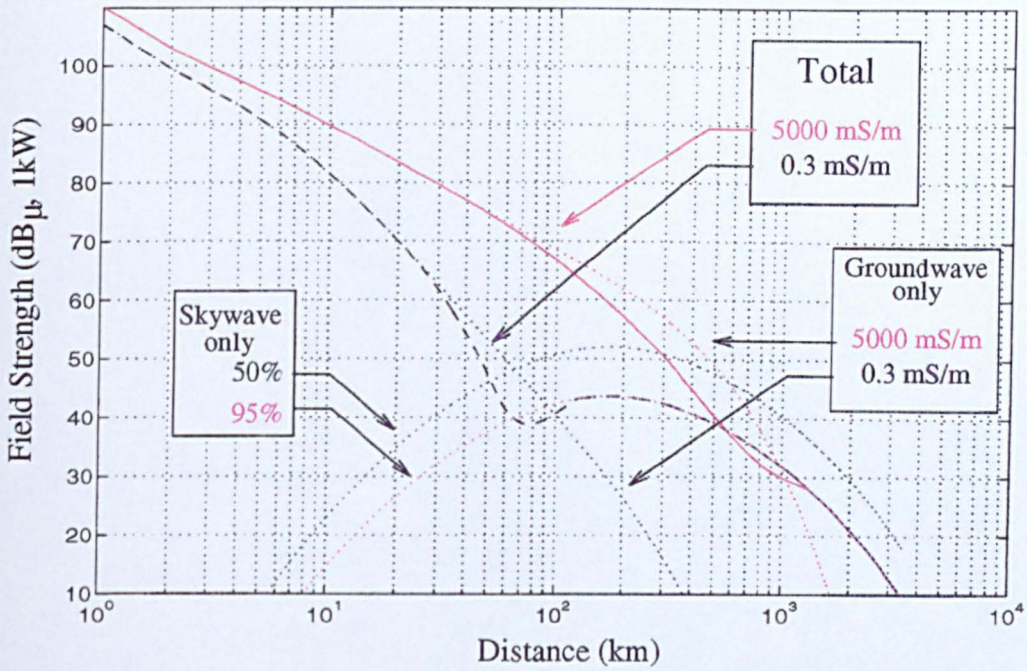

Figure 6.10: Curves of 95%-ile total field strength (*Total*) versus distance over sea water and over low-conductivity ground. Near the beacon, the total field strength is dominated by the groundwave. In the fade zone, own-skywave interference causes the total field strength to fall below both the groundwave-only and skywave-only curves. Recovery to skywave-only levels is seen in the skywave-dominated zone far from the beacon.

path the groundwave signal is negligible and the signal is coming via the skywave path alone. In fact, one might say that the low-conductivity path is experiencing pure skywave and the skywave signals over the sea-water path are suffering fading due to groundwave interference!

The relative levels of groundwave and skywave are, of course, independent of the beacon's radiated power. The groundwave and median skywave over a sea-water path are comparable, between 500 km and 600 km, for either a 1 kW, or a 1 W, beacon. This means that the curves of total field strength for 300 kHz may be adjusted for use with beacons of other power in the same way as the groundwave-only curves described in 4.1.1. It also means that the degree of fading at a given distance is the same for all beacons, regardless of their nominal ranges.

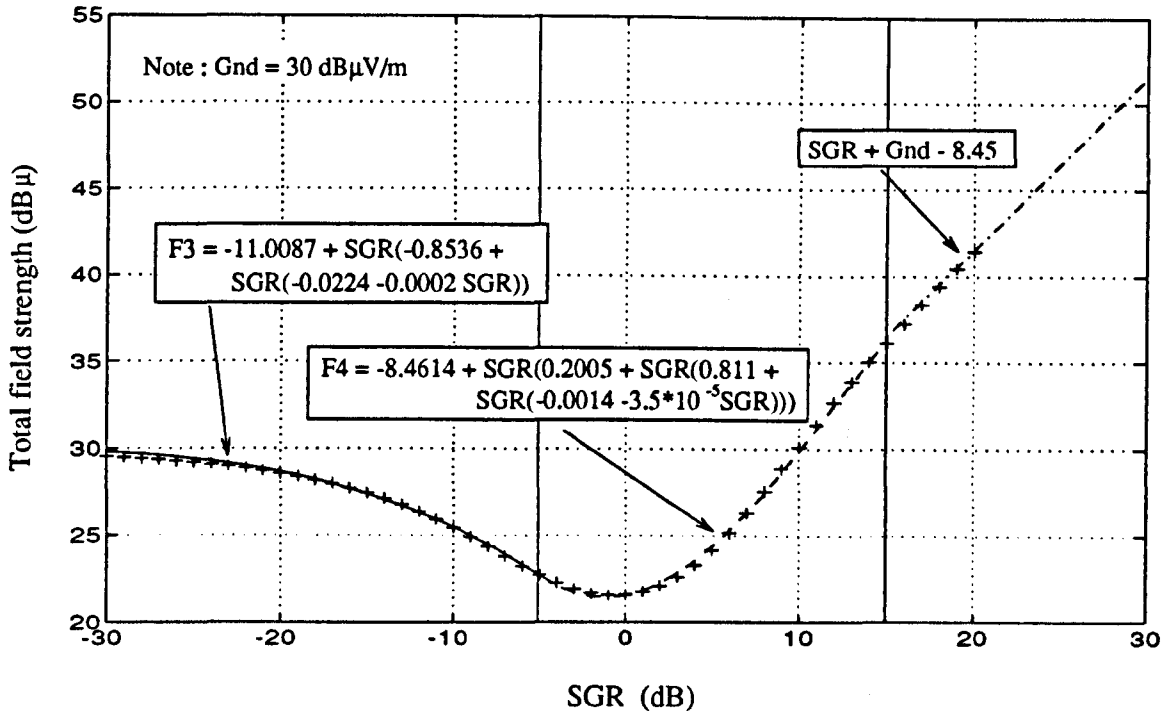

Figure 6.11: *Total* field strength as a function of *SGR*, assuming a groundwave field strength of 30 dBμ. The curve is composed of three sections: the 3rd-order *F3*, the 4th-order *F4* and the skywave-only asymptote. The '+'s are the calculated points to which the curves are fitted.

6.3 Modelling own-skywave interference

Calculation of field strength values using the new method is extremely time-consuming. It was decided, therefore, to apply a polynomial curve fit to the results for inclusion in the DGPS model. In the following examples, a curve fit to the 95%-availability fade depth as a function of *SGR* (in dB) has been employed. To keep the order of the polynomial low, different curves are applied over various ranges of *SGR*, as follows:

$$Total_{dB} = \begin{cases} Gnd_{dB}, & SGR < -30, \\ Gnd_{dB} + F3(SGR), & -30 \leq SGR < -5, \\ Gnd_{dB} + F4(SGR), & -5 \leq SGR < 15, \\ SGR + Gnd_{dB} - 8.45, & 15 \leq SGR \end{cases} \tag{6.33}$$

F3 and *F4* are third- and fourth-order polynomial fits, as shown in Fig. 6.11, where $Total_{dB}$ is plotted as a function of *SGR* assuming a *Gnd* strength of 30 dBμ.

Fig. 6.12 shows the effect of own-skywave interference on the coverage of Porkkala. These contours represent the levels of night-time field strength available 95% of the time

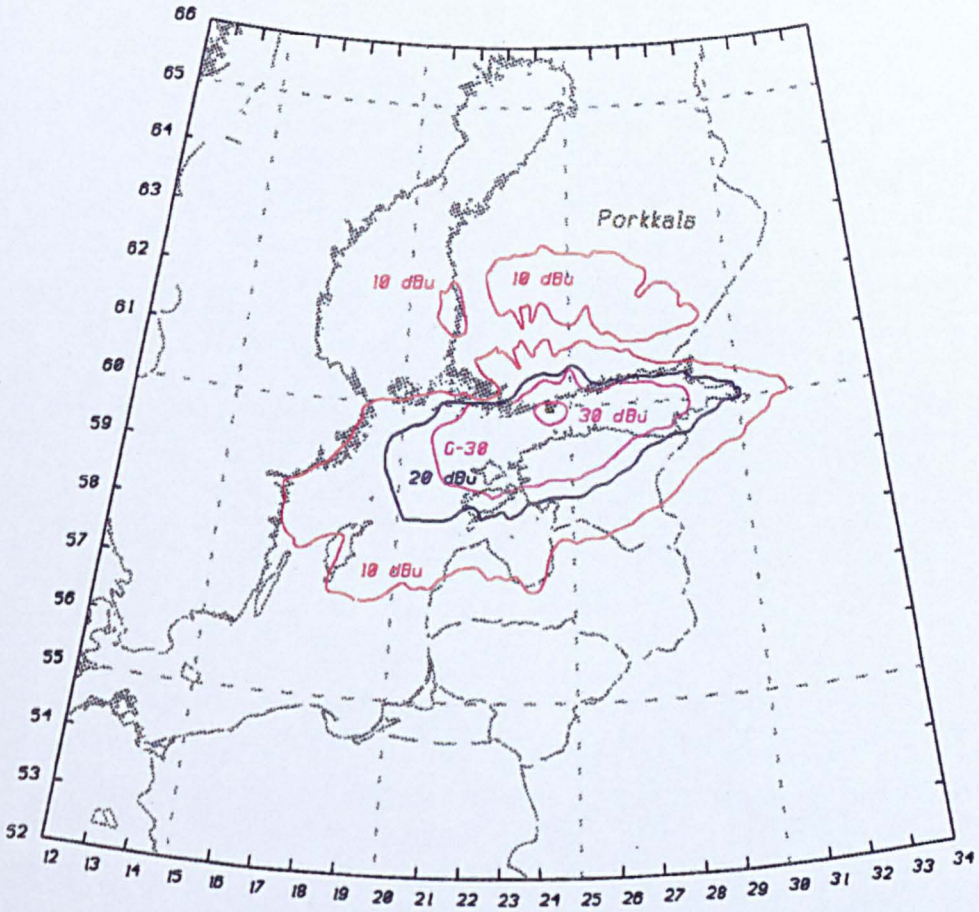

Figure 6.12: Contours of combined groundwave and skywave signal strength around the beacon Porkkala. The outer, 10 dBμ contour encloses three regions: the groundwave-dominant area around the beacon; and, over Finland, two smaller, separated sections. The two northerly ones are regions of skywave recovery, beyond the fade zone.

around the beacon. The outer, 10 dBμ, contour encloses three regions: the groundwave-dominant area around the beacon; and, over Finland, two smaller, separated sections. The gap separating the inner-zone from the two outer ones is the fade zone, where the own-skywave interference causes the available signal to fall below the contoured level. The two sections to the north constitute the skywave-recovery zone, where the levels of available signal due to skywave alone rise above the contour level. Skywave-recovery is seen only over the low-conductivity land, where the groundwave is attenuated very rapidly allowing the skywave to become dominant. Over the sea-water paths, the groundwave is attenuated more slowly, with the result that the fade zone persists over a longer range and by the time the skywave has become dominant its strength is below the contour level.

The serious reduction in range due to fading can be seen by comparing the *G-30* (groundwave 30 dBμ contour) to the *30 dBμ* contour in Fig. 6.12. Note that the inner two field strength contours of 20 and 30 dBμ show no skywave-recovery. In fact, the 95%-availability skywave field strength of this 180 km beacon never rises above 20 dBμ. This is why the very low strength of 10 dBμ has been used to illustrate skywave recovery. It is important to note, however, that if the beacon power were to be increased by 10 dB, the outer contour would then represent the 20 dBμ signal level and the signal would be usable for DGPS. The fade zone is, of course, independent of the beacon power.

6.4 Validation

In validating the calculation of own-skywave interference, two different types of comparisons have been made. The first examines the behaviour of the method at its limits and compares it to physical reality. At one extreme, close to the beacon, the groundwave is known to dominate and the fading to be negligible. This is correctly predicted by the New Method (Fig. 6.9, which yields a fade depth of 0 dB for groundwave-dominant SGR). The other extreme occurs at ranges such that the groundwave has disappeared into the noise and any received signal is due to the skywave-propagated component. The method correctly predicts this skywave-dominant situation, with the statistical distribution of field strength corresponding more accurately to those of the skywave alone. This is again physically correct.

For the second check, to determine if the depth of fading is predicted correctly when skywave and groundwave are of similar strength, we compare the calculated results with experimental measurements. Using a CEI *Sidekick* receiver, we record the received signal strengths from the UK beacon at Flamborough. This beacon is located on the east-coast of England, approximately 280 km from the test site on the Isle of Anglesey. It is a rare beacon in that it shares its frequency channel of 302.5 kHz with only one other beacon: a 33 km marine beacon located in Russia! As will be seen in Chapter 8, a European beacon normally has to share its channel with five or ten other beacons.

Beacon	Propagation Mode	Predicted (dBμ)	Measured (dBμ)	
			Uncalibrated	Calibrated
Point Lynas	Groundwave	52	63	52
Flamborough	Groundwave	22	31	20
	Skywave	17.5	-	-

Table 6.1: Comparison between signal strengths measured at the test site on the Isle of Anglesey and those predicted by the model for two UK beacons. Point Lynas is a strong, local, beacon used to calibrate the receiver. Flamborough, several hours of whose signal strength data has been recorded, was predicted to have a 4.5 dB skywave-to-groundwave ratio at the test site which places the site inside its fade zone.

Since it is the only beacon in Western Europe broadcasting at 302.5 kHz, we can be very confident that the measured signal strength results from Flamborough's signals alone and that there is no contribution by groundwave or skywave from other beacons. In fact, Flamborough has such a quiet channel because of the coverage prediction work being done here at Bangor (see Chapter 8 for details): its original allocation was shown to suffer from severe levels of interference at almost any point beyond its nominal range, yet its co-located marine beacon located on the adjacent channel was predicted to have none. A swap between the two frequencies was proposed and has been implemented!

The 280 km range over land places the test site inside Flamborough's fade zone, with an SGR of -4.5 dB predicted by the DGPS model (see Table 6.1). The table also shows the 'uncalibrated' measured daytime signal strength values. The receiver and antenna combination employed gave a linear response to received field strength, but had not been calibrated to indicate absolute values. This calibration was achieved as follows. The predicted and measured groundwave signals of a very local beacon, 'Point Lynas' at a range of 18.5 km, were measured (see the Table). The difference between Point Lynas' measured and predicted daytime field strength was used to calibrate the receiver signal strength reading, indicating a correction factor of 11 dB. Applying this calibration factor to Flamborough's received signal strength gives good agreement between the measured and predicted groundwave values, 20 and 22 dBμ, respectively.

The signal strength from Flamborough was recorded once per minute for 48 hrs in early April, 1995. Fig. 6.13 plots calibrated signal strength (dBμ) against local time.

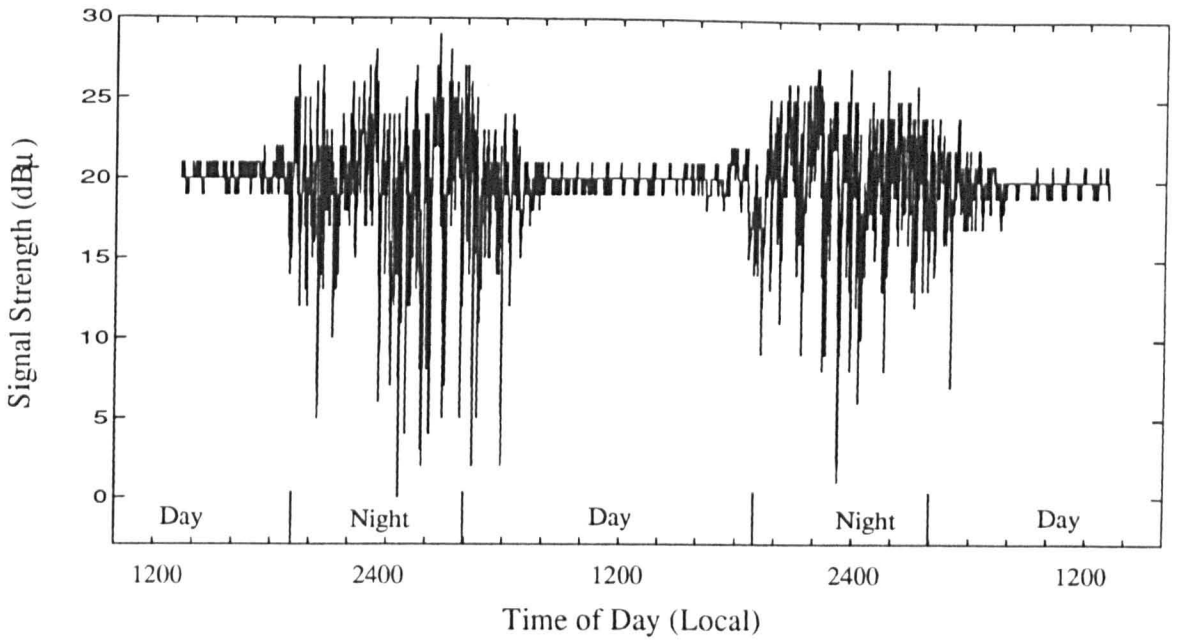

Figure 6.13: Variation of measured signal strength received from Flamborough over two days and nights. The constant signal strength measured during the daytime is due to the groundwave-propagated signal. The variations in strength during the night are due to the additional presence of a skywave component and the complex interference between the two.

The outstanding feature of this plot is the 29 dB variation (from 0–29 dB) in the signal strength recorded during the night. This labelling of a specific period as 'night' was based on the use of a Decca Navigator skywave period chart (see Chapter 7), which indicated that night skywave conditions at the beginning of April at that site normally run from about 1900–0400 h. The variations in the night time signal strengths contrast strongly with the stable daytime measurements.

The next step in verifying the own-skywave interference calculation was to calculate the distribution of the measured night-time signal strength. From Fig. 6.9, for an SGR of -4.5 dB, our analysis predicts that the signal available 50% of the time will be 1.5 dB above the daytime groundwave signal strength. The signal available 90% of the time will be 5 dB, and 99% of the time 14 dB below the groundwave. Certainly looking at the range of signal strength measurements in Fig. 6.13, with its minimum value 19 dB below the daytime level, the pattern of fading appears broadly as predicted. In Fig. 6.14, the 'o' show the percentage of time a given signal strength was exceeded; *e.g.* the 'o' at 60% indicates that 60% of the time a signal strength of 21 dBμ or stronger

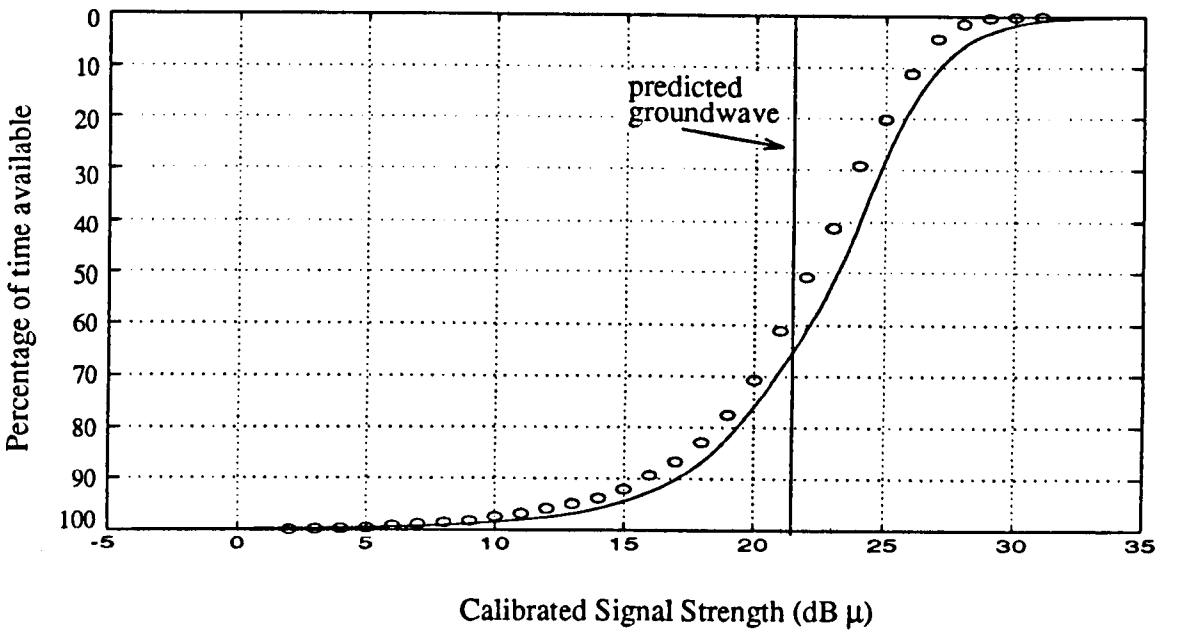

Figure 6.14: A remarkable comparison between the measured and predicted effect of own-skywave interference. The curve indicates the percentage of time that a given signal level is predicted to be available, the 'o's are the results of 18 h of measured night-time data.

was measured.

The last step in this verification was to compare the measured results with the values predicted by the New Method for calculating own-skywave interference. The solid line gives the percentage of time a field strength is predicted to be exceeded. The line is calculated using a groundwave of 20 dBμ and an $\overline{SGR}$ of -4.5 dB as predicted by the model. The excellent agreement between the 18 hours of measured night-time data and the calculated curve allow us to conclude that the new method has been correctly implemented and that it provides a very good model of the actual signal environment.

6.5 Conclusions

The predictions of groundwave and skywave field strengths show that signals can reach the receiver by both these modes at comparable strengths *within the desired ranges of DGPS beacons.* Although it was deduced that the difference in propagation time for the two modes is negligible compared to the MSK data rate, the presence of the

two signals causes fading to be experienced. This being the case, it was concluded that the effect of own-skywave interference needs to be included in the DGPS coverage prediction model.

This chapter began with a review of two existing methods of calculating the effect of own-skywave interference. Both these methods have been examined in detail and found to be inadequate for the DGPS model. The methods predict various degrees of fading when the groundwave and skywave signals are of comparable strength, but neither method predicts correctly the recovery of the signal to the CCIR-measured levels. Reasons for these discrepancies were identified.

A new approach to calculating own-skywave interference has been devised and presented. This New Method has sought to overcome the inadequacies of the existing methods by applying broader starting criteria. The resulting curves and equations have been incorporated into the DGPS model. Coverage contours around Porkkala demonstrate the predicted impact of this effect on a DGPS radiobeacon, showing both reductions in coverage due to fading and increases in coverage due to skywave recovery.

To verify the results of the new method, off-air measurements have been made from a beacon for which fading was predicted at the test site and for which the daytime and night-time signal strengths could be measured. The expected limits in both groundwave- and skywave-dominant conditions and the experimental measurements of fading depth provide a check on the results obtained using the New Method. The excellent agreement between the measured and predicted values leads to two conclusions: that own-skywave interference is a real factor in DGPS coverage, and that the New Method correctly predicts the effect of own-skywave interference from DGPS radiobeacons.

Chapter 7

Atmospheric Noise

The three preceding chapters have presented methods for predicting reliably the level of signal available from a beacon. This has been done for day conditions, that is, groundwave only and also for night conditions where both groundwave and skywave must be accounted for. In both cases examples of signal strength contours generated by the model have been shown. In practice, however, coverage depends not only on the available wanted signal, but also on the levels of noise and unwanted signals affecting the receiver. This noise will primarily be atmospheric noise, the unwanted signals interference from other radiobeacons. This chapter will discuss the levels of atmospheric noise affecting a beacon receiver, signal-to-noise ratio requirements, methods for including this noise in the DGPS model and its impact on coverage prediction. Interference will be the subject of the next chapter.

At frequencies in the LF and MF bands (30–3000 kHz), atmospheric activity is the major source of radio noise. Atmospheric noise is characterised by low-level Gaussian noise mixed with high-level, short duration, noise spikes. These spikes are due to lightning discharges during electrical storms. Multiple discharges, where a major lightning stroke is quickly followed by numerous other strokes, cause the spikes to occur in bursts. Large numbers of storms occur in the equatorial latitudes, with the noise propagating by groundwave and skywave to the mid- and high-latitudes [91, 103]

Local 'weather' may also cause *precipitation static (P-static)*, which is radio noise

resulting from the dissipation of charge that has accumulated on an antenna and/or its surroundings. This build-up of charge on ships and aircraft is due primarily to electrical storms or electrically-charged precipitation [91] and has been reported chiefly at higher latitudes [104]. It can be reduced by eliminating sharp points on the antenna and its surroundings, including the use of encased whip antennas [95]. Preliminary work, reported in [104], indicates substantial theoretical and experimental advantages for H-field loop antenna systems under P-static conditions. As more data becomes available, the incorporation of precipitation noise as a coverage-limiting factor in the high latitudes may be appropriate. For the time being, this relatively rare phenomenon has been left out of the model.

7.1 Variation with time and season

Atmospheric noise varies greatly with the time of day and the season of the year. The results of extensive atmospheric noise measurement campaigns are recorded in CCIR Report 322-3 [69]. This report divides the year into the four standard seasons and into six, 4-hour, time blocks (0000-0400, 0400-0800, etc.). It then presents 24 world maps (*e.g.* Fig. 7.1) which contour the noise at 1 MHz in dB above thermal noise. The example is a daytime noise map for summer days between 1600–2000 hours local time. The high-levels of noise over land in the equatorial regions contrast strongly with the much lower levels in the mid- and high-latitudes. Each map has an associated set of curves to allow the contours to be converted to different frequencies: the curve for Fig. 7.1 is given in Fig. 7.2. Here it can be seen that when noise values ranging from 10–90 dB above thermal are experienced at 1 MHz, the values at 300 kHz will range from 36–114 dB above thermal. The actual rms noise field strength (dBμ) at any frequency is calculated by:

$$E_n = F_{am} - 95.5 + 20 \log f_{MHz} + 10 \log b_{Hz} \tag{7.1}$$

where:

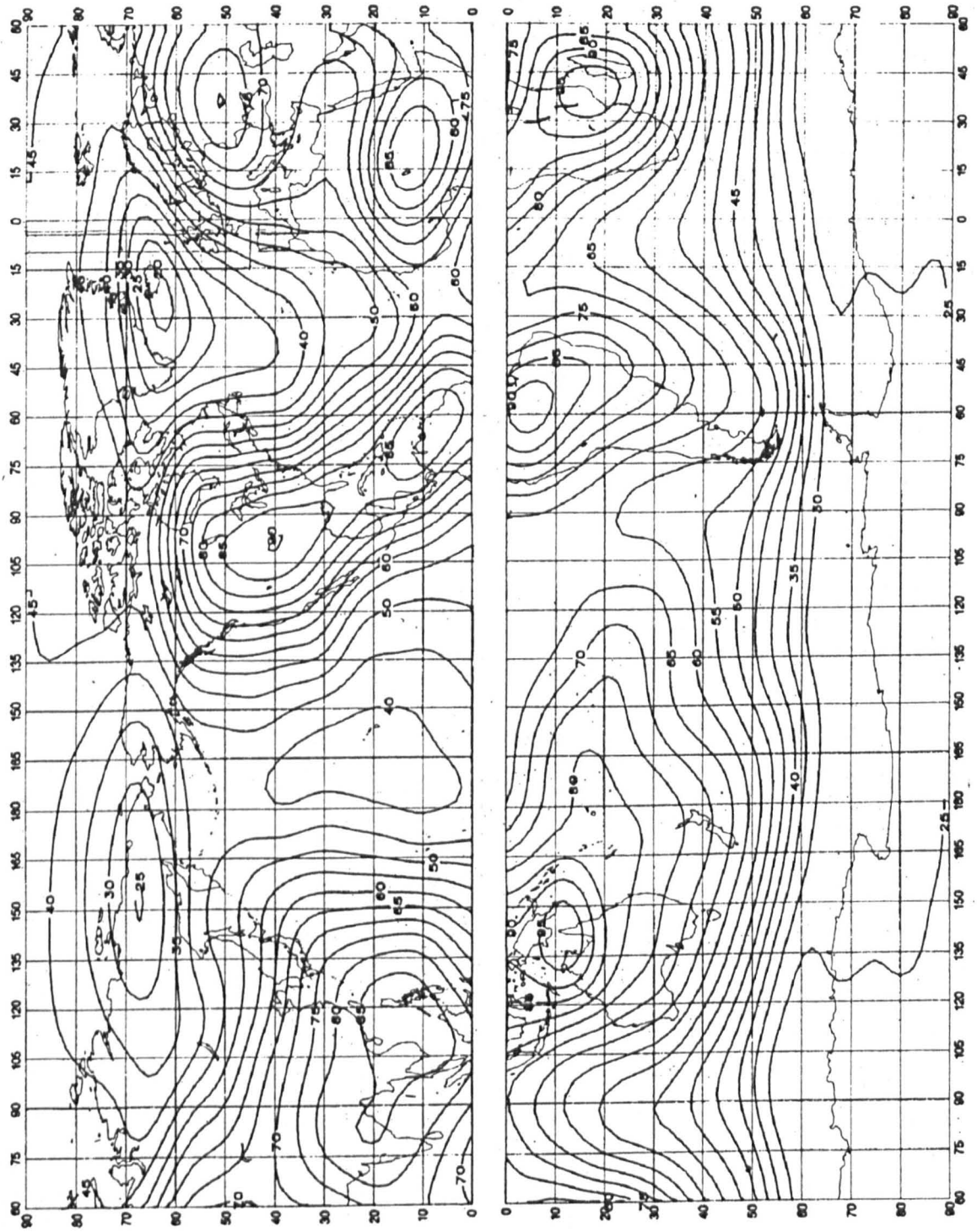

Figure 7.1: CCIR world map of 1 MHz noise values (dB above thermal noise) for the summer, 1600–2000, time-season block, from [69].

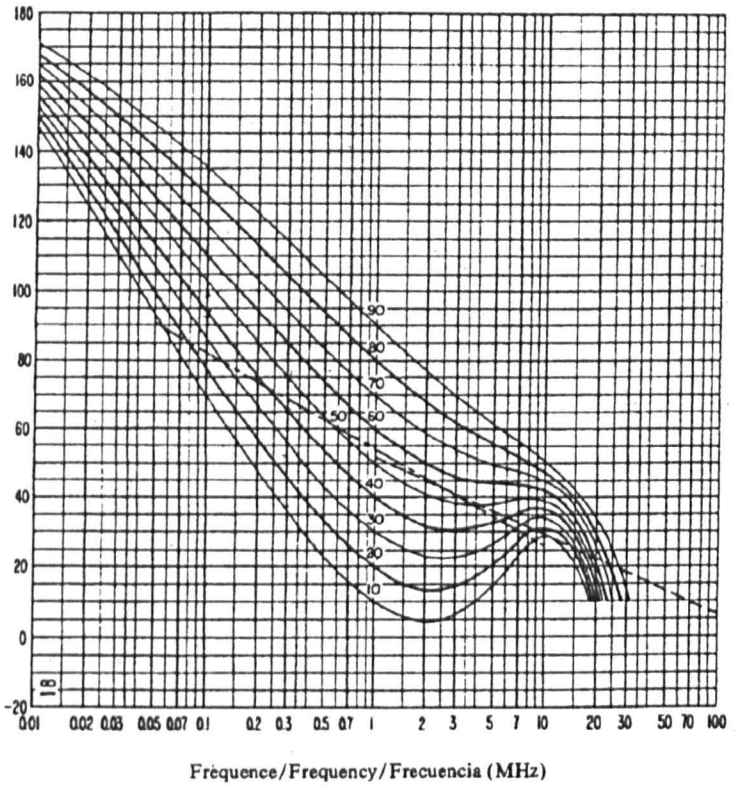

Figure 7.2: CCIR curves for converting from 1 MHz noise values to noise at other frequencies [69]. These curves correspond to the summer, 1600-2000, time-season block.

E_n: the rms noise field strength (dBμ) in bandwidth b at frequency f_{MHz},
F_{am}: the median noise level from the world map,
adjusted for the desired frequency by applying the conversion curves,
f_{MHz}: the desired frequency in MHz,
b_{Hz}: the desired noise bandwidth.

Thus CCIR gives us a way of predicting the noise strength at any point and time. Looking at the conversion curves in Fig. 7.2, it can be appreciated that reading values from these curves is difficult because of the limited resolution. It was deduced that the adjustment to the noise value could instead be implemented as a 'shift-and-scale' function, such that not every point needs to be read off the curve. To do this, the upper and lower limits of the 1 MHz values and the upper and lower of the 300 kHz values were determined. These can then be used to shift and scale any number of 1 MHz noise values read from the map in Fig 7.1. This would be implemented in following manner:

$$E_n = (F_a - L_{1MHz})S + L_{300kHz} - 95.5 + 20\log f_{MHz} + 10\log b_{Hz} \qquad (7.2)$$

where the 'shift-and-scale' terms not defined in Equation 7.1 are:

S: the scaling factor between 1 MHz and 300 kHz noise levels spread,
calculated as $(H_{300kHz} - L_{300kHz})/(H_{1MHz} - L_{1MHz})$.
L_{1MHz}: Lower noise limit, at 1 MHz, taken from the frequency conversion curve,
H_{1MHz}: Upper noise limit, at 1 MHz, taken from the frequency conversion curve,
L_{300kHz}: Lower noise limit, at 300 kHz, taken from the frequency conversion curve,
H_{300kHz}: Upper noise limit, at 300 kHz, taken from the frequency conversion curve,

Equation 7.2 calculates the 300 kHz noise strength for all values in any specific time-season block. These upper and lower limits vary from block to block, changing both the scaling and the shifting. The advantage of using the new Equation 7.2 instead of Equation 7.1 is not only the simplification in the noise calculation process, but also the consistency introduced into the frequency conversion process. The difficult process of reading values off the graph is limited to reading and recording only two points per time-season block, regardless of the number of geographical points at which a value of 1 MHz noise is read from the map. All the noise values in this chapter have been determined using this 'scale-and-shift' modification.

Table 7.1 gives, by way of example, the resulting 300 kHz median noise levels calculated at the point [60°N, 20°E] for each of the 24 different combinations of time and season.

Median Noise Values (dBμ) at [60N,20E]				
Time	Season			
	Winter	Spring	Summer	Autumn
0000-0400	7.7	1.0	11.7	4.2
0400-0800	-0.6	-18.1	-9.0	-7.7
0800-1200	-29.8	-25.9	-15.9	-27.1
1200-1600	-20.2	-16.8	-1.6	-19.3
1600-2000	-7.6	-10.1	-1.3	-4.5
2000-2400	0.7	3.5	8.4	5.0

Table 7.1: Median noise values at the point [60N,20E] in the Baltic Sea region for each of the 24 CCIR time-season blocks, demonstrating the substantial temporal variation, some 41.5 dB. The stronger noise signal during the night may be attributed primarily to better skywave propagation of noise from storms in equatorial latitudes.

Median Noise Strength (dBμ) during Summer, 1600-2000							
Degrees Latitude	Degrees Longitude						
	5	10	15	20	25	30	35
70	-25.6	-22.7	-20.8	-17.8	-15.9	-13.9	-12.0
65	-26.6	-21.7	-16.9	-13.0	-9.1	-6.1	-3.2
60	-15.9	-11.0	-6.1	-1.3	2.7	4.6	6.6
55	-7.1	-2.2	3.6	7.5	11.4	13.4	14.4
50	-2.2	3.6	8.5	12.4	14.4	15.3	17.3

Table 7.2: Median noise values during the single CCIR time-season block of summer, 1600-2000, over an array of regularly-spaced geographical points in Europe. The increase in the noise from north to south is typical and to be expected since the noise source is predominantly storms in the equatorial zones.

There is a huge temporal variation in the noise strength, with a 41.5 dB difference between highest and lowest median noise levels at this point. The higher noise levels at night are due to an increase in skywave-propagated noise from storms in the lower latitudes to this point in the Baltic Sea.

As was seen in Fig. 7.1, noise level also varies dramatically with location. For example, Table 7.2 lists the median noise levels calculated for a single time-season block over a variety of geographical points all in the same region. The noise in this example varies by as much as 10 dB over a distance of 550 km.

7.2 Statistical variation

The level of noise measured during each of the approximately 90 days which comprise a time-season block varies, depending on thunderstorm activity and propagation conditions. Information is provided in [69] to describe this variation for each block. The noise strength calculated by Equation 7.2 is the median 300 kHz noise, that is the level of noise which is not exceeded 50% of the time. The differences (in dB) between this median value and the upper and lower decile values are presented (90% and 10%, respectively), again as curves against frequency. A two-sided Gaussian distribution is used to compute other percentiles–two-sided because the Gaussian σ is defined by the 90% value for percentiles above median and by the 10% value for percentiles below median.

For coverage prediction, we want to know other noise strength probabilities than median and decile values. Since the distribution of the noise values is defined by a Gaussian distribution, any other percentile can be readily computed. However, each time-season block has its own decile values which must be applied in defining the Gaussian curves. Table 7.3 gives examples of the difference between the strongest noise level expected 50% of the time in any block and the strongest noise level expected during higher percentages of time, computed by applying a Gaussian distribution. This comparison is done for several different time-season blocks. As the percentage of time increases, so does the maximum measured noise strength because more of the less frequent, high level, noise events are experienced. During the spring 1600–2000 block, for example, the noise level measured 99.99% of the time is more than 50 dB above that measured 50% of the time. This would be characteristic of infrequent, but very strong, impulses or bursts of electrical noise. In contrast, summer 2000–2400 shows only a 26.8 dB increase in the noise levels measured 50% and 99.99% of the time.

Time-Season Block	dBs above median			
	90%	95%	99%	99.99%
Winter 0000-0400	10.8	13.9	19.9	31.4
Spring 1600-2000	18.5	23.9	34.0	53.8
Summer 1200-1600	17.1	22.1	31.5	49.8
Summer 2000-2400	9.2	11.9	16.9	26.8
Autumn 0400-0800	16.5	21.3	30.4	48.0

Table 7.3: The difference, in dB, between the median noise level (measured 50% of the time) and that measured during higher percentages of time, for several different time-season blocks. The values have been calculated by applying a Gaussian fit to the median and upper decile noise values for the block, taken from CCIR 322-3.

7.3 Averaging

CCIR Report 322-3 supplies a way to compute the noise strength in the radiobeacon band at any point in the world and for any percentage of time during each of 24 time-season blocks. Important as this information is, it is not a useful representation of the data for integrating into the DGPS model. It would still leave 24 values describing the noise throughout the year at any given point. When applying minimum SNR and availability criteria, this would result in 24 coverage contours, one for each time-season block. Coverage prediction tends to be more useful if there is a single coverage contour, or at most only a few different ones, to be considered. The problem is to decide what noise information to include in forming the contour.

7.3.1 Worst-case noise

One way of simplifying the situation would be to consider the worst-case noise which might affect a system. This would result in a single value of noise to be compared with the available signal strength, the result being compared against the minimum SNR required. Designing systems around the worst-case noise, however, would result in gross over-engineering, with too much emphasis being placed on conditions obtained intermittently in a single time-season block in which the system might be little used. Unless an error-correcting capability is added to the signal, [88, 105], this

Annual Average, 95% Noise Strength (dBμ)							
Degrees Latitude	Degrees Longitude						
	5	10	15	20	25	30	35
70	0.9	2.2	3.5	4.5	5.2	5.6	5.9
65	3.8	5.6	6.9	7.8	8.4	8.7	8.7
60	7.4	9.0	10.2	11.0	11.4	11.4	10.7
55	9.9	11.7	12.7	13.1	12.9	12.6	11.7
50	11.8	13.1	13.7	14.0	13.8	12.9	11.9

Table 7.4: Annual average of the 95% noise values over an array of regularly spaced geographical points covering the Baltic Sea area.

over-engineering would demand orders of magnitude more radiated power than are really required. Whether this was achieved through higher transmitter power or higher antenna efficiency, the installation and operating expenses of the site would be substantially increased. Additionally, in the European environment, radiating more power would increase the problems of interference (see Chapter 8).

7.3.2 Average noise

To avoid placing all the emphasis on a single time-season block, some sort of averaged noise value could be applied in the coverage prediction process. The simplest option here would be to calculate the *annual average* noise strength at each point, with all 24 time-season blocks contributing equally. Table 7.4 gives the annual average of the 95% noise values at points spaced 5°×5°over the Baltic Sea region. The spacing of the points was chosen to be small enough keep the maximum difference between adjacent points below 5 dB.

Recall, however, that two different signal-propagation periods have been characterised: a night period when both groundwave and skywave signals are present and a day period when only the groundwave component is considered. Since atmospheric noise in the mid-latitudes is due in large part to noise propagating from the equatorial regions, it would be expected that there would be a correlation between high noise levels and conditions which favour skywave propagation. This correlation can indeed be seen in

Table 7.1, where the noise strength is considerably higher during the 0000-0400 night-time slot, say, than during the 1200-1600 daytime slot. If it were possible to determined whether a time-season block corresponded to night or to day propagation conditions, then the appropriate group of blocks could be averaged to give a *night* and a *day* noise strength. This would then lead to two coverage contours, *Night* and *Day*. The *Night* contour would take into account the combined groundwave- and skywave-propagated beacon signals and the averaged night-time noise strength. The *Day* contour would only include the groundwave-propagated beacon signal and the averaged daytime noise strength.

Whether a time-season block falls into the *Day* or *Night* category depends on the ionospheric characteristics associated with the block. In deciding this division, the information available from the Decca Navigator system is employed [79]. Decca Navigator is a system whose coverage is limited by skywave-propagated signals alone; thus skywave is a factor which Decca have analysed in great detail. In fact, Decca publish separate coverage contours for each of five different *skywave periods*: winter night, summer night, dawn/dusk, half light and full daylight. Although the actual level of skywave intensity experienced during a given Decca skywave period may be different at 300 kHz from that in the Decca band around 100 kHz, the hours and months during which each skywave period occurs would be expected to be the same. If this hypothesis is correct, then a correlation will be seen between the weighted averages of the 300 kHz noise values and the corresponding Decca skywave periods.

Fig. 7.3 shows a standard Decca skywave diagram for the UK latitudes in digitised form [79]. The five skywave periods are plotted against the time blocks and seasons over the whole year. Table 7.5 shows the fraction of the CCIR time-season blocks, and thus the overall proportions of the year, which falls within each of the Decca skywave periods and also into *Day* and *Night* divisions.

Table 7.5 provides the information necessary to compute a separate noise value for each Decca period based on weighted averages of the CCIR time-season blocks. Representing each of the CCIR time-season blocks by a letter (W for winter, G for spring, S for

CCIR Time-Season Block		Decca Time Period					*Night*	*Day*
		winter night	summer night	dawn/ dusk	half light	full daylight		
winter	0000-0400	0.58	0.42	–	–	–	1.00	–
	0400-0800	–	0.83	0.17	–	–	0.83	0.17
	0800-1200	–	0.08	0.67	0.25	–	0.08	0.92
	1200-1600	–	–	0.75	0.25	–	–	1.00
	1600-2000	–	0.67	0.33	–	–	0.67	0.33
	2000-2400	.42	0.58	–	–	–	1.00	–
spring	0000-0400	–	0.92	0.08	–	–	0.92	0.08
	0400-0800	–	0.08	0.17	0.50	0.25	0.08	0.92
	0800-1200	–	–	–	0.08	0.92	–	1.00
	1200-1600	–	–	–	–	1.00	–	1.00
	1600-2000	–	0.08	0.08	0.42	0.42	0.08	0.92
	2000-2400	–	0.75	0.17	0.08	–	0.75	0.25
summer	0000-0400	–	0.83	0.17	–	–	0.83	0.17
	0400-0800	–	–	0.08	0.25	0.67	–	1.00
	0800-1200	–	–	–	–	1.00	–	1.00
	1200-1600	–	–	–	–	1.00	–	1.00
	1600-2000	–	–	–	0.08	0.92	–	1.00
	2000-2400	–	0.50	0.33	0.17	–	0.50	0.50
autumn	0000-0400	0.08	0.92	–	–	–	1.00	–
	0400-0800	–	0.58	0.25	0.17	–	0.58	0.42
	0800-1200	–	–	0.33	0.25	0.42	–	1.00
	1200-1600	–	–	0.25	0.25	0.50	–	1.00
	1600-2000	–	0.25	0.42	0.25	0.08	0.25	0.75
	2000-2400	0.08	0.84	0.08	–	–	0.92	0.08
Total number of time-season blocks in period		1.16	8.33	4.33	3.00	7.18	9.49	14.51

Table 7.5: Division of CCIR time-season blocks into Decca time periods and into *Day* and *Night*. The fraction of each time-season block falling within each Decca period has been determined from the Decca diagram. The total number of such time-season blocks contained within each Decca period is given as the column total at the bottom. *Night* is composed of the Decca periods 'winter night' and 'summer night'. *Day* consists of the remaining three periods, 'dawn/dusk', 'half light' and 'full daylight'.

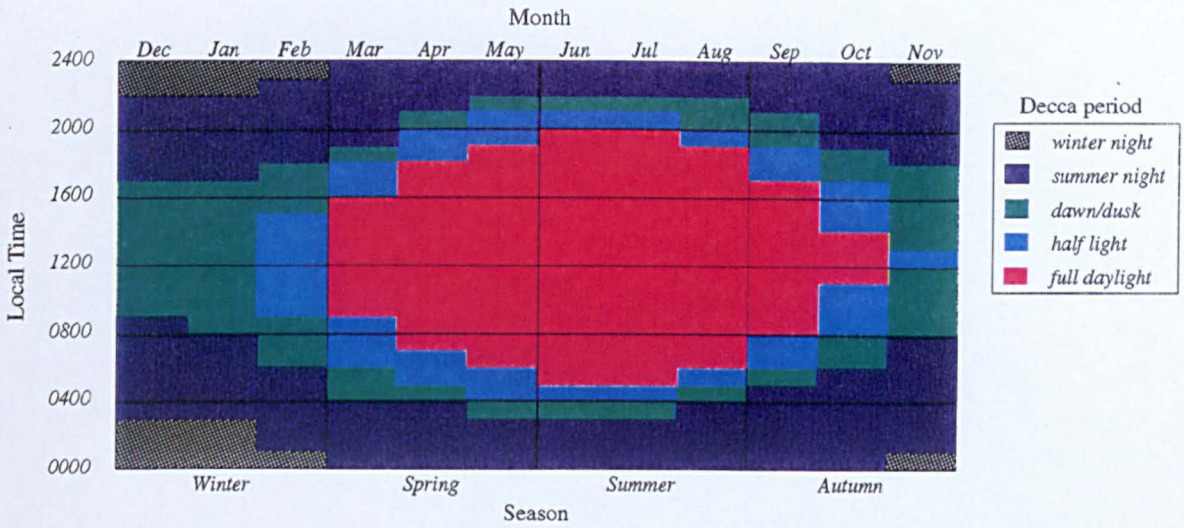

Figure 7.3: Digitisation of the Decca skywave periods. This diagram forms the basis of a weighted translation of the 24 CCIR time-season blocks into the five skywave periods characterised by Decca.

summer and A for autumn) and a number (1 for 0000-0400, 2 for 0400-0800, etc.), the five equations are:

$$winter\,night = \frac{1}{1.16}\{0.58W1 + 0.42W6 + 0.08(A1 + A6)\} \tag{7.3}$$

$$\begin{aligned} summer\,night = \frac{1}{8.33}\{&0.42W1 + 0.83(W2 + S1) + 0.08(W3 + G2 + G5) \\ &+0.67W5 + 0.58(W6 + A2) + 0.92(G0 + A0) + 0.75G6 \\ &+0.50S6 + 0.25A5 + 0.84A6\} \end{aligned} \tag{7.4}$$

$$\begin{aligned} dawn/dusk = \frac{1}{4.33}\{&0.17(W2 + G2 + G6 + S1) + 0.67W3 + 0.75W4 \\ &+0.33(W5 + S6 + A3) + 0.08(G1 + G5 + S2 + A6) \\ &+0.25(A2 + A4) + 0.42A5\} \end{aligned} \tag{7.5}$$

$$\begin{aligned} half\,light = \frac{1}{3.00}\{&0.25(W3 + W4 + S2 + A3 + A4 + A5) + 0.50G2 \\ &+0.08(G3 + G6 + S5) + 0.42G5 + 0.17(S6 + A2)\} \end{aligned} \tag{7.6}$$

$$\begin{aligned} full\,daylight = \frac{1}{7.18}\{&0.25G2 + 0.92(G3 + S5) + G4 + S3 + S4 \\ &+0.42(G5 + A3) + 0.67S2 + 0.50A4 + 0.08A5\} \end{aligned} \tag{7.7}$$

Applying Equations 7.3– 7.7 yields averaged noise values for each of the five Decca periods. These have been calculated for two different points, [55°N, 15°E] and [60°N, 20°E] and listed in Table 7.6. Indeed the expected correlation between the averaged noise

Location Lat Lon)	Decca Period	95% averaged noise value (dBμ)	Bangor Model
55N 15E	winter night	18.0	*Night*
	summer night	16.1	*Night*
	dawn/dusk	3.9	*Day*
	half light	3.8	*Day*
	full daylight	4.4	*Day*
60N 20E	winter night	18.6	*Night*
	summer night	17.0	*Night*
	dawn/dusk	5.2	*Day*
	half light	5.8	*Day*
	full daylight	8.6	*Day*

Table 7.6: Averaged noise strengths for the five Decca periods at two points, [55°N, 15°E] and [60°N, 20°E]. The natural separation into the *Night* and *Day* divisions is emphasised by the ≈10 dB difference in noise strength between the two periods.

values and the skywave periods is apparent. At both sites, the values are in the expected order. Also the winter night and summer night averages are much higher than those of the other three periods. This confirms that there is more noise propagating, via skywave, from the equatorial-latitudes during these two periods.

Adopting now the approach to this problem taken in the Loran-C model [66], there *Night* is comprised of 'winter night' and 'summer night' and *Day* is composed of 'dawn/dusk', 'half light' and 'full daylight'. That the use of this approach at 300 kHz is reasonable is confirmed by the fact that the two night averages are similar to one another and that they differ from those of the day values by some 10 dB. Distribution of the 24 time-season blocks into *Night* and *Day* is included in Table 7.5. The equations for the weighted averages of *Night* and *Day* are:

$$\begin{aligned} Night &= \frac{1}{9.49}\{W1 + W6 + A1 + 0.83(W2 + S1) + 0.08(W3 + G2 + G5) + 0.67W5 \\ &\quad +0.92(G1 + A6) + 0.75G6 + 0.50S6 + 0.58A2 + 0.25A5\} \end{aligned} \tag{7.8}$$

$$\begin{aligned} Day &= \frac{1}{14.51}\{0.17(W2 + S1) + 0.92(W3 + G2 + G5) + W4 + G3 + G4 \\ &\quad +S2 + S3 + S4 + S5 + A3 + A4 + 0.33W5 + 0.08(G1 + A6) \\ &\quad +0.25G6 + 0.50S6 + 0.42A2 + 0.75A5\} \end{aligned} \tag{7.9}$$

Thus three possible ways of averaging the 24 time-season blocks into a single noise value have been examined: annual average, day and night. The next step is to incorporate these averaged noise values into the model, so that we can create SNR contours. The *annual average* noise strengths can be compared to either the groundwave or the total field strength. The *Day* noise strengths will be compared to the groundwave field strength alone and the *Night* noise strengths to the total field strength.

7.4 Implementing SNR contours

A way needs to be selected to give the DGPS model access to the calculated noise values. This will allow the model to compare the wanted signal strength with the calculated noise strength to determine the atmospheric noise SNR at each calculation point. A simple way to do this would be to construct a database composed of the noise strengths at the regularly-spaced points shown in Tables 7.2 and 7.4 with their point spacing of 5° × 5°.

In the first version of this method implemented, the model employed at all 500 calculation points in the 5°-square box centred on any noise point the single 95%-ile noise value stored here; recall that the point-spacing was selected so that there was no more than 5 dB variation between adjacent noise points. The noise and signal strengths were then compared at each calculation point and a contour drawn around all points at which the SNR exceeded a user-specified level. This approach was found to be promising, but the resulting SNR contour had 'steps' at the boundaries between noise values. These were undesirable and unnecessary artifacts; after all, the model employs a fine calculation resolution and the CCIR atmospheric noise map shows a continuous distribution of noise.

To recreate this continuous noise characteristic, it was decided to interpolate between the regularly-spaced noise values. Table 7.2 demonstrates the way these values vary with location. Although steep, the noise gradient over any 'local' area is relatively smooth. That is, the spatial variation of the noise is such that linear interpolation

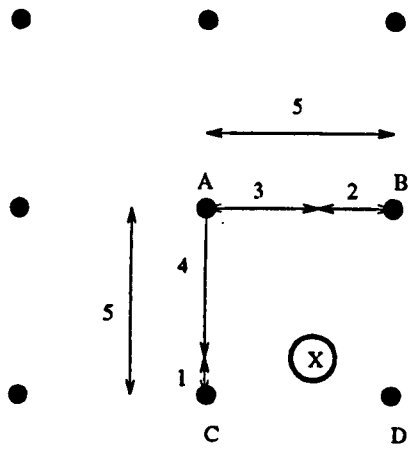

$$X = \frac{1}{5}\left(\frac{2}{5}A + \frac{3}{5}B\right) + \frac{4}{5}\left(\frac{2}{5}C + \frac{3}{5}D\right)$$

Figure 7.4: Simple example of four-way interpolation between equally-spaced noise points. Here the interpolated value at point X depends, as shown, on the known values at points A,B,C and D.

between noise values spaced 5°× 5°would result in an estimated noise value at least as accurate as could be attained by reading the value off the CCIR map. The interpolation method is illustrated in Fig. 7.4. This method allows for smooth transitions between calculated noise values, with an interpolated noise value being computed individually at each calculation point.

Fig. 7.5 plots the contours of the resulting noise contours obtained by interpolation in this way. These values are those not exceeded 95% of the time during the summer, 1600-2000, time-season block. As can be seen, the interpolation does indeed result in a continuous approximation to the CCIR noise maps.

7.5 Effects of atmospheric noise on coverage

The model can now be used to calculate the values of several factors at each calculation point: the wanted beacon's groundwave field strength, the wanted beacon's skywave field strength and, as a result of the work in this chapter, atmospheric noise. The

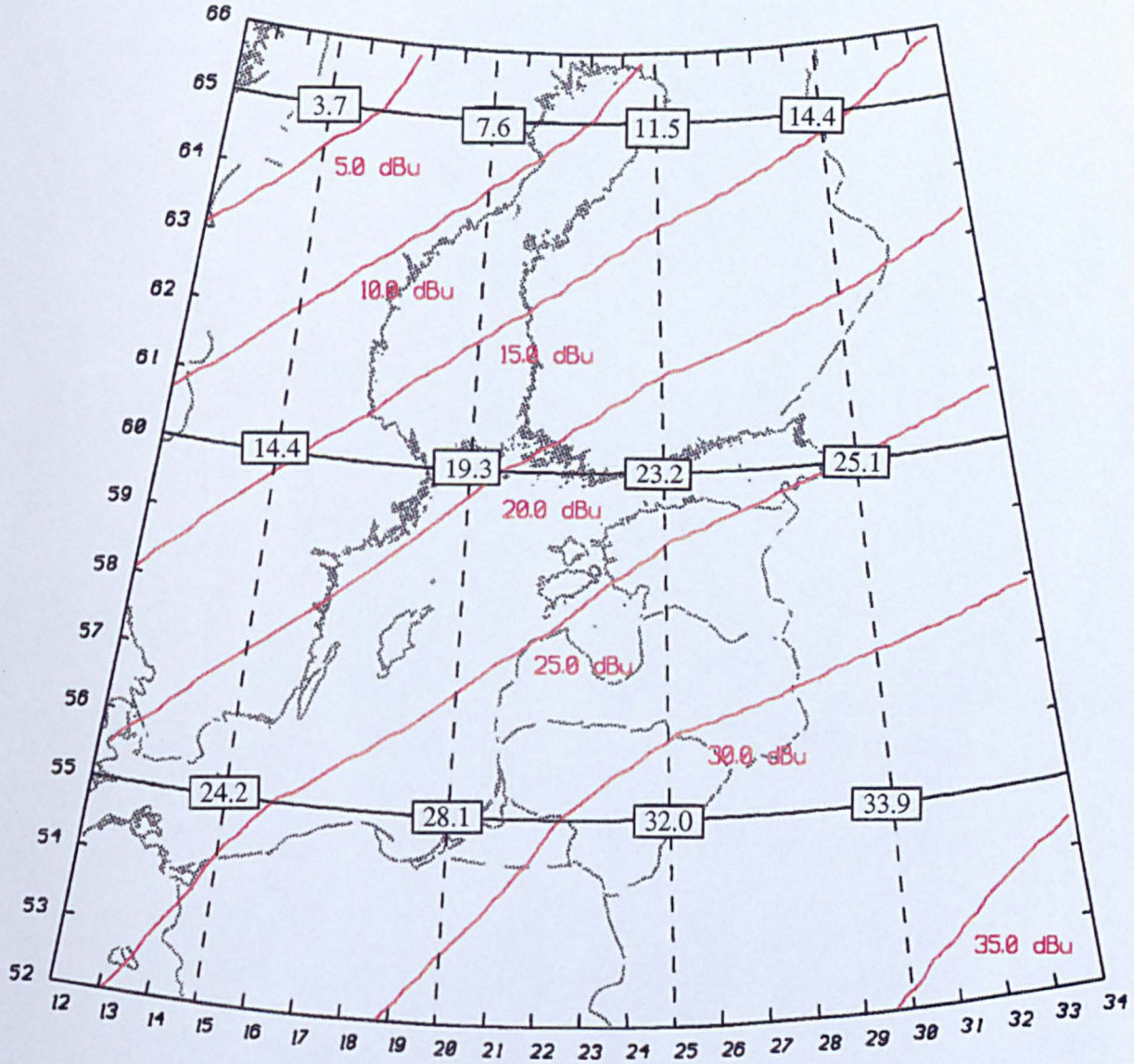

Figure 7.5: Contours of equal noise strength, interpolated from the values stored at the 5°–spaced noise points. The interpolation results in a smooth variation of noise values over the area of interest. These noise strengths are the values not exceeded 95% of the time in summer, 1600-2000.

next step is to compare the resulting SNR to the required SNR. Both USCG and ITU specify 7 dB as the minimum SNR (see Chapter 9) [11, 44].

SNR contours around Porkkala are shown in Fig. 7.6. The contours include the calculation points at which Porkkala's groundwave signal exceeds the 95% atmospheric noise by 7 dB or more. The differences between the three contours are in how the noise is defined. Within the outer-most contour labelled *1-point*, the level of noise employed at every calculation point is 11.4 dBμ, this being the 95% annual average of the noise at the noise database point closest to Porkkala, [60° N, 25° E]. The *Interp* contour uses a noise value at each calculation point calculated by interpolating the 95% annual average database values. These two contours are quite similar, but as the noise level decreases from north to south, the *1-point* contour slightly under-estimates the coverage to the north and slightly over-estimates it to the south, compared to the *Interp* contour. The inner-most contour *Worst* includes a dramatically smaller area than the other two contours. *Worst* employs as the noise value at every calculation point the worst-case value of the 95% noise, for any time-season block, at the point [60° N, 25° E]. This worst-case noise value, 24.1 dBμ, is 12.7 dB above the annual average value at the point; it occurs during the summer, 0000-0400, time-season block. This comparison demonstrates the effect that using this worst-case noise value has on coverage, resulting in what is certainly an overly pessimistic usable range for Porkkala.

Let us now consider the degree to which SNR limits coverage by studying the boundaries when both the 7 dB SNR and the 20 dBμ field strength minima are employed. In Fig. 7.7, the solid-line *Day* contour employs Porkkala's groundwave field strength and the interpolated, 95%, *Day* noise strength at each point to calculate SNR and compare it to 7 dB, with the added requirement that the field strength also meets its threshold. For comparison, the dashed-line *Day* contour drops this minimum field strength requirement. As can be seen, the factor limiting the *Day* coverage in this case is not atmospheric noise, but minimum field strength.

The *Night* coverage contours are produced in a similar way, except that now Porkkala's

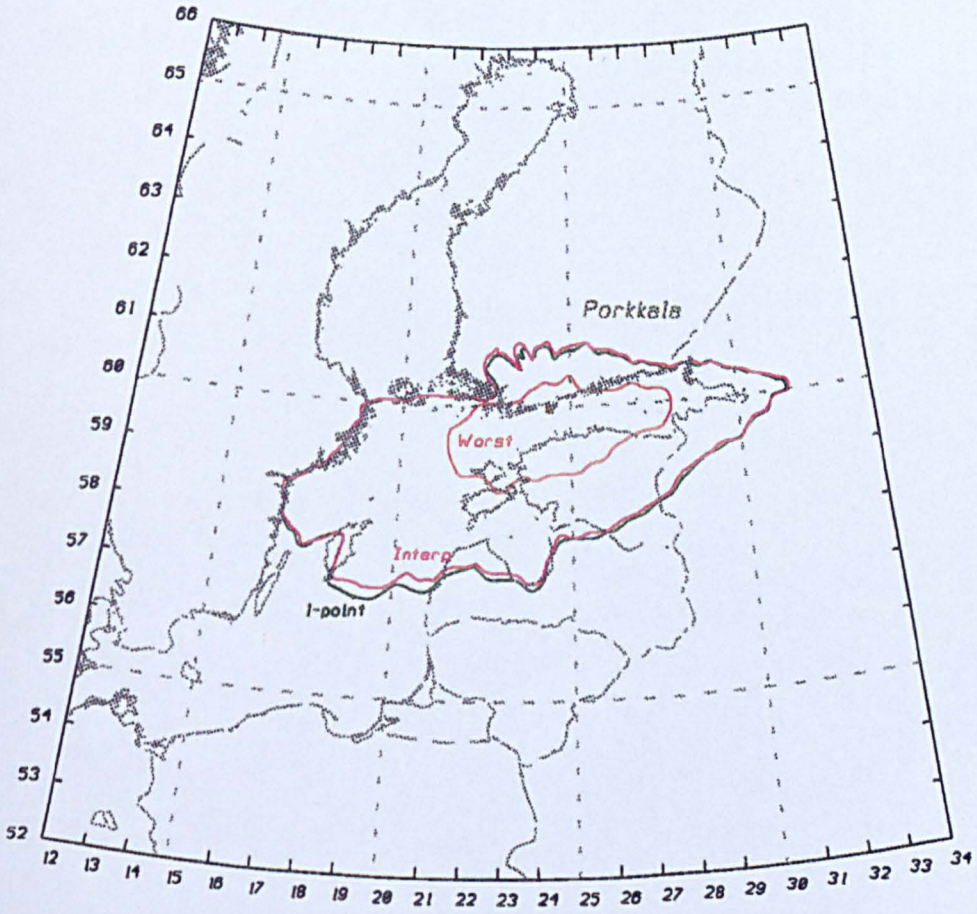

Figure 7.6: Three different SNR contours around Porkkala. *1-point* and *Worst* employ a single value of atmospheric noise, while *Interp* calculates an interpolated noise value at each calculation point.

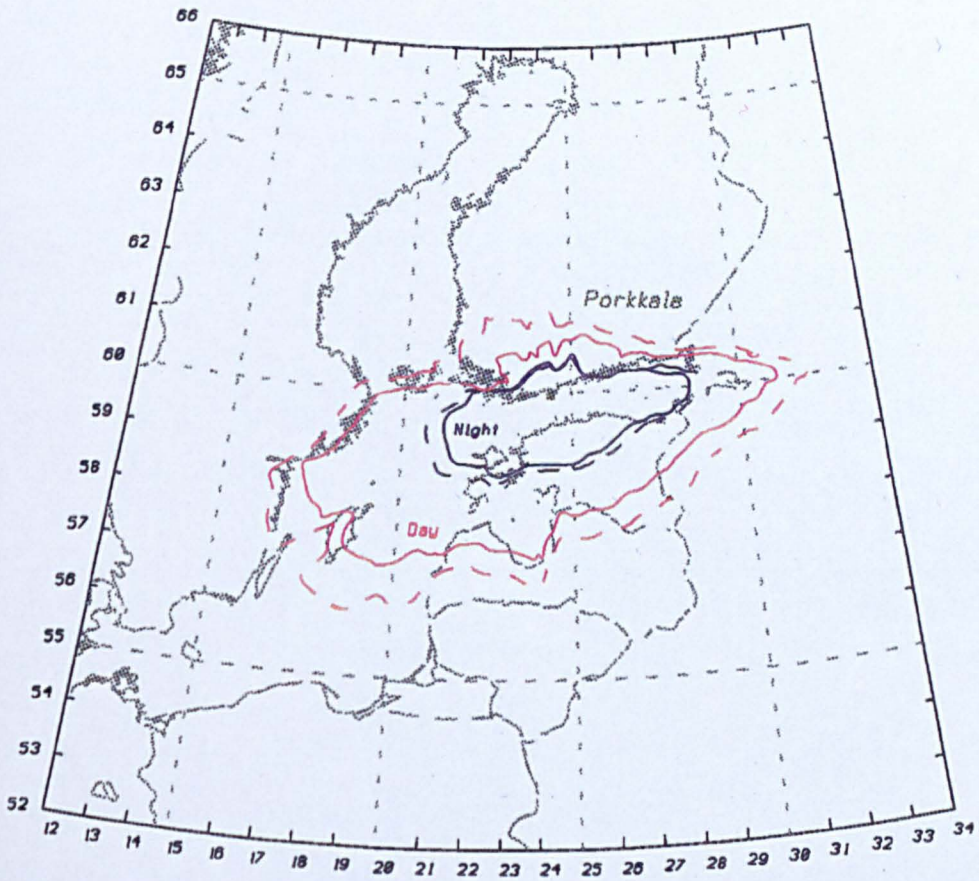

Figure 7.7: *Day* and *Night* contours around Porkkala. The solid line in each case employs the 7 dB SNR and 20 dBμ field strength minima, while the dashed line employs only the 7 dB SNR minimum. The SNR minimum nowhere appears to be the limiting criterion.

wanted field strength is computed using the skywave as well as the groundwave. The total field strength is compared to the 95% *Night* noise. Because of the skywave fading, the *Night* coverage is seen to be much less than the *Day* coverage. Yet by comparing the solid-line contour which includes that 20 dBμ threshold and the dashed-line contour which does not, we see that still it is the minimum field strength, and not the atmospheric noise, that limits the coverage. This is despite the inclusion of the higher levels of *Night* noise, the use of the 95% value and, what is, by European standards, a relatively-powerful beacon.

It could thus be deduced that in Northern Europe, where beacons are relatively low-powered and located well north of the equatorial storms, DGPS radiobeacon coverage may be limited by minimum field strength and not by atmospheric noise. To state

that, however, would be to assume that the SNR requirement of 7 dB specified reflects a realistic receiver specification in an atmospheric noise environment. This issue will be dealt with further in Chapter 9.

There are parts of the world, especially equatorial regions, where the atmospheric noise may be 50–60 dB stronger than here in Finland (see Appendix C). There, as can be imagined, atmospheric noise is generally the dominant factor limiting coverage.

7.6 Conclusions

Atmospheric noise in the radiobeacon band is due to storms, primarily in equatorial latitudes, with the noise propagating by both groundwave and skywave. CCIR publishes world maps of atmospheric noise levels for different time-season blocks, which show the noise strength to vary tremendously with both location and time and to a lesser, but still significant, extent with the season of the year. The statistical variation of the noise within the time-season blocks is also detailed by CCIR.

This noise information has been implemented in the radiobeacon band. In working with the CCIR data, a novel 'shift and scale' method was applied which both simplified the calculation of noise strengths and increasing the accuracy of the resulting value compared with reading each value from the curve. To allow noise to be incorporated into coverage predictions, it was determined that some sort of average strength should be considered. This average could consist of a simple annual average or separate night and day averages. In determining night and day averages, it has been demonstrated that the Decca skywave period information could be used to determine a weighted average of the different CCIR time-season blocks.

The noise information derived from the CCIR method has been implemented in the DGPS model as noise strengths at each of a series of regularly-spaced geographical points. To then recreate the 'continuous' noise distribution and allow each of the higher-resolution calculation points to have its own noise value, interpolation between

the noise points is performed. This results in smooth SNR contours, reflecting to a high degree the spatial variation in the atmospheric noise.

Interestingly, when the model was asked to include both the minimum signal strength requirements and the minimum SNR requirements for beacons in the Baltic region, the resulting coverage was seen not to be limited be atmospheric noise. It was questioned whether this occurred because the minimum SNR requirement does not accurately reflect receiver performance in the atmospheric noise environment. This issue will be dealt with in detail in Chapters 8 and 9.

Chapter 8

Interference

The previous chapter discussed the effect of atmospheric noise on the coverage provided by a beacon. Receivers may also be affected by the signals coming from other, *unwanted*, beacons. Unwanted beacons may broadcast on the same frequency as the wanted DGPS signal or on the adjacent channels. As the numbers of DGPS radiobeacons increase, so do the requests for frequency allocations in the limited marine radiobeacon bandwidth. The result is a crowded frequency band in which a receiver is listening to a complex blend of signals, one of which is the wanted signal, with many others which constitute unwanted interference. The level of interference will depend on the geographical and spectral distances between the wanted and unwanted beacons. As the strength of the interference becomes significant with respect to that of the wanted signal, the receiver's performance will be adversely affected and the DGPS correction data corrupted.

DGPS radiobeacons are relatively new additions to the marine radiobeacon band, originally reserved for direction-finding beacons for ships and aircraft. There are currently more than 400 marine, aeronautical and DGPS radiobeacon allocations in the European Maritime Area of ITU Region 1 (EMA). They occupy 64 channels between 283.5 and 315.0 kHz, with a channel spacing of 500 Hz. Their nominal ranges vary from 9 to 370 km. The European spectrum is definitely not a quiet environment in terms of interference! Table 8.1 shows a portion of the EMA radiobeacon list [85] which includes the now familiar beacon Porkkala, at its frequency of 285.0 kHz.

FREQ (kHz)	NAME	TYPE	COUNTRY	NR (km)
283.0	Kobbe	NDB	Norway	55
	Kolsnes	NDB	Norway	30
	Sandefjordlang	NDB	Norway	90
283.5	Bressey	NDB	Belgium	48
284.0	Almeria	NDB	Spain	24
	Gotska Sandoen	MB	Sweden	98
	Lizard Lstn	DGP	UK	129
	Memmingen	NDB	Germany	44
	Ninian Central	NDB	UK	46
	Ninian North	NDB	UK	48
	Pnt Silla	MB	Spain	88
284.50	C Machichaco	MB	Spain	183
	Duesseldorf	NDB	Germany	27
	Lizard Lstn	MB	UK	129
	Namdalseid	NDB	Norway	88
	Porkkala	MB	Finland	111
285.00	Barth	NDB	Germany	151
	C de la Nao	MB	Spain	88
	Granada	NDB	Spain	27
	Linkoeping	NDB	Sweden	31
	Nieuwpoort	MB	Belgium	9
	Ordjonikidzegr	NDB	Russia	201
	Porkkala	**DGP**	**Finland**	**160**
	Sollefteaa	NDB	Sweden	31
285.50	- None -			
286.00	Boden	NDB	Sweden	24
	C Figuera	DGP	Spain	74
	Hohenfels	NDB	Germany	44
	N E Frolois	NDB	France	46
	Sylt	NDB	Germany	185
	Tuskar Rock	MB	Ireland	92
286.50	Almagrundet	MB	Sweden	24
	Baily	MB	Ireland	9
	C Ferret	MB	France	183
	C Figuera	MB	Spain	88
	Daugavgriva	MB	Russia	59
	Frehel	MB	France	38
	Inchkeith	MB	UK	27
	La Chippa	MB	France	183
	Villacoublay	NDB	France	44
287.00	Almagrundet	DGP	Sweden	88
	C Ferret	DGP	France	74

Table 8.1: A portion of the EMA list of radiobeacons, including the Porkkala DGPS beacon. MB=marine beacon, DGP=DGPS beacon, NDB=aeronautical non-directional beacon, NR means Nominal Range.

8.2 Interfering ranges

The IALA frequency allocation procedure was designed for conventional marine and aeronautical beacons. These types of beacons are normally used only within their nominal ranges, with a relatively strong signal of 34 dBμ (or 37.5 dBμ, as appropriate) being guaranteed at the edge of coverage. DGPS radiobeacons, on the other hand, are customarily used well beyond this nominal range, out to signal levels of only 20 dBμ [11, 44]. This extension of range causes many potential interference problems, as the frequency allocations do not provide protection down to these signal levels [85]. When a user moves beyond a beacon's nominal range, the wanted signal becomes weaker and, in many cases, the interfering signals become stronger.

The IALA frequency allocation procedure is based on establishing that two beacons are sufficiently separated, taking into account the nominal range of one and the *interfering distance* of the other. A beacon's interfering distance is the range at which its field strength has fallen to 15 dB, (the co-channel protection ratio), below its value at nominal range. Ref. [107] then explains that the "minimum *protection distances* separating pairs of" (presumably co-channel) "radiobeacons is the lesser of the sum of the" (nominal) "range of one and the interfering distance of the other." For beacons at latitudes above 43°north, this means that the protection distance is the sum of the range at which one beacon's field strength is 34 dBμ plus the range at which the other's is $34 - 15 = 19$ $dB\mu$. The IALA method does consider both groundwave field strength and median skywave field strength in determining interfering distances. It is also suggested that some account be made of the reduction in the ranges over land paths, but the procedure is not well defined [107].

The IALA method is inadequate for ensuring there is no interference to the DGPS radiobeacon service. DGPS radiobeacons would need protection distances sufficiently great to allow for the range at which their field strengths had fallen to 20 dBμ; a range which would most likely, depending on ground losses, be greater than the nominal range. Additionally, ITU and USCG both specify protection ratios not just for the

beacon's own channel, but also for the four adjacent channels either side of it (Table 8.2). Since interference has the potential to reduce coverage, the calculation of the signal-to-interference ratio must be included in the DGPS model. In principle, the field strength of every unwanted beacon on each of these nine channels, received by both groundwave and skywave paths, must be calculated at every point in the wanted beacon's calculation array.

The field strengths of the groundwave- and skywave-propagated signals from the unwanted beacons can, of course, be calculated using the same methods as were employed for the wanted beacon's signals (see Chapters 4 and 5). Thus it would be straightforward to implement a 'brute force' approach to calculating the field strengths of all the many unwanted signals. This would require the model to read the EMA frequency list [86], identify all unwanted beacons within 2 kHz of the wanted beacon's frequency and calculate the groundwave and skywave field strengths for every beacon at every calculation point. However, this would be a huge computational task and, for the model to be a valuable tool for coverage prediction and planning, its running time must be kept acceptably short. Thus it is desirable to find ways of excluding from the calculation those beacons whose interference is, in fact, negligible.

One way of identifying those beacons is by determining the maximum range at which the signal from any potential interfering beacon can reduce the SIR below its allowed minimum, assuming that the wanted signal has fallen to its minimum field strength of 20 dBμ. This is similar, in principle, to determining the IALA interfering distance; let us call what we are computing the *DGPS interfering range.* This range is the maximum range at which an unwanted beacon can exceed a field strength of 20 dBμ minus the appropriate protection ratio. We will need separate groundwave and skywave DGPS interfering ranges.

8.2.1 Groundwave DGPS interfering ranges

Consider a worst case. The most powerful in-band beacon of any kind in the EMA has a nominal range of 370 km. If this were an unwanted, co-channel, transmission its groundwave DGPS interfering range would be that range at which its field strength had fallen to $20 - 15 = 5$ dBμ over an all sea-water path (from Table 8.2). We choose an all sea-water path because we want to find the *maximum* range at which this can occur. By using the curves of groundwave field strength versus range, adjusted for a 370 km beacon, the 5 dBμ field strength is found to lie at a range of 1188 km. This, therefore, is the maximum groundwave DGPS interfering range.

Now consider the wanted DGPS signal. The most powerful *DGPS* radiobeacon in the EMA currently is the Finnish station Mantyluoto which has a nominal range of 180 km. Mantyluoto's groundwave signal strength falls to the 20 dBμ threshold at a maximum range of 550 km, again assuming a sea-water path. Taking this to be the maximum range of any wanted DGPS beacon and adding to it the unwanted beacon's maximum DGPS interfering range of 1188 km gives a maximum *DGPS protection range* for co-channel beacons of 1738 km. Thus, if an unwanted, co-channel, beacon is located further from the wanted beacon than 1738 km, the interference it can cause need not be taken into account and the beacon may be dropped from the list of potential interferers.

If the unwanted beacon has a shorter nominal range, its DGPS interfering range is correspondingly reduced. Similarly, if the unwanted beacon is located on an adjacent frequency channel, then it is subject to a less stringent protection ratio and again its DGPS interfering range is reduced. Table 8.3 lists the calculated groundwave DGPS interfering ranges for all the protection ratio values specified and for five different bands of nominal range. The nominal range bands have been introduced to help eliminate the large numbers of relatively short-range beacons; it would be inefficient to apply the worst-case limit to them.

Combining these maximum interfering ranges with the maximum, 550 km range of a wanted beacon gives the worst-case protection ranges between beacons needed to avoid

Maximum Groundwave DGPS Interference Ranges (km)					
Protection Ratio (dB)	Nominal Range of Interferer(km)				
	370 - 300	299 - 200	199 - 100	99 - 50	49 >
15	1188	1100	958	763	588
-22	195	145	87	42	22
-25	144	105	62	31	16
-36	44	32	19	10	4
-42	23	17	10	4	2
-45	17	12	7	3	1
-47	13	9	5	2	1
-50	10	7	4	2	—
-55	6	4	3	1	—

Table 8.3: Maximum *DGPS interfering ranges*, in km, for unwanted groundwave-propagated signals. As the protection ratio and the nominal range decrease, so does the the DGPS interfering range.

groundwave-propagated interference. As we have seen, for strong, co-channel, interfering beacons, geographical separations of up to 1738 km may be necessary to avoid interference via groundwave. Even the lowest-powered group of co-channel beacons still need to be about 1000 km away if the area in between is sea-water. For interfering beacons on the adjacent channels, the required DGPS protection ranges are much less, but interference is still possible from powerful beacons located less than 750 km away. If these beacons are of lower power, groundwave DGPS interfering ranges become small, requiring only that the unwanted beacon be not located inside the wanted beacon's coverage area. If this rule is broken, even low-power beacons may cause interference in their immediate vicinity.

8.2.2 Skywave DGPS interfering ranges

The same considerations should now be applied to interference propagated by skywaves at night. Again considering a minimum wanted signal strength of 20 dBμ, maximum skywave DGPS interfering ranges have been calculated and are given in Table 8.4. With skywave, the field strength has a statistical distribution (see Chapter 5). At percentiles up to 97.1%, the only interfering beacons which are significant are co-

Maximum Skywave DGPS Interfering Ranges (km) Co-Channel Signals					
Skywave Percentile	Nominal Range of Interferer(km)				
	370 – 300	299 – 200	199 – 100	99 – 50	49 >
50%	2050	1790	1400	920	540
95%	3602	3104	2563	1822	1217
96.5%	3680	3309	2675	1903	1298

Table 8.4: Maximum skywave *DGPS interfering ranges*, in km, for unwanted skywave-propagated signals. Due to the protection ratios, skywave interference is only possible from co-channel beacons. As the skywave percentile increases, so does the maximum interference range.

channel ones; the skywave signal from beacons on the adjacent channels never reach strong enough levels to cause the adjacent-channel SIRs to fall below their limits. However, because the skywave signals propagate over long distances with relatively uniform field strengths, the maximum skywave DGPS interfering ranges for these co-channel skywave-propagated signals are very great. Powerful interfering beacons need to be separated by more than 2000 km to avoid night-time interference.

8.3 Implementation

Recall that the calculated arrays of groundwave and skywave field strengths of wanted beacons have been restricted to points located within 550 km of the beacon (see Chapter 4). It is at these points that the field strengths of the unwanted beacons need to be calculated, subject to the points also being within the unwanted beacons' DGPS interfering ranges. It is very possible that a calculation point may fall inside the DGPS interfering range of more than one unwanted beacon. Apparently, the ITU protection ratios apply to each unwanted signal on an individual basis [11]; that is, the DGPS model should not combine these multiple signals by using, say, a root-sum-square or some other method. Instead, the model should determine which of the unwanted beacons is the strongest interferer at that point, then store its strength in an array. That has been done. It will be seen that, employing the model has shown that if there is significant interference at any point it is usually due to a single, dominant, interfering

signal. The total interference at any point is thus well approximated by the strength of that strongest interferer.

8.3.1 Interfering strength

Determining which unwanted beacon is the strongest interferer is not entirely straightforward. A way needed to be found for comparing the field strengths of unwanted beacons on different channels which are, consequently, subject to different protection ratios. A novel method has been devised which not only allows these comparisons to be made, but simplifies the later procedure of checking the SIR at each point to determine whether the point meets the coverage limitations. This new method requires the model to convert the field strength received from an unwanted beacon into an *interfering strength*, defined as the unwanted beacon's field strength weighted by its protection ratio, which depends on its frequency and type, as given in Table 8.2. So, for a co-channel beacon of any type, the interfering strength is the unwanted field strength plus 15 dB; an MB on one of the *first adjacent* channels (±500 Hz) would have an interfering strength given by the unwanted field strength plus -25 dB. These two interfering signals can now be compared directly and the larger saved in the array. This compare-and-store operation is done separately for groundwave and skywave signals, so allowing day and night coverages to be predicted. The model now contains a *groundwave interference array* and a *skywave interference array.* As was the case with groundwave and skywave wanted signal strengths (Chapters 4 and 5), these interfering strengths need be calculated once only, stored to file, and subsequently called up when coverage is being determined.

To allow the dominant source of interference to be more easily identified, the DGPS model actually stores three interfering strengths at each point: the groundwave-propagated co-channel, the groundwave-propagated adjacent-channel (*i.e.* that on any of the 8 adjacent channels) and the 50% skywave-propagated co-channel. In practice it is found that the greatest losses of coverage are due to co-channel interference. An adjacent-channel beacon must be located relatively close to the edge of the wanted beacon's

area to cause any problems, as was indicated in Tables 8.3 and 8.4.

8.3.2 Flow of the model

Let us trace through the steps for calculating the groundwave interference arrays for Porkkala. The calculation of the single, co-channel, skywave protection array is done in a similar manner. The details of the groundwave field strength calculation are to be found in Chapter 4.

The model first gets the name, location, beacon window and frequency of Porkkala. It then scans the EMA frequency list to locate all unwanted beacons within 2 kHz of Porkkala's frequency. As each is found, its distance from Porkkala is calculated and compared with the appropriate protection range. If the unwanted beacon is located within this protection range, it is put on a list of potential interferers. The resulting list of potential groundwave interferers to Porkkala is shown in Table 8.5. These eight unwanted beacons are a subset of the 40 unwanted beacons within 2 kHz of Porkkala's frequency (Table 8.1). Notice that there are four co-channel beacons, two of which are quite powerful: 'Barth' in Germany, with a nominal range of 151 km and 'Ordjonikidzegr' in Russia, with 201 km. For each of the eight potential interferers, the model must now calculate the Δ_P strength adjustment that adjusts the CCIR groundwave attenuation curves for each beacon's nominal range (see Chapter 4). The model than adds to this Δ_P the appropriate protection ratio, based on the frequency separation between the unwanted beacon and Porkkala and its type. This step implements the conversion from groundwave field strength to groundwave interfering strength.

Next, the groundwave interfering strength is calculated point-by-point. At each point, the model determines if each unwanted beacon is within its interfering range of the point. If it is, then the groundwave interfering strength is calculated. This is done by following the same steps as were used in calculating groundwave field strength of the wanted beacon, with the protection ratio information now incorporated into Δ_P. The process is repeated for all (eight) unwanted beacons. The resulting interfering

Potential Interferers to Porkkala				
Name	Type	NR (km)	Protection Ratio (dB)	Range from Porkkala (km)
Barth	NDB	151	15	936
Linkoeping Mal	NDB	31	15	536
Ordjonikidzegr	NDB	201	15	954
Sollefteaa	NDB	31	15	526
Porkkala	MB	111	-25	co-located
Gotska Sandoen	MB	98	-45	342
Almagrundet	MB	111	-50	307
Almagrundet	DGP	88	-47	307

Table 8.5: Potential groundwave interferers to Porkkala. The first four of these are co-channel beacons, the last four are adjacent-channel beacons.

strengths of all the co-channel beacons within range are compared and the greatest strength saved. Separately, the greatest interfering strength of all the adjacent-channel beacons is determined and stored.

The results of these operations are a co-channel and an adjacent-channel groundwave interference array for Porkkala. Fig. 8.1 plots a 3-d contour of the co-channel array, the height of the contour showing the strength of the co-channel interference. Remember that these interfering strengths, which exceed 60 dBμ, are 15 dB stronger than the field strengths of the unwanted beacon. The outstanding feature here is the high level of interference to the south-west of Porkkala. This comes from Barth, the signals of which reach the Porkkala area primarily via sea-water paths. Barth's DGPS interfering range reaches just past Porkkala towards the north-east, beyond which its interfering strength is no longer calculated. The peaks to the west and north-west of Porkkala are due to the 'Linkoeping Mal' and 'Sollefteaa' beacons, respectively. With nominal ranges of only 31 km, these beacons cause significant interference only locally. To the south-east of Porkkala is Ordjonikidzegr with its nominal range of 201 km. Although a more powerful beacon than Barth and located about the same range from Porkkala, its resulting groundwave interfering strengths are much lower since they must reach the area via overland propagation paths.

In determining interference arrays, priority has been given to ensuring that the model

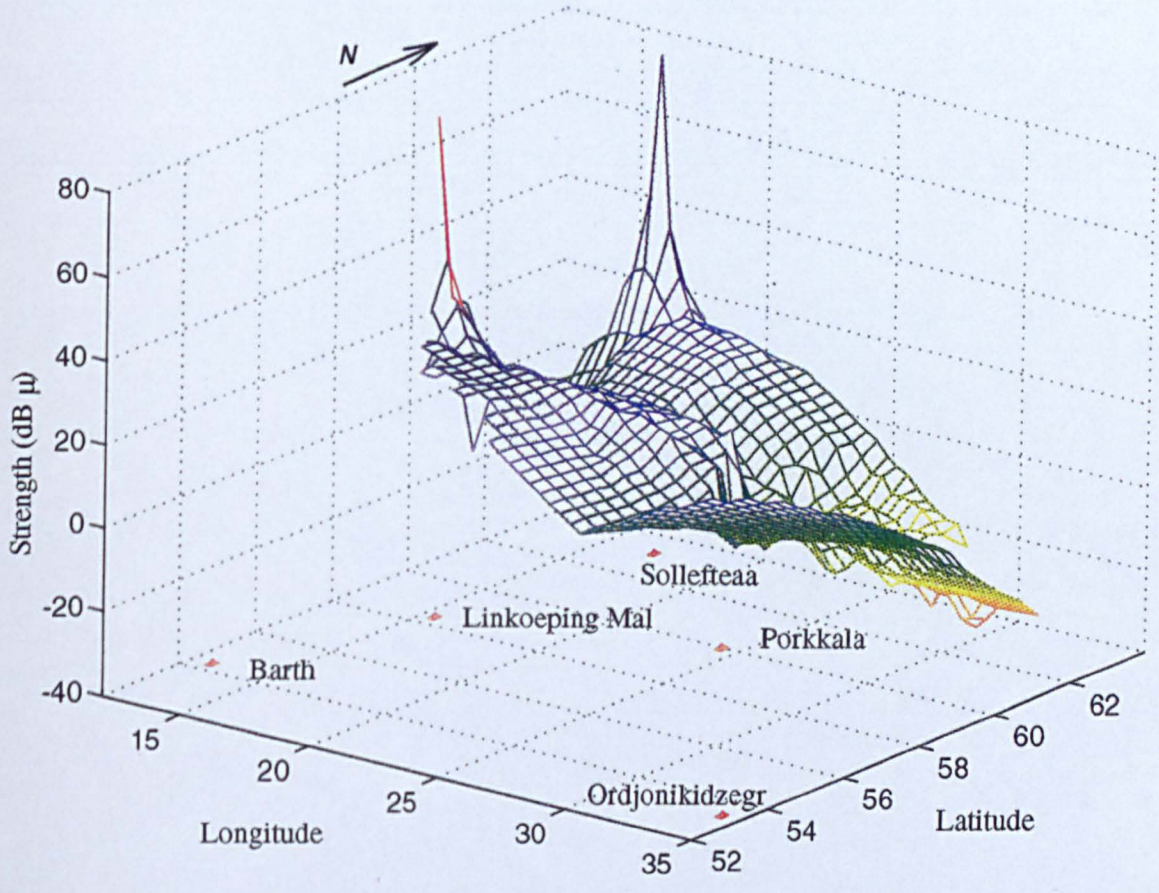

Figure 8.1: A 3-d contour plot of groundwave, co-channel, interfering strengths around the wanted beacon Porkkala. This beacon has four co-channel interferers, as indicated, all of which are located within 1000 km.

Frequency Separation kHz	Wanted Beacon Type : DGPS	
	Interfering Beacon Type	
	MB, NDB	DGPS
0.0	15	15
0.5	-25	-22
1.0	-45	-36
1.5	-50	-42
2.0	-55	-47

Table 8.2: ITU *protection ratios*, in dB, between wanted DGPS and interfering transmissions. The left-hand column is the frequency separation between the wanted and unwanted signals. Different protection ratios are prescribed when the interference is caused by a marine beacon (MB) or aeronautical NDB from those when a DGPS transmission is the interferer.

8.1 Protection ratios

The burden of coping with interference is shared between the system planner and the receiver designer. The link between them is formed by the *protection ratios* which define the minimum signal-to-interference ratio (SIR) which a receiver must tolerate within a beacon's coverage area. The receiver design must include filtering and processing such that it can operate with these specified minimum level of SIR [87, 106]. In turn, the system planner must verify that a beacon's coverage includes only those areas in which these protection ratios are not exceeded. This means ensuring that any neighbouring beacons are sufficiently separated in distance or frequency from the wanted beacon.

Table 8.2 lists the protection ratios specified by ITU and USCG for the DGPS radiobeacon service [11, 44]. These are the minimum SIRs allowed between the wanted beacon signal and any other beacon signal; *15 dB* means a wanted signal at least 15 dB greater than the unwanted signal. The protection ratios vary with the frequency separation between the wanted and unwanted signals, with co-channel (0 Hz separation) protection ratios, of course, being the most stringent. Different values are prescribed when the interference is caused by a marine beacon (MB) or aeronautical non-directional beacon (NDB) from those when a DGPS transmission is the interferer, since the first two transmit only carrier-waves while the latter is a narrow-band modulated signal.

works efficiently. If the model were to apply a 'brute force' method in calculating Porkkala's groundwave interference arrays, it would take about 10 hours. There are, after all, 40 potential interferers and 20,000 calculation point for each one! After taking into account the frequency and geographical separations of the unwanted beacons, eliminating negligible interferers and limiting the calculation range of those remaining, this time is reduced to only about 10 *minutes*!

8.3.3 Coverage examples

The effect of interference on Porkkala's coverage is shown in Fig. 8.2. To explain the figure, the *G-20* contour contains all points at which Porkkala's field strength exceeds the minimum value of 20 dBμ. The *Gnd* contour adds the requirement that the signal-to-groundwave-interference ratio meets ITU protection ratio criteria. The effect of interference from Barth is evidenced by the large loss in coverage over the Baltic Sea. Note the effect of the island Gotland, which attenuates Barth's groundwave signal so that the coverage of Porkkala is not reduced to the north of the island. There is no other coverage loss due to groundwave interference.

The *T-20* contour includes all points at which Porkkala's combined, groundwave-plus-95% skywave, field strength (*i.e.* the night value) exceeds 20 dBμ. The *Total* contour adds the requirement that both the groundwave interference and the 95% skywave interference levels meet ITU protection ratio criteria. The effect of long-range, skywave, interference is seen here, with the coverage reduced in all directions. This interference comes from both Barth and Ordjonikidzegr, with the latter's signal no longer attenuated by its overland propagation path.

Fig. 8.3 shows similar contours for Almagrundet. Here, in contrast, is a beacon that suffers NO loss of coverage due to interference. Thus the *Gnd* contour extends out to the groundwave signal's 20 dBμ range and the *Total* contour extends out to the 95% combined signal's range. The reason for this lack of interference is seen by examining Table 8.6, which lists the potential interferers to Almagrundet. There are no co-channel

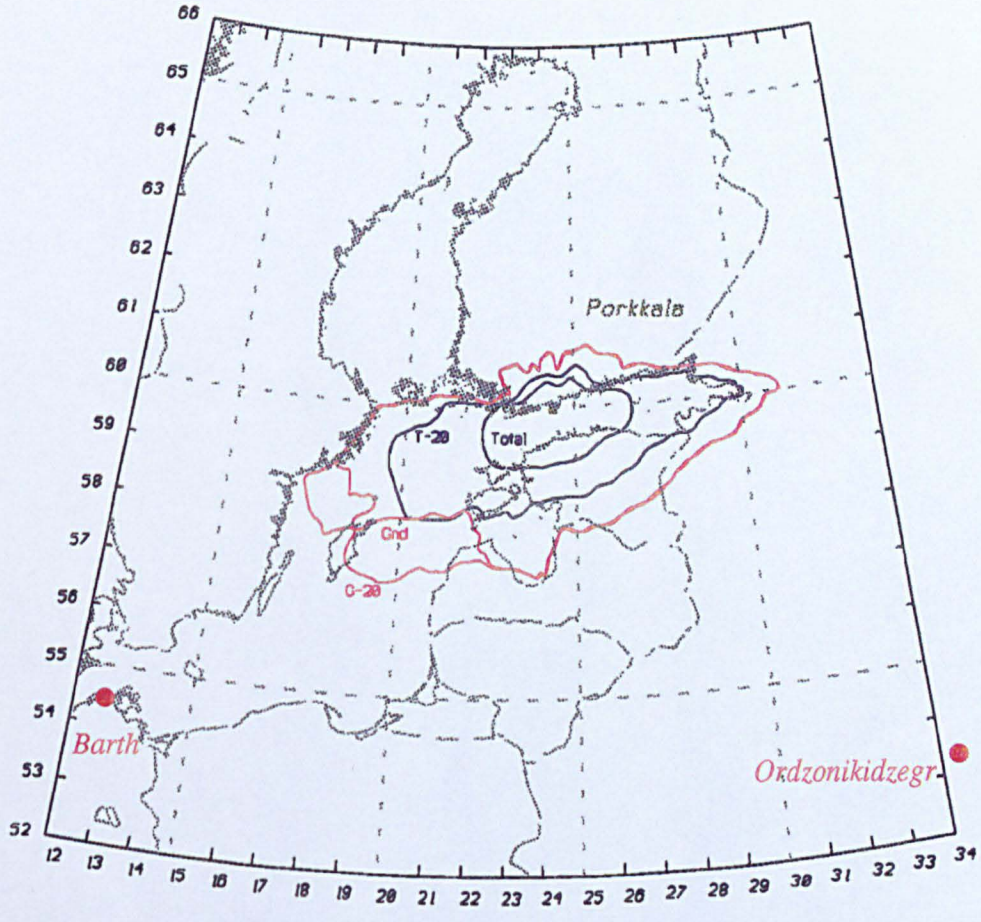

Figure 8.2: The effect of interference on Porkkala's coverage. The *G-20* contour is Porkkala's 20 dBμ groundwave contour. The *Gnd* contour adds the effect of interference; a loss of coverage is seen over the Baltic Sea. Similarly, at night, *T-20* is the 95% combined field strength contour and *Total* adds the effect of both groundwave and 95% skywave interference. This night skywave interference (from Barth and Ordjonikidzegr) causes the coverage to be reduced substantially in all directions.

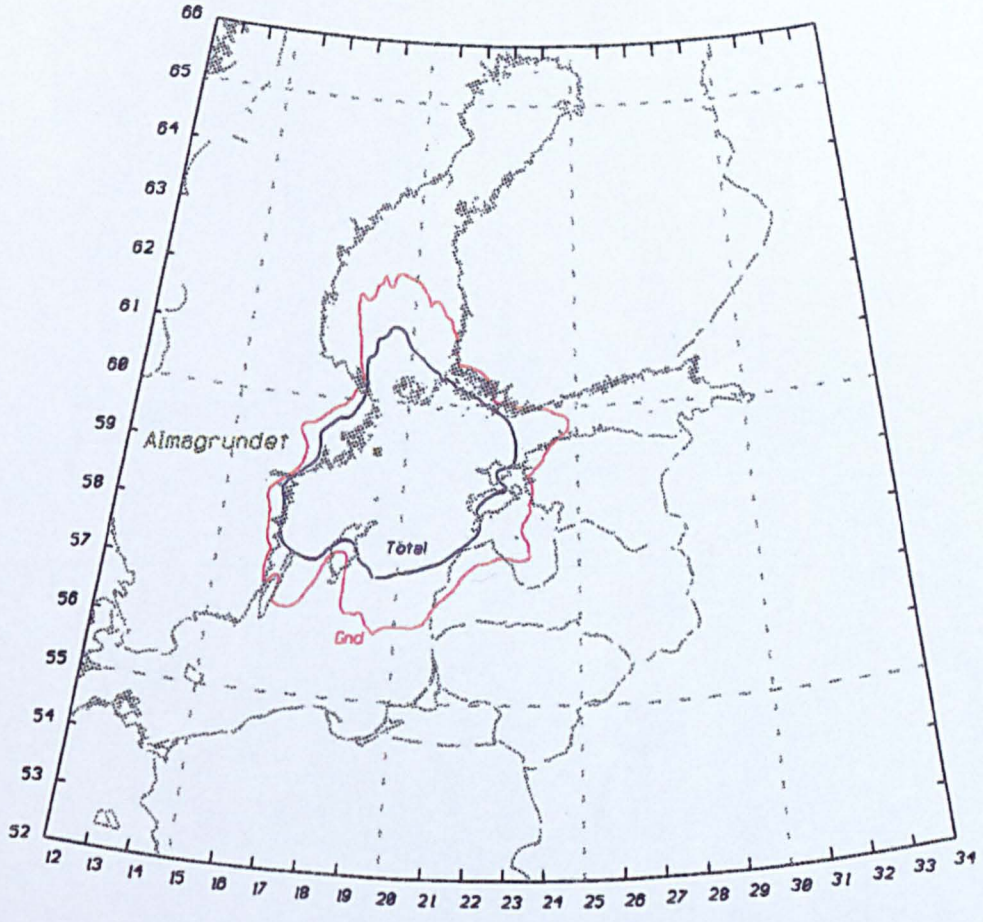

Figure 8.3: The coverage around Almagrundet, which suffers no loss due to interference by day or by night. Almagrundet's only co-channel beacon is located in western France! *Gnd* and *Total* as in Fig. 8.2

beacons at all, so no skywave interference is experienced. In fact, Almagrundet's only co-channel beacon is 'C Ferret', located in western France!

The ranges of Almagrundet from its adjacent-channel potential interferers are long enough that, as it turns out, no significant groundwave interference is experienced. What is most outstanding is that the predicted night-time coverage of Almagrundet is a much larger area than that of Porkkala, yet Almagrundet has only some half the nominal range of Porkkala, only 88 km versus 160 km! This highlights how essential it is to include interference in the coverage prediction process.

The model's new abilities have been applied to current DGPS system planning. In one instance, the model has highlighted the sources of severe groundwave- and skywave-

Potential Groundwave Interferers to Almagrundet				
Name	Type	NR (km)	Protection Ratio (dB)	Range from Almagrundet (km)
Almagrundet	MB	111	-25	co-located
Braemoen	MB	129	-25	349
Faerder	MB	127	-25	494
Halli	NDB	31	-45	426
Faerder	DGP	103	-36	494
Hammerodde	DGP	88	-47	503
Porkkala	DGP	160	-47	307

Table 8.6: Potential interferers to Almagrundet. All these are adjacent-channel beacons, so only groundwave interference is possible. In fact, this also turns out to be negligible.

interference to the DGPS beacon Flamborough, in the UK. This beacon had been giving a disappointing service and, examining Flamborough's predicted coverage, this interference could be clearly attributed to two specific co-channel interferers. Table 8.7 shows the co-channel beacons, with 'Myggenaes' and 'I D'Yeu Phare' relatively close and powerful, a situation not unlike Porkkala's. Because of these interferers, Flamborough's usable range was reduced to its 129 km nominal range, even less over land paths. It was suggested that it would be prudent to swap frequencies with the co-sited marine beacon and so greatly improve coverage. The marine beacon had only one co-channel beacon, a 33 km NDB in Russia, a situation similar to that of Almagrundet. The frequency swap was implemented and the now adjacent-channel interferers cause little or no loss of coverage to the DGPS beacon. The increased interference to the marine beacon is not significant within its nominal range which is, of course, much less than the '20 dBμ range' of the DGPS beacon.

8.4 Conclusions

The European radiobeacon band is crowded with marine, aeronautical and now DGPS radiobeacons. The IALA frequency allocation procedure is designed to guarantee simply that the minimum, co-channel, protection ratio is met within each beacon's nominal

NAME	TYPE	COUNTRY	NR (km)
Bjoernoeya	MB	Norway	185
Falserborev	MB	Sweden	79
I D'Yeu Phare	MB	France	185
Marjaniemi	MB	Finland	129
Myggenaes	MB	Denmark	277
Rota	MB	Spain	146

Table 8.7: The co-channel interferers to Flamborough's DGPS beacon, before its frequency was swapped with that of its co-located MB.

range. This procedure has been examined and found to be inadequate for guaranteeing that DGPS radiobeacon systems are free from interference. The inadequacies result from the system specifications requiring protection not only against co-channel interference, but also interference on four adjacent-channels each side. The frequency allocation procedure considers only the co-channel beacons to be potential interferers. The underlying problem, though, is that DGPS radiobeacons are used use well beyond their nominal range field strengths, down to 20 dBμ.

A method has been developed for predicting the effect of interference on coverage, with priority being given to ensuring that it works in an efficient manner. The method employs the techniques for calculating groundwave and skywave field strengths described in Chapters 4 and 5 to compute interference arrays around a wanted beacon.

Time-efficiency is achieved by reducing wherever possible the number of points at which an interferer's field strengths must be calculated. By taking into account the frequency and the geographical separations between wanted and unwanted beacons, the number of unwanted beacons for which point-by-point calculations must be done has also been greatly reduced. Unwanted beacons causing negligible interference are eliminated and the area over which point-by-point field strength calculations must be made for potential interferers is limited to within their interfering ranges. A technique of comparing interfering strengths has been implemented to determine the strength of the strongest interferer at each calculation point.

By comparing the calculated interfering strength and the wanted beacon's field strength,

the model can identify points at which coverage is lost due to interference. This procedure has been demonstrated using the beacons Porkkala and Almagrundet, one of which is severely hampered by both groundwave and skywave co-channel interference and the other which enjoys a quiet channel and interference-free coverage. These examples also serve to emphasize that coverage loss due to interference is usually caused by co-channel interferers.

Chapter 9

Performance Contouring

Accuracy contouring identifies the areas within which the user will meet various minimum positioning accuracies. The estimated DGPS positioning accuracy depends on all the factors described in Chapters 4 to 8, which predict the levels of signal, noise and interference affecting the radiobeacon receiver. If no differential corrections are received, the achievable accuracy is that of stand-alone SPS GPS, that is 100 m 95% of the time, or 500 m 99.7% of the time [1]. Positioning results achievable by applying RTCM corrections received via a DGPS radiobeacon link have been extensively evaluated and found to be generally better than 10 m, often reaching the 1 m level [19, 108, 109, 110]. To achieve this high accuracy, the reference station and the user must experience the same pseudorange errors; differences of pseudorange error may be due to either temporal or spatial decorrelation. These factors will now be examined, with a view to devising a way of determining contours of position accuracy within the coverage boundary.

9.1 Spatial decorrelation

Spatial decorrelation of the pseudorange corrections is due mainly to differences between the ionospheric delays affecting the signals measured by the reference station and those measured by the user. It is not expected to be a limiting factor at reference station-user separations within the coverage ranges of DGPS radiobeacons. The worst-case difference may be estimated from Fig. 9.1, from [18]. The plot shows the

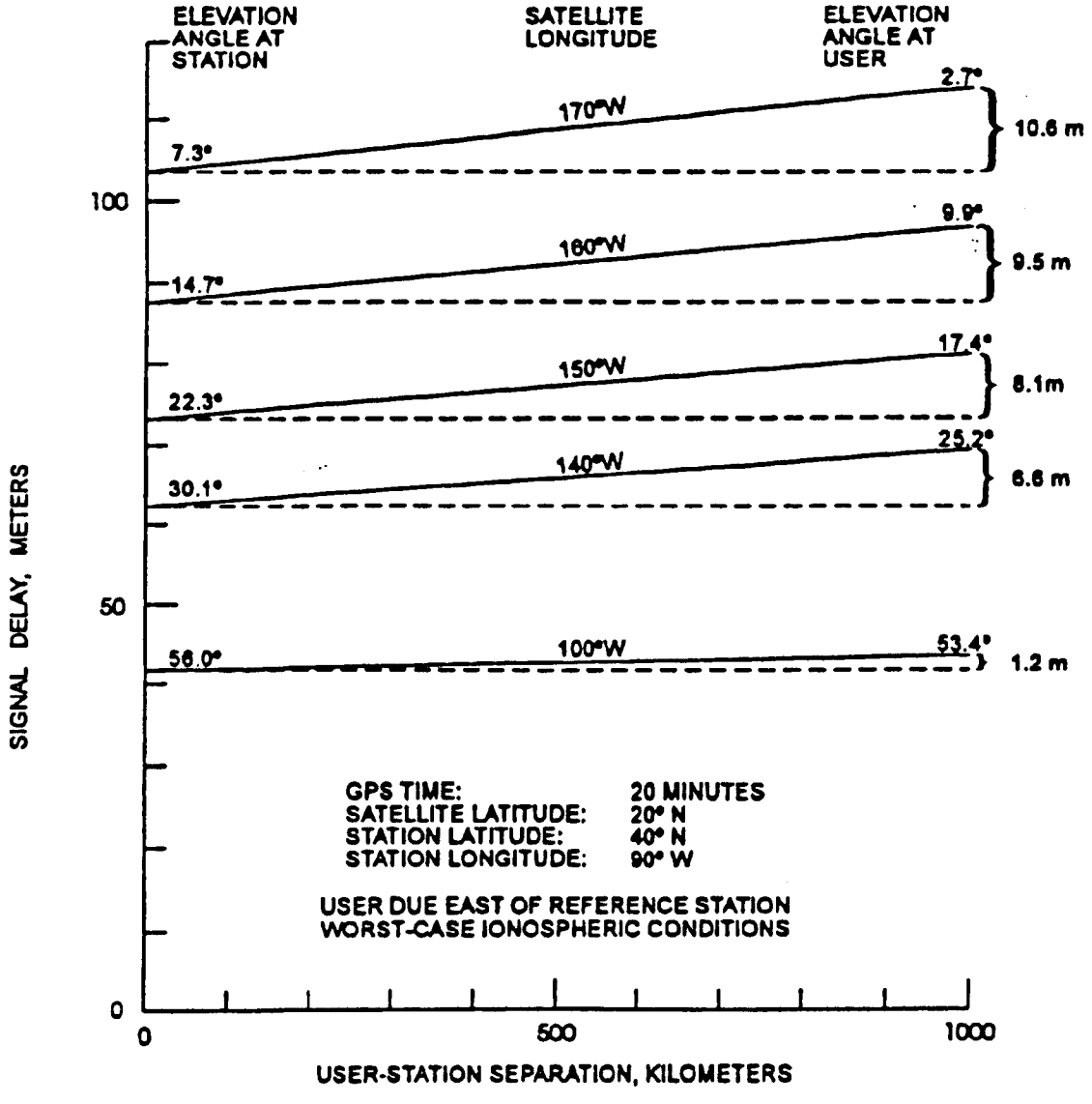

Figure 9.1: The variation in ionospheric signal delay as a function of user-reference station separation distance and satellite elevation, from [18]. The plot shows a typical satellite over-pass, and assumes worst-case ionospheric conditions for the GPS ionospheric model employed.

signal delay as a function of the separation between the user and the reference station, as derived by RTCM using the standard GPS ionospheric model [18, 24]. This plot assumes that no ionospheric correction is applied by either the user or the reference station; RTCM decided that, in normal operations, that should be the case for the reference station. Their justification for this decision considers two scenarios: at small separations, the reference station and user will experience similar errors and the PRCs will remove most of the ionospheric effect. At greater distances, the reference station and the user may experience different delays. In this case, the ionospheric model can be applied to the received PRCs by the user using the reference station's known location and to the receiver's pseudoranges using the user's location. This places the decision on whether or not to apply the model in the user's hands and also simplifies the implementation, at a later date, of better ionospheric correction models, as only the user equipment would then need to be upgraded.

The difference in the ionospheric signal delays at the reference station and the user's location depends on the angle of the elevation of the satellite and the spatial variations in the TEC of the ionosphere (see Chapter 2). In Fig. 9.1, the largest difference in signal delay is seen to occur when the satellite is at a longitude of 170° west and the elevation angle at the user is only 2.7°. This is a much lower-elevation satellite then would normally be used, but even so it results in a spatial decorrelation of only 10.6 m at 1000 km separation. Increasing the user's viewing angle to a more realistic 10°reduces the spatial decorrelation to 9.5 m. At the edge of coverage of a DGPS radiobeacon of the maximum nominal range used in Europe, 550 km, the spatial decorrelation is 5.5 m. This error would be reduced if the user were to apply an ionospheric correction model at the edges of coverage. As these worst-case ionospheric conditions result in errors of the order of the best-case DGPS positioning results, it can be concluded that the spatial decorrelation of the PRCs is not a limiting factor for DGPS radiobeacons.

Because information about the spatial variation of the ionosphere is quite limited [21, 23] and the worst-case ionospheric conditions suggest that it is not a limiting factor, it was decided that this factor should not be included in the model.

9.2 Temporal decorrelation

Temporal decorrelation of the PRCs is due to the time-varying nature of the GPS error sources. As the time between the calculation of a PRC by the reference station and its application by the user increases, the accuracy of the user's differential position solution decreases. Most GPS error sources vary relatively slowly, the pseudorange value only changing significantly over hours. This is the case for the ranging errors due to ionospheric and tropospheric delays, clock bias, ephemeris error and SA ephemeris manipulation. The exception is the SA clock dither, by far the most rapidly-varying (and largest) of the SPS error sources, which causes a typical position error velocity of 0.5 m/s, say 15 m over 30 s [17].

The RTCM message format has been designed to reduce the 30 s positioning error from 15 m to 5 m. As was discussed on Chapter 2, this is done by sending not only the pseudorange corrections but also range-rate corrections, that is the rate of change of each PRC. Doing this allows the user to extrapolate the PRC forward in time by assuming that it changes at a linear rate [18]. The convention is for the PRC to be added to the user-measured pseudorange:

$$PR(t) = \rho(t) + PRC(t), \tag{9.1}$$

$$PRC(t) = PRC(t_0) + RRC(t - t_0). \tag{9.2}$$

At time t, $PR(t)$ is the differentially-corrected pseudorange, $\rho(t)$ is the pseudorange measured by the user, $PRC(t)$ is the pseudorange correction. $PRC(t_0)$ and $RRC(t_0)$ are the pseudorange and range-rate corrections calculated by the reference station at time t_0. The resulting growth in the error is given by

$$E(t) = HDOP \cdot (k_1 + a \cdot t^2), \tag{9.3}$$

where $E(t)$ is the 2drms error at time t, $HDOP$ is the Horizontal Dilution of Precision, k_1 is the 1-σ reference station positioning error due to surveying inaccuracies and a the 1-σ SA acceleration, typically 0.0037 m/s^2. This value of SA acceleration is an experimental value, the determination of which is detailed in [17]. The expected growth

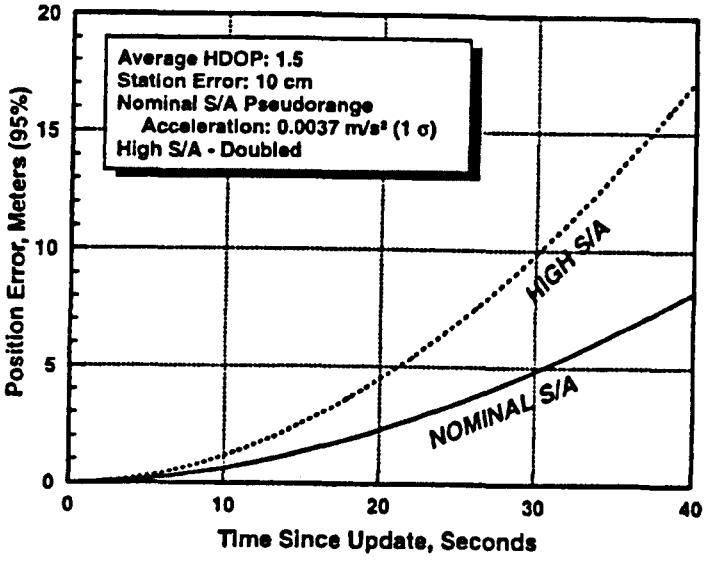

Figure 9.2: The expected error growth due to SA, after applying the RTCM-type corrections, from [18].

of the positioning error due to SA, after applying the RTCM-type corrections, is shown in Fig. 9.2, which is taken from [18]. As can be seen, the growth in positioning error is in fact reduced to 5 m over 30 s for nominal SA and twice that for 'high' SA. This RTCM graph assumes an HDOP of 1.5, a level which should be achievable under 'normal' operational conditions [7, 18].

The user will always want to apply the most recently received set of PRCs. Current DGPS radiobeacon systems have the robust error *detection* capabilities provided by the RTCM message format, but no error *correction* [95, 105]. So the user needs to receive error-free messages in order to up-date the PRCs. The predicted accuracy at any point in the coverage-prediction array depends on the age of the PRCs at that point. This in turn depends on the probability of receiving a set of error-free PRCs, given the SNR computed from the strengths of the wanted signal, noise and interference. Published work has established a relationship between message error rate and the resulting magnification of position errors. We need, therefore, to establish a relationship between the computed SNR and message error rate. Let us start by considering the existing state of knowledge.

Number of PRCs	Number of RTCM words	
	Type 1	Type 9
3	7	7
6	12	-
8	16	-
9	17	-
10	19	-
11	21	-

Table 9.1: The number of 30-bit words in a Type 1 or Type 9 message. The Type 9 message always includes three PRCs. Messages either cycling through the available satellites, or schedule satellites with rapidly varying PRCs more often than satellites with slowly-varying ones.

9.2.1 RTCM message Types 1 and 9

The original RTCM PRC message format is the Type 1 message, which constitutes the minimum RTCM message requirement for a DGPS radiobeacon (see Chapter 2). Most DGPS radiobeacon systems initially employed Type 1 messages. These are increasingly being replaced by Type 9 messages. The Type 1 message is a long message, containing PRCs and RRCs for all satellites in view of the reference station. The alternative Type 9 message has the same format as the Type 1, but includes PRCs and RRCs for only three satellites. All RTCM messages are composed of 30-bit words, referred to in the following sections as *RTCM words* or *words*. Table 9.1 gives the message length in words when PRCs for different numbers of satellites are transmitted.

The major disadvantage of Type 1, and the reason for the introduction of the Type 9 message, is that as the number of satellites increases, so does the length of the message, and the chance of it being corrupted. This results in a longer time between of error-free messages. Since if, during reception, any individual 30-bit word fails a parity check, the whole message must be discarded and the user must wait for the next message. We say that the delay, or *latency*, in the message is high.

The Type 9 message, being shorter, is more likely to be received intact. If a message is corrupted, the time lost is short, regardless of the number of satellites being tracked.

Using Type 9 messages is also advantageous in a higher noise environments, as the more frequent repetitions of the preamble allow for faster re-synchronisation when necessary.

9.2.2 Expected accuracy

Predicting the accuracy which can be achieved at points around a beacon requires prediction of the ages of the PRCs. Good work has been done by Enge and others in calculating the expected message latency given the probability of there being an error in a demodulated RTCM word, although this information is often buried in the analysis of the performance of specific coding or messaging schemes [56, 88]. This section presents the information on message latency which has been extracted from the sources cited.

A message will age due to transmission delay, even if no corruption occurs. At an MSK rate of 100 bps, a Type 1 message containing 8 PRCs will take 4.8 s to transmit (16 words, 30 bits per word, a total of 480 bits). As the whole message must be received before any part may be applied, the minimum age of this message is 4.8 s. Any additional aging will depend on the probability of receiving the next up-date. P_m is the probability of each up-date arriving successfully. It can be written in terms of the probability of receiving all its words uncorrupted:

$$P_m = [1 - P_w]^W , \tag{9.4}$$

where P_w is the probability of an RTCM word failing its parity check, and W is the number of RTCM words in the message [88]. The variable P_w will be dealt with in the next section.

Let us first look at the expected message latency as a function of P_m.

Again, interpreting Enge [88], the 1-σ pseudorange error is given by

$$e(t) = k_1 + \frac{a}{2}t^2. \tag{9.5}$$

The term k_1 is the reference station error due to errors in the surveyed position of the reference station and the effect of multipath reception there. The second term, a, is

the acceleration due to SA, with its typical 1-σ value of 0.0037 m/s [17, 18]. We are interested in knowing the minimum, maximum and expected values of t^2, the latency of a message of length M bits and MSK data rate of R_d bps. The minimum value of t^2, t^2_{min} is experienced when the PRCs are received without error:

$$t^2_{min} = M^2/R^2_d. \tag{9.6}$$

This latency is due solely to the transmission delay of the link.

The maximum value of t^2, t^2_{max}, is experienced after N attempts to receive a message up-date:

$$t^2_{max} = ((N+1)M/R_d)^2, \tag{9.7}$$

$$= M^2/R^2_d(\overline{N^2} + 2\overline{N} + 1) \tag{9.8}$$

where [88] relates the expected number of attempts, N, to the probability of message success, P_m:

$$\overline{N} = \sum_{N=1}^{\infty} NP_m(1-Pm)^{N-1} = 1/P_m, \tag{9.9}$$

$$\overline{N^2} = \sum_{N=1}^{\infty} N^2P_m(1-Pm)^{N-1} = (2-P_m)/(P^2_m). \tag{9.10}$$

The expected latency $\overline{t^2}$ will be between these two limits, and may be interpreted as showing:

$$\overline{t^2} = \frac{M^2}{3R^2_d}(\overline{N^2} + 3\overline{N} + 3) \tag{9.11}$$

Substituting this back into Equation 9.5, we determine the expected 1-σ pseudorange error to be:

$$\overline{e(t)} = k_1 + \frac{a}{2}\overline{t^2}. \tag{9.12}$$

The *positioning* accuracy may be calculated from the 1-σ pseudorange error, by using the following formula from [16],

$$Accuracy \approx 2 \cdot e(t) \cdot HDOP, \tag{9.13}$$

where $\overline{e(t)}$ may be used in place of $e(t)$.

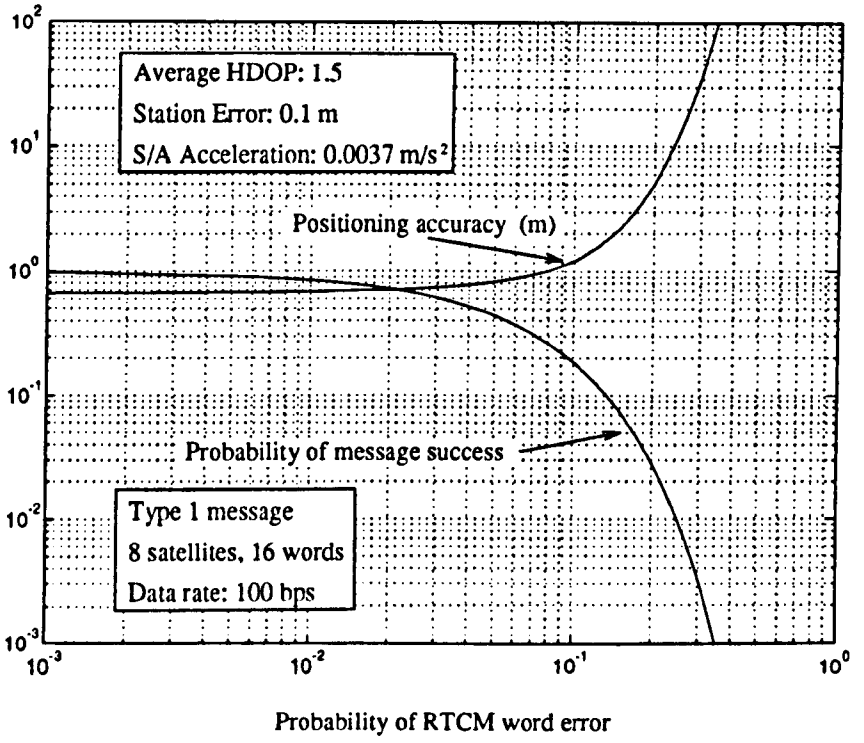

Figure 9.3: Variation in positioning accuracy (and probability of message success) with probability of RTCM word error. A Type 1 message containing the PRCs for 8 satellites is assumed. The reference station error, which determines the minimum positioning error, is set to 0.1 m.

Thus, given the probability P_w of an RTCM word error occurring, Equation 9.13 may be used to predict the resulting position accuracy. Fig. 9.3 shows this accuracy for a Type 1 message containing 8 PRCs. This curve has been calculated using the same reference station error, SA acceleration and HDOP as Fig. 9.2, except now we are looking at the positioning accuracy as a function of *word error rate (WER)* instead of time delay. The predicted error is seen to rise very rapidly as the probability of RTCM word error increases above about $3 \cdot 10^{-2}$, and the probability of message success decreases correspondingly. Looking at the rising edge of the curve, the positioning accuracy is seen to increase from 5 m for a P_w of 0.2 to more than 30 m for a P_w of 0.3.

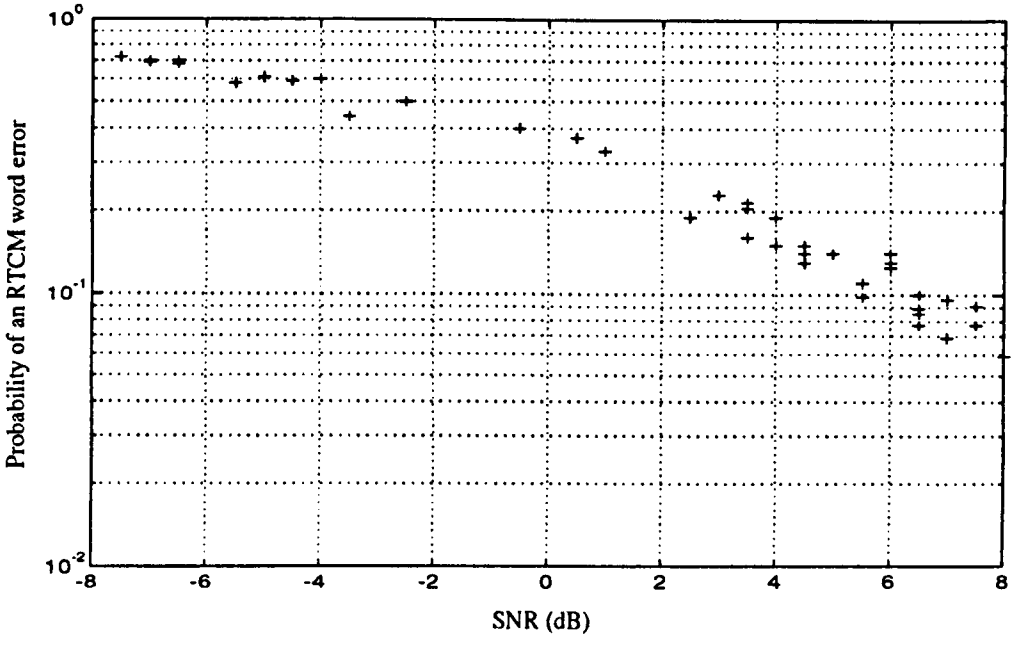

Figure 9.4: The probability of RTCM word error versus logged SNR as reported in [87], from measurements made on the East Coast of the US.

9.2.3 Probability of RTCM word error

The preceding section analysed the position accuracy as a function of the probability of RTCM word error. To implement accuracy contouring in the model requires a method of predicting position accuracy as a function of SNR. The highly non-Gaussian nature of atmospheric noise (see Chapter 7) makes it difficult to *calculate* the probability of RTCM word error due to a particular value of SNR. In 1988, a limited measurement campaign was undertaken at the University of New Hampshire, Durham, (UNH) to measure *bit error rate (BER)* versus SNR. It used a test bed composed of an MSK signal modulator and demodulator [81]. The test bed generated an MSK test signal, mixed in actual off-air noise, demodulated the resulting noisy MSK signal and compared the demodulated signal with an appropriately delayed version of the transmitted signal. The actual sequential-pattern of errors in the decoded signal was logged, as was the SNR, although the technique used to measure SNR was unfortunately not specified.

The pattern of the bit errors was used to determine what the RTCM WER would have been had the signal been composed of 30-bit RTCM words. This was done simply

by checking to see whether there were any bit errors in each group of 30 sequential bits. One or more bit errors would have caused a word error. The resulting plots of the probability of RTCM word error versus logged SNR are shown in Fig. 9.4 [81, 88]. Here were experimental curves relating the RTCM WER to the SNR, but even though the noise is off-air, this is not actually an off-air RTCM WER. The question is whether the WER measured in this way and calculated from the off-air BER accurately reflects the requirements not only for a word to pass parity, but also for the decoder to stay synchronised to the RTCM message frames and preambles. If synchronisation is lost, it cannot be regained until the next message preamble occurs. This aspect would not have been taken into account in the analysis of the UNH data.

Further, the UNH paper did not specify how SNR had been determined, only that a single value for each 15 minute data sample was recorded. Additionally, the test-bed employed only an MSK data rate of 100 bps, whereas information is needed on the performance of both 100 and 200 bps broadcasts. Because of these short-comings, it was decided to establish a test-bed and experimentally sample the off-air RTCM WER.

9.3 Receiver performance measurements

In order to have data on WER as a function of SNR and MSK data rate during actual RTCM message reception, measurements were made at a test site near Bangor during the summer of 1995. These measurements used a modulator and a receiver loaned by Cambridge Engineering, Inc. (Fig. 9.5). This Sidekick-T MSK modulator allows a low-powered, short range, signal of variable strength to be radiated at a frequency and data rate selected by the user. One of the data options is a Type 1 message loop according to the USCG standard. Transmissions were made on 'unoccupied' channels in the radiobeacon band, well separated in frequency from nearby beacons. The test-bed was located in a carefully chosen, electrically quiet, environment.

The goal of the experiment was to use the MSK receiver to sample both the RTCM WER and the associated receiver SNR. The WER measurements would thus include

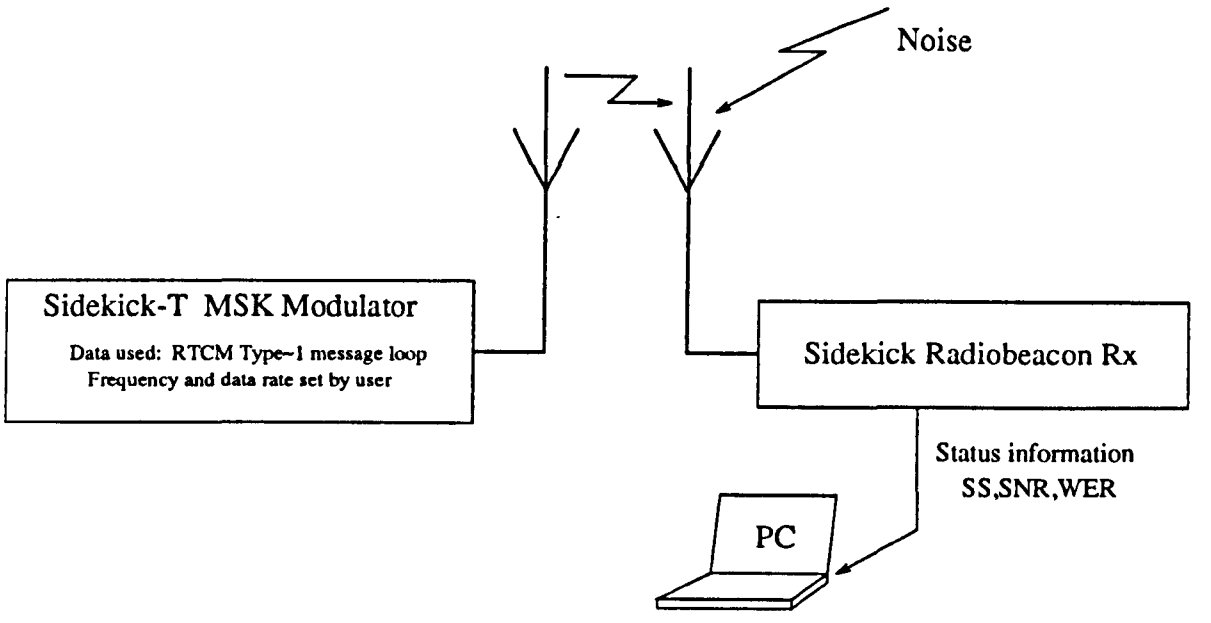

Figure 9.5: Setup of the modulator and receiver for measuring WER versus SNR.

the effects on error rates of failures not only of individual message bits, but also of message and word synchronisation, as the beacon receiver checks both the preamble and the parities of the messages.

Once per minute, the receiver reported the SNR and the number of RTCM words, from the last 14, which had passed the RTCM parity check. The receiver determined the SNR value by measuring the variation and the mean value of the signal amplitude *after* noise processing has taken place [87]. It thus takes into account the effect on atmospheric noise impulses of the 'blanking' or 'clipping' of this receiver, which is typical of that found in all current, high-grade, MSK, radiobeacon receivers [56, 87].

There are no unused beacon channels in Europe, as may be found in the US. So, to avoid possible transient interference from co-channel and adjacent channel beacons, the measurements were carried out only during the day when long-range skywave signals experience their greatest attenuation. Careful checks were carried out to ensure that the noise and (lack of) signal levels of the channel chosen were typical of those of unoccupied channels. The frequency was chosen to sit mid-way between two relatively quiet channels, such that additional protection from interference was afforded by the receiver's filters. The amplitude of the signal output by the modulator was adjusted

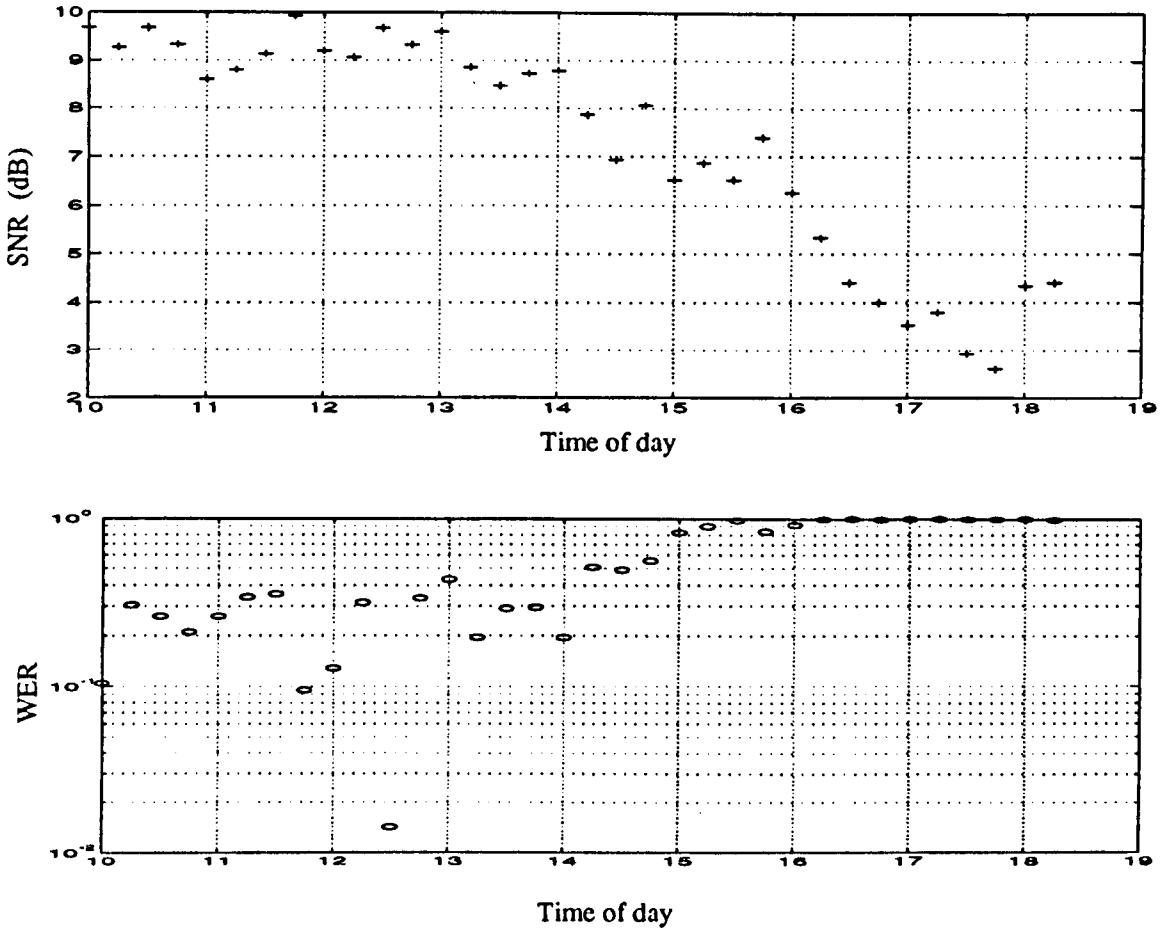

Figure 9.6: SNR and WER versus local time. This plot shows 8 hrs of data logged on July 11th, at a frequency of 295.25 kHz and a data rate of 100 bps. The frequency was chosen to sit between two relatively quiet channels, so that additional protection from interference was afforded by the receiver filtering.

at the start of the day to yield an SNR around 8 to 10 dB, since SNR values above 12 dB give few errors and those below 6 dB unusable signals.

The SNR and WER are plotted against local time in Fig. 9.6. The SNR is seen to have decreased (noise increased) by some 5 dB by the afternoon. By comparing the two plots, the clear correlation between SNR and WER is seen as the noise level increased into the afternoon.

A resulting plot of WER versus SNR is shown in Fig. 9.7. The raw measurements, shown as 'o's, have been averaged into 15-minute blocks, the averaged points indicated by '*'s. This averaging has been done to permit direct comparison of these results with the UNH data, which used single values of SNR and WER over the same periods of

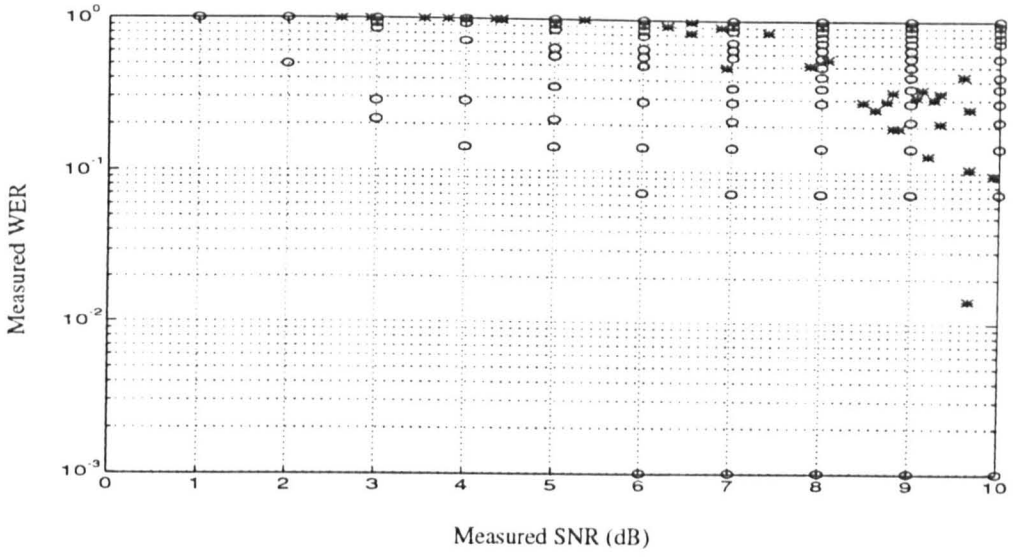

Figure 9.7: Measured WER versus SNR at 100 bps. The raw measurements are shown as 'o', the 15-min averaged values as '*'.

Date	Duration (hrs)	Frequency (kHz)	Data Rate (bps)
1 July	8	295.50	200
2 July	8	283.50	100
11 July	8	295.25	100
13 July	4	295.25	200

Table 9.2: Test schedule for measurements shown in Fig. 9.8. The data rates of 100 and 200 bps are standard RTCM rates being used in current DGPS systems.

time. This plot shows 8 hrs of data logged on July 11th, at a frequency of 295.25 kHz and a data rate of 100 bps. As would be expected, the probability of a word error occurring tended to decrease as the SNR increase.

These receiver performance measurements were made using the two RTCM standard data rates, 100 and 200 bps. The results are shown in Fig. 9.8. These plots are the results of measurements taken over four days (see Table 9.2). Third-order polynomials have been fitted to the data sets, resulting in the curves plotted. At usable levels of WER, the higher data rate of 200 bps is seen to require about 2 dB more SNR to achieve the same performance as does 100 bps. The receiver bandwidth for the 200 bps was approximately twice that at 100 bps. The rapid transition between very good and

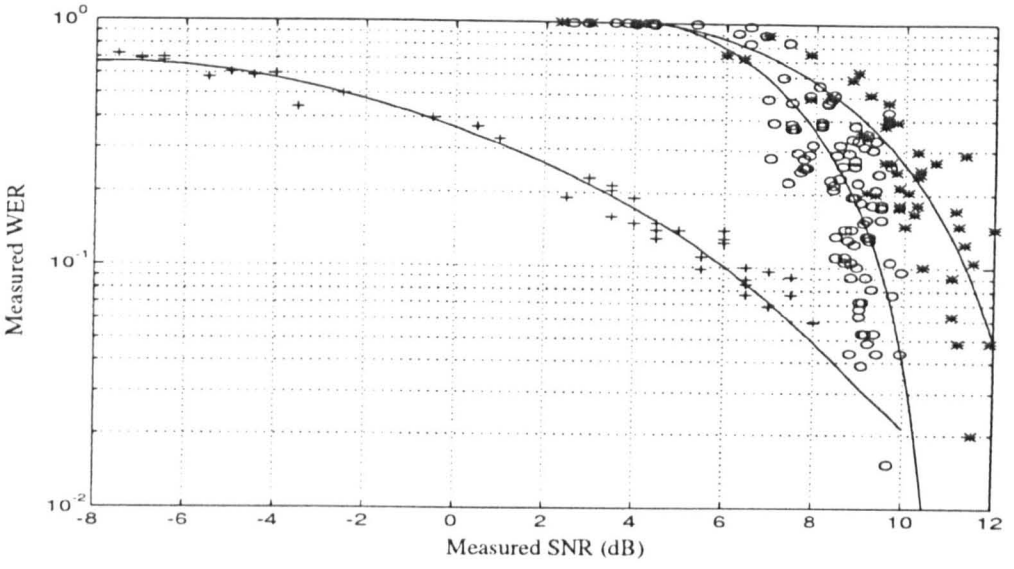

Figure 9.8: WER versus SNR for several days of data. Data at 100 bps shown by 'o' and 200 bps by '*'. For comparison, the UNH data is also included as '+'.

very bad WER as the SNR changes by only a few dB emphasizes the need for precise and comprehensive coverage prediction.

The UNH data is again included for comparison; the large difference between the two sets of results is obvious. The UNH data predicts usable signals down to -2 dB (which is in conflict with experience), with a much more gradual change in WER as the SNR increases. In fact, by 9 dB SNR the new curve for 100 bps predicts lower WERs than the UNH curve. The successful demodulation of data at low and negative SNRs by UNH would suggest that the noise bandwidth used in their measurements was wider than the receiver filter bandwidth. The Sidekick receiver will not normally ever report SNRs below about 2 dB since the receiver 'blanks' out strong impulses by ignoring these digital samples. This blanking approach is adopted rather than just narrow-band filtering, since the filters would cause these impulses to be smeared out over time and contaminate additional digital samples. The effect on the SNR is to cause an under-estimation of very high noise levels. It is of little practical interest, as the signal is unusable at these SNRs anyway. We conclude that an SNR of at least 6 dB is required for 100 bps reception and by 10 dB WER is very low. The corresponding figures at 200 bps are a couple of dB higher.

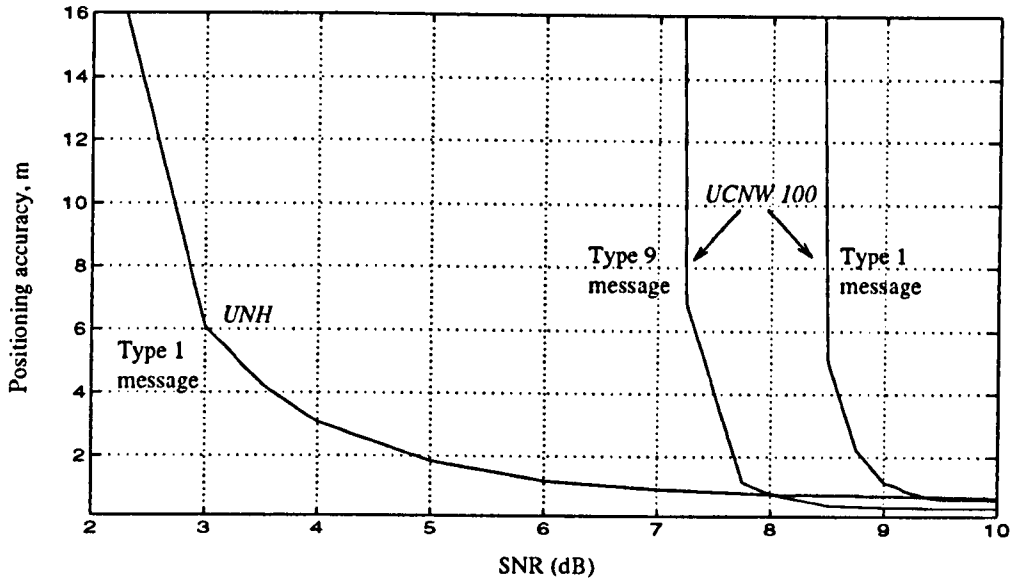

Figure 9.9: Accuracy as a function of SNR for a Type 1 message containing 8 PRCs and a Type 9 message. The *UNH* curve makes use of the data in Fig. 9.4 and *UNCW 100* the data in Fig. 9.7 for 100 bps.

These measurements give us the required relationships between WER and SNR.

9.4 Implementation

In Section 9.2, we determined the relationship between positioning accuracy and WER, Section 9.3 presented the results of measuring WER as a function of SNR and MSK data rate. These two relationships are combined in Fig. 9.9 to show accuracy as a function of SNR for a Type 1 message containing 8 PRCs and for a Type 9 message containing 3 PRCs. The *UNH* curve makes use of the data in Fig. 9.4 and *UCNW 100* curves the 100 bps data in Fig. 9.8. For the latter, the rapid transition from good to poor message throughput is evidenced by the sharp rise in the accuracy curve between 8.5 and 8.0 dB SNR. The benefit of the shorter, Type 9, message is also demonstrated by the fact that lower values of SNR yield acceptable accuracies. A method for building this information into the DGPS model needed to be selected, so that *performance contours*, that is the areas within which the DGPS positioning accuracy exceeds a user-defined level, could be determined.

Two methods were considered for implementing the conversion from a positioning accuracy requirement to a corresponding minimum SNR. The first method would be to fit a polynomial to the data points in Fig 9.9. The second method would be to invert the equations of Sections 9.2 and 9.3 so that they solve for P_w given positioning accuracy and then apply this P_w to a polynomial curve which calculates SNR as a function of P_w. The first is certainly the simpler, but it was rejected because it would require several parameters to be fixed, including: message Type, message length, data rate, HDOP and the station error.

The second option is the more complex, but notice that it is not actually necessary to calculate the positioning accuracy at every point in order to perform accuracy contouring. The problem can be simplified considerably by employing the results obtained in Sections 9.2 and 9.3 which relate accuracy to SNR. The model need only determine the minimum value of SNR which corresponds to the accuracy required and then draw a contour using that SNR (see Chapter 7).

Let us derive the equations for calculating P_w as a function of positioning accuracy. The model takes the positioning accuracy requirement and converts this into a 1-σ pseudorange error, $\overline{e(t)}$, based on the HDOP. From Equation 9.13:

$$\overline{e(t)} = Accuracy/(2 \cdot HDOP). \tag{9.14}$$

The probability of successfully receiving a message, P_m, depends not only on this 1-σ pseudorange error, but also on the reference station error k_1, the data rate R_d, the message length M in bits and the SA acceleration parameter a. From Equations 9.9–9.12 (requiring the solution of a quadratic):

$$P_m = \frac{1 + \sqrt{1 + 2X}}{X}, \tag{9.15}$$

where X is defined to be:

$$X = \frac{6R_d^2(\overline{e(t)} - k_1)}{M^2 \cdot a}. \tag{9.16}$$

The probability of a word being in error depends on the probability of a message success and the number of words, $W = M/30$, in the message. From Equation 9.4:

$$P_w = [1 - P_m]^{1/W}, \tag{9.17}$$

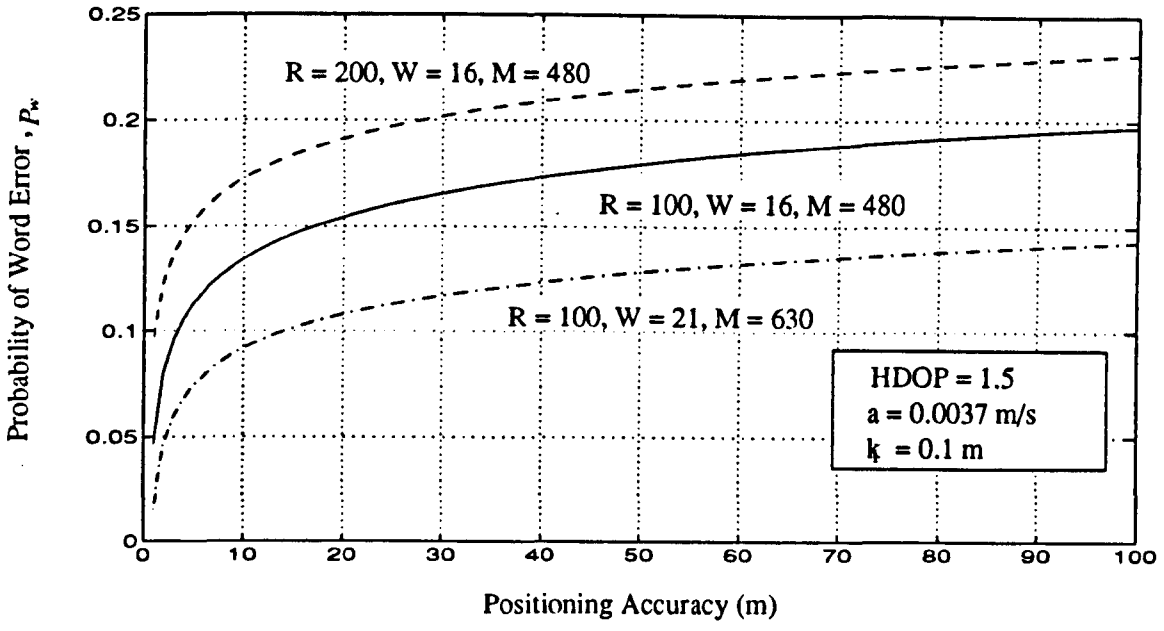

Figure 9.10: Examples of calculated P_w as a function of positioning accuracy. Three scenarios are shown: a 16 word message broadcast at 200 bps, a 16 word message at 100 bps and a 21 word message at 100 bps. The minimum P_w increases as the data rate increases and as the message length decreases.

Fig. 9.10 shows the result of calculating the maximum P_w as a function of accuracy, with the various parameters taking the values indicated. Notice that the maximum P_w which can be tolerated decreases, that is fewer word errors can be tolerated, if the data rate remains the same and the message length is increased. In the 100 bps example, if we wished to achieve an accuracy of 10 m then an increase in message length from 16 words to 21 words would require P_w to decrease from 0.135 to 0.092. This is because we need to get more words through without errors occurring. If the message length is left the same and the data rate doubled to 200 bps, P_w increases, meaning that more word errors can be tolerated. This is because when the message is sent at twice the rate, it is only half as old when it is received. Looked at the other way, every second message could be lost at the higher data rate and still yield the same message latency as the lower data rate. In this example, with a message length of 21 words, the tolerable P_w increases from 0.135 to 0.173 when the data rate is increased from 100 to 200 bps. Unfortunately, as was shown in Section 9.3, when the data rate is increased, the probability of a word error is also increased for the same level of SNR. This leads us to the final step, which is determining the minimum level of SNR required to achieve

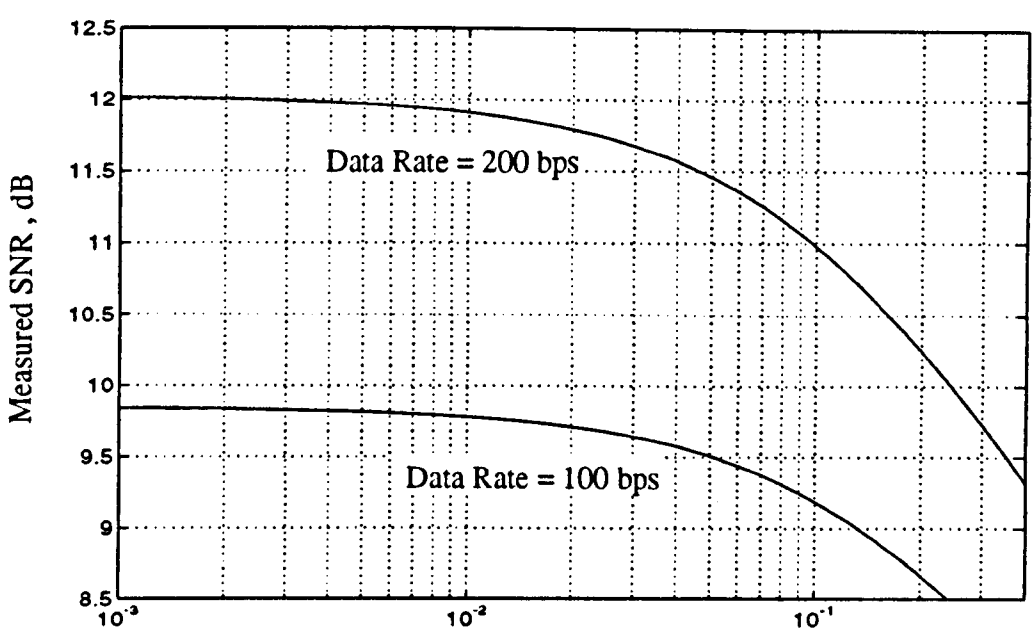

Figure 9.11: Polynomial curves of SNR as a function of P_w, from experimental data at 100 and 200 bps. At probabilities below approximately 10^{-2}, the SNR is relatively insensitive to the value of P_w

a given level of positioning accuracy.

From the experimental data collected in Section 9.3, a polynomial for calculating SNR as a function of P_w has been determined. Fig 9.11 shows the data points and curves. Now, employing these polynomials, we can calculate the SNR required to achieve a level of positioning accuracy for different data rates and message lengths, as shown in Fig. 9.12. The most remarkable feature of this figure is that to improve upon the stand-alone GPS accuracy of 100 m requires an SNR of about 10 dB for 200 bps link and about 9 dB for the 100 bps link. The SNR requirement for 5 m positioning accuracy only increases by about 0.5 dB, indicating the sensitivity of the accuracy to the SNR value and the need for accurate coverage and performance modelling. Both experimental SNR numbers are several dB above the SNR specification of 7 dB (see Chapter 7), suggesting that the specification does not reflect the performance capabilities of current MSK receivers in atmospheric noise conditions.

From this figure we can also conclude that although at 200 bps we can tolerate more word errors, this does not result in a reduction in the required SNR. In fact the opposite:

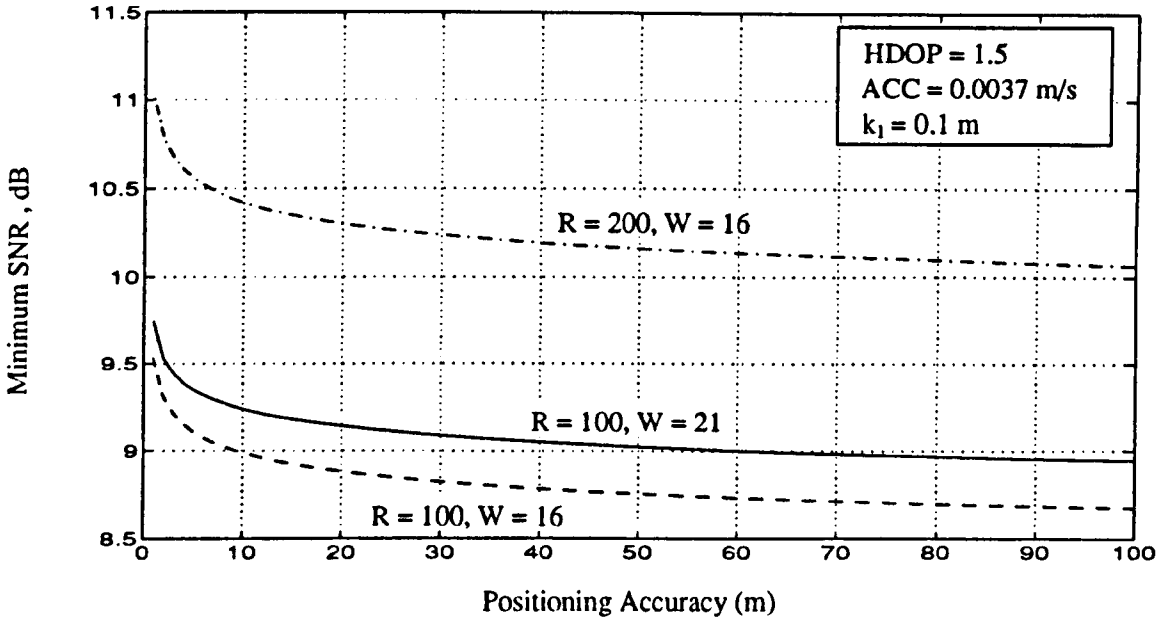

Figure 9.12: Minimum SNR as a function of positioning accuracy. These curves are the combined results of theoretical and experimental data. The minimum SNRs for three combinations of data rate, R bps, and message length, W words, are shown.

the 200 bps data rate requires a good 2 dB more SNR to achieve the same performance as the 100 bps channel, all other parameters being identical. Experimental measurements, conducted by Young *et. al.* and USCG, to determine if the 200 bps data rate offers an improvement compared to the 100 bps when used to transmit the shorter, Type 9, messages resulted in significant performance improvement [44, 56, 111].

The method for determining accuracy contours which has been devised for use in the DGPS model is based on the combination of the theoretical and the experimental information from Sections 9.2 and 9.3. This implementation allows different data rates, message lengths and reference station errors to be accommodated. It will also simplify the expansion of the model, if desired at a later date, to include computation of the accuracy which results from using Type 9 messages.

9.5 Examples of performance contouring with the model

Using the DGPS model, the 5 m performance contour around the beacon Porkkala has

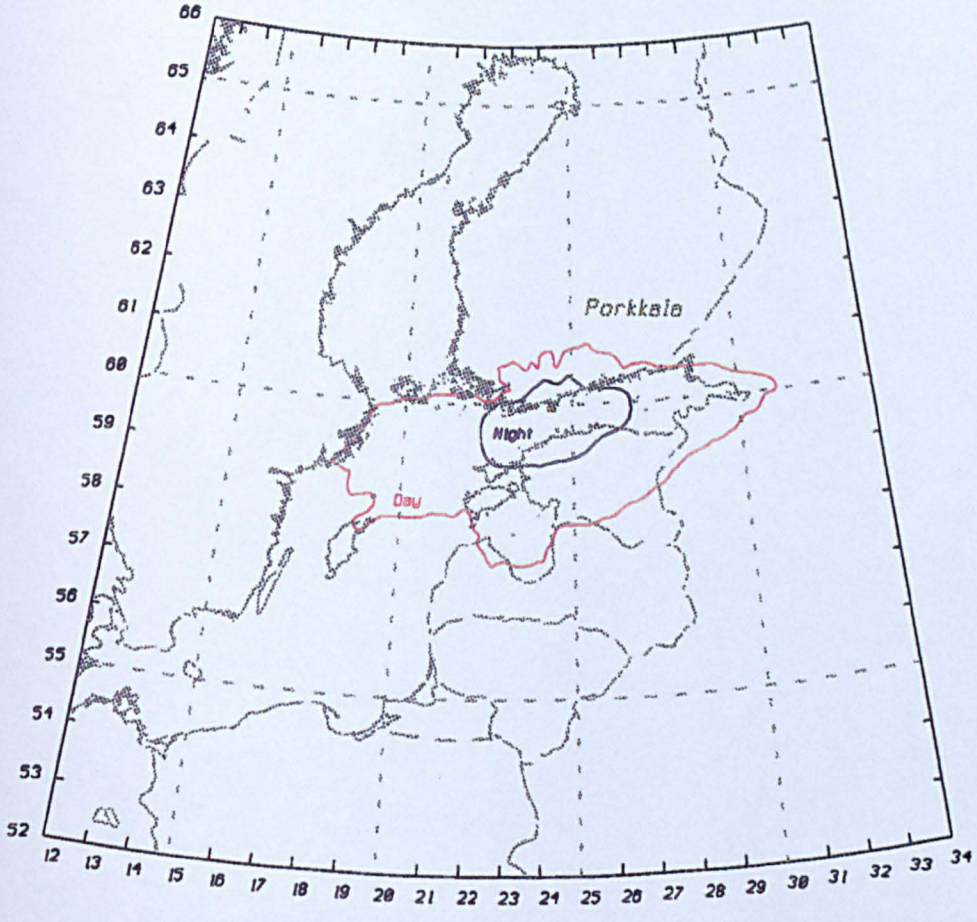

Figure 9.13: Performance contours around the Finnish beacon Porkkala, nominal range of 160 km, at a data rate of 100 bps. Within the boundary, the user would expect to achieve positioning accuracies of 5 m (95% confidence) or better. Both *Day* and *Night* contours are shown.

been calculated and is shown in Fig. 9.13. The beacon has a nominal range of 160 km and uses a data rate of 100 bps. The *Day* contour combines the newly implemented method for calculating accuracy with the factors of Chapters 4, 7 and 8. It encloses all points at which the signal strength exceeds 20 dBμ, the 95% annual average SNR exceeds 7 dB, IALA protection ratios are met by all unwanted signals and the positioning accuracy is expected to be 5 m or better. Before determining that a calculation point will meet the accuracy limit, the point must first meet or exceed the minimum signal strength requirement and also the minimum SIR requirement. If these conditions are not met it is assumed that no DGPS corrections can be received.

Porkkala's *Night* contour also includes the factors of Chapters 5, 6 and 7, adding the effect of own-skywave fading and accounting for the 95% night-time skywave interference levels from other beacons. As has been the case in previous chapters, the *Night*, 5 m, performance contour is greatly reduced compared to the *Day* contour. This reduction is solely due to these additional night-time factors, as all other parameters are left the same.

As the user moves further from the beacon, beyond the 5 m contour boundaries, the accuracy will fall until finally it becomes that of stand-alone GPS. During the daytime, this limiting condition will normally be reached at the 20 dBμ signal strength contour requirement but, if not, it becomes an SNR limit, as seen in Fig. 9.9. At night there are the additional limitations from the own-skywave effect and skywave interference reducing the ranges of the field strength and SNR contours.

9.6 Conclusions

The positioning accuracy achievable using the corrections broadcast by DGPS radiobeacons have been shown to be limited by temporal decorrelation of the PRCs and not by spatial decorrelation. The accuracy has been shown to be strongly dependent on the probability of RTCM word errors occurring, on the broadcast data rate and on the RTCM message length. Rather that select a single scenario, the equations

have been incorporated into the model to provide greater flexibility.

Published data relating receiver word error rates to SNR were found to be inadequate because of the post-processing method of determining WER and the lack of information on how SNR had been defined. To provide the required WER information, experimental measurements of RTCM word error as a function of receiver SNR have been made at two standard data rates, typical of what is experienced during navigation. The results of these measurements differed greatly from the previously available data, they also showed the WER to be very sensitive to changes in the SNR. This new data has been curve fitted and implemented in the model for use in determining performance contours.

Using the newly-implemented method, performance contours around Porkkala have been shown as examples. Significant deterioration in the night-time performance of a receiver using this signal has been predicted. This is now a familiar problem, due not only to the need to achieve the minimum field strength and protection ration criteria, but now also to the relationship between accuracy and SNR.

Chapter 10

Conclusions

The primary objective of this research was to develop more precise and comprehensive techniques for predicting the coverage and performance of DGPS radiobeacon systems. Two existing coverage prediction models were examined and found to be inadequate for DGPS radiobeacon use. One because it was designed for modelling the Loran-C radionavigation system, the other because it oversimplifies the task, taking into account only groundwave field strength and atmospheric noise. This research has investigated a number of other possible coverage-limiting factors and developed and implemented methods for predicting their effects.

Comparisons between predicted and measured data have been used to verify that the methods have been correctly developed and implemented. Groundwave field strength predictions have been compared with independent measurements from various parts of the world. In order to validate the predictions of the novel own-skywave calculation technique, measurements have been made for a beacon where fading was predicted. These measurements all showed excellent agreement between the measured and predicted values.

10.1 Review of the thesis

Chapter 2 gave an introduction to GPS and how it works, followed by a discussion of the causes of positioning error. An overview of civilian positioning and navigational requirements which demand DGPS was followed by an introduction to DGPS, discussing in particular radiobeacon system specifications and error sources.

An analysis of relevant existing coverage prediction techniques was given in Chapter 3. The reasons for their inadequacy were discussed and a number of major factors affecting coverage were identified which have previously been ignored. A framework for an improved DGPS model was proposed, in which the effects of these factors were to be incorporated. Chapters 4 to 9 discussed in detail each of these factors and methods for analysing them.

Chapter 4 discussed groundwave field strength attenuation. It explained the importance of knowing the ground conductivity and described the implementation, for DGPS radiobeacon use, of a calculation method. Examples generated by the DGPS model were used to demonstrate the effect of ground loss on beacon coverage. The model's point-by-point predictions were compared to measurements made in the UK and in the Arabian Gulf and found to be in very close agreement.

Chapter 5 discussed the method adopted for calculating skywave field strength. It included details of the many parameters which must be taken into account in this calculation and the need for statistical modelling of this field strength. This factor was included only as a night-time factor in the model, when it was predicted to have a significant field strength over long ranges.

Chapter 6 began with an analysis of existing methods of calculating fading due to the combination of the groundwave- and skywave-propagated components of the signal. Reasons were given as to why these methods had proved inadequate for DGPS coverage prediction. A novel fade-calculation method for use in the model was developed and implemented. Examples were presented which showed that this night-time effect caused

major coverage limitations. The predictions showed excellent agreement with night-time measurements.

The calculation of an atmospheric noise database was described in Chapter 7. Averaging techniques were developed to determine the noise levels corresponding to different characteristic time periods. Methods for approximating a continuous noise distribution in the model were described. It was concluded that this factor was of major importance for coverage prediction in the equatorial latitudes, but not as crucial in temperate latitudes where coverage is dominated by other factors.

Chapter 8 developed methods for identifying potential interference sources and calculating their effective interference levels. In calculating interference values, priority was given to finding methods which reduced the time needed for the task. Coverage contours for beacons in Europe showed interference to be a dominant factor for both day and night.

In Chapter 9 the predicted levels of field strength, noise and interference were related to the achievable radiobeacon DGPS positioning accuracy. Discussions of both the spatial and temporal decorrelation of DGPS data were included. An analysis of the relationship between accuracy and word error was presented and new measurements showing the dependence of word error on signal-to-noise ratio were described. Methods for calculating performance contours were implemented in the model and examples were given.

10.2 The Bangor DGPS coverage prediction model

As part of this work, a coverage and performance model has been developed. The Bangor DGPS coverage prediction model is a suite of five programs, implemented and tested by the candidate, which allow coverage and performance predictions to be made for DGPS radiobeacons. The candidate is responsible for the coverage prediction methods used in the model and for the implementation, testing and verification of

its output. During its development, the model has been used to produce coverage diagrams for system planning by several organisations, examples of which are included in Appendix C. A guide to operating the Bangor DGPS coverage prediction software is included in Appendix D.

10.3 USCG COAST model

The USCG COAST model, under development at the start of this research and recently made public, is now beginning to be used to determine the coverages of existing DGPS radiobeacons and to plan future system additions in North America [65]. It is of interest to see how this model compares to the Bangor DGPS model. The following description is based on the information in the COAST manual [65].

The COAST package requires a UNIX environment which supports X Windows and Motif, 20 Mbytes of hard disk space, 16 Mbytes of memory; a minimum of a 33 MHz 80486-based platform with a baths co-processor is recommended. The software uses a framework of radial beacon-cells, as shown in Fig. 10.1. The incremental radius and the number of beacon-cells per ring is chosen such that each beacon-cell's maximum edge length is less than a user definable 'resolution' parameter. Each beacon-cell has an associated signal strength value and a noise value. Based on these values and the coverage thresholds, the beacon-cell is determined to be either inside or outside the coverage area.

10.3.1 Groundwave attenuation

Groundwave attenuation of the wanted signal is calculated in the same way as in the Bangor model, using CCIR attenuation curves and Millington's method for inhomogeneous paths. The default ground conductivity database is composed of $0.25° \times 0.25°$ cells, with a single conductivity value for each cell derived from [73].

The USCG COAST model applies a conductivity database, but sacrifices some of

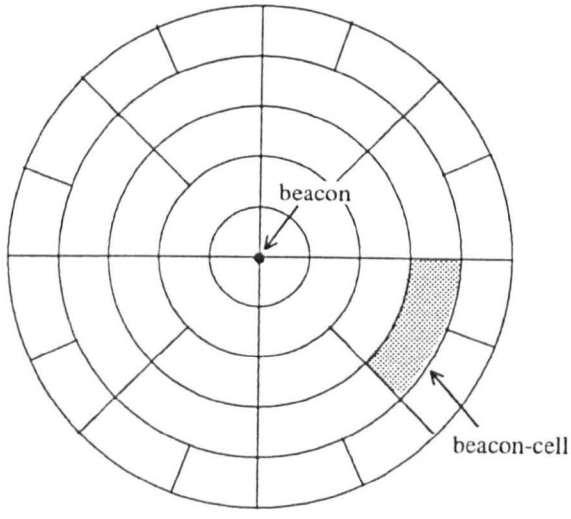

Figure 10.1: The COAST radial beacon-cells, after [COAST]. The desired coverage resolution determines the size of the beacon-cells.

the available resolution of the data in [67] by using this coarse quantisation size of 0.25° by 0.25°. This block size, approximately 28 km by 20 km, loses details of both the land-to-sea coastline transitions and the irregular borders between areas of different ground type.

10.3.2 Noise

Atmospheric noise is assumed to be the dominant noise source and the COAST model uses values derived from [69]. The default noise database for the program consists of a median noise value and statistical data associated with each of a number of irregularly sized, rectangular noise-cells. The size of the rectangle is defined such that, at any point inside it, the difference between the assigned median noise value and the CCIR median noise value is 6 dB or less. In applying this database, the first point of overlap of a beacon-cell and a noise-cell determines the noise value of that beacon-cell, even if the beacon-cell also overlaps other noise-cells.

Although the way COAST includes the statistical data allows for an easier transition between different percentiles than the Bangor model, the ±6 dB default seems extremely coarse. We have seen in Chapter 9 how sensitive coverage and performance are to small changes in SNR.

10.3.3 Accuracy

The COAST program determines the DGPS position accuracy within each cell through a complex relationship between the SNR, the expected BER and the expected lag for each PRC update. The user defines such parameters as the MSK transmission rate of the beacon, whether the primary RTCM message being broadcast is Type 1 or Type 9, a level of transmission overhead to account for the broadcast of any messages other than this primary type and whether or not a forward-error correcting code is encrypting the transmission. All these parameters affect the expected latency of received PRCs at a given BER. Additionally, the user can define the contribution to the pseudorange error due to spatial decorrelation of the tropospheric delay, ionospheric delay and ephemeris error.

The implementation of accuracy calculations in the COAST model is impressive: it includes algorithms for determining the latency of the PRCs for each satellite depending on the RTCM message type broadcast. COAST determines an expected BER given an SNR, although the relationship between the two is not stated and may not compare well with measurements of off-air WERs in North America.

Unfortunately, COAST totally fails to consider skywave propagation and own-skywave fading in calculating SNR. As has been shown in Chapter 6, *own-skywave fading is a real, measurable, effect* that can cause serious limitations of night-time coverage. As such, it can be concluded that the COAST predictions are applicable only during the daytime. There is no inclusion of an interference factor either, but this may not be as necessary for planning in North America where beacons are few and far between.

The type of coverage displayed by the COAST model may be one of five types:

Signal Strength - displays the region where the signal level meets or exceeds a user-set threshold parameter,

Signal to Noise - displays the region within which the SNR meets or exceeds a user-set threshold,

Bit Error Rate - displays the region within which the BER is expected to be below a user-set threshold with a user-specified probability,

Accuracy - displays the region where the expected accuracy is below a user-set threshold with a user-specified probability,

Required Range - displays the region where coverage is required, based upon a user-set required range.

So, in summary, the Bangor DGPS model has a more solid foundation for predicting the total, reliably available, field strength around a beacon. For European use, it also has the advantage of including the effect of interference. The COAST model is an extremely complex, yet flexible, planning tool suitable for use in North America. It is, however, built like an inverted pyramid with all its complexity balanced on top of a very questionable, groundwave-only, assumption!

10.4 Suggestions for further work

The Bangor DGPS model could be improved by adopting the method for calculating accuracy that have been used in the USCG COAST model. This would expand the abilities of the model to include the prediction for DGPS radiobeacon systems utilising different message Types.

The navigational tasks described in Chapter 2 not only specify minimum accuracy, but also integrity, availability and reliability requirements. These parameters are not always well defined and need to be pinned down and included in the coverage prediction process. Neighbouring beacons with overlapping coverage will impact these factors; the availability *etc.* of groups of beacons would be predicted.

There may be an improvement in DGPS position accuracy when the information from more than one beacon is utilised. There is a large body of work on Wide-Area DGPS which may provide information on how this could be done and how its effect could be

predicted.

Measurements performed as part of this work have been limited in quantity. For accuracy contouring, more extensive measurements of 'typical' receiver performance characteristics would be desirable.

The output of the model would be more useful to the navigator if it indicated which beacon was recommended for use in each part of areas of overlapping coverage. These boundaries would depend in a complex way on the field strengths, propagation paths, time of day, message Type and data rates broadcast by the reference stations. The raw information to do this already exists in the model, but a method of processing it and presenting the output needs to be determined.

10.5 Conclusions

This work has introduced, analysed and implemented more precise and comprehensive methods for predicting the coverage and performance of DGPS radiobeacons than existed previously or have been developed elsewhere. The model brings together broadcasting and navigational information to include the effects of groundwave attenuation, skywave propagation, own-skywave fading, atmospheric noise, groundwave interference, skywave interference and temporal decorrelation. Throughout the period of this work, the Bangor DGPS model has been used to evaluate and design DGPS radiobeacon systems and will continue to be so used in the foreseeable future.

References

[1] DOT and DOD. '1994 Federal Radionavigation Plan'. Technical Report DOT-VNTSC-RSPA-95-1/DOD-4650.5, NTIS, 1994.

[2] S.D. Thompson. *Everyman's Guide to Satellite Navigation.* Interstate Electronics Corp., 1994.

[3] P. Diederich. 'The Development of Civil Satellite Navigation in Europe'. *NAVIGATION*, 36(1):127–136, 1989.

[4] G.B. Green. 'The GPS 21 Primary Satellite Constellation'. *NAVIGATION*, 36(1):9–24, 1989.

[5] D.H. Alsip, J.M. Butler, and J.T. Radice. 'The Coast Guard's Differential GPS Program'. *NAVIGATION*, 39(4), 1992.

[6] R. Conley. 'An Overview of the GPS Standard Positioning Service Signal Specification'. In *ION Satellite Division's Technical Meeting*, pages 179–188, September 1994.

[7] R. Conley. 'GPS Performance: What is Normal?'. *NAVIGATION*, 40(3):261–281, 1993.

[8] R.W. Blank and W.D. Rhodes. 'Field Test Results Prove GPS Performance and Utility'. In *IEEE PLANS Symposium*, pages 287–296, 1986.

[9] B.W. Parkinson *et al.* 'A History of Satellite Navigation'. *NAVIGATION*, 42(1,Special Issue):109–164, 1995.

[10] R.B. Langley. 'The GPS Observables'. *GPS World*, 4:52–59, 1993.

[11] ITU. 'Technical Characteristics of Differential Transmissions for Global Navigation Satellite Systems (GNSS) from Maritime Radiobeacons in the Frequency Band 285–325 kHz (283.5–315 kHz in Region 1)'. Technical Report : Draft Revision of Recommendation 823, ITU, 1994.

[12] A.J. Van Dierendonck. 'Understanding GPS Receiver Technology: A Tutorial'. *GPS World*, 6(1):34–44, 1995.

[13] P. Mattos. 'GPS 2: Receiver Architecture'. *Electronic World and Wireless World*, pages 29–32, 1993.

[14] G.R. Lennin. 'A NAVSTAR GPS C/A Code Digital Receiver'. *NAVIGATION*, 36(1):115–126, 1989.

[15] T. Allison *et al.* 'C/A Code Dual Frequency Surveying Receiver – Architecture and Performance'. In *IEEE PLANS Symposium*, pages 434–441, 1988.

[16] B. Forssell. *Radionavigation Systems.* Prentice Hall, 1991.

[17] G.T. Kremer *et al.* 'The Effect of Selective Availability on Differential GPS Corrections'. *NAVIGATION*, 37(1):39–52, 1990.

[18] RTCM SC-104. 'RTCM Recommended Standards for Differential NAVSTAR GPS Service'. Technical Report : Special Publication 94–30, National Telecommunications and Information Administration (NTIA), 1994.

[19] D. Pietraszewski *et al.* 'US Coast Guard Differential GPS Navigation Field Test Findings'. *NAVIGATION*, 35(1):55–72, 1988.

[20] P. Loomis, L. Sheynblatt, and T. Mueller. 'Differential GPS Network Design'. In *ION Satellite Division's Technical Meeting*, pages 511–520, September 1991.

[21] L. Wanninger. 'Effects of Equatorial Ionosphere on GPS'. *GPS World*, 4(7):48–54, 1993.

[22] W.A. Feess and S.G. Stephans. 'Evaluation of GPS Ionospheric Time Delay Algorithm for Single-Frequency Users'. In *IEEE PLANS Symposium*, pages 206–213, 1986.

[23] R.L. Greenspan *et al.* 'The Effects of Ionospheric Errors on Single–Frequency GPS Users'. In *ION Satellite Division's Technical Meeting*, 1991.

[24] P.S. Jorgensen. 'An Assessment of Ionospheric Effects on the GPS User'. *NAVIGATION*, 36(2):195–204, 1989.

[25] J.A. Klobuchar. 'Design and Characteristics of the GPS Ionospheric Time Delay Algorithm for Single Frequency Users'. In *IEEE PLANS Symposium*, pages 280–286, 1986.

[26] C. Cohen, B. Pervan, and B. Parkinson. 'Estimation of Absolute Ionospheric Delay Exclusively Through Single Frequency GPS Measurements'. In *Proceedings of the ION*, 1992.

[27] F.K. Brunner and W.M. Welsch. 'Effect of the Troposphere on GPS Measurements'. *GPS World*, 4(1):42–51, 1993.

[28] H.Z. Abidin. 'Multi–Monitor Station 'On the Fly' Ambiguity Resolution: The Impacts of Satellite Geometry and Monitor Station Geometry'. In *IEEE PLANS Symposium*, pages 412–418, 1992.

[29] U.S. Department of Commerce. 'A Technical Report to the Secretary of Transportation on a National Approach to Augmented GPS Services'. Technical Report : Special Publication 94–30, National Telecommunications and Information Administration (NTIA), 1994.

[30] W. Lechner. 'Real Time DGPS Service for Precise Positioning–Activities in the Federal Republic of Germany'. In *IEEE PLANS Symposium*, pages 398–402, 1992.

[31] R. Johannesen. 'International Future Navigation Needs: Options and Concerns'. *NAVIGATION*, 34(4):279–289, 1987.

[32] N.H. Keeler. 'Maritime Future Navigation Needs and Plans'. *NAVIGATION*, 34(4):290–296, 1987.

[33] G. Gibbons *et al.* 'Automatic Vehicle Location: GPS Meets IVHS'. *GPS World*, 4(4):22–34, 1993.

[34] E.O. Frye. 'GPS Signal Availability in Land Mobile Applications'. *NAVIGATION*, 36(3):287–302, 1989.

[35] R.M. Kalafus. 'GPS Integrity Channel RTCA Working Group Recommendations'. *NAVIGATION*, 36(1):25–44, 1989.

[36] K. Kovach and R. Conley. 'SATZAP: A Novel Approach to GPS Integrity'. *NAVIGATION*, 38(2):163–190, 1991.

[37] L. Caporicci and C. Soddu. 'GPS Integrity monitoring and System Improvement with Ground Station and Multistationary Satellite Support'. In *IEEE PLANS Symposium*, pages 559–565, 1992.

[38] A. Brown, J. King, and J. Spaulding. 'Differential GPS Autonomous Failure Detection'. In *ION Satellite Division's Technical Meeting*, 1991.

[39] 'Notice Advisory to Navstar Users – 014-95023'. www.navcen.uscg.mil.

[40] 'Notice Advisory to Navstar Users – 257-92290'. www.navcen.uscg.mil.

[41] A.W. Hartberger and D.H. Alsip. 'Introduction to the USCG DGPS Program'. In *IEEE PLANS Symposium*, pages 450–456, 1992.

[42] R.B. Langley. 'RTCM SC-104 DGPS Standards'. *GPS World*, 5(5):48–53, 1994.

[43] R.B. Langley. 'Communication Links for DGPS'. *GPS World*, 4(5):47–51, 1993.

[44] DOT and USCG. 'Broadcast Standard for the USCG DGPS Navigation Service'. Technical Report COMDTINST M16577.1, USCG, 1993.

[45] F. Forbes, S. Ryan, and S. Wee. 'The Canadian Coast Guard DGPS Project'. In *ION Satellite Division's Technical Meeting*, pages 1451–1460, September 1994.

[46] R.J. Wilson. 'Decision Making for a Public Differential GPS Service'. In *ION Satellite Division's Technical Meeting*, pages 937–953, September 1991.

[47] F. Howard *et al.* 'A Comparison of Data Transmission Methods for Realtime Differential GPS'. In *ION Satellite Division's Technical Meeting*, 1991.

[48] J.R. Nagle. 'Wide Area Differential Corrections (WADC) from Global Beam Satellite'. In *IEEE PLANS Symposium*, pages 383–390, 1992.

[49] C. Kee and B. Parkinson. 'Algorithms and Implementation of Wide Area Differential GPS'. In *ION Satellite Division's Technical Meeting*, pages 565–572, 1992.

[50] 'Industry News'. *Marine Electronics – The official Publication of the National Marine Electronics Association (NMEA)*, 5(7), 1995.

[51] S. Pasupathy. 'Minimum Shift Keying: A Spectrally Efficient Modulation'. *IEEE Communications Magazine*, pages 14–22, 1979.

[52] B. Boehm, J.A. Schoonees, and R.M. Braun. 'Data to Frequency Mapping in Various MSK Schemes'. *IEE Electronics and Communication*, 6(1):13–20, 1995.

[53] D.H. Pianka *et al.* 'Medium Frequency DGPS Data Link'. In *ION Satellite Division's Technical Meeting*, pages 845–854, September 1991.

[54] I. Korn. 'Simple Expression for Interchannel an Intersymbol Interference Degradation in MSK Systems with Application to Systems with Gaussian Filters'. *IEEE Transactions on Communication*, 30(8):1968–1972, 1982.

[55] J.G. Proakis. *Digital Communications.* McGraw–Hill, 1989.

[56] P. Enge *et al.* 'DGPS/Radiobeacon Field Trials Comparing Type 1 and Type 9 Messaging'. *NAVIGATION*, 4(4):395–408, 1993–94.

[57] D.R. Cragg *et al.* 'Application and Impact of RTCM SC–104 Type 9 Messages'. In *ION Satellite Division's Technical Meeting*, 1991.

[58] P.M. Creamer, D.H. Alsip, and J.P. Radziszewski. 'Performance Requirements for the Coast Guard's Differential GPS Service'. *NAVIGATION*, 40(4):375–393, 1993–94.

[59] G. Harkleroad, W. Tang, and N. Johnson. 'Estimation of Error Correlation Distances for Differential GPS Operation'. In *IEEE PLANS Symposium*, pages 378–382, 1990.

[60] J.D. Last, M.D. Searle, and R.G. Farnworth. 'Coverage and Performance Predictions for the North-West European Loran-C System'. *Simulation (USA)*, pages 181–189, 1993.

[61] M.D. Searle *et al.* 'Prediction of Loran-C Additional Secondary Phase Factors'. In *8th National URSI Colloquium*, Jul 1991.

[62] M.D. Searle, J.D. Last, and J. McCulloch. 'Calculation of ECD Variations Over Inhomogeneous Terrain Using Millington's Method'. In *22nd Annual Tech. Symposium, Wild Goose Assoc.*, 1993.

[63] J.D. Last, M.D. Searle, and R.G. Farnworth. 'Coverage and Performance Predictions for the North–West European Loran–C System'. In *Proc. 21st Ann. Tech. Symp., Wild Goose Assoc.*, August 1992.

[64] P.K. Enge *et al.* 'Coverage of DGPS/ Radiobeacons'. *NAVIGATION*, 39(4):363–381, 1992.

[65] TASC. 'COAST User's Manual'. Technical report, DOT, USCG, 1993.

[66] R.G. Farnworth. *Loran–C Coverage Prediction in Western Europe.* PhD thesis, University College of North Wales, 1992.

[67] CCIR. 'World Atlas of Ground Conductivities'. Technical Report 717–2, ITU, Geneva 1988.

[68] J.D. Last, R.G. Farnworth, and M.D. Searle. 'Effect of Skywave Interference on the Coverage of Loran–C'. *IEE Proc–F*, 139(4):306–314, 1992.

[69] CCIR. 'Characteristics and Applications of Atmospheric Radio Noise Data'. Technical Report 322–3, ITU, Geneva 1988.

[70] J.D. Last, R.G. Farnworth, and M.D. Searle. 'A Thousand Signals – Carrier-wave Interference in Europe'. In *Proc. 21st Ann. Tech. Symp., Wild Goose Assoc.*, October 1991.

[71] G. Millington. 'Ground-wave Propagation Over an Inhomogeneous Smooth Earth'. *Proc. IEE*, 96(Part III):53–64, 1949.

[72] P.E. Gill, W. Murray, and M. Wright. *Practical Optimization.* Academic Press.

[73] H. Fine. 'An Effective Ground Conductivity Map for the Continental United States'. *Proceedings of the IRE*, 42, 1954.

[74] CCIR. 'Electrical Characteristics of the Surface of the Earth'. Technical Report 229–2, ITU, Geneva 1974.

[75] J.D. Last, R.G. Farnworth, and M.D. Searle. 'Ionospheric Propagation and Loran-C Range – The Sky's the Limit!'. In *Proc. 20st Ann. Tech. Symp., Wild Goose Assoc.*, October 1991.

[76] CCIR. 'Sky-wave Propagation and Circuit Performance at Frequencies Between About 30 kHz and 500 kHz'. Technical Report 265–5, ITU, 1982.

[77] CCIR. 'Prediction of Sky-wave Field Strength Between 150 and 1600 kHz'. Technical Report : Recommendation 435–6, ITU, 1990.

[78] CCIR. 'Methods for Predicting Sky-wave Field Strengths at Frequencies Between 150 kHz and 1705 kHz'. Technical Report 575–4, ITU, 1990.

[79] Racal-Decca Marine Navigation Ltd. Marine data sheets, updated periodically.

[80] CCIR. 'Ionospheric Propagation Characteristics Pertinent to Terrestrial Radio-communication Systems Design (Fading)'. Technical Report 266–5, ITU, 1982.

[81] P.K. Enge and K.E. Olsen. 'Medium Frequency Broadcast of Differential GPS Data'. *IEEE Transactions on Aerospace and Electronic Systems*, 26(4):607–617, 1990.

[82] W.Q. Crichlow, C.J. Roubique, A.D. Spaulding, and W.M. Beery. 'Determination of the Amplitude–Probability Distribution of Atmospheric Radio Noise From Statistical Moments'. *Journal of Research of the National Bureau of Standards – D. Radio Propagation*, 64D(1):49–56, 1960.

[83] B. Peterson *et al.* 'Analysis of DGPS MSK Receivers in a Non–Gaussian Noise Environment'. In *ION National Technical Meeting*, January 1993.

[84] B. Tryggo and S. Fogelberg. 'Signal Optimization and Field Results of Radio Beacon DGPS'. In *Differential Satellite Navigation Symposium*, 1995.

[85] 'Final Acts of the Regional Administrative Conference for the Planning of the Maritime Radionavigation Service (Radiobeacons) in the European Maritime Area'. Technical report, ITU, 1985.

[86] 'International Frequency List'. CD-ROM, updated periodically.

[87] M.C. Poppe and Cambridge Engineering Inc. 'Improved DGPS Data Reliability through the Use of Advanced Signal Processing Techniques'. Technical Report DTRS–57–91–C–00084, DOT Contract, 1995.

[88] P.K. Enge. 'Forward Error Correction for Radiobeacon Broadcast of Differential GPS Data'. *IEEE Transactions on Aerospace and Electronic Systems*, 29(1):223–233, 1993.

[89] T.G. Collett. *Coverage Prediction of Aeronautical Non-Directional Beacons.* Honours dissertation, University of Wales, Bangor, 1995.

[90] CCIR. 'Report to the Regional Administrative Radio Conference for the Planning of Frequencies for the Maritime Radiobeacons in the European Maritime Area'. Technical report, ITU, 1984.

[91] International Telephone and Telegraph Corporation. *Reference Data for Radio Engineers.* Howard W. Sam and Co., 1975.

[92] N. Ward and J.D. Last. 'Implementation and Performance of DGPS on a Helicopter'. In *Differential Satellite Navigation Symposium*, April 1995.

[93] W.H. Hundley *et al.* 'Flight Evaluation of a Basic C/A-Code Differential GPS Landing System for Category I Precision Approach'. *NAVIGATION*, 40(2):161–178, 1993.

[94] G. Lachapelle *et al.* 'GPS System Integration and Field Approaches in Precision Farming'. *NAVIGATION*, 41(3):323–335, 1994.

[95] R. Backstrom *et al.* 'Establishment of a Joint Governmental Differential Service for Marine Use in the Baltic Sea'. In *ION Satellite Division's Technical Meeting*, September 1991.

[96] Ylesradio OY. 'DGPS-beacon measurements: Baltic sea and Saimaa Lake areas'. Technical report, Finnish Maritime Administration, May 1995.

[97] K. Jansen, C. Goodman, and Z. Harrington. 'Draft – DGPS Commissioning Records'. Technical report, GLA, 1993.

[98] J.D. Last. 'Differential GPS Feasability Trial Conducted by MENAS in December 1994 and January 1995'. Technical report, MENAS, 1995.

[99] J.D. Last. 'Differential GPS Signal Measurements Conducted for MENAS on L.T. Relume in March 1995'. Technical report, MENAS, 1995.

[100] P.K. Enge. 'Approximate Performance of Coded Systems in Combined Atmospheric Noise and Skywave'. In *Proceedings of the 1986 Conference on Information Sciences and Systems*, pages 573–578, 1986.

[101] A. Papoulis. *Probability, Random Variables, and Stochastic Processes.* McGraw–Hill, 1984.

[102] S. Haykin. *An Introduction to Analog and Digital Communications.* John Wiley and Sons, 1989.

[103] M. Kotaki. 'Global Distribution of Radio Noise Derived from Thunderstorm Activity'. *Journal of Atmospheric and Terrestrial Physics*, 46(10):867–877, 1984.

[104] P.K. Enge *et al.* 'The Impact of Precipitation Static on the Range and Availability of a Radiobeacon Broadcast of Differential GPS Data'. In *DSNS '95*, 1995.

[105] D. Poppe. *Burst-Error Correcting Coding for Medium Frequency Broadcasts of Differential GPS Signals.* MSEE thesis, Worcester Polytechnic Institute, 1991.

[106] U.L. Rohde and T.T.N. Bucher. *Communications Receivers, Principles and Design.* McGraw-Hill, 1988.

[107] IALA. 'Interfering Distances of Maritime Radiobeacon *(sic)* in the European Maritime Area of Region 1'. Technical Report YBSAAV, 1985.

[108] X. Qin. 'Very Precise Differential GPS-Development Status and Test Results'. In *ION Satellite Division's Technical Meeting*, pages 615–624, 1992.

[109] K. Hervig. 'DIFFSTAR - A Project Based on Differential GPS in Northern Norway'. In *IEEE PLANS Symposium*, pages 297–302, 1986.

[110] J.R. Clynch *et al.* 'Monterey Bay Precise Positioning Experiment: Comparisons of GPS Receiver Solutions Under Dynamic Condition'. In *ION Satellite Division's Technical Meeting*, 1991.

[111] D. Young *et al.* 'DGPS/Radiobeacons: Noise Cancellation and Type 9 Messaging'. In *DSNS '95*, 1995.

Appendix A

RTCM Message Format

For more details on these or other RTCM messages, see Ref. [18].

All RTCM messages are composed of 30-bit words, the last 6 bits of which form a parity count. The parity algorithm, identical to that of GPS, is designed to provide a strong error detection capability. Figure A.1 shows the format of the first two words of every message: a message header providing a synchronisation preamble and message sequence number, the message type and length, the reference station ID and health and a time-tag indicating when the message was generated. This header is followed by a variable length subframe, depending on the message type and the number of PRCs being transmitted.

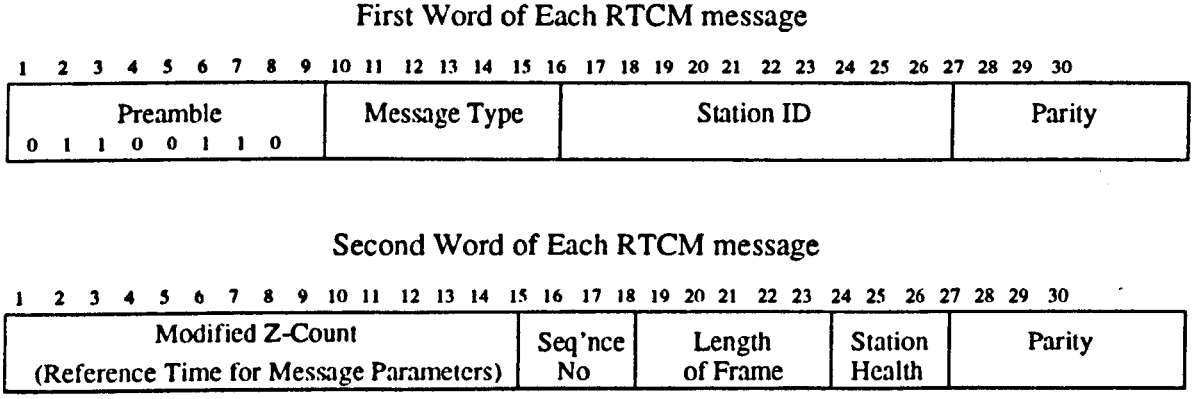

Figure A.1: The 2-word header of all RTCM messages, providing information for word synchronisation, reference station identification and PRC time-stamping.

The Type 1 and the Type 9 messages have identical subframe structures, as given in Fig. A.2. The Type 1 message, which is of variable length, includes PRC ad RRC information for all satellites in view of the reference station. The Type 9 message, which is seven words long, contains the PRC and RRC information for exactly three satellites.

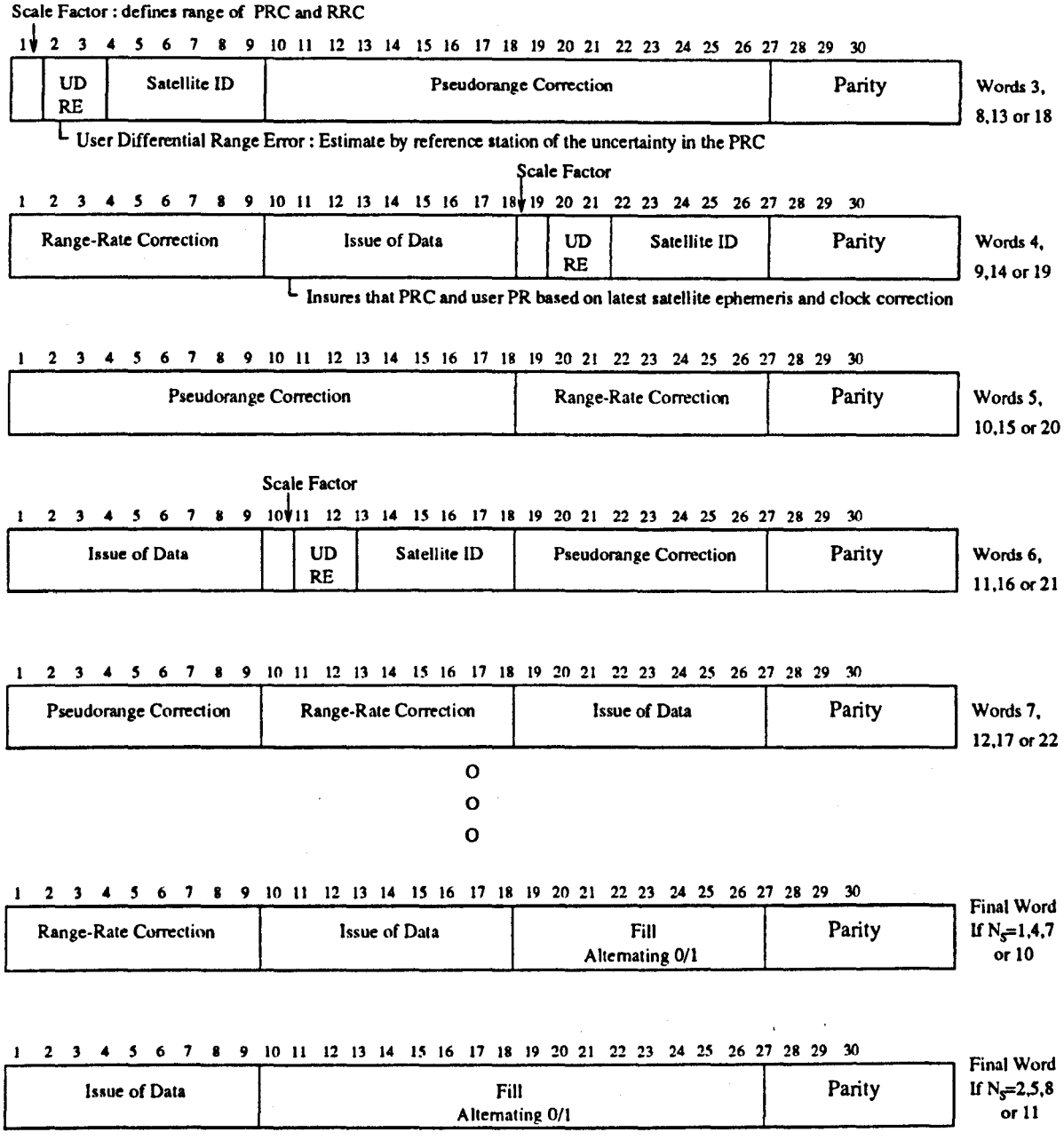

Figure A.2: The subframe format of a Type 1 or Type 9 message, providing PRCs and RRCs. If the number of satellite corrections, N_s, in a Type 1 message is not a factor of 3, then the *Final Word* will need to be filled with alternating 0s and 1s, as indicated. A Type 9 message is always exactly 7 words long, containing the corrections for 3 satellites and no *Fill*.

Appendix B

IALA DGPS Reference Station Survey

The following is the January 1994 version of the DGPS reference station list being compiled by IALA.

Station name	Location Lat, Lon	NR (km)	Freq. (kHz)	Rate bps	Station in operation
Country : AUSTRALIA Range based on 50 μV/m					
Cape Schanck	38°30'S, 114°53'E	280	314.0	100	June 1994
Karratha	20°45'S, 116°27'E	230	304.0	100	Dec. 1994
Country : BELGIUM Range based on 50 μV/m					
Oostende	51°14'N, 02°55'E	70	311.5	100	April 1995
Country : BERMUDA Range based on 50 μV/m					
St. David's Head	32°22'N, 64°38'W	320	323.0	100	yes
Country : CANADA Range based on 75 μV/m					
Alert Bay BC	50°35'N, 125°55'W	450	TBA	100	mid 1996
Tofino BC	48°55'N, 125°32'W	350	TBA	100	mid 1996
Pt. Atkinson BC	49°19'N, 123°15'W	90	320.0	100	yes
		170	320.0	200	mid 1996
St.Jean Richelieu QUE	46°19'N, 73°18'W	200	308.0	100	yes
		330	308.0	200	mid 1996
Trois-Rivieres QUE	46°23'N, 72°27'W	115	321.0	100	yes
		170	321.0	200	mid 1996
Lauzon QUE	46°48'N, 71°09'W	200	314.0	100	yes
		330	314.0	200	mid 1996
Partridge Isl. NB	45°14'N, 66°03'W	90	311.0	100	yes
		300	311.0	100	mid 1996
Cardinal ON	44°47'N, 75°25'W	300	TBA	200	mid 1996
Halifax NS	44°40'N, 63°36'W	180	TBA	200	mid 1996
East Pt. PEI	46°27'N, 61°58'W	300	314.0	100	mid 1996
Cape Race NFLD	46°39'N, 53°04'W	310	288.0	100	yes
		525	288.0	200	mid 1996
Wiarton ON	44°42'N, 81°08'W	250	TBA	100	1997
Riviere du Loup QUE	47°45'N, 69°36'W	300	TBA	100	1997
Miosie QUE	50°12'N, 66°07'W	300	TBA	100	1997
Pt. Escuminiac NB	47°04'N, 64°47'W	300	TBA	200	1997
Western Head NS	43°59'N, 64°39'W	110	296.0	100	yes
		300	296.0	200	1997
Cranberry Isl. NS	45°19'N, 60°55'W	300	286.0	100	1997
Port aux Basques NFLD	47°34'N, 59°09'W	170	290.0	100	yes
		350	290.0	200	1997
Rigolet NFLD	54°15'N, 58°30'W	300	TBA	100	1997
Sandspit BC	53°14'N, 128°48'W	350	TAB	100	1997
Cap de Rosiers QUE	48°51'N, 64°12'W	300	TBA	100	1997
La Romaine QUE	50°12'N, 60°41'W	300	TBA	100	1997
Devil's Head NFLD	49°07'N, 58°24'W	300	TBA	100	1997

Station name	Location Lat, Lon	NR (km)	Freq. (kHz)	Rate bps	Station in operation
Postolet Bay NFLD	51°29'N, 55°48'W	310	317.0	100	yes
		350	317.0	100	1997
Cape Bonavista NFLD	48°42'N, 53°05'W	200	TBA	100	1997
Race Rocks BC	48°18'N, 123°32'W	75	309.0	100	yes
Triple Isl. BC	54°17'N, 130°52'W	90	308.0	100	yes
Pt. Petrie ON	43°50'N, 77°09'W	115	303.0	100	yes
Port Weller ON	43°15'N, 79°13'W	30	302.0	100	yes
Sombra ON	42°43'N, 82°29'W	32	306.0	100	yes
Country : DENMARK/FAROE ISL/GREENLAND Range based on 50 μV/m					
Hammer Odde	55°18'N, 14°46'E	90	289.0	100	yes
Skagen	57°45'N, 10°35'E	90	298.0	100	yes
Blaavandshuk	55°34'N, 08°05'E	90	296.5	100	yes
Country : ESTONIA Range based on 50 μV/m					
Ristna	58°56'N, 22°04'E	90	307.0	100	Dec 1994
Country : FINLAND Range based on 50 μV/m					
Porkkala	59°58'N, 24°23'E	90	285.0	100	yes
Mantyluoto	61°36'N, 21°28'E	90	298.0	100	yes
Puumala	61°24'N, 28°14'E	90	301.5	100	yes
Outokumpu	62°41'N, 26°01'E	90	293.5	100	Dec 1994
Country : FRANCE Range based on 50 μV/m					
Gatteville	49°42'N, 01°16'W	75	297.5	100	yes
Echmuhl	47°48'N, 04°22'W	75	312.5	1995/1996	
Les Baleines	46°15'N, 01°34'W	75	299.5	100	1994
Cap Ferret	44°39'N, 01°15'E	75	287.0	100	1995/1996
Cap Bear	42°31'N, 03°08'W	110	313.0	100	1995/1996
La Revellatta	42°35'N, 08°44'E	110	294.5	100	1995/1996
Country : GERMANY Range based on 50 μV/m					
Wustrow	54°20'N, 12°23'E	90	314.5	200	April 1994
Helgoland	54°11'N, 07°53'E	130	313.0	200	Dec. 1994
Country : ICELAND Range based on 50 μV/m					
Reykjanes	63°49'N, 22°42'W	310	292.5	100	Dec.92
Bjargtangar	65°30'N, 24°32'W	200	289.0	100	Oct 1994
Skagata	66°07'N, 20°06'W	200	304.5	100	Oct 1993
Raufarhofn	66°27'N, 15°57'W	200	301.5	100	Feb 1994
Djupivogur	64°39'N, 14°17'W	200	295.5	100	Jul 1994
Skardsfjara	63°31'N, 17°59'W	200	313.0	100	Aug 1993
Country : IRELAND Range based on 50 μV/m					
Tory Isl.	55°16'N, 08°15'W	129	313.5	100	yes
Mizen Head	51°27'N, 09°49'W	129	300.5	100	yes

Station name	Location Lat, Lon	NR (km)	Freq. (kHz)	Rate bps	Station in operation
Country : JAPAN					
Turugi-zaki	35°08'N, 139°40'E	TBA	309.0	TBA	end1995
Daioh-zaki	34°16'N, 136°54'E	TBA	288.0	TBA	end1995
Country : THE NETHERLANDS Range based on 50 μV/m					
Hoek van Holland	51°59'N, 04°07'E	88	287.5	100	yes
Ameland	53°27'N, 05°37'E	92	299.5	100	end 1996
Country : NORWAY Range based on 50 μV/m					
Faerder	59°01'N, 10°31'E	70	288.0	100	Oct 1993
Lista	58°06'N, 06°34'E	70	301.0	100	Oct 1994
Utsira	59°18'N, 04°30'E	70	307.0	100	Oct 1992
Utvaer	61°02'N, 04°30'E	70	300.0	100	Oct 1993
Svinoey	62°19'N, 05°16'E	70	293.5	100	Sept 1993
Halten	64°10'N, 09°24'E	70	313.5	100	Sept 1993
Sklinna	65°12'N, 10°50'E	70	288.5	100	mid 1995
Skomvaer	67°24'N, 11°52'E	70	300.0	100	Sept 1993
Torsvaag	70°14'N, 19°30'E	70	291.5	100	mid 1995
Vardo	70°23'N, 31°09'E	70	307.0	100	Oct 1004
Country : POLAND Range based on 50 μV/m					
Dziwnow	54°01'N, 14°44'E	130	288.0	100	1995
Rozewie	54°49'N, 18°20'E	130	311.0	100	1995
Country : RUSSIA Range based on 20 μV/m					
Baltiisk	54°38'N19°54'E	500	312.5	100	1995/1996
Shepelevskiy	59°59'N, 29°29'E	500	298.5	100	1995-1996
Set. Navolock	69°24'N, 32°29'E	500	318.5	100	1996
Dgedginsky	65°13'N, 36°49'E	500	298.5	100	1996
Canin-Nose	65°13'N, 43°18'E	500	285.5	100	1996
Tonky	69°51'N, 61°06'E	500	303.5	100	1996
Sterlegov	75°24'N, 88°45'E	500	318.5	100	1996
Andrea	76°44'N, 110°28'E	500	291.5	100	1996
Camenka	69°28'N, 161°14'E	500	291.5	100	1996
Yarangai	69°54'N, 170°32'E	500	291.5	100	1996
Russian Cat	64°34'N, 178°33'E	500	315.5	100	1997
Caraginsky	58°33'N, 163°33'E	500	301.5	100	1997
Africa	56°33'N, 163°33'E	500	291.5	100	1997
Petropavlovsky	52°53'N, 158°42'E	500	291.5	100	1997
Vasilieva	50°04'N, TBA	500	303.5	100	1997
Alevina	58°50'N, 151°21'E	500	303.5	100	1997
Crutogrova	55°05'N, 155°35'E	500	300.5	100	1997
Elizarova	54°25'N, 143°43'E	500	318.5	100	1997
Corsakovsky	46°37'N, 142°48'E	500	312.5	100	1997
Gamov	42°33'N, 131°13'E	500	306.5	100	1997

Station name	Location Lat, Lon	NR (km)	Freq. (kHz)	Rate bps	Station in operation
Astyrahnasky	44°28'N, 48°01'E	500	291.5	100	1997
Anapsky	44°53'N, TBA	500	315.5	100	1996
Vize	79°30'N, 76°59'E	500	294.5	100	1997
Oleniy	72°35'N, 77°39'E	500	294.5	100	1996
Enisey	68°25'N, TBA	500	315.5	100	1996
Begichev	47°31'N, 112°15'E	500	300.5	100	1996
Stolbovoy	74°10'N, TBA	500	306.5	100	1996
Cotelny	75°59'N, TBA	500	310.5	100	1996
Indygirsky	71°16'N, 150°17'E	500	324.5	TBA	1996
Vrangelia	70°59'N, 178°29'E	500	309.5	100	1996
Dedgneva	66°01'N, 169°43'E	500	303.5	100	1996
Van-der-Linda	45°35'N, 149°24'E	500	312.5	100	1997
Country : SWEDEN Range based on 50 μV/m					
Bjuroklubb	64°29'N, 21°35'E	103	303.5	100	May 1994
Skags Udde	63°11'N, 19°01'E	103	306.5	100	June 1994
Orskaer	60°32'N, 18°23'E	74	291.5	100	April 1994
Almagrundet	59°09'N19°10'E	88	287.0	100	Jan 1994
Hoburg	56°55'N, 18°09'E	74	302.0	100	Feb 1994
Kullen	56°18'N, 12°27'E	103	293.5	100	Jan 1994
Hjortons Udde	58°38'N, 12°40'E	74	297.0	200	Jan 1996
Country : UNITED KINGDOM Range based on 50 μV/m					
Lizard	49°57'N, 05°12'W	129	284.0	100	yes
St. Catherines	50°34'N, 01°17'W	129	293.5	100	yes
N'Foreland	51°22'N, 01°26'E	129	310.5	100	yes
Flamborough	54°06'N, 00°04W	129	302.5	100	yes
Girdle Ness	57°08'N, 02°03'W	129	311.5	100	yes
Rinns of Islay	55°40'N, 06°31'W	129	293.5	100	yes
Butt of Lewis	58°31'N, 06°16'W	129	289.5	100	yes
Sumburgh	59°51'N, 01°16'W	129	304.5	100	yes
Pt. Lynas	53°24'N, 04°17'W	129	304.5	100	yes
Country : USA 100 bps range based on 75 μV/m 200 bps range based on 100 μV/m					
Wisconsin Pt WI	46°42'N, 92°01'W	65	296.0	100	Nov 1995
Upper Keweenaw MI	47°13'N, 88°32'W	210	298.0	100	Oct 1995
Whitefish Pt MI	46°46'N, 84°52'W	160	318.0	100	yes
Neebish Is. MI	46°19'N, 84°09'W	100	309.0	200	May 1995
Sturgeon Bay WI	44°48'N, 87°19'W	175	322.0	100	Sept 1995
Cheboygan MI	45°39'N, 84°28'W	130	293.0	200	Aug 1995
Saginaw MI	43°38'N, 83°50'W	140	301.0	100	Aug 1995
Milwaukee WI	43°00'N, 87°53'W	225	298.0	100	Sept 1995
Detroit MI	42°18'N, 82°58'W	160	319.0	200	Aug 1995

Station name	Location Lat, Lon	NR (km)	Freq. (kHz)	Rate bps	Station in operation
Youngstown NY	43°14'N, 79°01'W	240	322.0	100	1995
Brunswick ME	43°54'N, 68°–'W	160	316.0	100	Jun 1995
Portsmouth NH	43°04'N, 70degree44'W	160	288.0	100	yes
Chatham MA	41°40'N, 69°57'W	155	304.0	200	Jun 1995
Montauk Pt NY	41°04'N, 71°52'W	210	293.0	100	yes
Sandy Hook NJ	40°28'N, 74°00'W	160	286.0	200	yes
Cape Henlopen DE	38°47'N, 75°05'W	290	298.0	100	yes
Cape Henry VA	36°56'N, 76°00'W	210	289.0	100	yes
Fort Macon NC	34°42'N, 76°41'W	210	294.0	100	Jul 1995
Charleston SC	32°45'N, 79°51'W	240	298.0	100	Aug 1995
Cape Canaveral FL	28°28'N, 80°33'W	400	289.0	100	Aug 1995
Miami FL	25°45'N, 80°10'W	195	322.0	100	Aug 1995
Key West FL	24°–'N, 82°–'W	175	286.0	100	Dec 1995
San Juan PR	18°–'N, 66°–'W	200	295.0	100	Dec 1995
Egmont Key FL	27°36'N, 82°46'W	340	312.0	100	yes
Mobile Pt AL	30°14'N, 88°01'W	275	300.0	200	Aug 1995
English Turn LA	29°53'N, 89°57'W	275	293.0	200	yes
Galveston TX	29°20'N, 94°44'W	290	296.0	100	yes
Aransas Pass TX	27°50'N, 97°04'W	290	304.0	100	yes
Cape Hinchenbrook AK	60°14'N, 146°39'W	290	292.0	100	yes
Potato Pt AK	61°03'N, 146°42'W	160	298.0	100	yes
Kenai AK	60°36'N, 150°13'W	275	310.0	100	Oct 1995
Cape Kodiak AK	57°37'N, 152°11'W	290	313.0	100	Oct 1995
Cold Bay AK	55°15'N, 162°46'W	290	289.0	100	Oct 1995
Gustavus AK	58°25'N, 135°42'W	275	288.0	100	Oct 1995
Annette Isl	55°04'N, 131°36'W	275	323.0	100	Oct 1995
Upola Pt HI	20°15'N, 155°53'W	275	285.0	100	Nov 1995
Kokole Pt HI	22°04'N, 159°47'W	485	300.0	100	Nov 1995
Whidbey Isl WA	48°19'N, 122°42'W	145	302.0	100	yes
Robinson Pt WA	47°23'N, 122°22'W	95	323.0	200	yes
Fort Stevens OR	46°12'N, 123°57'W	290	287.0	100	Aug 1995
Cape Mendocino CA	40°26'N, 124°24'W	290	292.0	100	Aug 1995
Pigeon Pt CA	37°11'N, 122°23'W	290	287.0	100	Sept 1995
Pt Blunt CA	37°51'N, 122°25'W	95	310	200	June 1995
Pt Arguello CA	34°35'N, 120°39'W	290	321.0	100	July 1995
Pt Loma CA	32°40'N, 117°15'W	290	302.0	100	July 1995
Vicksburg MS	32°20'N, 90°35'W	190	313.0	200	yes
Memphis TN	35°28'N, 90°12'W	190	310.0	200	yes
St Louis MO	38°37'N, 89°46'W	190	322/0	200	yes
Rock Isl IA	42°01'N, 90°14'W	240	311.0	200	1995
St Paul MN	44°18'N, 91°54'W	240	317.0	200	1995
Millers Ferry AL	32°05'N, 87°24'W	240	320	200	1995

Appendix C

Coverage Examples

The following diagrams have been generated using the Bangor DGPS coverage prediction model. These are examples of the model being employed for system planning in four different areas.

Fig.*NOR 12* –Night-time coverage for a system of 13 beacons in Norway. Notice the fading zone north of 'Torungen' and the effect of interference on 'Utsira' in contrast to the extensive coverages of the more northerly beacons. Reproduced by permission of the Norwegian Coast Directorate.

Fig.*AUS SE2* –Night-time coverage of six beacons in South-East Australia. The high atmospheric noise levels at these latitudes causes severe loss of coverage for these beacons. Reproduced by permission of the Australian Maritime Safety Authority.

Fig. *ME 6* –Night-time individual coverage contours for four beacons in the Arabian Gulf. Overlapping coverage is desired in these hazardous waters. Reproduced by permission of the Middle East Navigation Aids Service.

Fig. *British Isles* –The groundwave field strength contour (not coverage) for a system of 11 beacons in the British Isles, after [91].

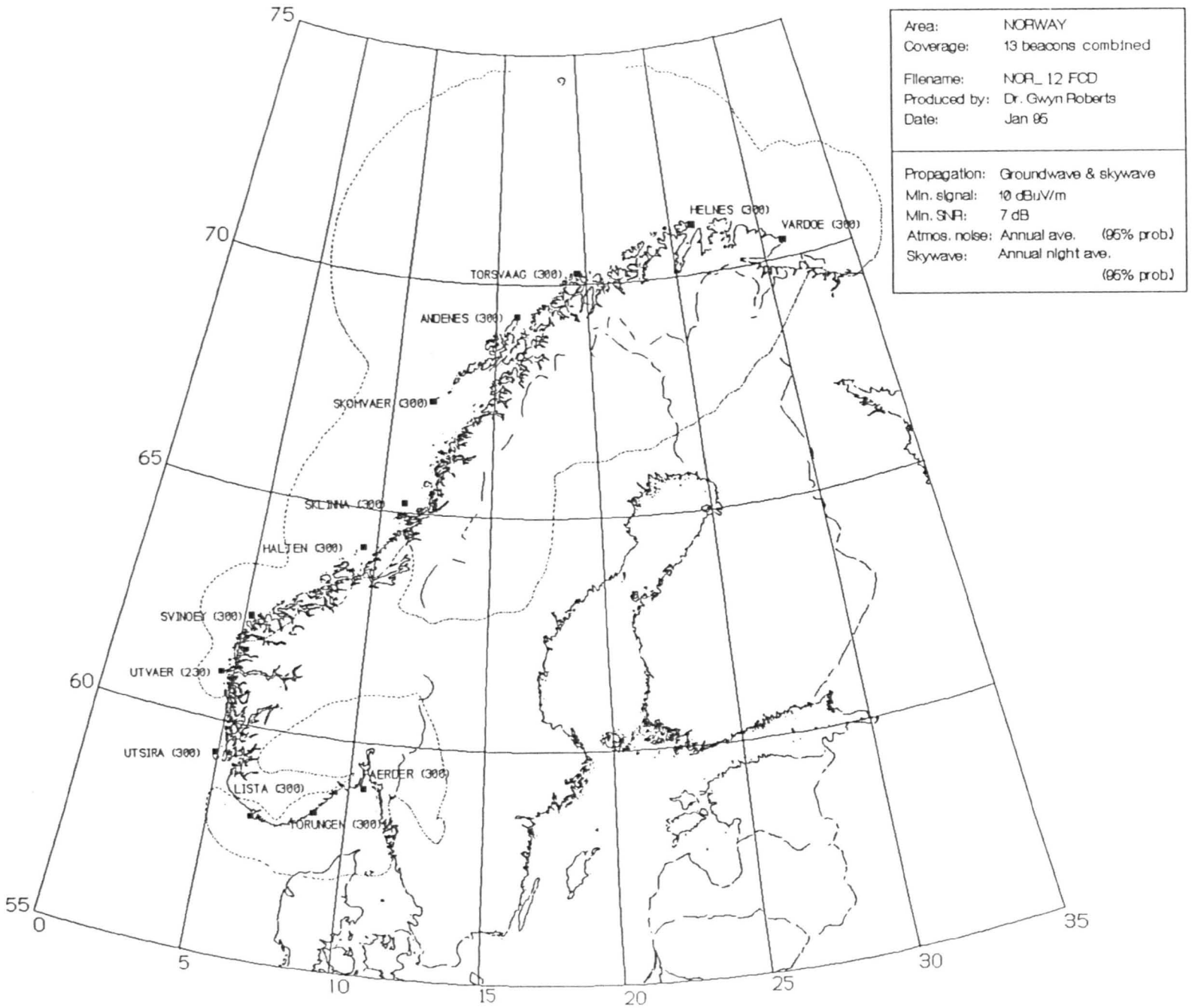
Area: NORWAY
Coverage: 13 beacons combined
Filename: NOR_12.FCD
Produced by: Dr. Gwyn Roberts
Date: Jan 95
Propagation: Groundwave & skywave
Min. signal: 10 dBuV/m
Min. SNR: 7 dB
Atmos. noise: Annual ave. (95% prob.)
Skywave: Annual night ave. (95% prob.)
HELNES (300)
VARDOE (300)
TORSVAAG (300)
ANDENES (300)
SKOMVAER (300)
SKJNNA (300)
HALTEN (300)
SVINOEY (300)
UTVAER (230)
UTSIRA (300)
LISTA (300)
TAERDER (300)
TORUNGEN (300)
75
70
65
60
55
0
5
10
15
20
25
30
35

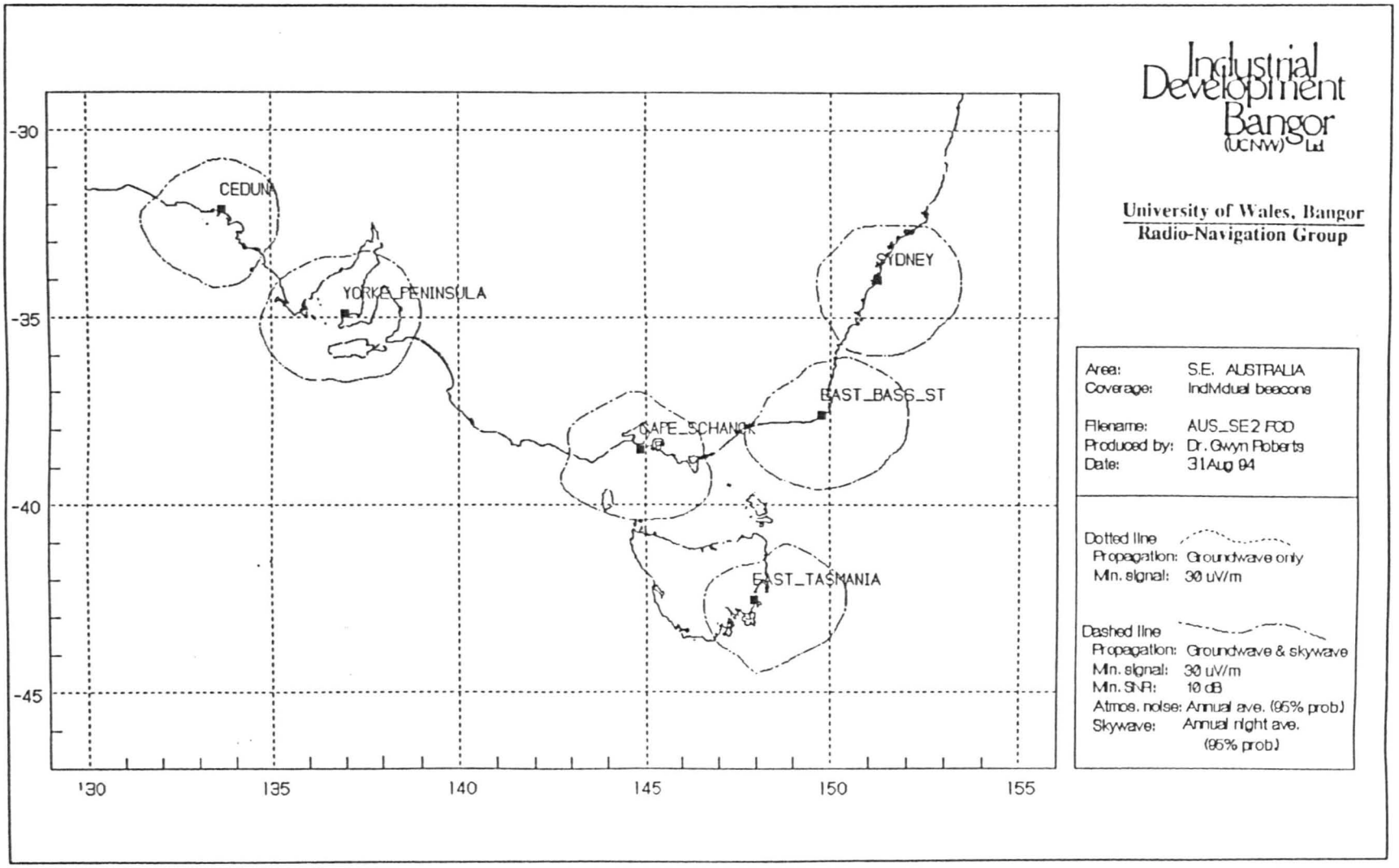
Industrial Development Bangor (UCNW) Ltd
University of Wales, Bangor
Radio-Navigation Group
-30
-35
-40
-45
130
135
140
145
150
155
CEDUNA
YORKE_PENINSULA
SYDNEY
EAST_BASS_ST
CAPE_SCHANCK
EAST_TASMANIA
Area: S.E. AUSTRALIA
Coverage: Individual beacons
Filename: AUS_SE2.FOD
Produced by: Dr. Gwyn Roberts
Date: 31Aug 94
Dotted line
Propagation: Groundwave only
Min. signal: 30 uV/m
Dashed line
Propagation: Groundwave & skywave
Min. signal: 30 uV/m
Min. SNR: 10 dB
Atmos. noise: Annual ave. (95% prob.)
Skywave: Annual night ave. (95% prob.)

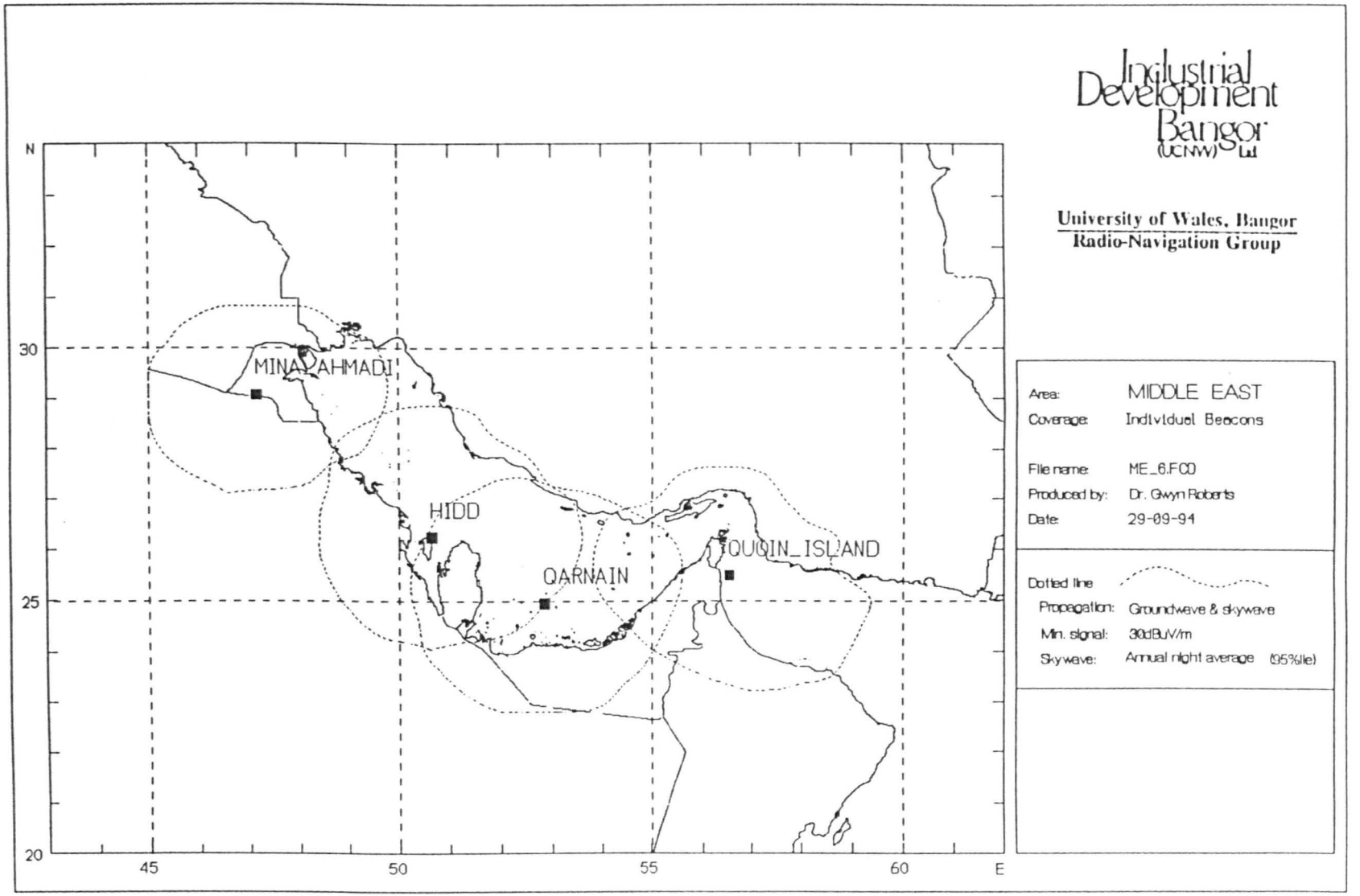
Industrial Development Bangor (UCNW) Ltd
University of Wales, Bangor
Radio-Navigation Group
N
30
25
20
45
50
55
60
E
MINA AHMADI
HIDD
QARNAIN
QUOIN_ISLAND
Area: MIDDLE EAST
Coverage: Individual Beacons
File name: ME_6.FCD
Produced by: Dr. Gwyn Roberts
Date: 29-09-94
Dotted line
Propagation: Groundwave & skywave
Min. signal: 30dBuV/m
Skywave: Annual night average (95%ile)

Ward & Last
Implementation and performance
of DGPS on a helicopter

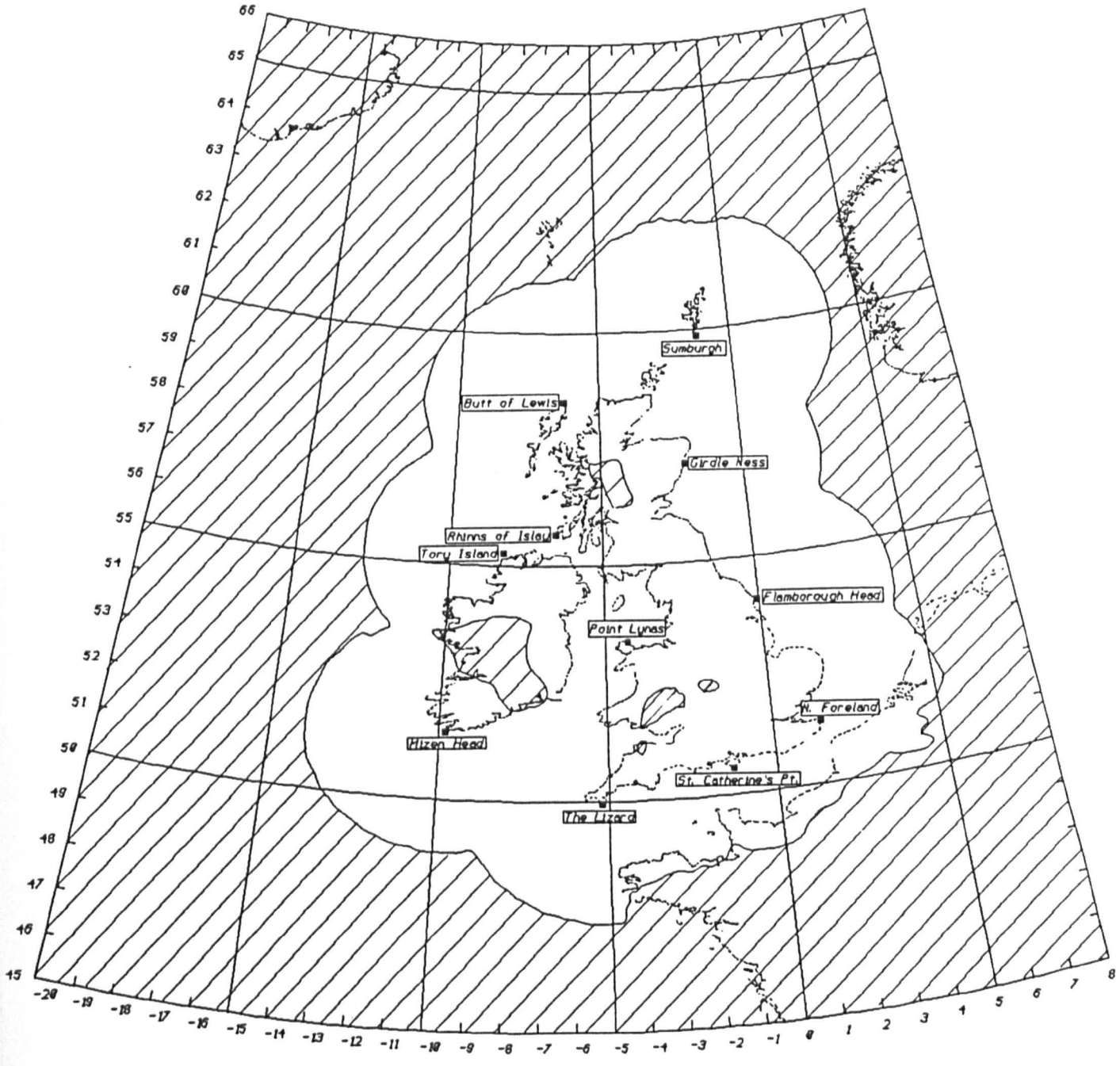

British Isles DGPS radiobeacons. The shaded areas are where the field strengths are below 20 μV/m. The boundary occurs at a range over sea water of 150 n.m..

Appendix D

Guide to the Bangor Radiobeacon Coverage Prediction Software

The Bangor Radiobeacon DGPS Coverage Prediction Software (CPS) is a suite of five C-programs used to generate coverage diagrams for DGPS radiobeacons. The main program, *PLOTBECN*, determines the actual coverage contours based on a series of parameters selected by the user at run-time. *PLOTBECN* draws on pre-calculated files generated for each beacon by the four other programs; *GNDWANT, SKYWANT, GNDIFR* and *SKYIFR*. These four programs, which calculate arrays of groundwave field strength, skywave field strength, groundwave interference levels and skywave interference levels respectively, need only be run once to install each beacon, being re-run if additions or modifications are made to the beacon list. Coverage diagrams are viewed in the CAD package EasyCAD, available from FastCAD Distributions, Watford, UK.

The CPS has been successfully tested on 80286 to 80486 PC machines. The executable versions (*.EXE* files) delivered are for use on a 80286 or better with a math co-processor. Figure D.1 shows the directory structure used by the CPS and the files associated with each directory. The specified structure needs to be used, as the CPS will look for database files only in their specified locations.

input.lst

All five programs make use of the *input.lst* file to determine which beacons the user wishes to have a program work with. The basic format of *input.lst* is given in Figure D.2. It contains first the number of beacons for which the software is to be run, followed by the names of these beacons. Any names beyond the number specified are ignored, so that the user need never re-type names but only cut and paste the desired names into the top lines of the file. If all 11 beacons are to be run, then their order is unimportant.

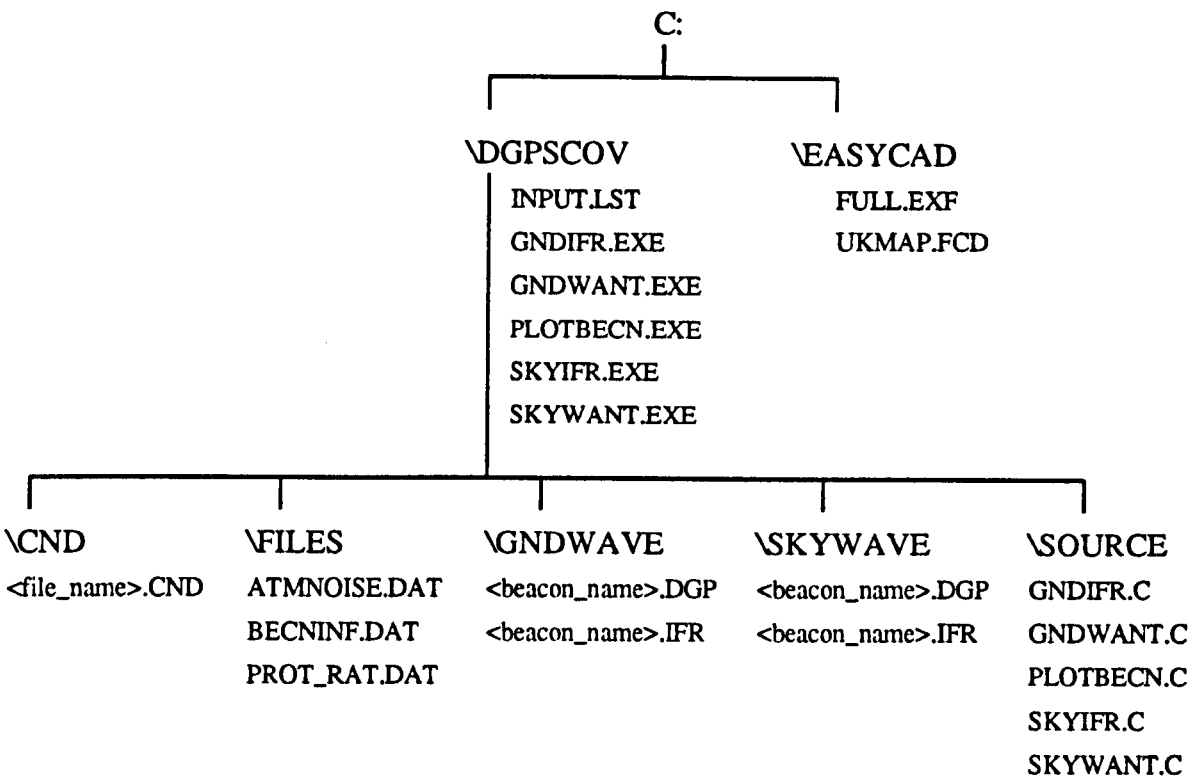

Figure D.1: The directory structure used by the Bangor CPS.

The spelling of the names must exactly match those given for the beacons in the *becninf.dat* file. All names are in upper case letters, with underscores instead of spaces.

GNDWANT

GNDWANT calculates the groundwave attenuation of the wanted DGPS beacons, creating the files */gndwave/⟨beacon_name⟩.dgp*. These files need to be created after installation of the software and re-created if modifications are made to any beacon's location. Adjustments to a beacon's nominal range can be made during the generation of a contour using *PLOTBECN*, although it is desirable to re-run *GNDWANT* if a permanent change is made to the nominal range of a beacon. To generate files for the beacons selected in *input.lst*, change into the *c:/dgpscov* directory and type *GNDWANT*.

For each beacon, a rectangular latitude/longitude window is defined which contains an array of calculation points spaced every 0.1° of latitude by 0.1° of longitude. The window is automatically set to include all calculation points within 550 km of the beacon, subject to the additional requirement that the window not extend outside the geographical box with its edges located at 44° North latitude, 65° North latitude, 18° West longitude and 8° East longitude. These define the edges of the master window for the British Isles. For a given beacon, *GNDWANT* must be run before *SKYWANT*, *GNDIFR* or *SKYIFR*, as the latter three use the beacon window defined by *GND-*

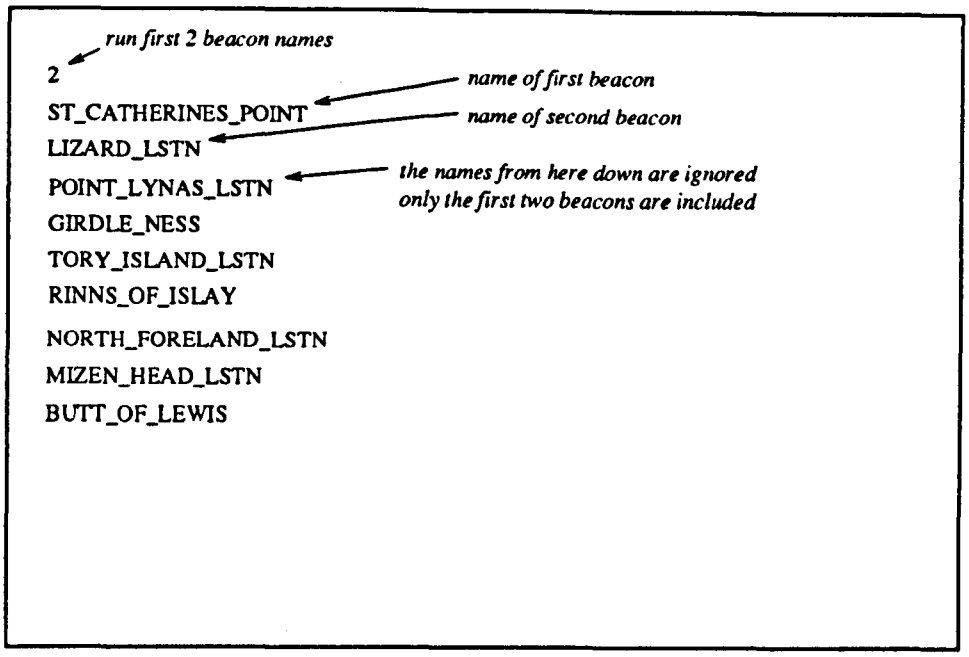

Figure D.2: The format of *input.lst* for a system of two beacons. The spelling of beacon name must exactly match that given in the *becninf.dat* file.

WANT.

The flow of the *GNDWANT* program is as follows :

1 Read *input.lst* to determine how many beacons are to be run,
2 Read a beacon name from *input.lst,*
3 Read the beacon's location and nominal range from *becninf.dat,*
4 Determine the latitude and longitude of the window around the beacon, such that it includes all calculation points within 550 km of the beacon,
5 Open the file */gndwave/⟨beacon_name⟩.dgp* and save the size and location of the beacon window,
6 Read in the conductivity files for the relevant area, that is, the **.cnd* files,
7 For each calculation point,
 7a Determine the great circle path between beacon and calculation point,
 7b Determine the path conductivity,
 7c Apply Millington's method to calculate the field strength attenuation at the calculation point,
 7d Save the attenuation in the */gndwave/⟨beacon_name⟩.dgp* file,
8 Repeat 7 until all the points are done,
9 Save the completed */gndwave/⟨beacon_name⟩.dgp* file,
10 Repeat 2 until the specified number of beacons have been run,
11 Done.

SKYWANT

SKYWANT calculates the skywave attenuation of the wanted DGPS beacons, creating the files */skywave/(beacon_name).dgp* . These files need to be created after installation and re-created if modifications are made to the beacon's location. Adjustments to a beacon's nominal range can be done during the generation of a contour using *PLOTBECN,* although it is desirable to re-run *SKYWANT* for a beacon with a permanent change to its nominal range. To generate files for the beacons selected in *input.lst,* change into the *c:/dgpscov* directory and type *SKYWANT. GNDWANT* must already have been run for the beacon. For each beacon, the size and location of the rectangular latitude/longitude window defined by *GNDWANT* is retrieved from the */gndwave/(beacon_name).dgp* file. This window defines an array of calculation points spaced every 0.1° of latitude by 0.1° of longitude. The flow of the *SKYWANT* program is as follows :

1 Read *input.lst* to determine how many beacons are to be run,
2 Read a beacon name from *input.lst,*
3 Read the beacon's location and nominal range from *becninf.dat,*
4 Retrieve the window size and location from the */gndwave/(beacon_name).dgp* file,
5 Open the file */skywave/(beacon_name).dgp* and save the size and location of the window,
6 Read in the conductivity files for the relevant area, that is, the **.cnd* files,
7 For each calculation point,
 7a Determine the great circle path between beacon and calculation point,
 7b Determine the slant distance between beacon and calculation point,
 7c Determine the geomagnetic latitude of the mid-point of the path,
 7d Determine the basic median skywave attenuation,
 7e Correct for antenna gain,
 7f Use the conductivity information to correct for sea gain,
 7g Save the attenuation in the */skywave/(beacon_name).dgp* file,
8 Repeat 7 until all the points are done,
9 Save the completed */skywave/(beacon_name).dgp* file,
10 Repeat 2 until the specified number of beacons have been run,
11 Done.

GNDIFR

GNDIFR calculates the groundwave interference to the wanted DGPS beacons, creating the files */gndwave/(beacon_name).ifr* . These files need to be created after installation and re-created if modifications are made to the wanted beacon's location. They must also be re-created if modifications of nominal range, beacon type or beacon location are made to any beacons on the same channel as the wanted beacons or any of the

Freq. Separation kHz	Wanted Beacon Type : DGPS	
	Interfering Beacon Type	
	MB, NDB	DGPS
0.0	15	15
0.5	-25	-22
1.0	-45	-36
1.5	-50	-42
2.0	-55	-47

Table D.1: ITU protection ratios, in dB, between wanted DGPS and interfering transmissions. The left-hand column is the frequency separation between the wanted and unwanted signals. Different values are prescribed when the interference is caused by a marine beacon or aeronautical NDB from those when a DGPS transmission is the interferer.

four adjacent channels either side. To generate files for the wanted beacons selected in *input.lst,* change into the *c:/dgpscov* directory and type *GNDIFR. GNDWANT* must already have been run for the beacon.

For each wanted beacon, the size and location of the rectangular latitude/longitude window defined by *GNDWANT* is retrieved from the */gndwave/⟨beacon_name⟩.dgp* file. This window defines an array of calculation points spaced every 0.1° of latitude by 0.1° of longitude. The *becninf.dat* file is used to assemble a list of potential groundwave interferers whose groundwave field strengths are then calculated at all relevant points. Potential interferers are determined based on both geographical and frequency separation from the wanted beacon and the protection ratio information contained in *prot_rat.dat.* Table D.1 lists the protection ratios applied by the CPS for the British Isles.

The flow of the *GNDIFR* program is as follows :

1 Read *input.lst* to determine how many beacons are to be run,
2 Read a beacon name from *input.lst,*
3 Read the beacon's location, nominal range and frequency from *becninf.dat,*
4 Retrieve the window size and location from the */gndwave/⟨beacon_name⟩.dgp* file
5 Open the file */gndwave/⟨beacon_name⟩.ifr* and save the size and location of the window,
6 Read in the conductivity files for the relevant area, that is, the **.cnd*files,
7 Read the protection ratio information from *prot_rat.dat*
8 Assemble a list of the potential interferers based on the frequency and geographical separation of the wanted beacon and the beacons in *becninf.dat*
9 For each calculation point,
9a Determine the great circle path between each interferer and calculation

point,
9b Determine the path conductivity for each interferer,
9c Apply Millington's method to determine the strength of each interferer at the calculation point,
9d Use the frequency separation to determine the interference level of each interferer relative to its protection ratio,
9e Determine the strongest co-channel interference level,
9f Determine the strongest adjacent channel interference level,
9g Save the strongest co-channel and adjacent channel interference level to the */gndwave/(beacon_name).ifr* file,
10 Repeat 9 until all points are done,
11 Save the completed */gndwave/(beacon_name).ifr* file,
12 Repeat 2 until the specified number of beacons have been run,
13 Done.

SKYIFR

SKYIFR calculates the skywave interference to the wanted DGPS beacons, creating the files */skywave/(beacon_name).ifr*. These files need to be created after installation and re-created if modifications are made to the wanted beacon's location. They must also be re-created if modifications of nominal range, beacon type or beacon location are made to any beacons on the same channel as the wanted beacons or any of the four adjacent channels either side. To generate files for the wanted beacons selected in *input.lst,* change into the *c:/dgpscov* directory and type *SKYIFR. GNDWANT* must already have been run for the beacon.

For each wanted beacon, the size and location of the rectangular latitude/longitude window defined by *GNDWANT* is retrieved from the */gndwave/(beacon_name).dgp* file. This window defines an array of calculation points spaced every 0.1° of latitude by 0.1° of longitude. The *becninf.dat* file is used to assemble a list of potential skywave interferers whose skywave field strengths are then calculated at all relevant points. Potential interferers are determined based on both geographical and frequency separation from the wanted beacon and protection ratio information from the *prot_rat.dat* file, as given in Table D.1.

The flow of the *SKYIFR* program is as follows :

1 Read *input.lst* to determine how many beacons are to be run,
2 Read a beacon name from *input.lst,*
3 Read the beacon's location, nominal range and frequency from *becninf.dat,*
4 Retrieve the window size and location from the */gndwave/(beacon_name).dgp* file
5 Open the file */skywave/(beacon_name).ifr* and save the size and location of the window,

6 Read in the conductivity files for the relevant area, that is, the **.cnd* files,
7 Read the protection ratio information from *prot_rat.dat*
8 Assemble a list of the potential interferers based on the frequency and geographical separation of the wanted beacon and the beacons in *becninf.dat*
9 For each calculation point,
 9a Determine the great circle path between each interferer and calculation point,
 9b Determine the slant distance between each interferer and calculation point,
 9c Determine the geomagnetic latitude of the mid-point of each path,
 9d Determine the basic median skywave field strength for each interferer,
 9e Correct for antenna gain,
 9f Use the conductivity information to correct for sea gain for each interferer,
 9g Determine the strongest co-channel interference level,
 9h Determine the strongest adjacent channel interference level,
 9i Save the strongest co-channel and adjacent channel interference level to the */skywave/⟨beacon_name⟩.ifr* file,
10 Repeat 9 until all the points are done,
11 Save the completed */skywave/⟨beacon_name⟩.ifr* file,
12 Repeat 2 until the specified number of beacons have been run,
13 Done.

PLOTBECN

PLOTBECN generates the file *c:/easycad/full.exf,* containing a coverage contour. To generate a contour for the system of beacons specified in *input.lst,* change into the *c:/dgpscov* directory and type the command *PLOTBECN.* The program presents the user with a menu screen as shown in Figure D.3. The default values are for the contour of standard nighttime coverage. Toggling parameters 2 and 4 to 'NO' would give the standard daytime coverage contour. This menu allows the user to specify the desired coverage limiting criteria for the contour. There are 10 parameters that may be adjusted, as detailed below.

Parameter 1. Wanted signal via Groundwave

The user may select whether or not the groundwave-propagated component of the wanted beacon signal is to be taken into account when computing coverage. This parameter toggles between YES and NO as the '1' key is pressed. Normally this parameter would always be set to YES, for both day and night conditions. The groundwave field strengths associated with this option are calculated by the *GNDWANT* program and

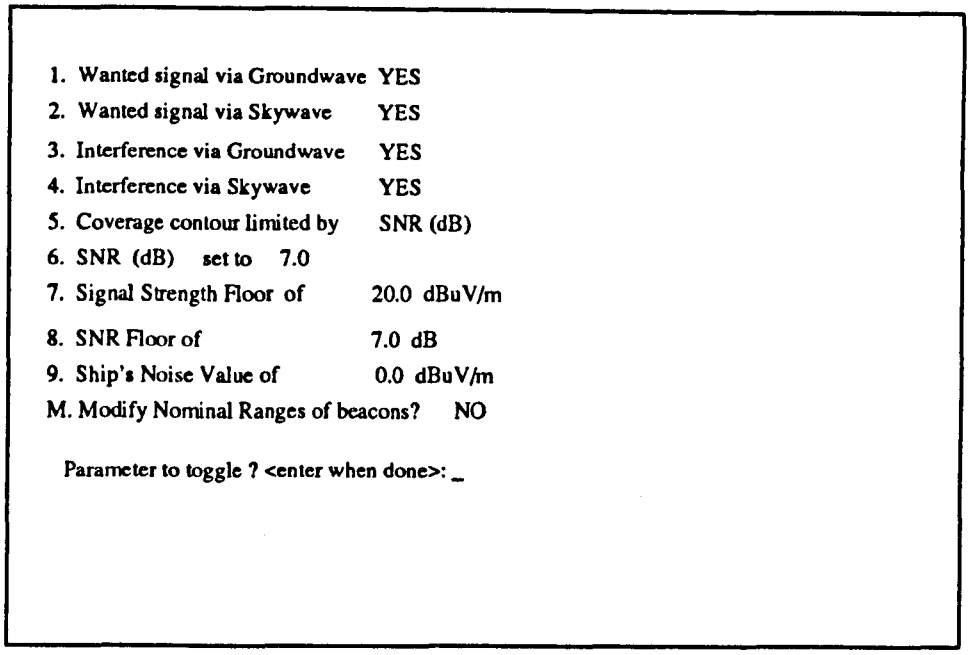

Figure D.3: The *PLOTBECN* menu presented to the user. Here the coverage limiting criteria for a contour may be specified. The default values are for the contour of standard nighttime coverage. Toggling parameters 2 and 4 to NO would give the standard daytime coverage contour.

stored in the */gndwave/⟨beacon_name⟩.dgp* files.

Parameter 2. Wanted signal via Skywave

The user may select whether or not the skywave-propagated component of the wanted beacon signal is to be taken into account when computing coverage. This parameter toggles between YES and NO as the '2' key is pressed. Normally this parameter would be set to YES for night conditions and NO for day conditions. If parameter 1 is set to NO and parameter 2 is set to YES, then the level of skywave signal available from the wanted beacon 95% of the time is applied to coverage criteria. If both parameters 1 and 2 are set to YES, then own-skywave interference is taken into account and the level of total wanted signal available 95% of the time is used in coverage calculations. The skywave field strengths associated with this option are calculated by the *SKYWANT* program and stored in the */skywave/⟨beacon_name⟩.dgp* files.

Parameter 3. Interference via Groundwave

The user may select whether or not the groundwave propagated component of any unwanted or interfering beacon signals are to be taken into account when computing coverage. This parameter toggles between YES and NO as the '3' key is pressed. Normally

this parameter would always be set to YES, for both day and night conditions. The numerical values associated with this option are calculated by the *GNDIFR* program and stored in the */gndwave/(beacon_name).ifr* files. If the level of groundwave interference exceeds the level of wanted signal, the point is deemed to be outside coverage. As explained in D, the level of groundwave interference saved in the*(beacon_name).ifr* files already incorporates an adjustment for the standard protection ratios.

Parameter 4. Interference via Skywave

The user may select whether or not the skywave propagated component of any unwanted or interfering beacon signals are to be taken into account when computing coverage. This parameter toggles between YES and NO as the '4' key is pressed. Normally this parameter would be set to YES for night conditions and NO for day conditions. The numerical values associated with this option are calculated by the *SKYIFR* program and stored in the */skywave/(beacon_name).ifr* files. If the level of skywave interference exceeds the level of wanted signal, the point is deemed to be outside coverage. As explained in D, the level of skywave interference saved in the*(beacon_name).ifr* files is the 95th% and already incorporates an adjustment for the standard protection ratios.

Parameter 5. Coverage contour limited by ...

The user may select the factor that defines the contour limits. This parameter toggles between SNR (Signal-to-Noise Ratio), ACCURACY and SS (Signal Strength) as the '5' key is pressed. If SNR is selected, the wanted signal will be compared to both shipboard and atmospheric noise. Shipboard noise is set with parameter 9, whereas atmospheric noise is interpolated from the database values supplied in */files/atmnoise.dat* and listed in Figure D.4. If ACCURACY is selected, a minimum SNR is determined by the program, based on the associated probability of message errors for a Type 1 message containing the corrections for 8 satellites. Again, the noise is both shipboard and atmospheric. No account is taken of noise levels if SS is selected. In all three cases, the inclusion or exclusion of interference is independently controlled by parameters 3 and 4. The numerical values of SNR, ACCURACY and SS are set with parameter 6.

Parameter 6. Value of contour limit set to ...

Having selected the contour-limiting criterion with parameter 5, the numerical value of the contour is set with parameter 6. Care should be taken in that any numerical value can be input here for SNR and SS. The standard minima are; 7 dB for SNR, 3 m for ACCURACY (and no lower value will be accepted) and 20 dBμ for SS. If

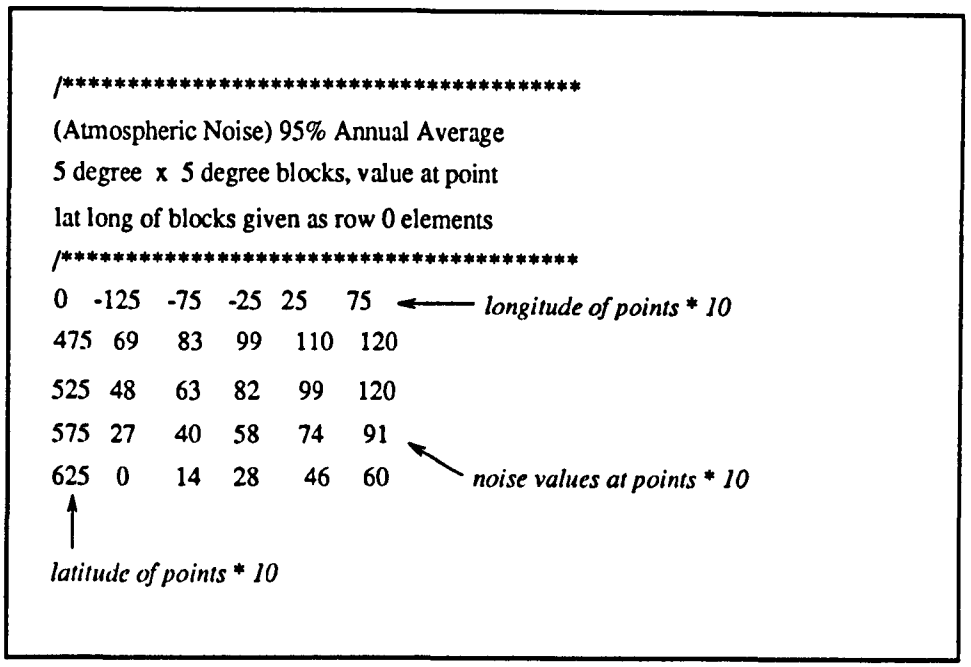

Figure D.4: The atmospheric noise values in dBμ at points spaced 5° by 5°over the region of the British Isles. The noise applied by the CPS at any point is the weighted interpolation of these values at that point.

the user enters values below these minima, a warning message appears which must be acknowledged by pressing any key.

Parameter 7. Signal Strength Floor of ...

The SS floor value selected by the user is applied as an additional coverage-limiting criterion when the coverage contour is limited by SNR or ACCURACY. It causes a point to be deemed out of coverage if it falls below this minimum acceptable SS, before the minimum SNR or ACCURACY criteria is checked. The standard minimum SS is 20 dBμ and the user must acknowledge a warning message if a lower value is chosen. If the coverage contour is limited by SS, this parameter has no effect.

Parameter 8. SNR Floor of ...

The SNR floor value selected by the user is applied as an additional coverage-limiting criterion when the coverage contour is limited by ACCURACY. It causes a point to be deemed out of coverage if it falls below this minimum acceptable SNR, before the ACCURACY criterion is checked. The standard minimum SNR is 7 dBμ, and the user must acknowledge a warning message if a lower value is chosen. If the coverage contour is limited by SS or SNR, this parameter has no effect.

Parameter 9. Ship's Noise Value of ...

This parameter allows the user to input a local, shipboard, noise level. Any value may be input. This parameter is taken into account when the coverage-limiting criterion is either SNR or ACCURACY. In these cases, the wanted signal level is compared to the larger of the two noise sources, either shipboard or the 95th% annual average atmospheric. Ship's noise has no effect if it is set at or below the minimum atmospheric noise level of 0 dBμ, as given in Figure D.4.

Parameter M. Modify Nominal Ranges of beacons?

The user has the option, at run-time, of changing the nominal range of any or all of the beacons in the system. With this parameter set to YES, the user will be reminded of the beacon's current nominal range and asked for a new range for each beacon as it is being added to the coverage of the system. If the user wishes NOT to modify the specified beacon's range, pressing ⟨*enter* ⟩ will cause the program to continue, using the current nominal range. The output plot will always carry a record of the nominal range of each beacon as it was applied to the given contour. This nominal range appears as a number in parenthesis following the beacon's name in the *full.exf* file.

Flow of *PLOTBECN*

With all the parameters adjusted and confirmed, the program sets up the master window of calculation points spaced by 0.1° latitude by 0.1° longitude. The pre-calculated data points for each beacon selected in *input.lst,* are aligned to the appropriate master window calculation point by using the local beacon window information stored as the header of the files. Each calculation point is declared to be either IN COVERAGE or NOT IN COVERAGE, depending on the wanted signal level, the interference levels, the noise levels and the coverage-limiting criteria. The coverage contour is 'drawn' around the IN COVERAGE area, excluding any areas NOT IN COVERAGE.

The flow of the program is as follows :

1 Open a file *c:/easycad/full.exf* and write the latitude/longitude lines,
2 Present the menu to the user, then save the parameter settings,
3 Read in noise data from *atmnoise.dat* file,
4 Read *input.lst* to determine how many beacon's are to be included in the system,
5 Read a beacon name from *input.lst,*
6 Read the beacon's location and nominal range from *becninf.dat,*
7 Query the user for a new nominal range, if the modification parameter is set,

8 Retrieve the beacon's window size and location from the */gndwave/⟨beacon_name⟩.dgp* file
9 For each calculation point in the local window,
9a Calculate the atmospheric noise level,
9b Read strengths from **.dgp* and **.ifr* files, depending on the setting of the user parameters,
9c Adjust the strengths read from **.dgp* files, if the nominal range was modified,
9d Compute own-skywave interference, depending on the settings of the user parameters,
9e Compare the wanted signal strength to the interference levels, the noise levels and the settings of the user parameters to determine if the point is in coverage,
9f Mark the point as IN COVERAGE or NOT IN COVERAGE, as appropriate,
10 Repeat 9 until all the points are done,
11 Repeat 4 until the specified number of beacons have been run,
12 Determine which points are on the border(s) between IN COVERAGE and NOT IN COVERAGE,
13 Save the border points as spline points in *full.exf* file,
14 Write all the parameter information to the *full.exf* file,
15 Done.

An example

This section provides a step-by-step guide to generating a coverage contour. It assumes that the beacons have already been installed. The specified contour is to indicate the area within which the user expects 5 m accuracy under daytime conditions. The user wishes to use either The Lizard or the St. Catherine's Point beacons and has a very good receiver, capable of working with a minimum signal strength of only 15 dBμ and a minimum SNR of 5 dB. Additionally, The Lizard's nominal range will be reduced to 100 km during the period of operation and the user's ship is extremely quiet electrically.

The steps for generating the specified coverage contour are show in Figures D.5 to D.18.

Step 1: Edit the *input.lst* file to select two beacons, LIZARD_LSTN and ST_CATHERINES_POINT.
Step 2: Start the *PLOTBECN* program by typing *PLOTBECN* at the *c:/dgpscov* prompt.
Step 3: Daytime conditions are specified, so parameters 1 and 3 are left as YES and parameters 2 is toggled to NO ...
Step 3 continued: ... and parameter 4 is toggled to NO.
Step 4: The contour required is an accuracy contour, so parameter 5 is toggled to ACCURACY.

Step 5: The accuracy limit of 5 m is specified, so select parameter 6, then type the input limiting value of 5.0 when queried.

Step 6: An SS Floor of 15 dBμ is specified, so select parameter 7, then type the input limiting value of 15.0 when queried. A key must be pressed to acknowledge the warning that this is below the standard minimum SS Floor of 20 dBμ.

Step 7: An SNR Floor of 5 dB is specified, so select parameter 8, then type the input limiting value of 5.0 when queried. A key must be pressed to acknowledge the warning that this is below the standard minimum SNR Floor of 7 dB.

Step 8: The Lizard's nominal range is to be modified, so set parameter M to YES. The program will ask for the New Range before accessing The Lizard's pre-calculated arrays.

Step 9: To proceed, press ⟨*enter* ⟩ and confirm that all parameters are correct by pressing 'Y'.

Step 10: When queried, press ⟨*enter* ⟩ to leave St. Catherine's nominal range as 129 km.

Step 11: When queried, type in the new range of 100 for The Lizard. When queried again, confirm 100 km by pressing ⟨*enter* ⟩.

Step 12: The program will indicate as a percentage how far along it is in the Spline Procedure, that is in defining the contour encircling the IN COVERAGE points. When the program has finished, change into the */easycad* directory.

Step 13: Import the coverage prediction file you have just generated by typing *import full.exf* at the DOS prompt and then enter EasyCAD by typing *ecad full.* For 'newer' versions of EasyCAD, first start EasyCAD by typing *ecad,* then import the file *full.exf* using the menu options (see your EasyCAD manual for details). The resulting diagram is shown. Notice that the parameter settings and warning messages appear on the right-hand side and that the nominal ranges used are given after the beacon names. If desired, the map supplied can be overlaid by using the 'part' function to add the *ukmap.fcd* file (see below).

Assembling diagrams

For more details of EasyCAD commands, please refer to the EasyCAD manual.

Each time *PLOTBECN* is run, a single coverage contour is produced in the file *full.exf.* This is then imported into EasyCAD and should be saved with a unique file name. To overlay several contours on one diagram, use the EasyCAD PART command to add each contour. A map can be added in the same way; one is supplied as *ukmap.fcd.* The final diagram may be output to hard copy using the EasyCAD PLOT command.

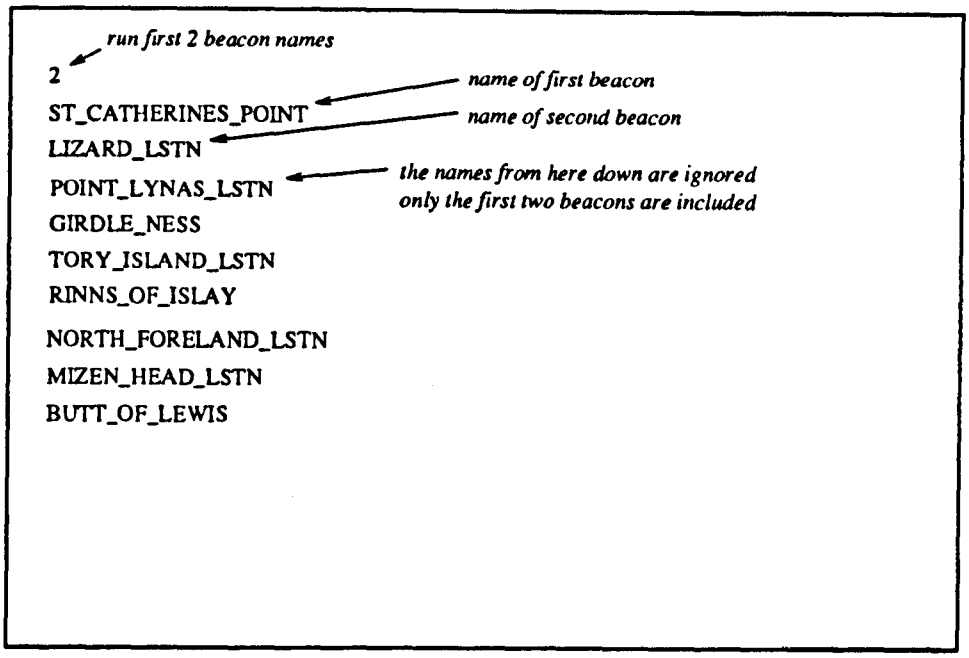

Figure D.5: Step 1: Edit the *input.lst* file to select two beacons, LIZARD_LSTN and ST_CATHERINES_POINT.

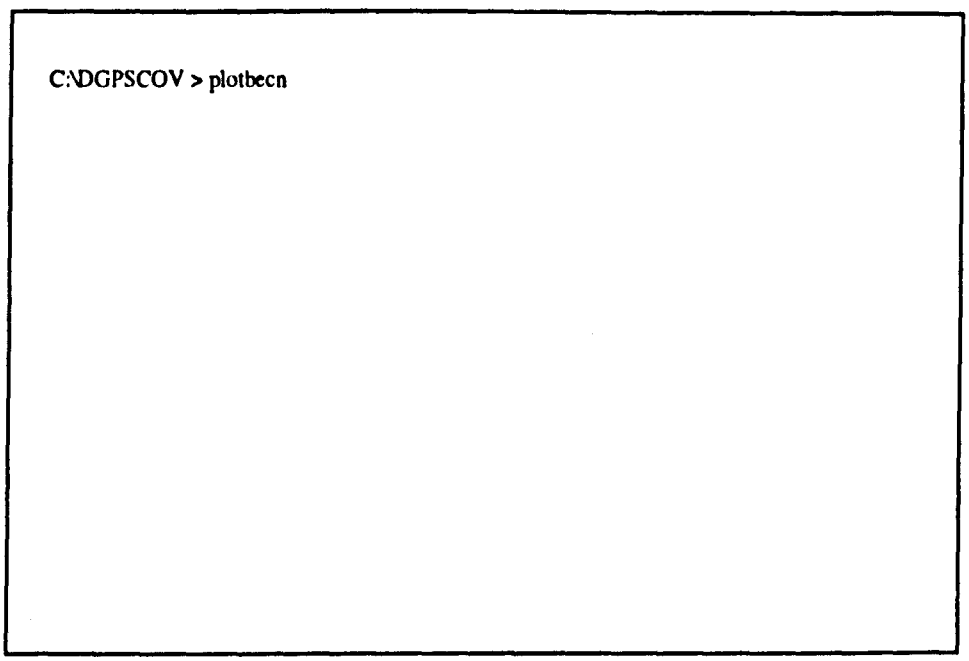

Figure D.6: Step 2: Start the *PLOTBECN* program by typing *PLOTBECN* at the *c:/dgpscov* prompt.

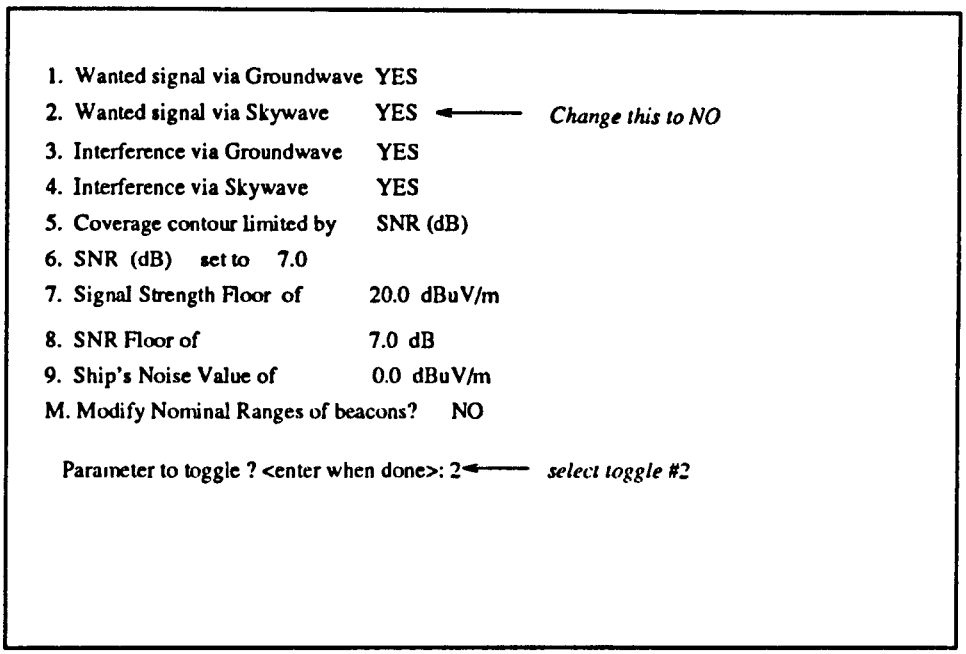

Figure D.7: Step 3: Daytime conditions are specified, so parameters 1 and 3 are left as YES and parameters 2 is toggled to NO ...

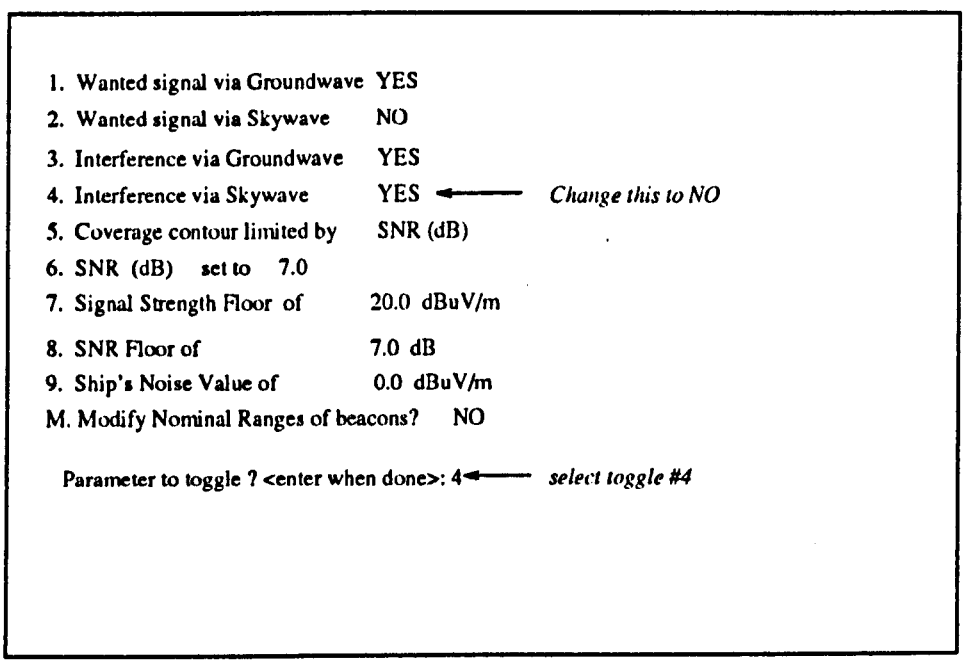

Figure D.8: Step 3 continued: ... and parameter 4 is toggled to NO.

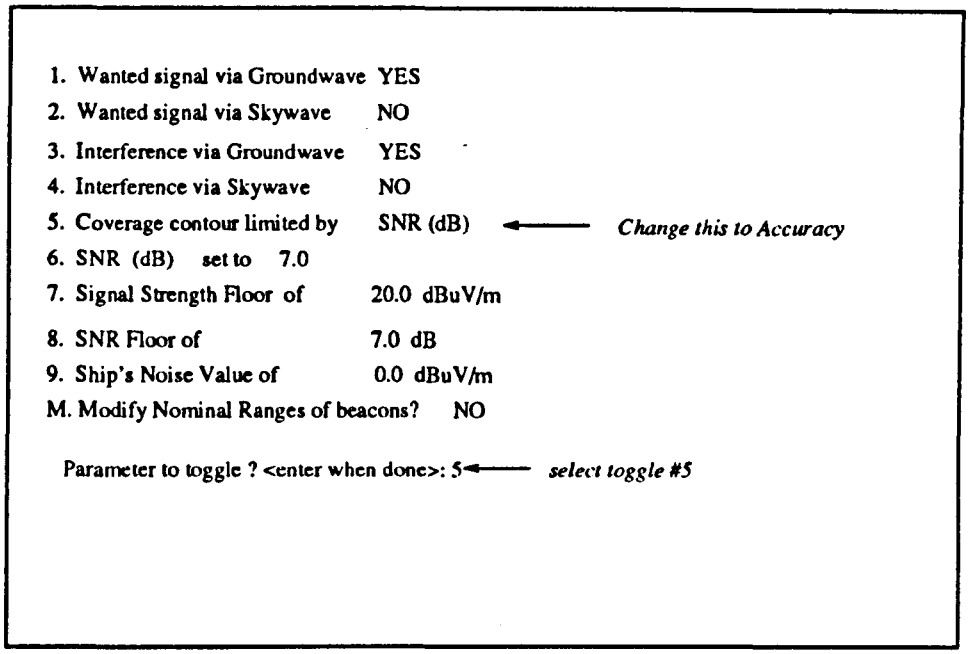

Figure D.9: Step 4: The contour required is an an accuracy contour, so parameter 5 is toggled to ACCURACY.

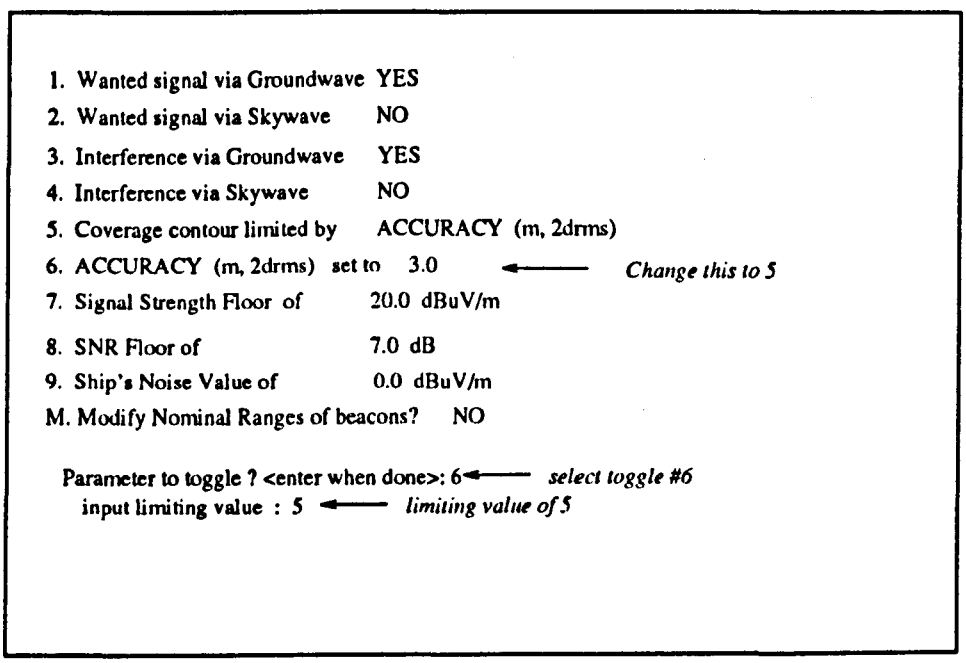

Figure D.10: Step 5: The accuracy limit of 5 m is specified, so select parameter 6, then type the input limiting value of 5.0 when queried.

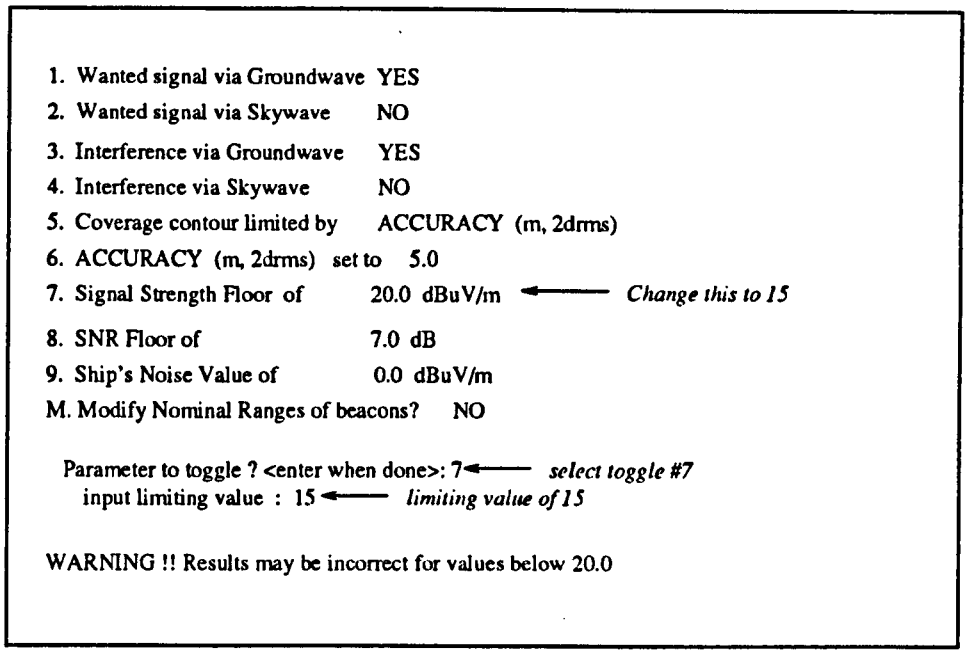

Figure D.11: Step 6: An SS Floor of 15 dBμ is specified, so select parameter 7, then type the input limiting value of 15.0 when queried. A key must be pressed to acknowledge the warning that this is below the standard minimum SS Floor of 20 dBμ.

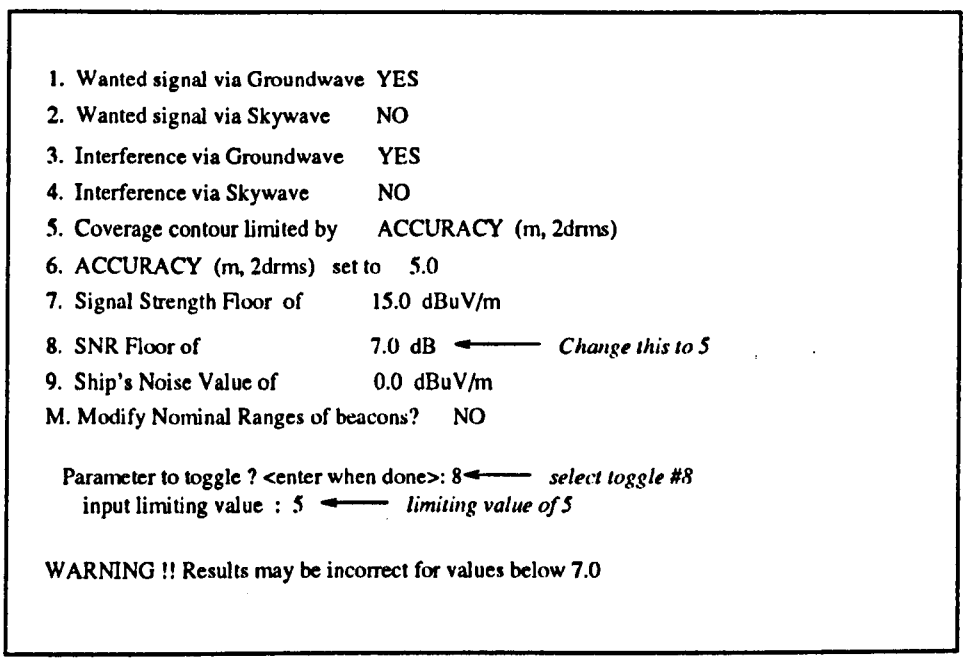

Figure D.12: Step 7: An SNR Floor of 5 dB is specified, so select parameter 8, then type the input limiting value of 5.0 when queried. A key must be pressed to acknowledge the warning that this is below the standard minimum SNR Floor of 7 dB.

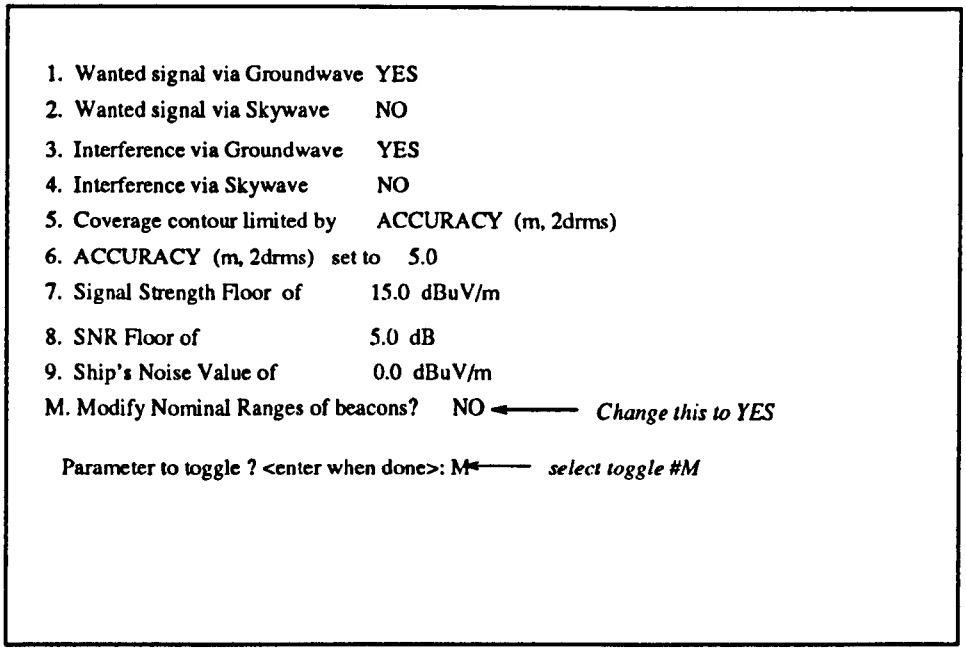

Figure D.13: Step 8: The Lizard's nominal range is to be modified, so set parameter M to YES. The program will ask for the New Range before accessing The Lizard's pre-calculated arrays.

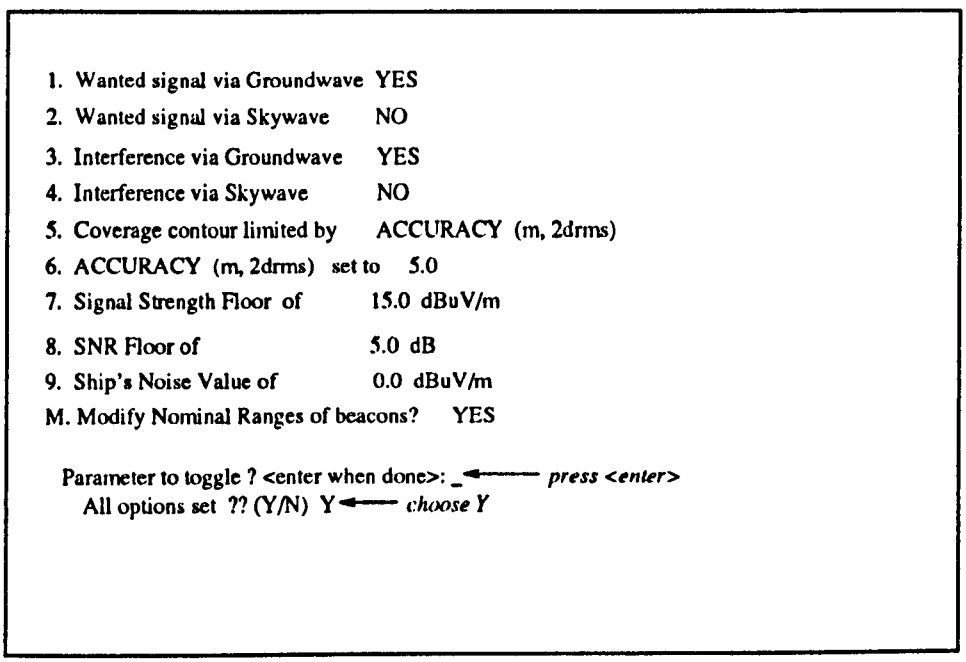

Figure D.14: Step 9: To proceed, press ⟨*enter* ⟩ and confirm that all parameters are correct by pressing **Y**.

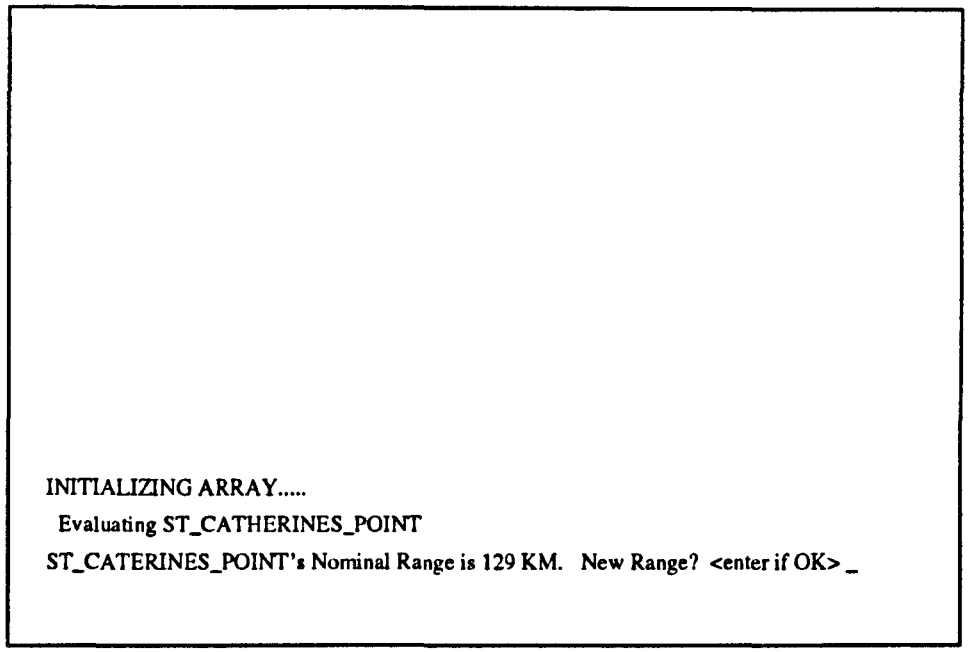

Figure D.15: Step 10: When queried, press ⟨*enter* ⟩ to leave St. Catherine's nominal range as 129 km.

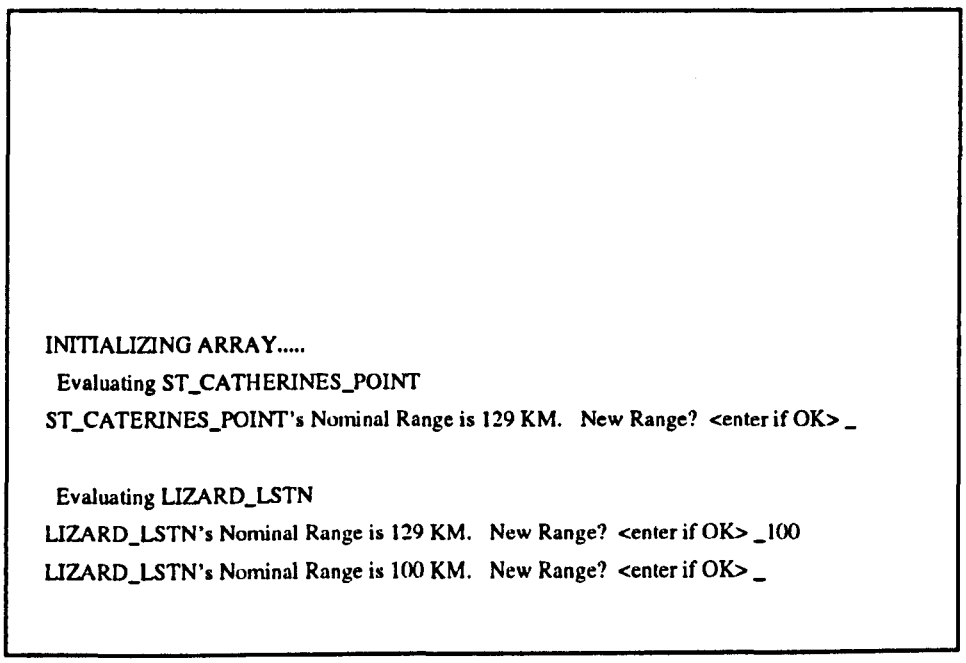

Figure D.16: Step 11: When queried, type in the new range of 100 for The Lizard. When queried again, confirm 100 km by pressing ⟨*enter* ⟩.

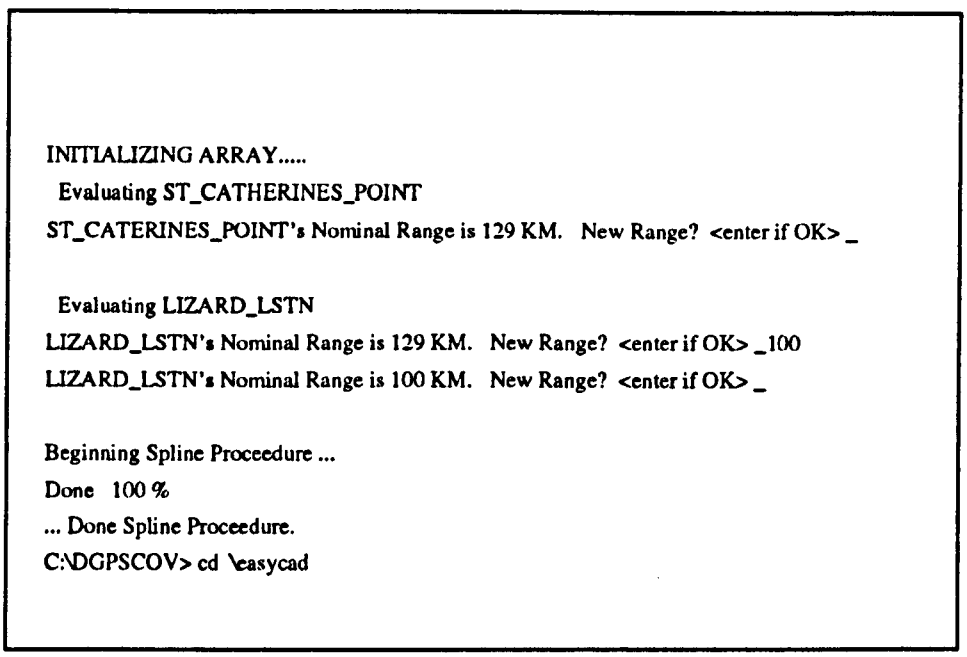

Figure D.17: Step 12: The program will indicate as a percentage how far along it is in the Spline Procedure, that is, in defining the contour encircling the IN COVERAGE points. When the program has finished, change into the */easycad* directory.

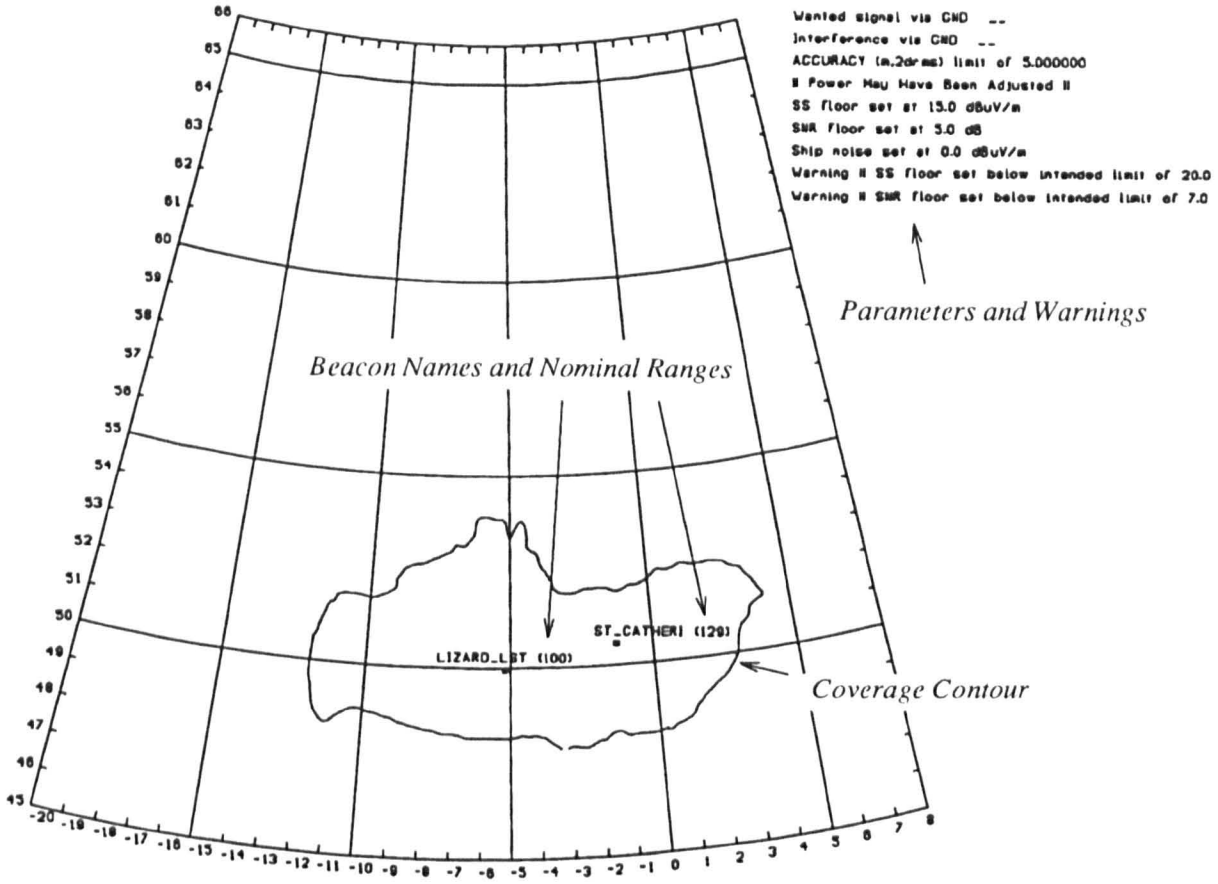

Figure D.18: Step 13: Import the coverage prediction file you have just generated by typing *import full.exf* at the DOS prompt and then enter EasyCAD by typing *ecad full.* For 'newer' versions of EasyCAD, first start EasyCAD by typing *ecad,* then import the file *full.exf* using the menu options (see your EasyCAD manual for details). The resulting diagram is shown. Notice that the parameter settings and warning messages appear on the right-hand side and that the nominal ranges used are given after the beacon names. If desired, the map supplied can be overlaid by using the PART function to add the *ukmap.fcd* file (see below).